# CONVERSION OF ALKANES AND ALKENES OVER Ga-MODIFIED ZSM-5 TYPE ZEOLITES AND METAL OXIDE CATALYSTS

**A**
**Thesis**
Submitted to the
**University of Pune**
For the degree of
**Doctor of Philosophy**
In
**Chemistry**

**By**

**SUBHABRATA BANERJEE**

**Chemical Engineering Division**
**National Chemical Laboratory**
**Pune - 411 008, INDIA**

**August, 2001**

***Dedicated***

***To***

***My Parents***
***and***
***My Sister***

***"Experiments are the only means of knowledge at our disposal. The rest is poetry, imagination."***

***Max Planck***

# *Acknowledgement*

*At the present moment let me in the beginning express my deepest sense of gratitude to my supervisor, Dr. Vasant R. Choudhary, for his invaluable guidance, meaningful teaching, constant support and advice throughout the course of this investigation. It is he, who introduced me to the world of catalysis, suggested my research problem and guided my sailing through the doctoral work. Working with him has at all times been a pleasant and stimulating experience for me and I shall be having long lasting gratitude and respect for him.*

*My sincere thanks are due to Dr. S. D. Sansare, Dr. S. G. Pataskar, Dr. A. M. Rajput, Dr. A. S. Mamman and Dr. A. G. Gaikwad for all the helpful discussion, encouragement and support. They not only extended their warm friendship, but they were always there whenever I needed them professionally.*

*I must then gratefully appreciate the help and cooperation of my lab-seniors Dr. V. H. Rane, Dr. S. A. R. Mulla, Dr. A. K. Kinage, Dr. P. Devadas, Dr. B. S. Uphade and Dr. C. Sivadinarayana. The help and cooperation received from Mr. V. L. Rajput, Mr. V. L. Chandekar and Mr. B. G. Pingale is also duly acknowledged. I wish to look back with warmth of my heart to the love and friendship that came my way from friends and colleagues like Abhijeet, Tushar and Kiran.*

*Association with colleagues Suman-da and Mantri in all these years has been a really wonderful experience. The very wholeness of their warmth, support, and encouragement has become a cherishing experience by now. Many thanks are due for my other lab-mates Rajamani, Joshi, Vijay, Jayant, Sachin, Deepa, Sonali, Kailash, Nilesh, Chanchal, Kartick and Pankaj. I have also enjoyed the company of the project students Smita, Geeta, Rajat and many others. My roommates in all these years, Raja, Chitto, Annyt, Sinchan and Babu, need a special mention. Away from home, it was they who provided a lively atmosphere around me.*

*The invaluable help and guidance received from Dr. Mandale for XPS, Dr. Sainkar for SEM, Dr. (Mrs.) A. Mitra for XRD, is also duly acknowledged.*

*The personnel from the C.E. office and from the supporting groups like glass blowing and electrical sections had been very friendly and generous with their assistance.*

*My sincere gratitude goes also to Subarno-da, Bikash, Karuna, Souvik-da, Dibakar-da, Mohuadi, Sumit, Snehasish, Jayati, Paramita, Aloke, Sukanto, Subhradipda and Priyamvada. It was their love and cooperation, which has inspired me to do good work.*

*I would like to thank all my seniors and friends in NCL, Somnath, Sujata, Ananda, Chandana-boudi, Koushik, Bibhas, Debdut, Debasish, Dilip, Samanta, Tarun, Anuradha, Laha-da, Utpal, Probal, Manas-da, Tapan-da, Somen-da, Debasish-da, Anil-da, Sanjoy-da, Sukhen-da, Soumen-da, Sruti-di, Sourabh-da, Sanjib-da, Tapas-da, Manna-da, Gour-da, Maji-da, Krishanu-da, Priyo-da, Saptarshi-da, Arindam, Dinu, Sukhen, Sriti, Subhas, Senapati, Ghota, Saikat, Kartick, Anamitra and all other friends in and around NCL. Thanks are due to Mr. Murugan and bhaviji. I am indebted to Syamasri-di, Lana-di, Pompa-di, Pinaki-da, Habu, Chat and Mousumi-di for their cooperation.*

*I also catch hold of this golden opportunity to express my deepest respect for Prof. S. P. Moulik, Dr. Arunava Sen, Dr. A. Sarkar and Mr. S. Ghosh and all my teachers who have not only taught me the basics of Chemistry, but also the basics of life and profession.*

*In all these years I have received love and affection from my relatives. I wish to particularly express my heartfelt gratitude to my Didu, Mama, Mami and Piku for their constant encouragement. I wish my dadu and thakuma were here by my side today, when I am submitting my thesis. They were the constant source of inspiration for me, their sad demise a painful reality though.*

*It gives me immense pleasure at this juncture to mention my parents and my sister in this regard. It is their teachings, their ideals, their affection, their encouragement, their patience, and their blessings, which have constituted a treasure for my life. I am sure this work could never have been possible but for their enthusiasm and sacrifice. Words cannot express my feelings towards them. They were there by my side in all these years, and I am sure that they will be, through the best worst of my times. Dedication of this thesis to them is just a very small token of love from my side.*

*My sincere gratitude remains there for Dr. B. D. Kulkarni, Head, Chemical Engineering Dvision, NCL, and Dr. P. Ratnasamy, Director, NCL, for allowing me to carry out this research work of mine at NCL and providing me with the infrastructure.*

*My thanks are due to the Council of Scientific and Industrial Research, New Delhi for awarding me a Junior Research Fellowship.*

*Pune* *(Subhabrata Banerjee)*
*August, 2001*

## *Certificate as per Form "A"*

Certified that the work incorporated in the thesis **"*CONVERSION OF ALKANES AND ALKENES OVER Ga-MODIFIED ZSM-5 TYPE ZEOLITES AND METAL OXIDE CATALYSTS"*** *submitted by* ***Mr. Subhabrata Banerjee*** *was carried out by the candidate under my supervision. Such material as has been obtained from other sources has been duly acknowledged in this thesis.*

*August, 2001*

*(Dr. Vasant R. Choudhary)*
*Research Guide*

# LIST OF CONTENTS

## SUMMARY AND CONCLUSIONS

The rapid growth of human civilization has seen a quantum jump in the consumption of energy. If the growth in the energy consumption continues at this rate, a rapid shortfall between the demand and supply of the fossil fuel is inevitable in the near future. The fossil fuel reserve in the earth is also not unlimited. This projected shortfall in the supply of fossil fuel can be best off-set by looking for some alternative natural energy resources, preferably a renewable one. Another immediate solution can be the better and effective utilization of the available fossil fuel resources through development of better and environmentally cleaner technologies. The world reserves of natural gas are almost equivalent to that of oil. Hence effective utilization of methane (which is the main constituent of natural gas) by its conversion into value-added products such as $H_2$ and ethylene is of great practical importance.

As part of a comprehensive research program going on in the National Chemical Laboratory (Pune, India), the various aspects related to the effective utilization of methane/natural gas and lower olefins through different catalytic conversion processes also the control of methane and propane emissions by catalytic combustion (at both lower and higher temperatures) have been studied in this dissertation.

The present Ph. D. work was undertaken with the following objectives:

1. To produce continuously CO-free $H_2$ by catalytic decomposition of methane and gasification of carbon by steam at low temperature in two parallel catalytic reactors operated in cyclic manner, using different Ni-based catalysts.
2. To study thoroughly the factors affecting the catalytic methane decomposition and gasification by steam of carbon formed on the catalyst in the step-wise steam reforming of methane operated in cyclic manner, using a $Ni/ZrO_2$ catalyst.
3. To study aromatization of dilute ethylene (< 5 mol%) over H-ZSM-5 and Ga-modified ZSM-5 type zeolite (viz. H-gallosilicate, H-galloaluminosilicate and Ga-impregnated H-ZSM-5) and to correlate the catalytic activity with the acidity and non-framework Ga-content of the zeolites.

4. To study the effect of different process parameters viz. temperature and space velocity on the aromatization of dilute ethylene over highly acidic H-GaAlMFI zeolite.

5. To study the aromatization of other lower olefins (viz. propylene and n-butene) over the highly acidic H-GaAlMFI zeolite.

6. To study the activation of low surface area perovskite oxides by their hydrothermal treatment and study the catalytic combustion of methane over them.

7. To study the catalytic combustion of propane over Mn-doped $ZrO_2$ (cubic) catalyst and to study in detail the effect of different catalyst parameters viz. Mn/Zr ratio, calcination temperature etc. on the propane combustion activity of the catalyst.

8. To study the complete combustion of propane over different transition metal (viz. Co, Mn, Fe, Cr and Ni) doped $ZrO_2$ (cubic) and to determine the various kinetic parameters (viz. activation energy and frequency factor) for the catalytic combustion process over these catalysts and also to study the involvement of lattice oxygen of the catalyst in the process.

9. To study the complete combustion of methane in presence or absence of oxygen over the Pd (or PdO)/$Al_2O_3$ catalyst oxidized (or reduced) to different extents in a pulse micro-reactor.

10. To study the high temperature (> $900^oC$) catalytic combustion of methane over thermally stable CoO-MgO catalyst and also to study the effect of different catalyst parameters viz. Co/Mg ratio, calcination temperature etc. on the methane combustion activity.

The thesis has been divided into four parts, as follows:

**PART – I: LITERATURE SURVEY AND EXPERIMENTAL**

This part is divided into two chapters.

### 1.1 GENERAL INTRODUCTION: LITERATURE SURVEY, OBJECTIVE AND SCOPE

This chapter presents the general background and also provides a summary of available literatures on the production of hydrogen from methane by its catalytic decomposition, aromatization of dilute ethylene and other lower olefins and the catalytic combustion of methane and propane over different catalysts viz. perovskites, noble metal catalysts and non-noble metal oxides along with the objectives and scope of the present work.

### 1.2 EXPERIMENTAL

This chapter deals with the preparation of different catalysts used in the present study, the techniques used for catalyst characterization and the experimental set-up used for different catalytic processes.

## PART – II DECOMPOSITION OF METHANE TO PRODUCE CO-FREE $H_2$

This part is divided into two chapters.

### 2.1. CONTINUOUS PRODUCTION OF $H_2$ AT LOW TEMPERATURE FROM METHANE DECOMPOSITION OVER Ni-CONTAINING CATALYST FOLLOWED BY GASIFICATION BY STEAM OF THE CARBON ON THE CATALYST IN TWO PARALLEL REACTORS OPERATED IN CYCLIC MANNER

CO-free $H_2$ in close to stoichiometric amounts was produced continuously at a constant $H_2$ production rate by the stepwise steam reforming of methane at low temperature ($500^oC$) in two parallel catalytic reactors operated in cyclic manner. The process involved two simultaneous reactions: one, catalytic decomposition of methane to $H_2$ and carbon (deposited on the catalyst) and second, gasification of the carbon deposited on the catalyst by steam to $H_2$ and $CO_2$. The two reactions were carried out separately in two parallel reactors (both containing the same Ni-containing catalyst), operated in cyclic manner by switching a methane containing feed and a steam containing feed between the two reactors at a predecided interval of time. The process shows best performance at an optimum value of the feed switch over time. Among the different Ni-containing metal oxide ($ZrO_2$, MgO, $ThO_2$, $CeO_2$, $UO_3$, $B_2O_3$ or $MoO_3$) and zeolite [HZSM-5, Hâ, HM, NaY, Ce(72)NaY or Si-MCM-41] catalysts, the $Ni/ZrO_2$ and Ni/Ce(72)NaY showed promising results for the cyclic process.

## 2.2. HYDROGEN FROM STEP-WISE STEAM REFORMING OF METHANE OVER $Ni/ZrO_2$: FACTORS AFFECTING CATALYTIC METHANE DECOMPOSITION AND GASIFICATION BY STEAM OF CARBON FORMED ON THE CATALYST

Decomposition of diluted methane (space velocity: 6450 $cm^3.g^{-1}.h^{-1}$) over $Ni/ZrO_2$ catalyst (for 1h) followed by gasification (carried out at the same temperature and period) by steam (50% steam in $N_2$, with a space velocity of 7740 $cm^3g^{-1}h^{-1}$) of the carbon formed on the catalyst at different concentrations of methane (2% - 75% $CH_4$ in $N_2$) in the feed and temperatures ($450^o$ – $600^oC$) has been thoroughly investigated. Both the methane decomposition and carbon gasification steps are strongly influenced by the concentration of methane in the feed and also by the temperature. In the methane decomposition step, the methane conversion is limited thermodynamically; it is decreased markedly with increasing the methane concentration but increased sharply with increasing the temperature. In the methane decomposition step, there is a little or no rise in the pressure drop across the catalyst for the initial reaction period, which can be considered as an induction period for the pressure drop increase due to the formation of filamentous carbon between the catalyst particles. When the methane concentration or temperature is increased, the induction period is decreased and also the pressure drop is increased at a larger rate. In the carbon gasification step, the degree of carbon gasification is decreased markedly with increasing the methane concentration, but it is increased sharply (approaching close to 100% at $600^oC$) with increasing the temperature. For achieving high methane conversions, particularly using methane without dilution for avoiding separation of the diluent from products, and also high degree of carbon gasification, both the methane decomposition and carbon gasification steps are required to be carried out at higher temperature (at $600^oC$ or above). However, at the higher temperature, a significant amount of CO is formed in the gasification step. XPS studies of the catalyst revealed that, the surface of Ni is covered to a very large extent by the carbon formed in the methane decomposition and the relative concentrations of the carbon species (viz. carbidic, semi-carbidic/semi-graphitic, graphitic and carbonate species) formed on the catalyst depends strongly on the methane decomposition temperature. The relative concentration of the carbon species is further changed after the gasification.

## PART – III AROMATIZATION OF LOWER OLEFINS

This part is divided into three chapters.

### 3.1. AROMATIZATION OF DILUTE ETHYLENE OVER Ga-MODIFIED ZSM-5 TYPE ZEOLITE CATALYSTS

Aromatization of dilute ethylene (5 mole% ethylene in $N_2$) over different Ga-modified H-ZSM-5 type zeolite catalysts [viz. Ga/H-ZSM-5 (Ga loading = 0, 1.4 and 4.7%), H-GaMFI and H-GaAlMFI (with different bulk and framework compositions of Si, Ga and Al)] at 400$^oC$ and atmospheric pressure was investigated at different space velocities (3,100 - 24,600 $cm^3g^{-1}h^{-1}$). The product selectivity and the distribution of aromatics and xylene isomers are strongly influenced by the space velocities and consequently show a strong dependence on the ethylene conversion. With decreasing the conversion, the selectivity for propylene is increased but that of aromatics is decreased, the concentration of $C_8$-aromatics and that of p- and o-xylene in xylenes are increased but that of benzene and toluene are decreased. Based on these observations a simplified reaction path for aromatization process is proposed. Because of their uniform distribution of non-FW Ga-species in the zeolite channels, the H-GaMFI and H-GaAlMFI zeolite catalysts show higher aromatics selectivity and/or higher ethylene-to-aromatics conversion activity in the ethylene aromatization than the Ga/H-ZSM-5 zeolite catalysts. The high zeolitic acidity is essential for the high ethylene conversion activity of the zeolite catalysts, but the high acidity alone is not enough for obtaining high aromatics selectivity or high ethylene-to-aromatics conversion activity. The aromatics selectivity does not show direct dependence on the acidity or non-FW Ga of the zeolite catalyst. For a Ga-modified ZSM-5 zeolite catalyst to be highly active and also highly selective in the ethylene aromatization, it should have both high acidity and an optimum ratio of non-FW Ga to strong acid sites, which is close to 1.0.

### 3.2. INFLUENCE OF TEMPERATURE AND SPACE VELOCITY ON THE PRODUCT SELECTIVITY AND DISTRIBUTION OF AROMATICS AND $C_8$ AROMATIC ISOMERS IN THE CONVERSION OF DILUTE ETHYLENE OVER H-GALLOALUMINOSILICATE (ZSM-5 TYPE) ZEOLITE

Product selectivity and distribution of the total and $C_8$ aromatics at the different iso-conversions (40, 60 and 80%) of dilute ethene (5 mol% $C_2H_4$ in $N_2$) over the H-GaAlMFI zeolite catalyst having high acidity (0.46 $mmol.g^{-1}$, measured in

terms of the pyridine chemisorbed at 400°C) and high concentration of non-framework Ga-oxide species (0.32 mmol.g$^{-1}$) at different temperatures (300° – 500°C) and space velocities have been investigated. A strong temperature and space velocity dependence of the selectivity for aromatics, propene and $C_4$ hydrocarbons and also of the distribution of aromatics and $C_8$-aromatic isomers has been observed. The results indicate that the aromatization involves $H_2$ transfer reactions predominantly at the lower temperatures and/or higher space velocities whereas dehydrogenation reactions become predominant at higher temperatures and/or lower space velocities. The primary aromatics produced in the process are found to be mainly p- and o-xylenes. The p-xylene/m-xylene ratio is decreased as expected, but the p-xylene/o-xylene ratio is increased with increasing both the space velocity and temperature. The increase of p-xylene/o-xylene ratio is found to be unusual, much above the equilibrium value. The distribution of xylene isomers is controlled by steric factors at 300°C but kinetically at 500°C.

### 3.3. AROMATIZATION OF PROPENE AND n-BUTENE OVER H-GALLOSILICATE (ZSM-5 TYPE) ZEOLITE CATALYST

Aromatization of propene and n-butene (at 400°C and atmospheric pressure) over H-GaAlMFI zeolite (bulk Si/Al = 37.5, bulk Si/Ga = 24.3, FW Si/Al = 40.3, FW Si/Ga = 49.9, Non-FW Ga = 0.32 mmol.g$^{-1}$, crystal size = 5.5 ± 1.5 μm) having high acidity (pyridine chemisorbed at 400°C = 0.41 mmol.g$^{-1}$) at different space velocities (3,100 - 58,100 cm$^3$g$^{-1}$h$^{-1}$) has been investigated. The catalyst was found to have a high olefin aromatization activity and high aromatics selectivity, which is attributed to the presence of a large number of both the non-framework Ga-species and protonic acid sites. The product selectivity and distribution was strongly influenced by the space velocity. The distribution of aromatics and xylene isomers were similar for the aromatization of both propene and n-butene, but that of aliphatic hydrocarbons differed in the two cases. The propene and n-butene aromatization reactions probably involved both the protonic acid sites mediated hydride transfer reactions and the direct dehydrogenation reactions over non-framework Ga-species, probably in combination with the zeolitic protons. Reaction path for the propene/n-butene aromatization has been proposed.

## PART – IV COMPLETE COMBUSTION OF LOWER ALKANES

This part is divides into five chapters.

### 4.1 ACTIVATION BY HYDROTHERMAL TREATMENT OF LOW SURFACE AREA $ABO_3$ TYPE PEROVSKTE OXIDES FOR COMPLETE COMBUSTION OF METHANE

Surface area and methane conversion in a complete combustion of methane of $LaCoO_3$ and $LaMnO_3$ perovskite- type oxides are increased very markedly by treating the perovskite-type oxides with water under autogeneous pressure (at $125^o$ - $300^oC$) and/or with steam (at $350^o$ - $800^oC$) at atmospheric pressure for 4h. The methane combustion activity per unit surface is, however, decreased markedly due to the hydrothermal water treatment of $LaCoO_3$ , but it is influenced only to a small extent because of the steam treatment of $LaCoO_3$ and the hydrothermal water treatment of $LaMnO_3$.

### 4.2 LOW TEMPERATURE COMPLETE COMBUSTION OF DILUTE PROPANE OVER Mn-DOPED $ZrO_2$ (CUBIC) CATALYSTS

Combustion of dilute propane (0.9 mol%) over Mn-doped $ZrO_2$ catalysts prepared using different precipitating agents (viz. TMAOH, TEAOH, TPAOH, TBAOH and $NH_4OH$), having different Mn/Zr ratios (0.05 - 0.67) and calcined at different temperatures ($500^o$ – $800^oC$) has been thoroughly investigated at different temperatures ($300^o$ – $500^oC$) and space velocities (25,000 – 100,000 $cm^3.g^{-1}.h^{-1}$) for controlling propane emissions from the LPG-fuelled vehicles. The Mn-doped $ZrO_2$ catalyst shows high propane combustion activity, particularly when its $ZrO_2$ is in cubic form, its Mn/Zr ratio is close to 0.2 and when it is prepared using TMAOH as a precipitating agent and calcined at $500^o$ – $600^oC$. Pulse reaction of propane in the absence of free-$O_2$ over the Mn-doped $ZrO_2$ (cubic) and Mn-impregnated $ZrO_2$ (monoclinic) catalysts has also been investigated for studying the relative reactivity and mobility of lattice oxygen of the two catalysts. Both the reactivity and mobility of lattice oxygen of the Mn-doped $ZrO_2$ are found to be much higher than that of the Mn-impregnated $ZrO_2$. The propane combustion over the Mn-doped $ZrO_2$ catalyst involves redox mechanism.

## 4.3 COMBUSTION OF DILUTE PROPANE OVER TRANSITION METAL-DOPED $ZrO_2$ (CUBIC) CATALYSTS

Combustion of dilute propane (0.9 mol% propane in air) over transition metal (viz. Co, Mn, Cr, Fe and Ni) doped $ZrO_2$ (cubic) catalysts (transition metal/Zr mole ratio = 0.25) at different temperatures ($200^o$ – $500^oC$) and space velocities (25,000 – 100,000 $cm^3g^{-1}h^{-1}$) has been investigated. The doping of transition metal in $ZrO_2$ was confirmed by XRD and temperature programmed reduction by $H_2$ of the catalyst. The catalysts have been compared for their propane combustion activity (measured in terms of the temperature required for 50% conversion at different space velocities and also the propane combustion rate at 50% conversion at different temperatures) and also for their activation energy and frequency factor in the propane combustion. The propane combustion performance of the catalysts was in the following order: Co-doped $ZrO_2$ > Mn-doped $ZrO_2$ > Cr-doped $ZrO_2$ > Fe-doped $ZrO_2$ > Ni-doped $ZrO_2$. Among the Co-, Mn- and Cr-doped $ZrO_2$ catalysts, for the Co-doped $ZrO_2$ catalyst, the activation energy is the lowest and the frequency factor was the highest. The propane combustion activity of the Co-doped $ZrO_2$ is found to be optimum for the Co/Zr ratio of about 0.25. The pulse reaction of pure propane in the absence of $O_2$ over the Co-doped $ZrO_2$ indicated the involvement of lattice oxygen from the catalyst in the propane combustion. It has also been shown that because of the doping of cobalt in $ZrO_2$, the lattice oxygen in the catalyst becomes mobile or the mobility of lattice oxygen is enhanced.

## 4.4 PULSE REACTION OF METHANE IN THE PRESENCE OR ABSENCE OF $O_2$ OVER Pd (OR PdO)/$Al_2O_3$ OXIDIZED (OR REDUCED) TO DIFFERENT EXTENTS

Initial methane combustion activity (at $160^oC$ – $280^oC$) of Pd(5%)/$Al_2O_3$ in its different reduced or oxidized forms [$Pd^o$/$Al_2O_3$ oxidized (by $O_2$ at $600^oC$) to different extents and PdO/$Al_2O_3$ reduced (by $H_2$ at $600^oC$) to different extents] has been studied in a pulse micro-reactor connected to GC [amount of catalyst: 0.1g; pulse: 0.1ml mixture of 7.9% $CH_4$ in air; carrier gas: He (flow rate = $30cm^3.min^{-1}$ at NTP); pressure: 338kPa]. The pulse reaction of methane in the absence of free-$O_2$ over the $Pd^o$/$Al_2O_3$ and PdO/$Al_2O_3$ catalysts has also been investigated. The oxidized catalyst (PdO/$Al_2O_3$) showed much higher methane combustion activity and also much higher

methane conversion in the absence of free-$O_2$ than the reduced catalyst ($Pd^o/Al_2O_3$). The combustion activity is increased with increasing the degree of the oxidation of the $Pd^o/Al_2O_3$. But it is decreased with increasing the degree of reduction of the $PdO/Al_2O_3$. For the partially reduced or oxidized catalysts with the same PdO content, the catalysts with the PdO in the outer skin of the catalyst (i.e. with a skin of the PdO over metallic Pd), shows a higher methane combustion activity than that having the PdO in the inner core (i.e. with a skin of metallic Pd over the PdO). Thus both the relative concentration and position of PdO (or $Pd^o$) in the partially oxidized (or reduced) catalyst play important role for deciding its methane combustion activity.

## 4.5 HIGH TEMPERATURE COMBUSTION OF METHANE OVER THERMALLY STABLE CoO-MgO CATALYSTS FOR CONTROLLING METHANE EMISSIONS FROM OIL/GAS-FIRED FURNACES

In order to control the concentration of methane in the hot (>800$^o$C) flue gases of oil/gas-fired furnaces, complete combustion of dilute methane (5000 ppm in $N_2$-air mixture) over thermally stable CoO-MgO (Co/Mg = 0.5 or 1.0) catalyst (calcined at 950$^o$C, 1200$^o$C and 1400$^o$C) at different space velocities (15000$h^{-1}$ - 120000$h^{-1}$, measured at 0$^o$C and 1 atm pressure) and temperatures (800$^o$C - 1100$^o$C) has been thoroughly investigated. The catalytic combustion was carried out in quartz reactor with a very low dead volume so that the contribution of homogeneous combustion, particularly at higher temperatures, could be kept low. Involvement of lattice oxygen of the catalyst in the methane combustion was confirmed by methane pulse experiments. The catalysts were characterized by XRD, XPS and also for their surface area and reduction by $H_2$ at different temperatures, using pulse technique. Surface area and methane combustion activity of the catalyst is decreased markedly with increasing its calcination temperature. However, the catalyst calcined at a temperature as high as 1400$^o$C, showed a good methane combustion activity. The catalyst was found to exist as a complete solid solution of CoO and MgO. Both the activation energy and frequency factor for the combustion were found to increase markedly with increasing the catalyst calcination temperature. At the higher reaction temperatures and/or lower space velocities, the contribution of homogeneous combustion occurring simultaneously in the voids of the catalyst bed was found to be appreciable. By using the catalyst (calcined at 1200$^o$C) in the combustion, a methane conversion close to 100% could be obtained at a contact time of about 15ms at 950$^o$C. Since, furnace flue

gases are at high temperatures and contain enough oxygen, the combustion of methane to $CO_2$ and water at high conversion can be accomplished just by passing the flue gases over the thermally stable CoO-MgO catalyst at a small contact time, depending upon the temperature of the flue gases.

# PART - I

## LITERATURE SURVEY AND EXPERIMENTAL

**CHAPTER 1.1: GENERAL INTRODUCTION: LITERATURE SURVEY, OBJECTIVES AND SCOPE**

**CHAPTER 1.2: EXPERIMENTAL**

# CHAPTER 1.1

## GENERAL INTRODUCTION: LITERATURE SURVEY, OBJECTIVES AND SCOPE

The development of mankind is intimately associated with the development in the energy sector. The rapid development of our society has been possible through a tremendous progress in the development of new technology for better utilization of available natural energy resources, particularly the fossil fuel. The rapid growth of human civilization has seen a quantum jump in the consumption of energy. If the growth in the energy consumption continues at this rate, a rapid shortfall between the demand and supply of the fossil fuel is inevitable in the near future. The fossil fuel reserve in the earth is also not unlimited. This projected shortfall in the supply of fossil fuel can be best off-set by looking for some alternative natural energy resources, preferably a renewable one. Research and development in this regard has already been initiated in different parts of the world. Another immediate solution can be the better and effective utilization of the available fossil fuel resources through development of better and environmentally cleaner technologies. The worldwide reserves of natural gas, which mainly consists of methane, can be an ideal energy source. Even a decade ago, a large part of the natural gas used to be flared up in various oilrigs. But the concerted scientific efforts to utilize the natural gas effectively have led to the development of a number of processes. Natural gas can be an attractive feed for hydrogen production. Hydrogen has already been projected as the green fuel for the future generation. It has also found use in various futuristic energy production processes, particularly in fuel cells. The development of a catalytic process to produce hydrogen from natural gas for fuel cells particularly for low temperature fuel cells which require CO-free hydrogen, can lead to a scientific and technological breakthrough. Oxidative coupling of methane (OCM) is another promising process, which converts methane to higher olefin, mainly ethylene and has been developed successfully in laboratory scale. But this process is associated with an inherent problem of separating the dilute ethylene from the product stream. An easy and economical solution can be the conversion of the dilute olefin stream directly into some value added products, which are less volatile (e.g. aromatics like benzene, toluene, xylenes), which can then be separated easily.

The increased awareness about the environmental pollution has led to the development of several cleaner and "green" technologies involving natural gas. Already efforts are on to substitute petrol and diesel in the automobiles by natural gas, which burn more cleanly. Compressed natural gas and LPG run automobiles are currently in use in metropolitan cities of various countries including India. The power generation units are also opting for natural gas instead of the conventional fossil fuel like coal etc. But despite having a substantially lower emission, these processes produce an appreciable amount of lower alkanes like methane and propane as emission products. These lower hydrocarbons particularly methane, which has 20 times more green house effect than $CO_2$, needs to be destroyed before being released in the atmosphere. Catalytic combustion can provide an alternative to check the emission of these gases. Depending on the nature of use, both high temperature and low temperature catalytic combustion can be employed. The catalytic combustion is associated with development of highly efficient low temperature and high temperature catalysts.

As part of a comprehensive research program in the National Chemical Laboratory (Pune, India), the various aspects related to the effective utilization of natural gas and lower olefins through different catalytic conversion processes also the control of methane and propane emissions by catalytic combustion (at lower and higher temperatures) from automobiles and industries which use them as fuel, have been studied in this dissertation. Decomposition of methane to produce hydrogen has been studied with the aim of generating fuel cell grade hydrogen and subsequently widening the resource base of the fuel for fuel cells. The aromatization of lower olefins (ethylene, propylene and 1-butene) over gallium modified ZSM-5 type zeolite has been studied as an effective down stream process for overcoming the difficulties in OCM processes (viz. separating ethylene and other lower olefins from the product stream of OCM processes) and also widening the raw material base for different industrially important products (viz. BTX). The high temperature combustion of methane has been studied to develop thermally stable catalysts to control methane emissions from the gas/oil-fired furnaces. The activation of conventionally synthesized $ABO_3$-type perovskites (which is a promising combustion catalyst) for low temperature methane combustion and catalytic combustion of propane over transition metal doped zirconia catalysts have been studied with the objective to

develop non-noble metal based highly efficient combustion catalysts. Some aspects of low temperature combustion of methane over noble metal-based catalyst (supported Pd catalyst), which is regarded as the most effective combustion catalyst was also investigated to get an insight into the various factors influencing the catalytic activities of this catalyst.

In the subsequent sections, a brief literature survey related to the work reported in this dissertation together with the scope and objectives of the work undertaken is presented.

### 1.1.1. Continuous Production of CO-free Hydrogen by Catalytic Methane Decomposition and Carbon Gasification by Steam

A tremendous development of science and technology has been witnessed in the last century in every aspects of human civilization. The energy sector is no exception. The devoted scientific research has led to an unbelievable development in the utilization of conventional non-renewable energy resources like fossil fuels etc. to produce energy. But the rapid consumption together with the resulting disappearance of the fossil fuel has already reached an alarming situation. The energy producing technologies are also very often not environment friendly. This alarming situation has left us at a crossroads. The last decades of the $20^{th}$ century can be really considered as a transition period when the mankind looked forward to adopt the eco-friendly and far-reaching futuristic alternatives for the energy sector. The best solution would have been the "going back to the basic life style". But the realistic viewpoint is the better technologies leading to a better utilization of fossil fuel and various other renewable energies.

Fuel cell is one of the several technologies, which has a lot of promise for the future energy needs. This is an electrochemical cell, which can continuously convert chemical energy of a fuel and an oxidant to electrical energy, by a process involving an essentially invariant electrode-electrolyte system [1]. Though the basic principle sounds similar to that of the electrochemical batteries, the main advantage of the fuel cell is that as long as the cell is supplied with the fuel and an oxidant, electrical power can be obtained. Fuel cells are also very efficient in converting upto 90% of the energy contained in its fuel into usable electric power and heat [2]. Besides, they are

modular, which means they can be developed for a wide range of power requirements from a few kilowatts to even megawatt size. They also have very low emission (produces water as the only by-product) and have very low noise levels - which is expected to be mandatory for all the next-generation power plants. Hydrogen has been found to be the most promising fuel for the fuel cells. The high electrochemical reactivity compared to that of the common fuels like hydrocarbons, alcohol etc. and its well-understood and relatively simple reaction mechanism has made it the only practical fuel for the present generation fuel cells [2].

The fuel cells can be primarily classified on the basis of their operating temperatures. The high temperature fuel cells, like molten carbonate fuel cells (MCFC) and solid oxide polymer fuel cells (SOFC), which operate above 923K, poses some problems during their maintenance and operation, and hence not suitable for small-scale and mobile operations like in automobiles. That way low temperature fuel cells like proton exchanged membrane (PEM) fuel cells, alkaline fuel cells (AFC), and phosphoric acid fuel cells (PAFCs) are advantageous. But these cells have very low $CO_x$ tolerance limits. AFCs have a few ppm $CO_2$ tolerance, whereas PAFCs can tolerate upto 2% CO and the most promising PEM cells can tolerate only a few ppm (<20 ppm) of CO. Thus $CO_x$ free production of hydrogen fuel for low temperature fuel cell is crucial to the successful development and commercialization of any fuel cell technology.

Water is the largest and probably the unlimited source of hydrogen. Electrolysis of water is to date the only industrial hydrogen production process, which does not directly rely on the fossil fuel. Though this technology produces the purest hydrogen, but this is presently not economically competitive with hydrogen produced from hydrocarbons.

There are several efficient economical and already commercialized processes for hydrogen production. These processes are following:

- hydrogen by catalytic steam reforming of natural gas
- partial oxidation of heavy hydrocarbons
- hydrogen from coal gasification
- methanol steam reforming
- steam iron process
- decomposition of non-carbonaceous fuel like $NH_3$, hydrazine etc., and

- methane decomposition

Except for methane decomposition and the decomposition of non-carbonaceous fuels, all the above mentioned processes produce a substantial amount of carbon monoxide. So, high and low temperature water gas shift reactors are to be employed to convert most of the CO to $CO_2$ ($CO + H_2O \rightarrow H_2 + CO_2$). The small amount of CO is then to be removed by a preferential oxidation reactor before using the hydrogen as a fuel in the low temperature fuel cells like PEM fuel cells. This tedious procedure makes the whole fuel-processing unit very bulky and complex and adversely affects the process economics.

The abundance of natural gas, which constitutes mainly methane, makes methane decomposition route very promising to produce the CO free hydrogen.

$$CH_4 \longrightarrow C + 2H_2 \qquad (1)$$

This is an endothermic reaction, the temperature dependence of enthalpy change ($\Delta H$) and equilibrium constant ($K_p$) are following:

700K : $\Delta H = 20.40$ kcal; $K_p = 0.111$

800K : $\Delta H = 20.82$ kcal; $K_p = 0.701$

1000K : $\Delta H = 21.40$ kcal; $K_p = 10.02$

Methane, having the highest H/C ratio, is also the most promising raw material for hydrogen production. This process, although long been known for producing carbon in its purest form, has not been fully explored for hydrogen production. But, in a rapidly changing energy scenario, the large abundance of natural gas, which constitutes above about 80% methane, makes the process very attractive. The successful development of this technology to produce hydrogen can lead to the effective utilization of the natural resources in an environmentally benign way.

But for the catalytic decomposition process, the carbon formed in the reaction can deactivate the catalyst rapidly by shielding the active catalytic sites and for a fixed bed reactor it can even block the catalyst bed, causing a large pressure drop across the reactor, which can be hazardous.

Regular removal of carbon, which is formed during the decomposition process, has to be done to make it suitable for commercial applications. One way to remove the carbon from the catalyst surface is its gasification by steam.

$$C + 2H_2O \longrightarrow CO_2 + 2H_2 \quad (2)$$

Some side reactions are also possible which can produce carbon monoxide viz. $C + H_2O \rightarrow CO + H_2$, but this reaction is favored at higher operating temperatures (> $1200^oC$), while the reaction (2) is favored at lower temperatures (<$538^o$ - $1000^oC$) [3].

The above reaction (reaction-2) removes the surface carbon and also produces hydrogen from water. If the two reactions (reaction 1 and 2) can be combined, then continuous production of CO-free hydrogen would be possible without any significant build up of carbon on the catalyst surface. The combination of the two processes also will produce 4 moles of hydrogen from one mole of methane.

Recently several researchers have reported the decomposition of methane to produce hydrogen. Barring a few, most of them have preferred Ni-containing catalysts. The unique process of carbon deposition on Ni-supported catalyst, which keeps the active Ni particle free from any encapsulation by carbon formed [4], may be the reason for selecting Ni-supported catalysts

Muradov et al. [5] has studied the cracking of methane over iron oxide catalyst. They achieved the equilibrium conversion above 1073K. They also reported no deactivation of the catalyst for several hours, in contrast to $Pt/Al_2O_3$ catalyst, which is deactivated within a few minutes under similar operating conditions.

Ishihara et al. reported [6,7] the methane cracking over a 10% $Ni/SiO_2$ catalyst at low temperatures, and they also observed no deactivation even after deposition of approximately 200 carbon per nickel atom.

Zhang and Amiridis reported [8] the hydrogen production via direct cracking of methane over silica supported Ni-catalyst. At 823K and at gas hourly space velocity (GHSV) = $30{,}000h^{-1}$, they observed a very slow deactivation of catalyst for the first two hours followed by a rapid deactivation. They found the formation of long, hollow, cylindrical filamentous carbon, having Ni-particle at the tip. They also studied the regeneration of deactivated catalyst by air and steam, and found that both methods were capable to restore the catalytic activity at 823K. But they did not combine the two processes to continuously produce hydrogen.

Avdeeva et al. [9] reported the methane decomposition to produce hydrogen over Co-alumina and Co-magnesia catalysts at $500^oC$ and at a methane stream space velocity of 45-60 $dm^3/g$ cat.h. The best performance was found with a coprecipitated 60-75 wt% Co-alumina. They found the Co-alumina catalyst as active as the Ni-

alumina. But no effort was made to remove the carbon deposited on the catalyst surface. They also found that the catalytic properties also depend on the nature of support.

Choudhary and Goodman reported [10] the step-wise production of CO-free hydrogen a pulse system at 648K - involving a methane decomposition step followed by carbon gasification by steam to produce CO-free hydrogen and simultaneously removing the carbon deposited on the catalyst. They observed the formation of 1.0 - 1.34 μmol of hydrogen per μmol of methane consumed. In carbon gasification step by steam, they found the presence of only $H_2$, $CH_4$ and $CO_2$. They also concluded that almost complete removal of surface carbon in carbidic form is possible almost quantitatively by water. Though their study was the first of its kind to combine both methane decomposition and carbon gasification steps, the study was a pulse one and not a continuous one, hence steady state was not achieved.

More recently Amiridis and co-workers [11] have carried out similar type of study over $Ni/SiO_2$ catalyst using a continuous flow reactor, where methane decomposition and catalyst regeneration by steam was done at 923K. They observed no deactivation of the catalyst even after 10 cycles of cracking and regeneration. The regenerated catalyst also showed no apparent structural changes. In one of their most recent work, Choudhary et al. has not ruled out the formation of trace amount of CO at a temperature as high as 923K, as CO-formation is thermodynamically favored at higher temperatures [12].

In continuation to their study on the CO-free hydrogen production, Choudhary et al. in another study [13] tried to optimize the process conditions for carrying out the two-step process. They found that the process could be optimally operated between 648-673K and at a surface coverage of 0.10 - 0.20 monolayer equivalent (MLE), without the CO formation. They also found that higher surface coverage of carbon has an adverse effect on the carbon removal by steam. Higher temperatures affect the nature of carbon formed on the catalyst, and a transition from an active carbon form to an inactive graphitic form occurs at higher temperatures, which has a negative impact on the carbon removal.

Choudhary et al has also addressed the various aspects of the methane decomposition step in their subsequent publications [14,15]. Methane decomposition reaction, when carried out over different Ni-supported catalyst, produced some

interesting time-on-stream activity pattern. The prolonged activity of $Ni/SiO_2$, $Ni/SiO_2/Al_2O_3$ and Ni/H-Y was attributed to the formation of long filamentous carbon, Ni being at the tip of the filament. But the carbon formed on the Ni/HZSM-5 was found to encapsulate the active Ni-particles, causing rapid deactivation. In fact common mechanism of filamentous carbon deposition for various Ni-based catalysts over different supports (e.g. silica, alumina, carbon) was reported earlier [16], however, accumulation of filamentous carbon was found to be strongly influenced by morphology and texture of the support.

From the brief literature survey, it is evident that catalytic methane decomposition study, though long been known, has not really been explored for the hydrogen production. Some recent literatures have addressed the topic in some details on several aspects of this catalytic process like nature of carbon filaments formed during the course of the reaction, effect of support on the carbon accumulation, the mechanism of filamentous carbon formation on the catalyst etc. But the issue of continuous production of CO-free hydrogen has rarely been addressed. The catalytic decomposition and subsequent removal of carbon by steam under a steady state condition is scarce. So, there is a great need to develop a process for continuously producing CO-free hydrogen by combining the reactions 1 and 2, without disturbing the feed for both the reactions.

### 1.1.2. Aromatization of Dilute Ethylene and Aromatization of Propylene and n-Butenes

The rapidly changing energy-scenario and the widening gap between the demand and supply of the petrochemical products has necessitated a comprehensive research for the effective and optimum utilization of the available natural resources. Natural gas is one of the natural resources. The worldwide research and developmental efforts have been made in the past two decades for developing novel processes for the conversion of methane/natural gas into value added products. Oxidative coupling of methane (OCM) for the production of $C_{2+}$ olefin is one such process, having a far-reaching futuristic importance. Despite the development of some active catalyst for the process, the process still suffers from one critical problem - that is the removal of very dilute ethylene produced in the OCM process from the product

stream. A typical OCM reaction generally produces ≤ 5 mol% ethylene, the balance being largely methane [17-19].

Several researchers have addressed this problem associated with the OCM process. They have suggested the removal of dilute ethylene based on primarily the condensation of the olefin on various solid adsorbents, followed by their recovery through thermal treatment [20-23]. Lunsford and coworkers described a process for removal of dilute ethylene from a OCM recycle stream involving absorption of ethylene through a porous membrane into a circulating $Ag^+$ solution, followed by subsequent decomposition of the resulting $Ag^+$-olefin complex [19].

But the inherent disadvantages of all the above processes is the introduction of a discontinuous multi-step olefin separation process, limited by the slow rate of olefin transport through the porous membrane and/or the slower complexation process [24]. An alternative approach could be the direct and continuous conversion of dilute olefin present in the OCM product stream into low boiling, higher molecular weight products, which can then be easily separated through condensation [25,26]. This relatively simple process would then require only an additional on-line catalytic reactor. The conversion of dilute ethylene/olefin into aromatics like benzene, toluene, xylenes (BTX) etc. has great commercial importance due to the high value and demand of the aromatic products. This approach was first disclosed by Choudhary et al. [25,26] in two US patents.

A detailed literature survey revealed that several studies have been reported on the aromatization of ethylene/lower olefins.

## Aromatization of ethylene

Lukyanov has developed a detailed kinetic model for ethylene aromatization over H-ZSM-5 zeolite under condition of catalyst deactivation [27]. Lukyanov et al. in another study has reported a kinetic modeling study of ethylene and propylene aromatization over H-ZSM-5 and Ga-HZSM-5 zeolite [28]. They established the contribution of Ga-species in formation of dienes and aromatics during the aromatization process.

Le Van Mao et al. has reported the effect of nature of coke on the activity and stability of the hybrid catalyst containing Zn or Ga used in the aromatization of ethylene [29].

Arishtirova et al. has studied the influence of copper on physico-chemical and catalytic properties of ZSM-5 zeolite in ethylene aromatization [30] and found that addition of copper enhances the activity and yield of aromatic products in the reaction.

Derouane et al. [31] in an earlier study reported the channel network effects in ethylene oligomerization and aromatization over H-ZSM-5, H-ZSM-11 and H-ZSM-48 catalysts. Bragin et al. [32] carried out ethylene oligomerization and aromatization over ferrisilicate zeolite and found that high temperature regeneration (at 550$^{o}$C) and aromatization causes a decrease in the lattice $Fe^{+3}$ concentration. They also observed that extra-lattice $Fe^{+3}$ does not participate in the catalytic reaction. Recently, Nakagawa [33] et al. has observed a promoting effect of $CO_2$ on aromatization of ethane and ethene over a $Ga_2O_3$ + HZSM-5 catalyst above 650$^{o}$C, aromatics yields were higher than those without $CO_2$. Solymosi et al. has studied reaction of ethylene on active methane aromatization catalysts [34]. In contrast to ZSM-5, they found that pure $Mo_2C$ exhibited low activity for cracking and transformation of ethylene. Preparation of pure $Mo_2C$ in highly dispersed state enhanced conversion of ethylene and only slightly decreased the selectivity to aromatics as compared to that measured on pure ZSM-5 under similar reaction condition. Brabec [35] et al. tested the catalytic activity of various Fe-modified MFI zeolites in aromatization of ethane and ethene and found that zeolite having Fe in its framework was much less active in aromatization compared to that in the case of HGaZSM-5. Berg et al. [36] found the evidence of catalytic formation of benzene from ethylene over tungstate ion.

## Aromatization of propene and n-butenes

Several studies on the aromatization of propylene and n-butene have also been reported in the recent literatures.

Popova et al. studied the aromatization of propene on Cu-ZSM-5, CuZn-ZSM-5 and H-ZSM-5 catalysts and found all the catalysts active for propene aromatization and have high selectivity for benzene, toluene and xylene [37]. Norval et al. studied the conversion of propene, 1-butene and 2-methylpropene over H-ZSM-5 zeolite at 663-773K [38]. Phillips and Virk also patented the aromatization of propylene (diluted in methane) over H-ZSM-5 zeolite [39]. Kustov et al. studied the effect of metal oxide modifiers on the catalytic properties of high silica pentasil type zeolites in conversion of $C_3$-$C_4$ olefin [40]. Wu et al. reported the catalytic dimerization and

aromatization of propylene over ZSM-5 type zeolites modified with Zn, P and Zn-P [41]. Some more literatures on the related subject were also found in the Chemical Abstracts, but only their abstracts were available. Karatun et al. reported propylene aromatization over Ga-containing pentasil zeolite [42]. Vorob'ev studied catalytic properties of high silica zeolites in the aromatization of ethylene and propylene [43]. Luo et al. reported aromatization of propylene on ZSM-5 and GaZSM-5 zeolite catalysts and found that selectivity and yield of aromatics were much higher on GaZSM-5 than on ZSM-5 zeolite [44]. Bragin et al. also found that formation of aromatics during aromatization of propane and propylene was greater for Ga-modified H-pentasil (H-ZVM) zeolites than the unmodified one [45]. Huang et al. studied the propene aromatization over alkali-exchanged ZSM-5 zeolites and found that the zeolite catalysts showed lower aromatization activity compared to HZSM-5, but higher benzene selectivity [46,47]. A mechanism involving Lewis acid-base pairs (alkali cation and neighboring basic oxygen) was proposed for observed product distribution. Inui et al. studied the synthesis of simple aromatics from propene over HZSM-5, H-Zn-silicate, Pt-ion exchanged H-ZSM-5, Pt-ion exchanged HZn-silicate and H-PtZn-bimetallosilicate and found that Pt-modified Zn-silicate was most active for propene aromatization [48]. Kwak et al. [49] prepared Ga/HZSM-5 by chemical vapor deposition technique and performed aromatization of propene and propane. With increasing Ga-loading [i.e. protons replaced by $(GaO)^+$], the propene conversion decreased but aromatics selectivity passed through a maximum, which was consistent with a bifunctional mechanism. They found optimum yield with catalysts having $Ga/(Ga + H^+)$ ratios between 0.4 and 0.5. Jiang et al. studied the active center of physically mixed $Ga_2O_3$/HZSM-5 catalyst in propene aromatization and found improved activity after its activation in $H_2$ at high temperatures. They attributed this to the migration of Ga-species into the zeolitic channels and the improved H-transfer properties of the catalyst [50].

Sivasanker et al. compared the activity of ZSM-5, ZSM-22 and EU-1 zeolites in aromatization of 1-butene [51] and attributed the difference in their activity and product distribution to their differences in acidity and pore characteristics.

De Jong et al. studied the activation and deactivation of the ferrierite zeolite for olefin conversions [52]. They found that carbonaceous deposits had an important role in modeling for activation/deactivation of FER for olefin conversion. Angelescu

et al. reported the aromatization of n-butane and n-butenes over $M_2O_3$-HZSM-5 zeolites (M= Ga, In, Tl) [53] and found that addition of $Ga^{3+}$ ions greatly improved the total conversion and aromatics selectivity compared to $In^{3+}$ and $Tl^{3+}$ ions. Angelescu et al. also reported the same reaction over H-ZSM-5 zeolite modified with Sr, Cd, Mg, Zn and Ag [54]. They correlated the aromatization activity with acid-base character of the corresponding oxides and found that Ag-HZSM-5 had catalytic performances comparable to those of Ga-HZSM-5 zeolite.

Ono et al. studied the aromatization of 1-butene over H-ZSM-5 and Zn-ZSM-5 zeolite [55]. They found beneficial effect of Zn when incorporated in H-ZSM-5 and borosilicate. Bhatia et al. reported aromatization of 1-butene over $AlPO_4$-11 as a function of temperature, time-on-stream, Ni-loading and methane dilution of the olefin feed [56]. Their experimental results supported a mechanism involving partial dehydrogenation of butene to butadiene, followed by oligomerization. But the activity of $AlPO_4$-11 was found to be less than that of H-ZSM-5.

A closer look at the available literatures on olefin aromatization process reveals that despite addressing the aromatization of olefin in detail, virtually all the studies involved highly concentrated olefin feed rather than the diluted one, which is typical of OCM reactions.

Another interesting point is the overwhelming use of the H-ZSM-5 zeolite (MFI structure) with or without modification by metal ions like Zn, Ga, Cu etc. Due to its unique shape selectivity that can discriminate between many molecules of commercial importance together with its acidity and high thermal/hydrothermal stability, H-ZSM-5 zeolite has always been an almost unanimous choice in the earlier studies. Its deactivation due to coking is also slower in comparison with zeolites having pore structure other than MFI-one. It has also been observed that H-ZSM-5 zeolite modified with metal oxides having redox function has high aromatization activity. In the critical reviews by Seddon, Guisnet et al., Ono and Giannetto et al., it has been demonstrated that modification of ZSM-5 zeolite by Zn or Ga leads to a higher aromatics yield in the aromatization of lower alkanes and alkenes [57-60].

A number of commercially important processes developed by various companies e.g. M2 forming from Mobil [61], cyclar from UOP and BP [62,63], Aroforming from IFP and Saltec [64,65] and Z-forming from Mitsubishi and Chiyoda [66] - use a medium pore zeolite (MFI-type doped with dehydrogenating species like

gallium. This illustrates the importance of presence of metal function like gallium or zinc during lower alkane/alkene conversion. The role of this metal function in lower alkane/alkene conversion has been a subject of extensive research, but the exact mechanism is yet to be fully established [28]. It is generally accepted that gallium species in the Ga-containing ZSM-5 zeolites ($Ga_2O_3$/HZSM-5, gallosilicate and galloaluminosilicate MFI structure) performs as a strong dehydrogenating function. It may be involved in dehydrogenation of either olefins to dienes or naphthenes to aromatics or both [28]. It is believed that Ga-species together with the Bronsted acid sites of the ZSM-5 zeolite imparts a bifunctional nature to the catalyst and the olefin aromatization proceeds through acid catalyzed olefin oligomerization and cracking and subsequent dehydrocyclization over the metallic function (i.e. Ga-species) [28,67,68].

It is evident from the above discussion that for any olefin aromatization process H-ZSM-5 zeolite with or without modification by a metallic function is a preferred catalyst.

Recently Lunsford and co-workers [24] have used Ga-oxide impregnated ZSM-5 zeolite having different Ga-loading, for catalytic aromatization of dilute (3%) ethylene-in-methane streams at 500-550$^oC$ and obtained a high ethylene conversion (93%) and aromatics selectivity (81%) at 520$^oC$ over a 5wt% Ga/ZSM-5 catalyst. They also concluded that the gallium species present both as $Ga^{3+}$ at zeolitic exchange sites and as Ga-oxide within the channels and on external surface promote dehydrogenation of acid catalyzed oligomerization and cyclization products. But there is ample scope to study the same reactions over gallosilicate and galloaluminosilicate zeolite having MFI structure, as related studies are scarce in the literature.

The study of aromatization of ethylene, propylene and n-butene is also important from the academic point of view. Zeolite catalyzed aromatization of low value LPG, consisting mainly of propane and butane provides a new and attractive route for the BTX production [69,70]. It is already established that Ga-containing catalysts are more preferable for industrial application due to higher conversion and aromatics selectivity and higher stability under standard process conditions [57]. As proposed by Inui et al. [71,72], Shibata et al. [73], Gnep et al. [74,75] and Kitagawa et al. [76], it is accepted generally that Ga-species provide new dehydrogenation route for alkane to alkene followed by olefin conversion into aromatics. The salient feature

is that for the aromatization of light paraffin/alkane like ethane, propane and butane, the corresponding olefin (e.g. ethylene, propylene and butylene) is the major intermediate. Hence a systematic study of aromatization of $C_2$-$C_4$ olefin over Ga-containing H-ZSM-5 zeolite can provide an insight into the reaction mechanism involved in the aromatization of light alkane and alkene and also provide valuable information about the role of Ga-species in the aromatics formation. This reveals that despite several literatures available on this subject, the role of Ga-species in the reaction and the exact reaction mechanism is still being debated. Hence, a systematic study of aromatization of $C_2$-$C_4$ olefins over Ga-containing ZSM-5 type zeolite, particularly over galloaluminosilicate zeolite, will be of practical interest and also useful to a better understanding of the reaction mechanism.

### 1.1.3. Complete Combustion of Methane over Perovskite-type Oxides

Natural gas (or methane) burns more cleanly than other fossil fuels like coal and petroleum, and produce smaller quantities of $CO_2$ and other pollutant gases. But one particular concern related to the use of natural gas (or methane) as a fuel is its emission as the unburned fuel. Methane being a green house gas, having green house effect 20 times larger than $CO_2$, can pose a serious environmental problem. So, considerable interests have been generated among the scientific and industrial community to develop catalytic material to combust methane at typical methane emission condition at a low temperature.

Perovskite-type oxides (i.e. $ABO_3$ type oxides) containing transition metals are good catalysts for the total oxidation of hydrocarbons and carbon monoxide and hence useful for the CO and hydrocarbon emission control by their complete combustion [77,78,79,80]. Perovskite-type oxides are also useful for a number of other catalytic processes, such as partial oxidation of hydrocarbons and oxygenates, hydrogenation and hydrogenolysis of hydrocarbons, hydrogenation of carbon oxides and decomposition of $N_2O$ [81,82,83,84].

Several methods based on the precursor preparation from mixed oxides, freeze-drying, spray drying, co-precipitation and sol-gel, followed by thermal decomposition of the precursor and/or thermal reaction between metal oxides are known for the preparation of perovskite-type oxides. However, because of the involvement of high reaction temperature in the formation of perovskite-type oxides,

the surface area of the resulting perovskite-type oxides is rather low. For example, the surface areas of the perovskite-type oxides obtained from mixed oxide technique is below 2 $m^2g^{-1}$ and the surface area of perovskite-type oxides obtained from coprecipitation technique are in the range of 1 to 10 $m^2g^{-1}$. Perovskite-type oxides having surface area upto 20 and 30 $m^2g^{-1}$ could be prepared by the spray drying and freeze-drying processes, respectively, of mutually soluble compounds and thereby achieving good chemical homogeneity for perovskite precursors, which are then fired at lower temperatures, to get high surface area perovskite-type oxides. However, the use of these processes is limited because of the requirements of mutually soluble compounds and specialized equipment and thereby the cost of perovskite-type oxide prepared by these processes is high [85,86]. Because of a very slow diffusion of metal cations and $O^{2-}$ anions in solid state, the formation of perovskite-type oxide from non-homogeneously mixed metal oxides requires high temperatures and long reaction period and hence the resulting perovskite-type oxide has a low surface area due to sintering or crystal growth. The temperature for the formation of perovskite-type oxide can however be reduced and thereby the surface area of the perovskite-type oxide can be increased if a homogeneously mixed metal oxides or compounds, which on decomposition or calcination are converted into metal oxides, are used as precursors for the preparation of perovskite-type oxides. But, in practice, it is very difficult to prepare such homogeneously mixed metal oxides, hydroxides or other compounds, which on decomposition or calcination are converted into metal oxides with homogeneous distribution of metal cations.

For perovskite-type oxides to be more active as catalysts, their surface area should be increased. The perovskite-type oxides deactivated due to sintering or crystal growth in the high temperature catalytic processes or other high temperature processes also need to be regenerated by increasing their surface area by some means. Hence there is a great need for developing some processes for increasing the surface area of the perovskite-type oxides prepared by conventional processes and thereby increasing the catalytic activity of the perovskite-type oxides. There is also a need for regenerating the perovskite-type oxides, deactivated due to sintering or crystal growth during catalytic processes, by increasing their surface area and thereby regaining the lost catalytic activity of the perovskite-type oxides. There is currently no such available literature, which deals with such problem. So developing a process for

activating the low surface area perovskite type oxides by increasing their surface area by some means is of great practical importance.

### 1.1.4. Complete Combustion of Propane

The growing problems of air-pollution particularly from the automotive sources in the urban areas have triggered a hectic research for the alleviation of the problem of air pollution. Because of its cleaner combustion, liquefied petroleum gas (LPG), which is a mixture of propane and butanes, is currently being used as a petrol substitute for automobiles in several metropolitan cities throughout the world including India. The reactivity of propane is less than that of butanes, and hence the concentration of propane in the unburned hydrocarbons in the auto-exhaust gases is much higher. For controlling the hydrocarbon emission from the LPG-fuelled automobiles, an efficient catalyst for the complete combustion of propane at low concentration (<1%) is essential.

A number of studies have been reported earlier on the catalytic combustion of propane at high concentrations over different noble metals and transition metal oxide catalysts, such as Pt or Pd/glass fiber [87], $Pt/TiO_2$ [88], $Pd/SiO_2$-$Al_2O_3$ [89], $Pt/Al_2O_3$ [90], Cu, Pd or Pt modified ZSM-5 [91,92], single or mixed transition metal oxides [93,94,95,96] and transition metal oxides supported on silica fiber [97].

Kiwi-Misker et al. found that Pt catalysts were more active than the Pd for the same metal loading on identical support [87]. Highest activity was observed on Pt-supported on glass fiber modified by titania. Yazawa et al. studied propane combustion on $Pd/SiO_2$-$Al_2O_3$ catalyst and correlated the catalytic activity with the oxidation state of palladium and found that the partially oxidized palladium, which has optimum ratio of metallic palladium to palladium oxide, shows the highest propane combustion activity [89]. Prasad et al [93] studied catalytic combustion of propane using oxides of Cr, Mg, Mn, Co and Fe, individually or in binary mixtures, in an adiabatic tubular reactor. The most suitable catalyst was found to be $Co_3O_4$ – $Cr_2O_3$. Busca et al. studied combustion of methane, CO, propane and phenanthrene over a number of transition metal mixed oxides (having spinel-type, corundum-type and perovskite-type structures). They also performed FT-IR experiments to find out the mechanism of combustion of $C_3$-organic compounds on spinel-type oxides viz.

$MgCr_2O_4$ and $Co_3O_4$ [94]. They concluded that nucleophilic oxygen species (lattice oxygen) was probably involved in both partial and total oxidation. Baldi et al. studied the catalytic combustion of $C_3$ hydrocarbons and oxygenates over $Mn_3O_4$ [95] and combustion of propane and propene over manganese and iron oxides [96]. The total combustion of propane over $Mn_2O_3$ was found to occur at 673 K, however pollutant products viz. propene from propane persists even at very high conversions [95]. A tentative reaction pathway was also proposed based on the reaction products. In another study they found that $\alpha$-$Mn_2O_3$ was more active than $\alpha$-$Fe_2O_3$ [96]. A substantial amount of propene formation was observed during propane combustion. Neyestanaki et al. tested the catalytic activity of different knitted $SiO_2$-fiber supported metal oxides (oxides of Co, Ni, Mn, Cr) and various combinations of them, Pt-activated Co and Ni oxides as well as noble metal (Pt, Pd) catalysts for combustion of propane and natural gas in a continuous flow tube reactor at 423-823K and GHSV of 23900 and 47800 $h^{-1}$ [98]. $Co_3O_4$ was found to be the most active single metal oxide catalyst in propane combustion. The low temperature activity of the catalyst was found to be improved by the use of Pt as an activator. Very recently, Teraoka et al. [99] have synthesized a high surface area $LaMnO_{3+\delta}$ which showed high propane combustion activity. In another recent study, Taylor and O'Leary [100] reported oxidative destruction of $C_1$-$C_4$ hydrocarbons over uranium oxide based catalysts. They observed that the oxidation activity of $U_3O_8$ is increased by its modification by Cr, which causes an increase in the defect structure of the oxide. However, the studies on the complete combustion of dilute propane are scarce.

Though a number of metal oxides either independently or in a mixture have been used for lower hydrocarbon combustion, particularly propane, the noble metal based catalysts still are the preferred one. Noble metal-based catalysts have in general high hydrocarbon combustion activity but they are quite costly and more prone to deactivation by poisoning [101]. Whereas, transition metal oxide based catalysts are generally less active but more resistant towards catalyst poisoning and also their cost is much lower. In the earlier communications, high activity of Mn-doped $ZrO_2$ in its cubic form for the combustion of butane [102] and dilute methane (1% in air) [103], comparable to that of noble metal catalysts were reported. It would be interesting to study the combustion of dilute propane over the various transition metal doped zirconia (e.g. Mn, Co, Cr, Fe or Ni-doped zirconia) catalysts.

### 1.1.5. Complete Combustion of Methane over Supported Pd-catalysts

Among the variety of catalytic material used till date for catalytic combustion of lower alkanes like methane, the noble metal based catalysts have drawn maximum attention. This is because of their higher catalytic activity per unit site and greater resistance to sulfur poisoning (below 773K). Pd and Pt are more volatile than the other noble metals, hence found ideal only for the low temperature combustion of hydrocarbons.

The Pd-based supported catalysts are particularly promising for the complete combustion of lower hydrocarbons, including methane.

Despite a plethora of literature dealing with the various aspects of the low temperature (< 800$^{o}$C) methane combustion over Pd-based catalysts, the controversy remains among the scientific community over the exact mechanistic aspects of methane combustion over Pd-catalysts. The extensive literature data can be briefed by noting the various aspects of Pd catalysts, which affects its methane combustion activity. These are following:

- Structure or nature of the active Pd species
- Time-on-stream effect on catalytic activity, and
- Effect of pre-treatment procedure on catalytic activity.

A recent review [104] has addressed the subject of methane combustion on supported palladium catalyst under lean conditions in some detail. In the following part, the most important aspects of low temperature methane combustion on supported Pd-catalysts will therefore be overviewed with a more emphasis on the very recent literatures. One of the key issues in literature has been whether methane oxidation on Pd is structure sensitive or structure insensitive. While many of the research groups have reported that the methane oxidation reaction is structure sensitive [105-109] there have been some contradictory suggestions [110]. Various research groups have investigated the effect of particle size on the methane oxidation turnover frequency (TOF). Hicks et al. observed a TOF of 0.02 and 1.3 $s^{-1}$ for small and large Pd particles respectively. However there was no significant difference in the activation energy values ($E_a$) for the two [111]. Most of the literature, which reported the increased TOF with increasing the Pd particle size, used Pd supported catalysts,

preconditioned in He or $H_2$. On the contrary, those catalysts used after pre-oxidation showed a wide variation of TOF with particle size, without any clear correlation [110,112,113]. The apparent anomaly was critically reviewed by Fujimoto et al. [114], who tried to identify the probable causes for the wide discrepancy between the literature data. The change in the oxidation state and morphology of Pd particle under operating condition, the product inhibition and the presence of an "induction period" in some catalysts may be the reasons for this apparent anomaly. After taking into account all these factors (accurate determination of surface Pd sites, product inhibition and induction/activation periods), the authors observed an increase in TOF with increase in the Pd particle size (at least for particles < 15 nm).

Several studies are available in literature, which deal with determining the nature of the active site and mechanistic details on the lower alkane oxidation reactions on Pd-based catalysts [115 - 126]. However, views for the nature of active surface Pd-species involved in the combustion are contradictory. Hicks et al. conducted a series of methane oxidation tests on Pd/alumina catalysts at 573 K, 50 Torr methane, 110 Torr oxygen and 900 Torr He [111]. Based on the experimental results the authors claimed that PdO dispersed on Pd crystallites was more active for methane oxidation than PdO dispersed over alumina. In general now it is acknowledged that Pd undergoes oxidation in course of the combustion reaction and the oxidation state of Pd plays an important role in determining the activity of the catalyst [101,105,111,115, 116, 117].

The initial "induction period" (i.e. the initial time period when the catalysts showed no activity after being exposed to the reaction mixture) of Pd-based catalyst was initially linked to the decomposition of inactive Pd-oxychloride species, which may be present in those catalysts for which metal chloride was used as precursor [111,127] for catalyst preparation. But even for some halogen free Pd-catalyst, an "activation period" (i.e. an initial time period needed to reach a higher steady state activity) has been observed [112,128]. The morphological change of Pd-particles under the reaction condition is attributed for this [126,129].

The kinetics of the methane combustion on Pd catalyst has also been widely investigated. Initially the Eley-Rideal mechanism was put forward, where the gaseous methane would be interacting with an adsorbed atomic oxygen [130]. It is now believed that the combustion reaction involves Mars van Krevelen mechanism, in

which the gaseous oxygen is initially adsorbed strongly on the metallic particle forming a surface PdO. It is followed by methane adsorption on the oxidic surface and ultimately oxidized and simultaneously the palladium is reduced back to the metallic state. The surface is thus alternating between an oxidized and a reduced state [126]. This mechanism was confirmed by recent $^{18}O$ isotope labeling experiments by Mueller et al. [118]. Pulse methane oxidation experiments on the $^{18}O$ labeled catalysts showed presence of $^{18}O$ in products ($CO_2$ and $H_2O$). They calculated that an estimated 20% of the product $CO_2$ was obtained by this redox mechanism. Fujimoto et al. has proposed a somewhat different mechanism. According to them, methane is first adsorbed on a coordinatively unsaturated Pd-site on the surface of the PdO crystallites. It is followed by the abstraction of H-atoms via the interaction with an adjacent PdO species to form a Pd-OH species. This hydrogen abstraction according to them was the rate-limiting one. Ultimately the combinative desorption of two OH species leads to the recovery of catalytic sites i.e. an unsaturated Pd and a PdO species.

It is now generally accepted that metallic Pd is less active than the PdO species. Oh et al. [131] have suggested that methane oxidation is inhibited by the adsorbed oxygen, because the O-atoms migrate into the bulk of Pd, forming an unreactive PdO. The active form of the catalyst according to them is a thin layer of PdO on metallic Pd, and the bulk PdO was claimed to be inactive. Bell and co-workers in a recent paper has studied the effect of metallic Pd-additive on the methane combustion in case of $Pd/ZrO_2$ catalyst [132]. They found that the activity of PdO for methane combustion could be enhanced by partially reducing the surface of the oxide to produce a small amount of metallic Pd. According to them metallic Pd has a better ability to dissociate methane, forming H and $CH_x$ (x=3-1) species, which are then diffused to Pd/PdO interface where they rapidly reduce PdO. The co-existence of metallic Pd and oxidized Pd on the surface of a crystallite at a low temperature has been opposed by Fujimoto et al. [114]. Bell and co-workers [132] also observed that the activity of the freshly reduced $Pd/ZrO_2$ catalyst for methane combustion initially increases with increasing the extent of oxidation. But after the formation of 6-7 monolayer (ML) of PdO, no further increase of catalytic activity was detected with increasing the extent of oxidation of metallic Pd. Burch and Urbano [116] also observed that the maximum activity of a Pd catalyst is shown by one in which the

surface Pd is oxidized to the equivalent of about 3-4 mono-layer of $O_2$, and hence concluded that combustion of methane is more favorable on a partially oxidized form of Pd.

X-ray photoelectron spectroscopy (XPS) and ellipsometric studies have been effectively employed to acquire insights into the Pd-based systems [107,122,133]. XPS study by Haack and Otto [107] revealed that smaller Pd particles had a greater tendency of carbon deposition from incomplete methane oxidation as compared to catalysts with larger Pd particles. The lower activity in case of smaller Pd particles was related to the partial poisoning of active sites by carbon. In a recent ellipsometric study, Graham et al. [122] studied both CO as well as methane oxidation on Pd film catalyst. Under oxygen rich conditions, dense PdO layers were observed for both the reactions, whereas, under fuel-rich conditions, a stable metal surface and porous PdO layer were seen in case of CO oxidation and methane oxidation, respectively.

From the literature survey of the available literatures, it is clear that despite several studies, addressing the nature of active site in supported Pd catalysts in case of lower hydrocarbon combustion, the controversy remains. So there is still enough scope to identify the active catalytic site in supported Pd catalysts, particularly by pulse studies. Pulse studies involving small pulse of methane can provide an insight into the initial activity of the Pd catalysts, which is not possible in the continuous flow reactors. Pulse studies for methane combustion over the supported Pd-catalysts are also scarce, so it would be interesting to carry out such studies.

### 1.1.6. High Temperature Complete Combustion of Methane

The catalytic hydrocarbon combustion for gas turbine and heating application, originally proposed by Pfefferle [134,135] has been a subject of active research in the past three decades. But the progress of this work was severely crippled due to the non-availability of the suitable catalytic materials. The main problems associated with the use of any catalyst at high operating temperatures ($\geq 900^{o}C$) (e.g. in gas turbines) are as follows:

1. Structural collapse and/or sintering with a drastic reduction in the surface area
2. Evaporation of catalytically active components, and

3. Solid-solid reactions of the active components of the catalysts among themselves or with reactive components of the catalyst support, ultimately deactivating the catalyst.

In short an ideal high temperature catalyst should be able to withstand at least one year of operation in a harsh environment, gas velocities around 25m.s$^{-1}$ and thermal shock of approximately 500$^{o}$C in a fraction of a second [136].

In the past decades or so, substantial research has been devoted for the development of catalysts for high temperature combustion. The development of stable support material as well as the active materials for combustion catalysts has been critically reviewed in recent literatures [136,137].

For a combustor of commercial importance, the fuel-gas mixture is fed at a very high space velocity (>$10^5$ h$^{-1}$), which risks the development of a large pressure drop across the catalytic substance. The monolithic honeycomb has been found to be the most technically advanced substrate which provides minimum pressure drop [138, 139]. Apart from having a low pressure drop, an ideal monolith should have the following properties:

- high hydrothermal stability
- high thermal shock resistance (upto 1000$^{o}$C/sec.)
- chemical inertness towards the active components of the catalyst
- very low thermal expansion
- high area to volume ratio (to avoid pressure drop), and
- stable performance for at least one year (ca. 8000h)

The usual catalyst poison like sulfur, arsenic or lead on catalyst surface have high vapor pressure and hence cannot be retained on catalyst surface during high temperature operation. Hence resistance to the "poisoning" is of trivial importance.

A variety of material has been developed for monoliths. They are α- and γ-alumina, aluminum titanate, silica, zirconia, silicon carbide, silicon nitride ($Si_3N_4$), mullite (3 $Al_2O_3$.2$SiO_2$), NZP ($Na_2O$-$ZrO_2$-$P_2O_5$-$SiO_2$), magnesia, spinel (MgO-$Al_2O_3$), cordierite (2 MgO. 2$Al_2O_3$.5$SiO_2$), FeCr alloy (15% Cr, 5% Al, trace Y, balance Fe) etc. Except the last one all the others are ceramic material. Compared to the ceramic materials, metallic monoliths e.g. FeCr alloy has several advantages, the most important being its smaller thin wall thickness, which reduces the pressure drop and also ensures higher wall conductivity and lower heat capacity. The metallic

monoliths are also very much stable against mechanical stress and strains. But compared to the ceramic materials, their maximum operating temperature is lower. Besides the coating of active material on them is also tedious and troublesome. These factors have been addressed in recent literature to develop highly active metal monolith [140]. Among the ceramic materials, cordierite has the highest thermal shock resistance, but its low melting point (ca. 1400$^{o}$C) prohibits its use for high temperature catalysis. That way aluminum titanate with the high operating temperature and low thermal coefficient seems promising. Mullite or zirconia is more suitable for high temperature operation, but the achievement of porosity, necessary for better adhesion of wash coat is rather difficult [141].

If the development of support is one aspect of developing a better high temperature catalyst, the other important aspect is the development of active materials which is generally used as a wash coat on the monolith type support. The ideal active material should possess at least the following qualities:

- low light-off (ignition) temperature, and
- sufficiently high catalytic activity to maintain complete combustion at the lowest levels of air preheat and the highest values of mass throughput [139].

Among the various active materials which has been reported in the literature, the following few class of materials seems promising:

- hexaaluminates
- perovskites
- spinels
- pyrochlores
- zeolites
- noble metals, and
- single metal oxides.

*Noble metals:* Noble metals possess the highest catalytic activity but its industrial use in the high temperature catalytic process is severely limited due to their high volatility, ease of oxidation and limited supply [142]. Among the noble metals only Pd and Pt appears to have promise as a combustion catalyst. The remarkable activity of these metals to activate $H_2$, $O_2$, C-H and O-H bond makes them an ideal choice. A lot of work has been done on the high temperature methane combustion over Pt and

Pd based catalysts at elevated temperatures. To improve their catalytic activity at high temperatures, some additives such as MgO have been successfully added [143].

*Metal oxides:* As an effective alternative to the precious noble metal catalysts, the non-noble metal oxides have aroused considerable interests among the researchers. The well-established correlation between the catalytic activity and physicochemical properties of the metal oxides [144] has the potential to substitute noble metal catalysts for practical application. Co, Mn, Cu, Ni and Cr oxides have been received substantial attention. But the chances of solid-solid reaction between active catalytic phase and supporting oxide and the vaporization of the active phase above 1000$^{o}$C still remains a major concern [136]. It has been observed that binary and ternary oxides often show higher stability and catalytic activity than the single metal oxides.

*Perovskites, Spinels and Pyrochlores:* Perovskites or $ABO_3$ type oxides has the advantage of high activity and thermal stability, though the stability is poor as compared to the hexa-aluminate based catalysts. Still they have been found promising catalytic material [145, 146]. But very low surface area at higher temperatures, coupled with heavy sintering has been a major obstacle towards its successful utilization as an effective high temperature catalyst.

Spinels, represented by a general formula $AB_2O_4$, has a good heat resistance and a suitable modification in its method of preparation can lead to a high surface area even at higher temperatures (>1000$^{o}$C) [147]. But their lower activity, often orders of magnitude less than the component oxide(s) makes them unsuitable as active catalyst phase [141].

Pyrochlores with a general formula of $A_2B_2O_7$ has a flexible structure in the sense that nature of A and B metal ions and the oxidation state of transition metal ion B cold be varied suitably to modify its catalytic property. But its low surface area at higher temperatures is not suitable for high temperature combustion [147,136].

*Hexaaluminates:* Since its invention, hexaaluminates has received tremendous attention of the scientific community. Hexaaluminate having a general formula $AB_xAl_{12-x}O_{19}$ (where A = alkali, alkaline earth or rare earth metal and B = metal having similar size and charge to that of Al) was developed by the Japanese group of

Arai and co-workers [148]. Despite having a poor thermal shock resistance due to high thermal expansion, hexaaluminate has enjoyed wide attention due to its high catalytic activity and low sintering. The unique crystal structure consisting of blocks of spinel structure divided by a mirror plane in which A atom are situated, suppress crystal growth along the c-axis compared to that along the direction normal to c-axis, which in turn increases its surface energy. But owing to the law of thermodynamics, the crystal tries to minimize the surface energy by keeping the crystal growth at a minimum, even at high temperature [149,150,151]. The state of hexaaluminates as combustion catalysts has been reviewed recently [152]. Manganese substituted hexaaluminate was found to possess high surface area and high catalytic activity at higher temperatures (ca. 1000$^{o}$C). But activity per unit area remained much lower than the noble metal catalysts [153]. Also during the long term testing (over 8000h) at 1300$^{o}$C, the surface area dropped significantly from 18$m^2g^{-1}$ to 5$m^2g^{-1}$ [154].

It is clear from the above discussion that high thermal/hydrothermal stability and high catalytic activity do not go hand in hand. One has to compromise with one characteristic to get a better combustion catalyst. Till date most active catalysts have been found to be a combination of metal oxides rather than the single one. Particularly the cobalt and manganese oxide based catalysts, which being the most active oxide by virtue of the twin-peak pattern of catalytic activity across the transition metal oxides [155,156,157] seems promising.

### 1.1.7. Objectives and Scope of Present Work

The present Ph. D. work was undertaken with the following objectives:

1. To produce continuously CO-free $H_2$ by catalytic decomposition of methane and gasification of carbon by steam at low temperature in two parallel catalytic reactors operated in cyclic manner, using different Ni-based catalysts.
2. To study thoroughly the factors affecting the catalytic methane decomposition and gasification by steam of carbon formed on the catalyst in the step-wise steam reforming of methane operated in cyclic manner, using a $Ni/ZrO_2$ catalyst.

3. To study aromatization of dilute ethylene (< 5 mol%) over H-ZSM-5 and Ga-modified ZSM-5 type zeolite (viz. H-gallosilicate, H-galloaluminosilicate and Ga-impregnated H-ZSM-5) and to correlate the catalytic activity with the acidity and non-framework Ga-content of the zeolites.

4. To study the effect of different process parameters viz. temperature and space velocity on the aromatization of dilute ethylene over highly acidic H-GaAlMFI zeolite.

5. To study the aromatization of other lower olefins (viz. propylene and n-butene) over the highly acidic H-GaAlMFI zeolite.

6. To study the activation of low surface area perovskite oxides by their hydrothermal treatment and study the catalytic combustion of methane over them.

7. To study the catalytic combustion of propane over Mn-doped $ZrO_2$ (cubic) catalyst and to study in detail the effect of different catalyst parameters viz. Mn/Zr ratio, calcination temperature etc. on the propane combustion activity of the catalyst.

8. To study the complete combustion of propane over different transition metal (viz. Co, Mn, Fe, Cr and Ni) doped $ZrO_2$ (cubic) and to determine the various kinetic parameters (viz. activation energy and frequency factor) for the catalytic combustion process over these catalysts and also to study the involvement of lattice oxygen of the catalyst in the process.

9. To study the complete combustion of methane in presence or absence of oxygen over the Pd (or PdO)/$Al_2O_3$ catalyst oxidized (or reduced) to different extents in a pulse micro-reactor.

10. To study the high temperature (> 900$^oC$) catalytic combustion of methane over thermally stable CoO-MgO catalyst and also to study the effect of different catalyst parameters viz. Co/Mg ratio, calcination temperature etc. on the methane combustion activity.

### 1.1.8. References


1. K. V. Kordesch and J. C. T. Oliveira, "*Fuel Cells"*, Ullman's Encyclopedia of Industrial Chemistry, 5th Ed., VCH, Weinheim, Germany, vol. A12, pp 55-83
2. K. Kordesch and G. Simander, "Fuel Cells and their Application", VCH, Weinheim, Germany, 1996.
3. H. F. Rase, *in* "Handbook of Commercial Catalysts – Heterogeneous Catalysts", CRC Press, USA (2000).
4. R. T. K. Baker, M. A. Barber, P. S. Harris, F. S. Feates and R. J. Waite, J. Catal., 26 (1972) 51.
5. N. Z. Muradov, Int. J. Hydrogen Energy, 18 (1993) 211.
6. T. Ishihara, T. Fujita, Y. Miyashita, Y. Takita, Shokubhai, 35 (1993) 324.
7. T. Ishihara, Y. Miyashita, H. Iseda and Y. Takita, Chem. Lett., (1995) 93.
8. T. Zhang and M. D. Amiridis, Appl. Catal. A, 167 (1998) 161.
9. L. B. Avdeeva, D. I. Kochubey and Sh. K. Shaikhutdinov, Appl. Catal. A, 177 (1999) 43.
10. T. V. Choudhary and D. W. Goodman, Catal. Lett., 59 (1999) 93.
11. R. Aiello, J. E. Fiscus, H-C. Z. Loye and M. D. Amiridis, Appl. Catal. A, 192 (2000) 227.
12. T. V. Choudhary, C. Sivadinarayana and D. W. Goodman, (2001) Unpublished work.
13. T. V. Choudhary and D. W. Goodman, J. Catal., 192 (2000) 316.
14. T. V. Choudhary, C. Sivadinarayana, C. Chusuei, A. Klinghoffer and D. W. Goodman, J. Catal., 199 (2001) 9.
15. T. V. Choudhary, C. Sivadinarayana, A. Klinghoffer and D. W. Goodman, Stud. Surf. Sci. Catal., (2001) (in press).
16. Sh. K. Shaikhutdinov, L. B. Avdeeva, B. N. Novgorodov, I. Zaikovskii and D. I. Kochubey, Catal. Lett., 47 (1997) 35.
17. J. H. Lunsford, Angew. Chem. Int. Ed. Engl., 34 (1995) 970.
18. L. Guczi, R. A. Van Santen, K. V. Sarma, Catal. Rev.-Sci. Eng., 38 (1996) 249.
19. E. M. Cordi, S. Pak, M. P. Rosynek and J. H. Lunsford, Appl. Catal. A,, 155 (1997) L1.
20. Y. Jiang, I. V. Yentekakis and C. G. Vayenas, Science, 264 (1994) 1563.

21. R. B. Hall and G. R. Myers, Prepr. - Am. Chem. Soc. Div. Petrol. Chem., 39(2) (1994) 214.
22 I. V. Yentekakis, M. Makri, Y. Jiang and C. G. Vayenas, Prepr. - Am. Chem. Soc. Div. Petrol. Chem., 41(1) (1996) 119.
23. A. Mashocki, Appl. Catal. A, 146 (1996) 391.
24. P. Qiu, J. H. Lunsford and M. P. Rosynek, Catal. Lett., 52 (1998) 37.
25. V. R. Choudhary, S. D. Sansare, A. M. Rajput, US Patent 5,306,854 (April 26, 1994).
26. V. R. Choudhary, S. D. Sansare, S. T. Chaudhari, US Patent 5,336,825 (August 9, 1994).
27. D. B. Lukyanov, Stud. Surf. Sci. Catal., 122 (1999) 299.
28. D. B. Lukyanov, N. S. Gnep and M. R. Guisnet, Ind. Eng. Chem. Res., 33 (1994) 223.
29. R. Le Van Mao, L. A. Dufresne, J. Yao and Y. Yu, Appl. Catal. A, 164 (1997) 81.
30. K. Arishtirova, Kh. Dimitrov, K. Dyrek, K. H. Hallmeier, Z. Popovaand S. Witkowski, Appl. Catal. A, 81 (1992) 15.
31. E. G. Derouane, C. Lefevre and J. B. Nagy, J. Mol. Cat., 38 (1986) 387.
32. O. V. Bragin, L. M. Kustov, T. V. Vasina and E. G. Khelkovskaya-Sergeeva, Kinet. Katal. 29 (1988) 1393.
33. K. Nakagawa, C. Kajita, Y. Ide, M. Okamura, S. Kato, H. Kasuya, N-O. Ikenaga, T. Kobayashi and T. Suzuki, Catal. Lett., 64 (2000) 215.
34. F. Solymosi and A. Szoke, Stud. Surf. Sci. Catal., 119 (1998) 355.
35. L. Brabec, M. Jeschke, R. Klik, J. Novakova, L. Kubelkova and J. Meusinger, Appl. Catal. A, 170 (1998) 105.
36. C. Berg, S. Kaiser, T. Schindler, C. Kronseder, G. Niedner-Schatteburg and V. E. Bondybey, Chem. Phys. Lett., 231 (1994) 139.
37. Z. Popova, K. Arishtirova and Kh. Dimitrov, React. Kinet. Catal. Lett. 41 (1990) 369.
38. G. W. Norval, M. J. Phillips, K. S. Virk and R. V. Simons, Can. J. Chem. Eng., 67 (1989) 521.
39. M. J. Phillips and K. S. Virk, Can. CA 1234159A1 (15 March, 1988).

40. L. M. Kustov, D. A. Kondrat'ev, T. B. Krasieva, V. Y. Borovkov, V. B. Kazanskii and Kh. M. Minachev, Kinet. Katal., 30 (1989) 169.
41. X. Wu, S. Wu and Z. Meng, Cuihua Xuebao, 12 (1991) 388.
42. O. N. Karatun and A. L. Proskurin, Neftekhimiya, 38 (1998) 294.
43. B. L. Vorob'ev, Y. N. Koshelev, A. A. Kharchenko, L. G. Kim and S. M. Zverev, Neftepereab. Neftekhim., 9 (1989) 16.
44. J. Luo, C. Tan and Q. Dong, Shiyou Huagong, 19(9) (1990) 587.
45. O. V. Bragin, T. V. Vasina, V. P. Sitnik, N. V. Nekrasov and V. I. Yakerson, Izv. Akad. Nauk. SSSR, Ser. Khim., 6 (1990) 1250.
46. M. Huang and S. Kaliaguine, J. Mol. Catal., 81 (1993) 37.
47. M. Huang and S. Kaliaguine, Stud. Surf. Sci. Catal., 73 (1992) 291.
48. T. Inui, J-B, Kim, T. Takeguchi and H. Nagata, Appl. Catal. A, 106 (1993) 83.
49. B. S. Kwak and W. M. H. Sachtler, J. Catal., 145 (1994) 456.
50. S. Jiang, S. Wu and Z. Meng, Appl. Catal. A, 103 (1993) 259.
51. D. Bhattacharya and S. Sivasanker, Catal. (Pap. Natl. Symp.) 12th, Meeting Date 1994, 191 (Eds. N. M. Gupta and D.K. Chakrabarty, Narosa, New Delhi, India (1996).
52. K. P. De Jong, H-H. Mooiweer, J. G. Buglass and P. K. Maarsen, Stud. Surf. Sci. Catal. 111 (1997) 127.
53. E. Angelescu, V. Parvulescu, G. Musca, F. Constantinescu, V. Dima, G. Gheorghe and G. Possa, Prog. Catal., 1 (1993) 32.
54. E. Angelescu, E. Stanescu, A. Cruceanu, G. Pop and F. Constantinescu, Prog. Catal., 4 (1995) 25.
55. Y. Ono, H. Kitagawa and Y. Sendoda, J. Chem. Soc. Faraday. Trans. 1, 83 (1987) 2913.
56. T. K. Bhatia and M. J. Phillips, J. Catal. 110 (1988) 150.
57. D. Seddon, Catal. Today, 6 (1990) 351.
58. M. Guisnet, N-S, Gnep and F. Alario, Appl. Catal., 54 (1992) 1.
59. Y. Ono, Catal. Rev.-Sci. Eng., 34 (1992) 179.
60. G. Giannetto, R. Monque and R. Galiasso, Catal. Rev.-Sci. Eng., 36 (1994) 271.
61. N. Y. Chen and T. Y. Yan, Ind. Eng. Chem. Process. Des. Dev., 25 (1986)151.
62. Chem. Brit., 20 (1984) 684.

63. R. T. Anderson, J. A. Johnson and J. R. Mowry, Presented at AIChE Spring National Meeting, Houston, TX, March, 1985).
64. G. N. Roosen, A. Orievx, J. Andrews, Dewitt's Houston Conf. March 1989.
65. L. Mank, A. Minkkinen and R. Shaddick, Hydrocarb. Technol. Int. p 69 (1992)
66. Z-Forming Process, Mitshubishi Oil Co. Ltd. And Chiyoda Corp. May 1994.
67. P. Meriaudeau, G. Sapaly and C. Naccache, Stud. Surf. Sci. Catal., 49 (1989) 1423.
68. Y. Ono, H. Nakatani, H. Kitagawa and E. Suzuki, Stud. Surf. Sci. Catal., 44 (1989) 279.
69. J. R. Mowry, D. C. Martindale and A. H. P. Hall, Arabian J. Sci. Eng., 10 (1985) 367.
70. J. R. Mowry, R. F. Anderson and J. A. Johnson, Oil Gas J., Dec. 2, 1985, pp. 128.
71. T. Inui, A. Miyamoto, H. Matsuda, H. Nagata, Y. Makino, K. Fukuda and F. Okazumi, Proc. Of the 7th Int. Zeolite Conf. (Eds. Y. Murakami, A. Iijima and J. W. Ward), Kodansha, Tokyo, 1986, pp. 859.
72. T. Inui, Y. Makino, F. Okazumi, S. Nagano and A. Miyamoto, Ind. Eng. Chem. Res., 26 (1987) 647.
73. M. Shibata, H. Kitagawa, Y. Sendoda and Y. Ono, Proc. of the 7th Int. Zeolite Conf. (Eds. Y. Murakami, A. Iijima and J. W. Ward), Kodansha, Tokyo, 1986, pp. 717.
74. N. S. Gnep, J. Y. Doyemet and M. Guisnet, J. Mol. Catal., 45 (1988) 281.
75. N. S. Gnep, J. Y. Doyemet, A. M. Seco, F. R. Ribeiro and M. Guisnet, Appl. Catal., 43 (1988) 155.
76. H. Kitagawa, Y. Sendoda and Y. Ono, J. Catal., 101 (1986) 12.
77. J. G. McCarty and H. Wise, Catal. Today, 8 (1990) 231.
78. N. Yamazoe and Y. Teraoka, Catal. Today, 8 (1990) 175.
79. T. Seiyama, Catal. Rev.-Sci. Eng., 34 (1992) 281.
80. B. Viswanathan, Catal. Rev.-Sci. Eng., 34 (1992) 337.
81. T. Shimizu, Catal. Rev.-Sci. Eng., 34 (1992) 355.
82. K. Ichimura, Y. Inoue and I. Yasumari, Catal. Rev.-Sci. Eng., 34 (1992) 301.
83. J. L. G. Fierro, Catal. Rev.-Sci. Eng., 34 (1992) 321.
84. C. S. Swamy and J. Christopher, Catal. Rev.-Sci. Eng., 34 (1992) 409.

85. R. J. H. Voorhoeve, D. W. Johnson Jr., J. P. Remeika and P.K. Gallagher, Science, 195 (1977) 827.
86. E. J. Baran, Catal. Today, 8 (1990)133.
87. L. Kiwi-Minsker, I. Yuranov, E. Slavinskaia, V. Zaikovskii and A. Renken, Catal Today, 59 (2000) 61.
88. K. Ruth, M. Hayes, R. Burch, S. Tsubota and M. Haruta, Appl. Catal. B, 24 (2000) L133.
89. Y. Yazawa, H. Yoshida, S. Komai, A. Satsuma and T. Hattori, Appl. Catal. B, 19 (1998) 261.
90. A. Chiba, M. Komoda, T. Kosumi, T. Nanba, N. Azuma and A. Ueno, Chem. Lett., 8 (1999) 801.
91. A. Kalantar Neyestanaki, N. Kumar and L.-E. Lindfors, Appl. Catal. B, 7 (1995) 95.
92. A. Kalantar Neyestanaki, N. Kumar and L.-E. Lindfors, Fuel, 74 (1995) 690.
93. R. Prasad, L. A. Kennedy and E. Ruckenstein, Combust. Sci. Technol., 22 (1980) 271.
94. G. Busca, M. Daturi, E. Finocchio, V. Lorenzelli, G. Ramis and R. J. Willey, Catal. Today, 33 (1997) 239.
95. M. Baldi, E. Finocchio, F. Milella and G. Busca, Appl. Catal. B, 16 (1998) 43.
96. M. Baldi, V. S. Escribano, J. M. G. Amores, F. Milella and G. Busca, Appl. Catal. B,, 17 (1998) L175.
97. A. Kalantar Neyestanaki and L.-E. Lindfors, Combust. Sci. Technol., 110/111 (1995) 303.
98. A. Kalantar Neyestanaki and L.-E. Lindfors, Combust. Sci. Technol., 110/111 (1995) 303.
99. Y. Teraoka, S. Nanri, I. Moriguchi, S. Kagawa, K. Shimanoe and N. Yamazoe, Chem. Lett., 10 (2000) 1202.
100. S. H. Taylor and S. R. O'Leary, Appl. Catal. B, 25 (2000) 137.
101. Y. Yazawa, H. Yoshida, S. Komai, A. Satsuma and T. Hattori, Appl. Catal. B, 19 (1998) 261.
102. A. Keshavaraja and A. V. Ramaswamy, Appl. Catal. B, 8 (1996) L1.
103. V. R. Choudhary, B. S. Uphade, S. G. Pataskar and A. Keshavaraja, Angew. Chem. Int. Ed. Engl., 35 (1996) 2393.

104. Y-H. Chin and D. E. Resaco, in "Catalysis - Specialist Periodical Report", Volume 14, Royal Society of Chemistry, UK, 1999.
105. R. F. Hicks, H. Qi , M. L. Young and R. G. Lee, J. Catal., 122 (1990) 280.
106. P. Briot and M. Primet, Appl. Catal., 68 (1991) 301.
107. P. L. Haack and K. Otto, Catal. Lett., 34 (1995) 31.
108. A. C. Mueller, M. Maciejewski, R. A. Koeppel and A. Baiker, Catal. Today, 47 (1999) 245.
109. H. Widjaja, K. Sekizawa, K. Eguchi and H. Arai, Catal. Today, 35 (1997) 197.
110. F. H. Ribeiro, M. Chow and R. A. Dalla Betta, J. Catal., 146 (1994) 537.
111. R. F. Hicks, H. Qi, M. L. Young and R. G. Lee, J. Catal., 122 (1990) 295.
112. T. R. Baldwin and R. Burch, Appl. Catal., 66 (1990) 337; ibid. 66 (1990) 359.
113. K. Muto, N. Katada and M. Niwa, Appl. Catal. A: Gen., 134 (1996) 203.
114. K. Fujimoto, F. H. Ribeiro, M. Avalos-Borja and E. Iglesia, J. Catal., 179 (1998) 431.
115. D. Rocha, M. G. Carneiro and R. Frety, Stud. Surf. Sci.. Catal., 110 (1997) 767.
116. R. Burch and F. J. Urbano, Appl. Catal. A, 124 (1995) 121.
117. M. Lyubovsky, R. Weber and L. Pfeferle, Symp(Int.) Combust., [Proc], 26th (Vol 1), 1779 (1996).
118. A. C. Mueller, M. Maciejewski, A. R. Koeppel, R. Tschan and A. Baiker, J. Phys. Chem., 100 (1996) 20006.
119. C. Descorme, P. W. Jacobs and G. A. Samorjai, J. Catal., 178 (1998) 668.
120. R. J. Farrauto, M. C. Hobson, T. Kennelly and E. M. Waterman, Appl. Catal. A, 81 (1992) 227.
121. S. C. Su, J. N. Carstens and A. T. Bell, J. Catal., 176 (1998) 125.
122. G. W. Graham, D. Konig, B. D. Poindexter, J. T. Remillard and W. H. Weber, Top. Catal., 8 (1999) 35.
123. A. K. Datye, J. Bravo, T. R. Nelson, P. Atanasova, M. Lyubovsky and L. Pfefferle, Appl. Catal., 198 (2000) 179.
124. J. A-Yeung, K. Chen, A. T. Bell and E. Iglesia, J. Catal., 188 (1999) 132.
125. Y. Yazawa, H. Yoshida, S-I Komai, A. Satsuma and T. Hattori, Appl.. Catal. B, 19 (1998) 261.
126. E. Garbowski, C. Feumi-Jantou, N. Mouaddib and M. Primet, Appl. Catal., A, 109 (1994) 277.

127. C. F. Cullis and B. M. Willatt, J. Catal., 86 (1984) 187.

128. C. F. Cullis and B. M. Willatt, J. Catal., 83 (1983) 267.

129. E. Garbowski and M. Primet, Appl. Catal., 125 (1995)185.

130. J. G. Firth and H. B. Holland, Trans. Faraday Soc., 65 (1969) 1121.

131. S. N. Oh, P. J. Mitchell and R. M. Siewert, J. Catal., 146 (1994) 537.

132. J. N. Carstens, S. C. Su and A. T. Bell, J. Catal., 176 (1998) 136.

133. D. Konig, W. H. Weber, B. D. Poindexter, J. R. McBride, G. W. Graham and K. Otto, Catal. Lett. 29 (1994) 329.

134. W. C. Pfefferle, Belgian Patent 814, 752; 1974.

135. W. C. Pfefferle, J. Energy, 2 (1978) 142.

136. E. M. Johansson, D. Papadias,P. O. Thevenin, A. G. Ersson, R. Gabrielsson, P. G. Menon, P. H. Bjorbom and S. G. Jaras, Catalysis - Specialist Periodic Report, vol. 14, Royal Society of Chemistry, Cambridge, 1999.

137. M. F. M. Zwinkels, S. G. Jaras and P. G. Menon in "Structured Catalysts and Reactors" (Eds. A. Cybulski and J. A. Moulijn), Marcel and Dekker, New York, 1998.

138. D. L. Trimm, Appl. Catal., 7 (1983) 249.

139. R. Prasad, L. A. Kennedy and E. Ruckenstein, Catal. Rev. - Sci. Eng., 26 (1984) 1.

140. M. F. M. Zwinkels, S. G. Jaras and P. G. Menon in Preparation of Catalysts VI, (Eds. G. Poncelet, P. A. Jacobs, P. Grange and B. Delmon), Elsevier Science B. V., Amsterdam, 1994.

141. D. L. Trimm, Catal. Today, 26 (1995) 231.

142. J. P. Kesselring, W. V. Krill, H. L. Atkins, R. M. Kendall, R. M. Kelley and J. T. Kelley, EPA - 600/7-79-181, August 1979.

143. T. Hayata, T. Furuya, S. Yamanaka and J. Koizuka, Shokubai, 31 (1989) 116.

144. A. A. Baladine in Advances in Catalysis (Eds. D. D. Eley, H. Pines and P. B. Weisz), vol. 10, Academic Press, New York, 1958, pg. 95.

145. L. J. Tejuca, J. Less-common Metals, 146 (1989) 251.

146. L. J. Tejuca, J. Less-common Metals, 146 (1989) 261.

147. M. F.M. Zwinkels, S. Druesne, E. Bjornbom, P. G. Menon and S. G. Jaras, Ind. Eng. Chem. Res., 37 (1998) 391.

148. M. Machida, K. Eguchi and H. Arai, J. Catal. 120 (1989) 377.

149. K. Eguchi, H. Takahara, H. Inoue, K. Sekizawa and H. Arai, "Symp. Catalytic Combustion, San Fransisco". Am. Chem. Soc. Div. Petrol. Chem., 42, 1997.
150. M. Machida, A. Sato, T. Kijima, H. Inoue, K. Eguchi and H. Arai, Catal. Today, 26 (1995) 239.
151. H. Arai and M. Machida, Catal. Today, 10 (1991) 81.
152. G. Groppi, C. Cristiani and P. Forzatti in Catalysis - Specialist Periodical Reports, vol. 13, The Royal Society of Chemistry, Cambridge, UK, 1997, pg. 85.
153. R. L. Garten, R. A. Dalla Betta and J. C. Schlatter in Handbook of Heterogeneous catalysis, vol. 4 (Eds. G. Ertl, H. Knozinger and J. Weitkamp), VCH Weinheim, Germany, 1997, pg. 1668.
154. H. Arai, K. Eguchi, M. Machida and T. Shiomitsu in catalytic Science and Technology, vol. 1 (Eds. S. Yoshida, N. Takazawa, T. Ono), Kodansha, Tokyo, 1990, pg. 195.
155. D. L. Trimm, Design of Industrial catalysts, Elsevier, Amsterdam, 1980.
156. O. V. Krylov, Catalysis by Non-metals, Academic Press, New York, 1970.
157. M. F. M. Zwinkels, S. G. Jaras and P. G. Menon, Catal. Rev. Sci. Eng., 35 (1993) 319.

# CHAPTER 1.2

# EXPERIMENTAL

This chapter has been divided into three sections: Catalyst Preparation, Catalyst Characterization and Catalytic Reaction. In the first section the preparation of different catalyst used for different catalytic reactions will be discussed. In the second section, the techniques used to characterize the catalysts will be mentioned, and in the last section, the experimental set-up for various catalytic reactions carried out will be briefly discussed with diagrams.

## 1.2.1. Catalyst Preparation

In this section, the preparation procedure of different catalysts used for various catalytic reactions has been discussed.

### *1.2.1.1. Preparation of catalysts used for catalytic decomposition of $CH_4$ to produce $H_2$*

For catalytic decomposition of methane to produce CO-free hydrogen, different Ni-based catalysts were prepared, as follows:

$Ni/ZrO_2$ (Ni/Zr mole ratio = 1.0), $Ni/ThO_2$ (Ni/Th mole ratio = 1.0) and $Ni-Co/ZrO_2$ (Ni : Co : Zr mole ratio = 1 : 1 : 2) catalysts were prepared by coprecipitating the corresponding metal hydroxides from their aqueous solution containing respective metal nitrates using sodium hydroxide at a pH of 9.0 at room temperature. The precipitate was thoroughly washed, dried and then calcined at $600^oC$ for 2h under static air. Ni/MgO (Ni/Mg mole ratio = 1.0) catalyst was also prepared by the similar coprecipitation method except that the precipitating agent used was sodium carbonate.

$Ni/CeO_2$, $Ni/UO_3$, $Ni/MoO_3$ and $Ni/B_2O_3$ (Ni/M mole ratio = 1.0, where M = Ce, U, Mo and B) catalysts were prepared by thoroughly mixing nickel nitrate with ammonium cerium (IV) nitrate or uranyl acetate or ammonium molybdate or boric acid while grinding the mixed salts in the presence of water just enough to form a thick paste, which was then dried and calcined as above.

Ni/HZSM-5, Ni/Si-MCM-41, Ni/H-Mordenite, Ni/Hβ, Ni/NaY and Ni/Ce(72)NaY catalysts were prepared by impregnating nickel nitrate on HZSM-5 (Si/Al=40) or Si-MCM-41 or H-Mordenite (Z - 900 H, Norton Co., USA), or Hβ or

NaY or CeNaY (degree of $Ce^{+3}$ exchange = 72%), using the incipient wetness technique, followed by drying and calcining in air at 500°C for 4h. All the above catalysts were powdered, pressed and crushed to particles of 30-52 mesh size.

#### *1.2.1.2. Preparation of catalysts used for the aromatization of $C_2$-$C_4$ olefins*

For aromatization of $C_2$ - $C_4$ olefins, different Ga-modified ZSM-5 type zeolites, such as gallosilicate, galloaluminosilicate and gallium impregnated ZSM-5 zeolite, were prepared.

H-GaMFI (Si/Ga=30.1), H-GaAlMFI (Si/Ga=15.3 - 46.6 and Si/Al=17.7 - 49.6), ZSM-5 (Si/Al=35.0) zeolites have been synthesized by their hydrothermal crystallization from a gel consisting of Na-trisilicate (Fluka), gallium nitrate (Aldrich) and/or aluminum nitrate (BDH), TPA-Br (Aldrich), sulfuric acid and demineralized water in a stainless steel autoclave at 180°C for 96 hours. The zeolite crystals were washed thoroughly with deionized water and dried at 120°C for 10h and then calcined at 550°C under static air for 15h for removing occluded organic template from their channels. The calcined zeolites were exchanged with 1M ammonium nitrate solution at 80°C repeatedly (for four times) to convert them into their $NH_4$-form. After the exchange, the zeolite crystals were washed with deionized water and dried at 120°C for 10h. The $NH_4$-ZSM-5 zeolite was impregnated with aqueous gallium nitrate solution by incipient wetness technique and then dried as above. The $NH_4$-GaMFI ($NH_4$-form of gallosilicate with ZSM-5 type structure), $NH_4$-GaAlMFI ($NH_4$-form of galloaluminosilicate with ZSM-5 type structure), Ga/$NH_4$-ZSM-5 (Ga-impregnated $NH_4$-ZSM-5) zeolites were pressed binder-free and crushed to 52-72 mesh size particles and then calcined under static air at 600°C for 1h to convert the zeolites to their H-form. The H-GaMFI, H-GaAlMFI and Ga/H-ZSM-5 zeolites were pretreated in a flow of hydrogen (1030 $cm^3g^{-1}h^{-1}$) at 600°C for a period of 1h and then in a flow of air for 30 min. The detailed framework composition, bulk composition and other physicochemical properties are provided in the appropriate section in this dissertation.

### *1.2.1.3. Preparation of catalysts used for combustion of methane and propane*

For the complete combustion of dilute propane, different transition metal-doped zirconia (cubic) catalysts (M-$ZrO_2$; M = Mn. Co, Cr, Fe and Ni) were prepared. The Mn-doped $ZrO_2$ catalyst was prepared by mixing aqueous solutions of zirconyl nitrate and manganese acetate (Mn/Zr mole ratio varied from 0.05 to 0.67), coprecipitating metal hydroxides from the solution using tetramethyl ammonium hydroxide (25%) (TMAOH) under vigorous stirring at $30^o$ C and a pH of 8, washing (with deionized water) and drying (at $110^o$ C for 2h) the resulting precipitate and finally calcining it in air at $500^0$C for 8h. Other transition metal-doped $ZrO_2$ (cubic) catalysts (with transition metal/Zr mole ratio of 0.25) were prepared by a similar procedure described for the Mn-doped $ZrO_2$, using the respective transition metal nitrate instead of Mn-acetate in the coprecipitation. The Mn-doped $ZrO_2$ having Mn/Zr ratio 0.25 also was prepared by coprecipitating the mixed metal oxides from their aqueous solution using different precipitating agents e.g. tetramethyl ammonium hydroxide (25%) (TMAOH), aq. tetraethyl ammonium hydroxide (25%) (TEAOH), aq. tetrapropyl ammonium hydroxide (25%) (TPAOH), aq. tetrabutyl ammonium hydroxide (25%) (TBAOH) and aq. ammonium hydroxide (30%) The Mn-doped $ZrO_2$ having Mn/Zr ratio 0.11 was calcined at different temperature ($500^o$C - $800^o$C) for 8h. The Mn- impregnated $ZrO_2$ (Mn/Zr =0.25) was prepared by impregnating the $ZrO_2$ with Mn- acetate by incipient wetness method and calcining at $500^o$C for 8h. Co-impregnated $ZrO_2$ (Co/Zr = 0.25) was also prepared in a similar way using cobalt nitrate.

For low temperature complete combustion of methane, Pd (5%)/$Al_2O_3$ catalyst was used. This catalyst was obtained commercially from Lancaster, UK .

For low temperature complete combustion of methane, hydrothermally activated perovskite type oxides were used. The $LaCoO_3$ and $LaMnO_3$ perovskite were synthesized by conventional carbonate co-precipitation method as follows. La and Co (or Mn) carbonates were coprecipitated from their aqueous nitrate solution by drop-wise addition of an aqueous sodium carbonate solution under continuous stirring until the pH of the mixture was 8.2. The precipitate was aged in the mother liquor for 1h and then filtered and washed thoroughly with distilled water. The precipitate was then dried at $110^o$C for 16h and then calcined in static air at $500^o$C for 5h. The

calcined mass was washed with boiling water until the filtrate attained a pH of 6.8. The solid mass was then dried at 120°C for 3h, pelletized using a hydraulic pressure of 5 ton. The resulting pellets were then calcined at 925°C for 6h in static air and then crushed to 52-72 mesh size particles. The $LaCoO_3$ and $LaMnO_3$ catalysts were then subjected to various hydrothermal treatment, the details of which will be described in the appropriate section.

For high temperature complete combustion of dilute methane, CoO-MgO catalysts having different Co/Mg mole ratios and calcined at different temperatures were used. The CoO-MgO catalysts with two different Co/Mg mole ratios (Co/Mg = 0.5 and 1.0) were prepared by thoroughly mixing finely ground pure magnesium carbonate and cobalt nitrate, in desired proportions, with deionized water sufficient to form a thick paste, drying and decomposing in air at 600°C for 4h. Then the resulting mass was powdered, pressed binder-free, crushed to 22-30 mesh size particles and calcined in air at different temperatures (900°C - 1400°C). Before carrying out the reaction, the catalyst was pretreated in situ at 900°C in a flow of moisture free $N_2$ (30 ml/min) for 1h.

### 1.2.2. Catalyst Characterization

In this sub-chapter, various techniques used to characterize the catalysts used in the different catalytic reactions will be briefly discussed. The actual data obtained from different characterization techniques for different catalysts have been presented in the appropriate part.

#### *1.2.2.1. Surface area*

The surface area of the catalysts was measured by the single point BET method by measuring the adsorption of nitrogen at liquid nitrogen temperature and at the $N_2$ concentration of 30 mol% (balance helium), using a Monosorb Surface Area Analyzer (Quantachrome Corp., USA) based on dynamic adsorption/desorption technique. Before the measurement, the catalyst was pretreated in situ in the sample cell at 300°C for 1h in the flow of a mixture of helium and nitrogen (at a flow of 30ml/min) to remove the traces of moisture and also the analyzer was calibrated by injecting a known amount of air.

The surface area was calculated from the observed desorption counts instead of the adsorption ones, as follows:

*Surface area ($m^2.g^{-1}$) = (Desorption counts* X *2.84) / (Wt. of catalysts in gram* X *counts for 1$cm^3$ of air)*

[2.84 $m^2$ area = 1 $cm^3$ of $N_2$ or air; counts are expressed in terms of surface area, $m^2$]

#### *1.2.2.2. Scanning electron microscopy (SEM)*

The crystal size and morphology of the catalysts used in various catalytic processes were determined by using a Cambridge Stereoscan Model 150 scanning electron microscope.

#### *1.2.2.3. X-Ray diffraction (XRD)*

The XRD analysis of the catalysts was done by the X-ray powder diffraction method, using a Holland Philips, PW/1730 X-ray generator with the CuK$\alpha$ radiation scintillation counter.

#### *1.2.2.4. X-ray photoelectron spectroscopy (XPS)*

Surface chemical analysis of the catalysts was carried out by x-ray photoelectron spectroscopy (XPS) using a VG Scientific ESCA-3 MK II electron spectrometer. $C_{1s}$ (with binding energy = 285 eV) was used as an internal standard. The electron binding energies (with the accuracy of 0.2 eV) were determined from the observed electron kinetic energies using the relation:

Binding energy (B. E.) = h$\nu$ - Kinetic energy (K. E.)

The x-ray radiation (h$\nu$) used in the XPS was MgK$\alpha$ (1253.6 eV).

The atom ratio of two elements (say, A and B) on the catalyst surface was determined from the XPS peaks as follows:

A/B atom ratio = [(peak area of A/photoionization cross section of A) / (peak area of B/photoionization cross section of B)]

#### *1.2.2.5. Strong acidity*

Strong acid sites of the zeolites were measured in terms of the pyridine chemisorbed at 400$^oC$, using the GC adsorption/desorption method, the details of which has been elaborately given elsewhere [1].

### *1.2.2.6. Infra-red spectroscopy (IR)*

The IR spectra of different samples, particularly the MFI zeolites were recorded by Perkin-Elmer FTIR (1600 series), using and nujol medium.

### *1.2.2.7. Solid state magic angle spinning NMR (MAS-NMR)*

The MFI zeolites, modified with or without gallium (gallosilicate, galloaluminosilicate) was characterized by the MAS-NMR method. The incorporation of Ga in the framework of GaMFI and GaAlMFI was confirmed by the $^{71}$Ga MAS NMR peak at +156 ppm. The framework (FW) Si/Ga and Si/Al ratios were obtained from the $^{29}$Si MAS NMR peaks, Si (0Ga or Al) at about -112 ppm and Si (1Ga or Al) at about -104 ppm by the method described earlier [2]. The $^{71}$Ga, $^{29}$Si and $^{27}$Al MAS NMR was obtained using Bruker MSL 300MHz NMR instrument.

### *1.2.2.8. CO chemisorption*

The CO chemisorption uptake on the catalyst was obtained by pulse chemisorption technique using pure CO pulse (0.1 ml) at 40$^{o}$C for Ni-containing catalysts after reducing them insitu with $H_2$ at 500$^{o}$C for 2h. The pulse micro-reactor (Fig. 1.2.1b), operating in the catalyst reduction and in chemisorption modes, is shown in Figs. 1.2.2 a and b, respectively.

### *1.2.2.9. Temperature programmed reduction (TPR)*

The schematic diagram of the experimental set-up used for the measurement of temperature programmed reduction (TPR) with $H_2$ of the catalyst is shown in Fig. 1.2.3. The temperature programmed reduction of the unreduced catalysts was carried out in a quartz reactor (I. D. 4.5 mm), packed with 0.05 g catalyst in a flow (60 $cm^3.min^{-1}$) of $H_2$-Ar mixture (3.7 mol% $H_2$) from 100$^{o}$C to 600$^{o}$C at a linear heating rate of 10$^{o}$C.min$^{-1}$. The hydrogen consumed in the TPR was measured quantitatively by TCD.

### *1.2.2.10. Chemical analysis*

The bulk composition of some zeolites particularly the zeolites were determined by the chemical analysis of Si by the complete dissolution method [3], Ga

by the gravimetric method using 5,7 dibromo-8-hydroxyquinoline as a complexing agent [4,5], Al by gravimetric method using 8-hydroxyquinoline as a complexing agent [6] and Na by the flame photometric method.

### 1.2.3. Catalytic Reactions

#### *1.2.3.1. Catalytic decomposition of methane to produce hydrogen*

The reactor set-up used for the catalytic decomposition of methane and carbon gasification by steam in two parallel stainless steel fixed bed reactors, each containing a 0.4g catalyst, operated in cyclic manner is shown in Fig. 1.2.4. The two had different feeds but a common outlet. A flow switchover valve was connected to inlets of the two reactors to switch the two different gaseous feeds between the two reactors. One feed, (called Feed A) was a mixture of methane and nitrogen, and the other (called Feed B) was a mixture of steam and nitrogen. The two feeds were switched between the two reactors at a fixed interval of time (called feed switchover time). Before carrying out the reactions, the catalyst in both the reactors was reduced in a flow of $H_2$-$N_2$ mixture (50 mol% hydrogen) at 500$^oC$ for 4h. The reaction temperature in both reactors was controlled by a Cr-Al thermocouple located in the catalyst bed. The reactor effluent gases were cooled to about 2$^oC$ using a coiled condenser immersed in the ice-water slurry to remove the water from the product gases. The product gases were collected in a collapsible plastic bag for a reaction period of 2h and then analyzed by a gas chromatograph with TCD detector, using Porapak Q and Spherocarb columns. Also in the separate experiments, the product gases at a constant flow rate (35 $cm^3.min^{-1}$) were passed through the TCD and FID detectors connected in series (without any gas chromatographic column) using nitrogen as a carrier gas, for continuously measuring the concentrations of hydrogen (by TCD) and methane (by FID) present in the product gases as a function of reaction time (time-on-stream). The gas hourly space velocity (GHSV) of both the feeds was measured at 0$^oC$ and 1 atm pressure.

In the previous reaction set-up the reaction products from each of the two reactors had a common outlet. In a separate study, another reaction set-up was used where the reaction products from each reactor were collected/processed separately, as shown in Fig. 1.2.5. In this set-up, one additional switchover valve (product switchover valve) was connected to the reactor outlet of each of the reactor (reactor A

and B). When the switchover valve was switched between the two reactors, simultaneously the product switchover valve was also switched between two gas collectors. The reaction products of the two reactions (methane decomposition and carbon gasification) were thus collected separately in the gas collectors, and analyzed by GC with TCD and also by FID using Spherocarb and Porapak Q columns. The carbon gasification products were passed through a $CO_2$ trap containing saturated aqueous solution of $Ba(OH)_2$, which absorbs $CO_2$; the $BaCO_3$ formed was analyzed gravimetrically.

### *1.2.3.2: Aromatization of ethylene, propylene and n-butene*

The reactor set-up used for the aromatization of $C_2$-$C_4$ olefins is shown schematically in Fig. 1.2.6. It consists of a quartz continuous flow tubular reactor (i.d. 12 mm) (Fig. 1.2.1a) connected to a NUCON (model 5765) gas chromatograph with FID and two GC columns through three gas sampling valves (GSV1, GSV2 and GSV3). The reactor details are given in Fig. 1.2.1a.

The reactor packed with the catalyst, containing 0.2g zeolite catalyst diluted uniformly by an inert solid (the total volume being 1ml) was kept in a tubular furnace (25mm diameter) such that the catalyst bed lies in the constant temperature zone of the furnace. The furnace temperature was measured by a chromel-alumel thermocouple located in a gap between the reactor and the furnace wall, as shown in the Fig.1.2.6. The temperature of the catalyst was measured by the other thermocouple located axially in the catalyst bed. The GSV1 and the stainless steel (SS) gas connecting tubes (3mm o.d.) between the gas sampling valve and the reactor outlet or GC were heated by heating tapes to avoid condensation of higher hydrocarbons in the product stream. The product stream leaving GSV1 was cooled by passing it through a coiled condenser immersed in an ice-water slurry to condense $C_{5+}$ hydrocarbons. The gaseous hydrocarbons ($C_1$-$C_4$ hydrocarbons) were sampled using GSV2. Thus it was possible to sample the products with or without containing $C_{5+}$ hydrocarbons simultaneously using GSV1 and GSV2, respectively. Before entering the GC column B (Porapak Q), the gaseous sample from GSV2 was passed for a short period (which is just enough to elute the $C_1$-$C_4$ hydrocarbon fraction from the column) through a pre-column [Benton 34 (5%) and dinonylphthalate (5%) on Chromosorb W 3mm X 5m] for removing the traces of higher ($C_{5+}$) hydrocarbons present in the

gaseous sample. After the use, the pre-column was continuously back flushed by nitrogen to elute the higher hydrocarbons absorbed at the entrance of the column. GC column A [Benton-34 (5%) and dinonylphthalate (5%) on Chromosorb W (3mm X 5m)] was used for separating the individual $C_{5+}$ aliphatics and aromatics from the reaction products ($C_1$-$C_4$ hydrocarbons are not separated on this column, these are eluted as a single peak).

As mentioned above, the reaction products with and without containing $C_{5+}$ hydrocarbons, are sampled by GSV1and GSV2, respectively, at the same time. However, the sample (total products) from GSV1 is analyzed first and then the analysis of sample from GSV2 (i.e. gaseous sample containing $C_1$-$C_4$ hydrocarbon) is performed. An olefin-nitrogen mixture was used as a feed. The flow rates of feed gases were controlled by fine needle valves and measured by rotameters. For thorough mixing, the feed gases were passed through a long SS tube (6 mm o.d.; 5 mm i.d. and 4 m long) in form of a coil. The feed entered the reactor at the top and the reaction products left the reactor at the bottom.

#### *1.2.3.3: Catalytic combustion of methane and propane*

##### *a) Catalytic combustion in pulse micro-reactor*

The pulse reaction of methane (or propane) over the catalyst was carried out in a quartz micro-reactor (Fig. 1.2.1b) in presence or absence of gaseous oxygen, using the experimental set-up shown in Fig. 1.2.7.

The experimental set-up consisted of a micro-reactor (made up of quartz and having i.d. 4.0mm, o.d. 6 mm and length 30 cm) and flow switching valves, as shown in Fig. 1.2.7. The micro-reactor could be operated either in a catalyst pretreatment under He, $H_2$ or $O_2$ (i.e. catalyst pretreatment) (Fig. 1.2.7a) or in a pulse reaction mode (Fig. 1.2.7b) by operating the flow switching valves as shown in Fig. 1.2.7. Helium (> 99.99%) passed over the activated molecular sieves and oxysorb to remove the traces of moisture and oxygen, respectively, was used as a carrier gas (flow rate: 30 $cm^3.min^{-1}$).

A known mass of catalyst of desired particle size was packed between two quartz wool plugs in the constant temperature zone of the furnace. The catalyst temperature was measured by the Chromel-Alumel thermocouple located in the catalyst bed. Before carrying out the pulse reactions, the catalyst was calcined insitu

at 600°C in a flow of helium for 2h (Fig. 1.2.7a). After the pretreatment, the reactor was operated in the pulse reaction mode (Fig. 1.2.7b).

The pulse reaction of methane or propane in the absence of $O_2$ were carried out by passing pulses of methane (or propane) one after another at an interval of 5 min. Similarly the pulse reactions in presence of $O_2$ were carried out by passing the pulse of methane mixed with desired amount of $O_2$ over the fresh catalyst. The products formed in the each pulse experiment were analyzed by an on-line gas chromatograph (GC) with the TCD detector using Spherocarb column.

The activity (i.e. conversion) data was calculated from the carbon balance in the pulse before and after the reaction, taking into consideration the reaction stoichiometry as follows: conversion (%) of a particular reactant = $100[(R_i - R_o)/R_i]$, where $R_i$ and $R_o$ are the moles of reactant in the pulse before and after the reaction, respectively.

In order to study the pulse reactions over the reoxidized catalysts, the microreactor was operated in the pretreatment mode (Fig. 1.2.7a) and the reduced catalyst, after the pulse experiments carried out in the absence of $O_2$, was reoxidized in an air flow ($30cm^3.min^{-1}$) at 600°C for 1h. The reoxidized catalyst was then flushed with helium ($30cm^3.min^{-1}$) at 600°C for 30min to remove physically adsorbed oxygen on the catalyst, and its performance in the pulse reaction at the reaction temperature in the absence of -$O_2$ was then studied.

In order to study the pulse reaction over the completely reduced catalysts, the micro-reactor was operated in the pulse reaction mode, but in this case pure $H_2$ (in stead of air) was passed over the catalyst at 600°C for 2h.

In order to study the pulse reaction over the partially reduced (or oxidized) catalysts, the pulse micro-reactor was operated in the pulse reaction mode, and desired number of pulses of pure $H_2$ (or $O_2$) was passed over the completely oxidized (or reduced) catalysts at 600°C for 2h.

### *b) Catalytic combustion in continuous flow reactor*

The experimental set up used for the low temperature catalytic combustion of methane or propane in the continuous flow micro-reactor has been shown in Fig. 1.2.8. The quartz reactor used for the experiment is the same, used in the aromatization of lower olefins and has been shown in the Fig. 1.2.1a. The reactor packed with the catalyst, containing 0.1g catalyst diluted uniformly by 0.4g of an inert

solid was kept in a tubular furnace (25mm diameter) such that the catalyst bed lies in the constant temperature zone of the furnace. The temperature of the catalyst was measured by the chromel-alumel thermocouple located axially in the catalyst bed, as shown in the Fig.1.2.8. The product stream was passed through a condenser immersed in ice-water slurry to condense the water formed during the reaction. The product stream, free from water, was analyzed by an on-line GC (TCD and FID) using Porapak-Q and Spherocarb column. The product sample was injected into the GC by a gas sampling valve.

The experimental set-up used for the high temperature complete combustion of methane was same as that used for the low temperature operation (Fig.1.2.8). In this case, the quartz micro-reactor used (Fig. 1.2.1b) has a very low dead volume.

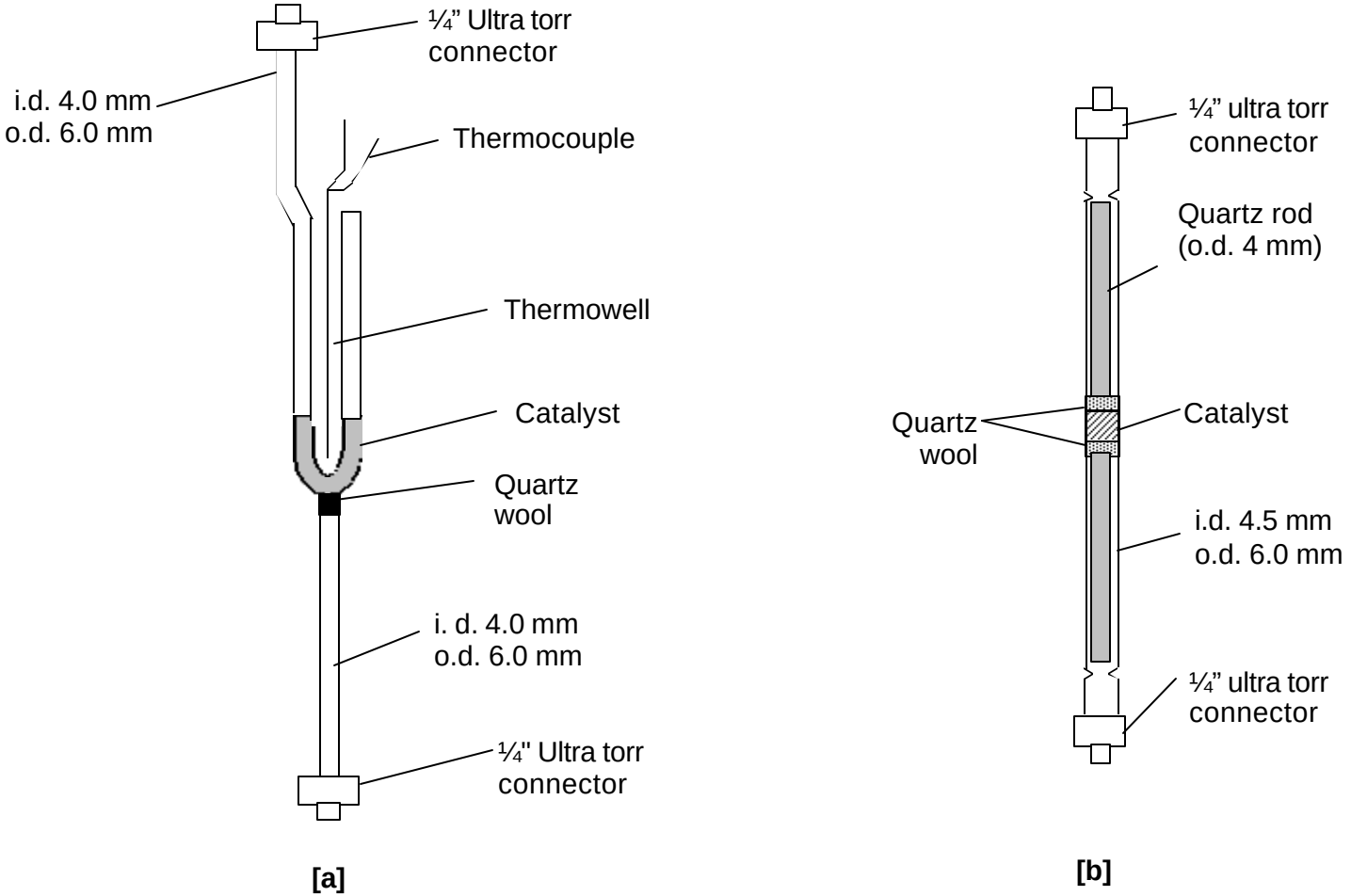


**Figure 1.2.1.** Different types of quartz reactors used in different catalytic processes

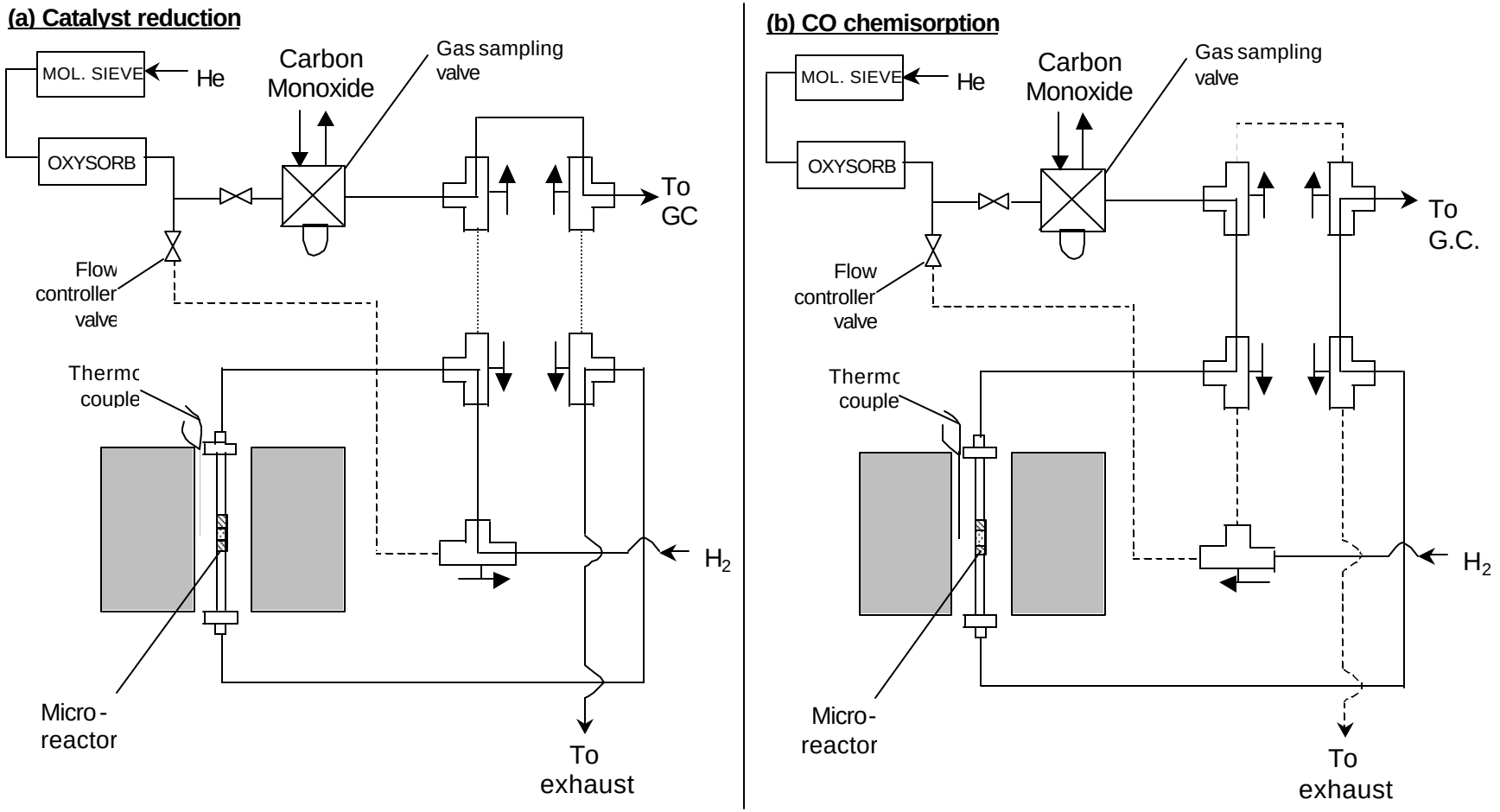


**Figure 1.2.2.** Experimental set-up for (a) insitu pretreatment (or reduction) of catalyst and (b) Carbon monoxide chemisorption on the catalyst in pulse microreactor [FCV = flow control valve; GSV = gas sampling valve; BV = three-way ball valve]

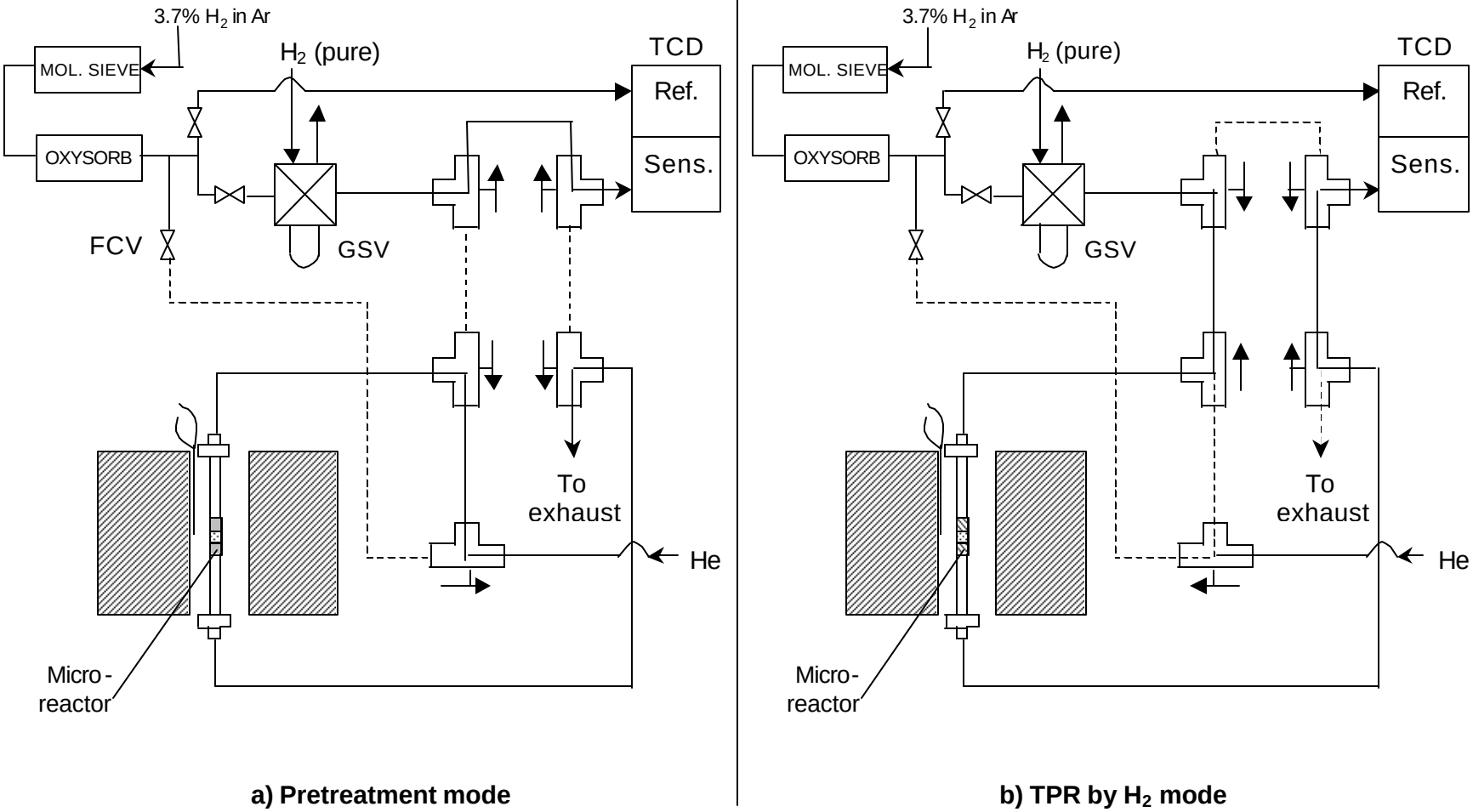


**Figure 1.2.3.** Experimental set-up for temperature programmed reduction (TPR) by $H_2$ (a) in situ pretreatment of catalyst and (b) TPR by $H_2$ [FCV = flow control valve; GSV = gas sampling valve; BV = three-way ball valve]

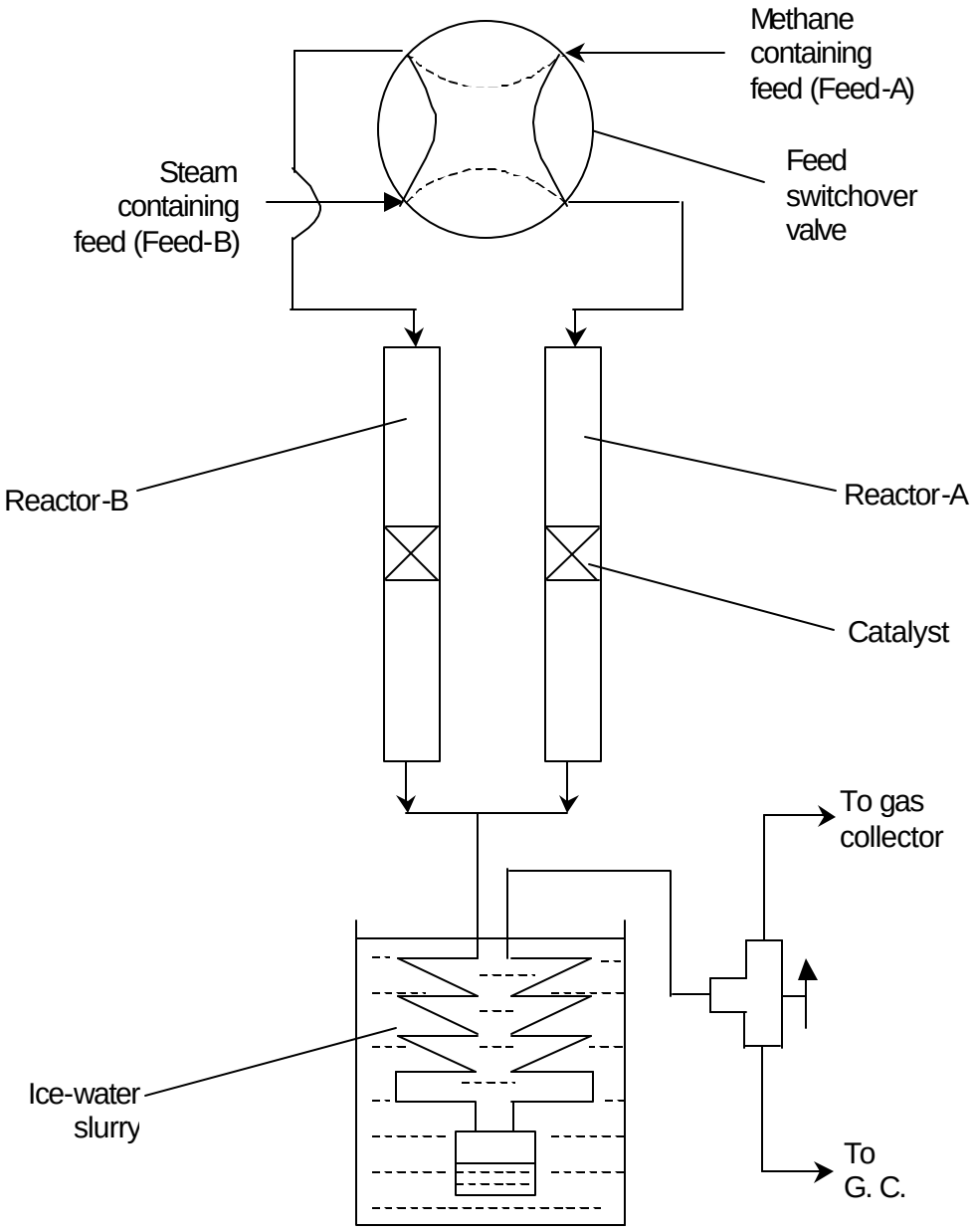


**Figure 1.2.4.** Schematic diagram of catalytic decomposition of methane and carbon-gasification by steam in two parallel reactor, having two different feeds but a common outlet, operated in a cyclic manner

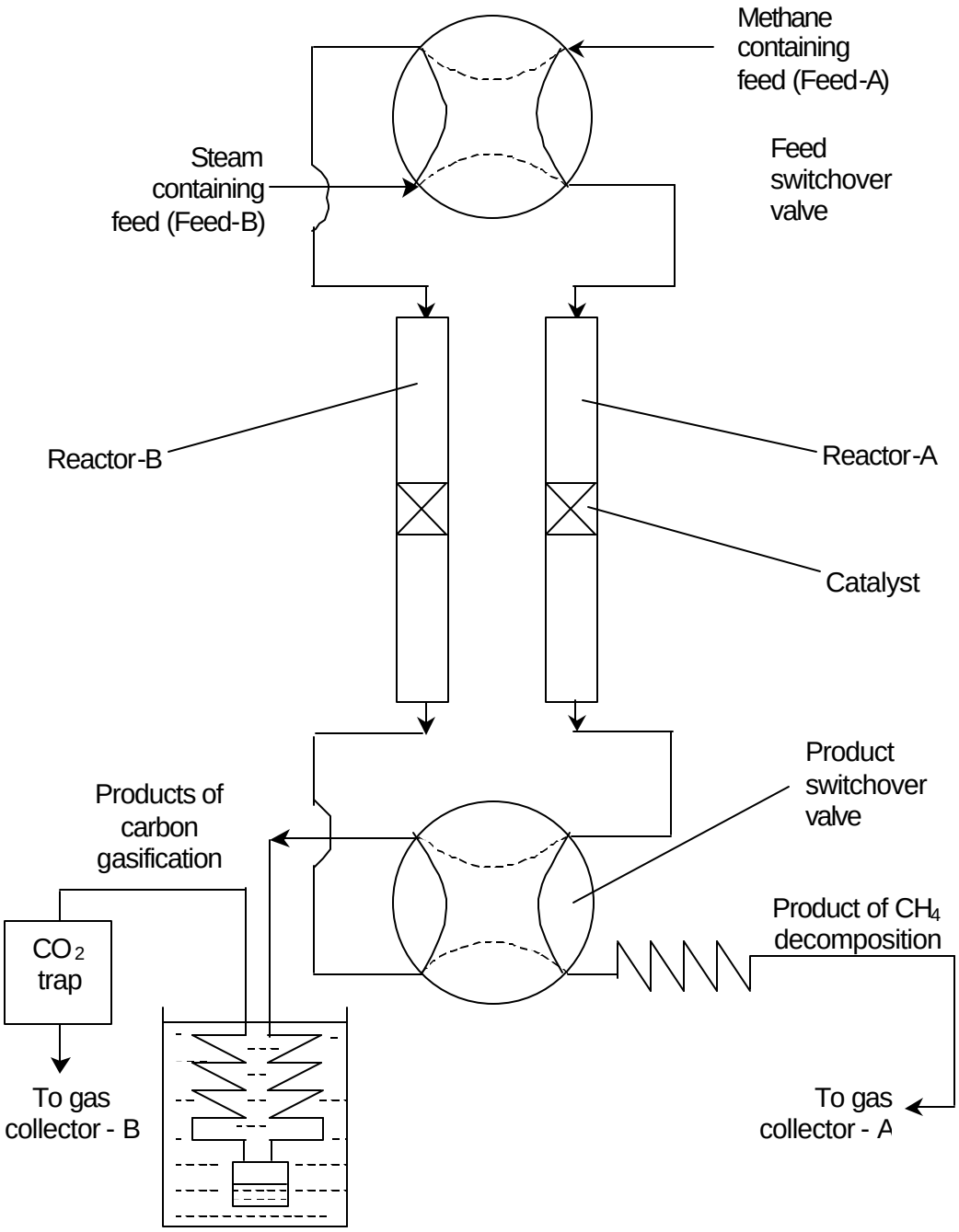


**Figure 1.2.5.** Schematic diagram for carrying out the catalytic methane decomposition and carbon gasification simultaneously in two separate parallel reactors in cyclic manner by switching two different feeds (feed-A and feed-B) between two reactors and also simultaneously switching two different product streams between two separate gas collector units.

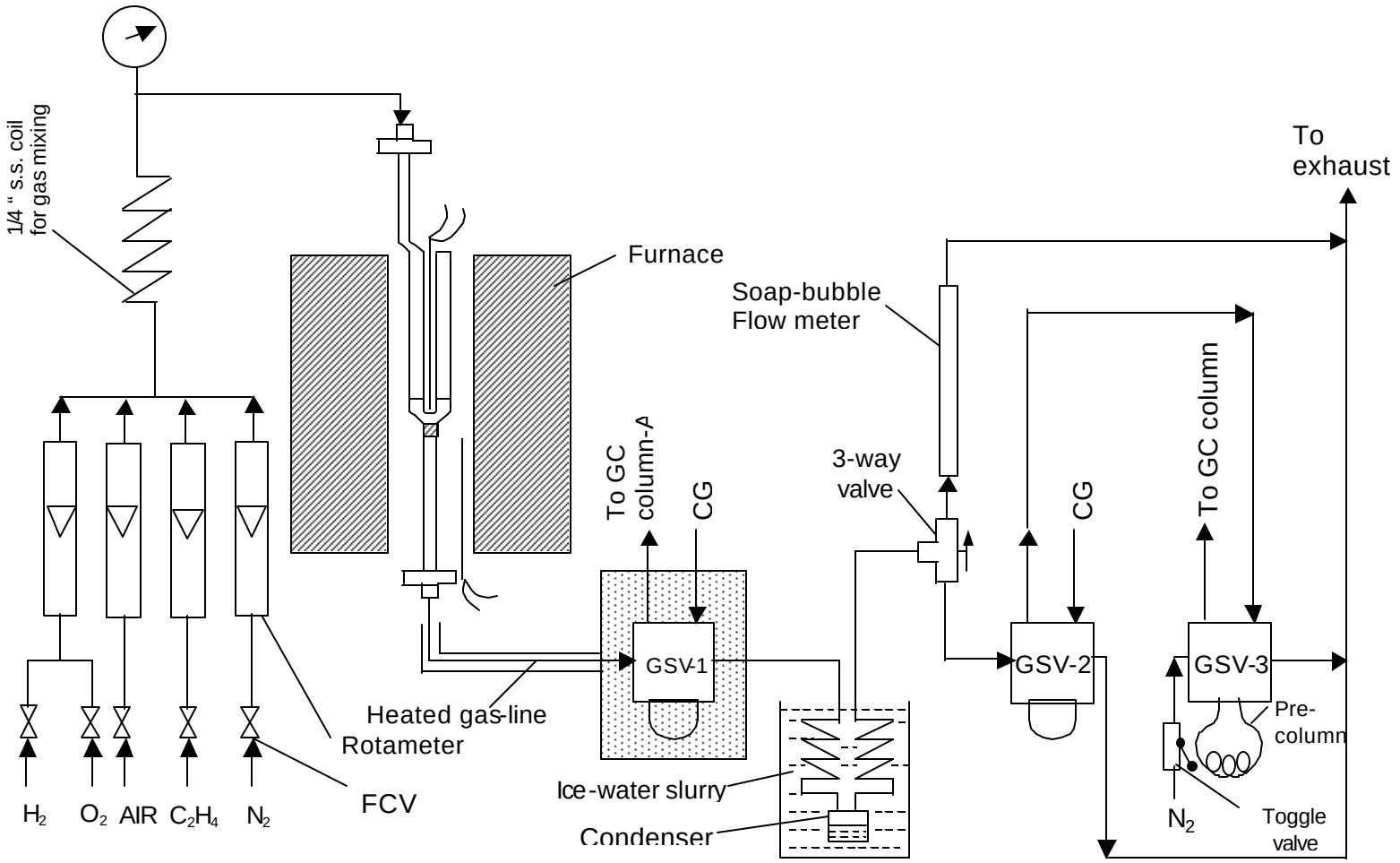


**Fig. 1.2.6.** Experimental set-up for olefin aromatization [GSV1 = heated gas sampling valve, GSV2 and GSV3 = gas sampling valves, Column A= Benton-34 (5%) and dinonylphthalate (5%) on Chromosorb-W, Column B = Porapak-Q, CG = carrier gas, FCV = flow control valve].

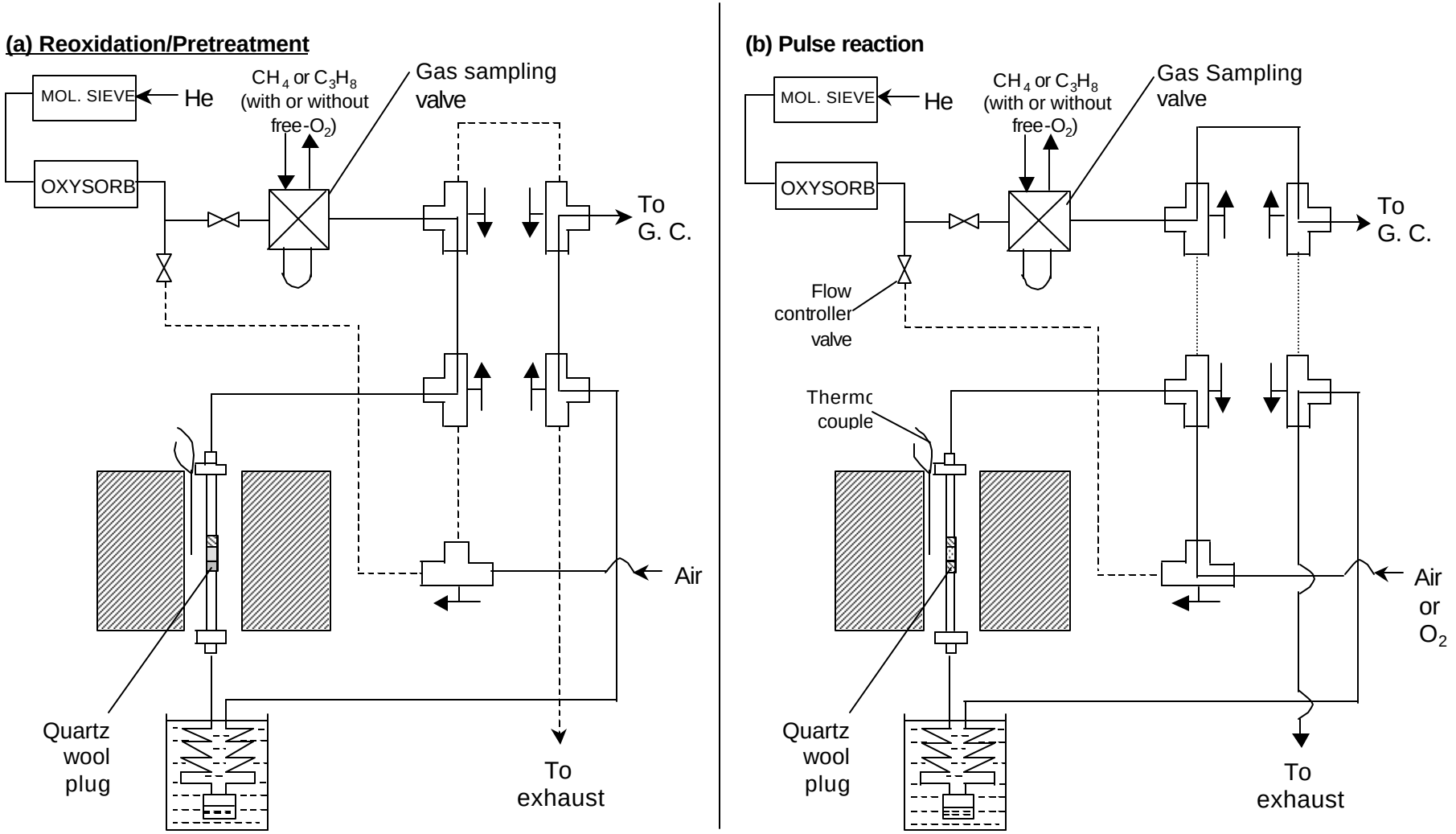


**Figure 1.2.7.** Experimental set-up for (a) insitu pretreatment (or reoxidation) of catalyst and (b) pulse methane (or propane) oxidation on the catalyst in pulse microreactor in presence or absence of free-$O_2$ [FCV = flow control valve; GSV = gas sampling valve; BV = three-way ball valve]

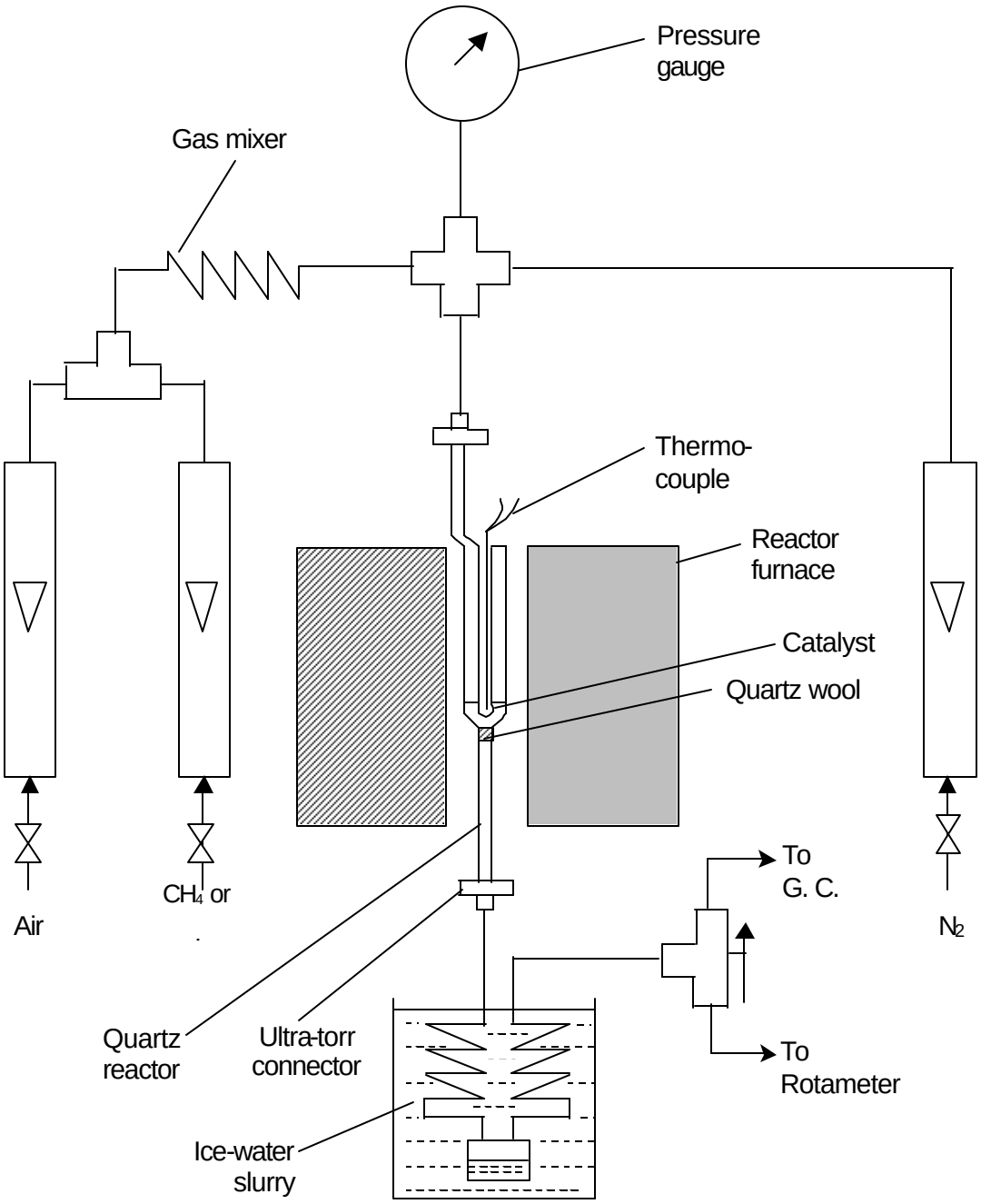


**Figure 1.2.8.** Experimental set-up for complete combustion methane (or propane) in a continuous flow fixed bed quartz reactor

### 1.2.4. References


1. V. R. Choudhary and V. S. Nayak, Appl. Catal, 4 (1982) 31.
2. X-S Lin, and J. Klinowski, J. Phys. Chem. 96 (1992) 3403.
3. J. H. C. Van Hooff and J. W. Roelofsen, Stud. Surf. Sci. Catal., 58 (1991).
4. E. Z. Gastinger, Anal. Chem., 126 (1944) 373.
5. C. Duval, Thermogravimetric Analysis, 2nd Ed., Elsevier, Amsterdam, (1963), pp. 416.
6. A. I. Vogel, Text Book of Quantitative Inorganic Analysis, 3rd Ed., Longmans, Green and Co. Ltd, London, (1961) pp. 514.

# PART – II

## DECOMPOSITION OF METHANE TO PRODUCE CO-FREE $H_2$

**CHAPTER 2.1:** **CONTINUOUS PRODUCTION OF $H_2$ AT LOW TEMPERATURE FROM METHANE DECOMPOSITION OVER Ni-CONTAINING CATALYST FOLLOWED BY GASIFICATION BY STEAM OF THE CARBON ON THE CATALYST IN TWO PARALLEL REACTORS OPERATED IN CYCLIC MANNER**

**CHAPTER 2.2:** **HYDROGEN FROM STEP-WISE STEAM REFORMING OF METHANE OVER $Ni/ZrO_2$: FACTORS AFFECTING CATALYTIC METHANE DECOMPOSITION AND GASIFICATION BY STEAM OF CARBON FORMED ON THE CATALYST**

# CHAPTER 2.1.

# CONTINUOUS PRODUCTION OF $H_2$ AT LOW TEMPERATURE FROM METHANE DECOMPOSITION OVER Ni-CONTAINING CATALYST FOLLOWED BY GASIFICATION BY STEAM OF THE CARBON ON THE CATALYST IN TWO PARALLEL REACTORS OPERATED IN CYCLIC MANNER

## 2.1.1. Earlier Work/Background and Objective of the Present Work

The demand for hydrogen is ever increasing due to its use in various hydrotreating processes in petroleum industries and also for hydrogen fuel cells. Hydrogen is a non-polluting fuel and its use as fuel in fuel cells used in automobiles is increasing day by day. However, the PEM (proton exchange membrane) fuel cells require CO-free hydrogen to avoid deactivation of its costly noble metal catalyst. Apart from water, methane is a preferred source of hydrogen due to its high hydrogen to carbon ratio. The conventional steam reforming and autothermal reforming processes for the production of $H_2$ from methane are high temperature processes (>800$^o$C) and produce CO as one of the major by-products. Hence, efforts are being made for producing CO-free hydrogen from low temperature catalytic step-wise steam reforming of methane (1-3), involving following reactions in consecutive steps:

$$CH_4 \rightarrow C \text{ (on catalyst)} + 2H_2 \quad (1)$$

$$C \text{ (on catalyst)} + 2H_2O \rightarrow CO_2 + 2H_2 \quad (2)$$

Zhang and Amiridis [1] have carried out the above two reactions alternatively (one after another) over $Ni/SiO_2$. Choudhary and Goodman [2] have passed alternative pulses of methane (5% $CH_4$ in He) and water (2μl) over $Ni/ZrO_2$ at 375$^o$C to obtain CO-free hydrogen from the above reactions. Very recently, Choudhary and Goodman [3] have studied the two steps of the process by carrying out the above two reactions alternatively as a function of temperature and surface coverage of carbon. They observed that the removal of surface carbon in reaction-2 becomes increasingly difficult at higher temperatures and surface coverage of carbon. In all the above investigations, the two reactions were carried out one after another in cyclic manner in the same reactor and there was no continuous decomposition of methane and/or gasification of carbon from the catalyst.

For the commercial application, both the reactions need to be carried out continuously without disturbing feed for reactions 1 and 2 for the continuous

production of $H_2$ from methane and water. The present work was therefore undertaken for the continuous production of $H_2$ from methane and water in two steps, reaction 1 followed by reaction 2, by carrying out the two reactions simultaneously and continuously in cyclic manner over a Ni-containing catalyst in two parallel fixed bed reactors at a low temperature (500°C) by switching two feeds - one, methane - $N_2$ mixture and second steam - $N_2$ mixture between the two reactors at a fixed interval of time. A number of Ni-containing catalysts were evaluated for their performance in the process.

### 2.1.2. Experimental

The preparation procedure of different Ni-based catalysts used for this purpose has been discussed earlier (section 1.2.1.1). In short, $Ni/ZrO_2$, $Ni/ThO_2$ and $Ni-Co/ZrO_2$ and Ni/MgO catalysts (Table 2.1.1) were prepared by coprecipitating the corresponding metal hydroxides from their aqueous solution containing respective metal nitrates using sodium hydroxide or sodium carbonate as precipitating agents; finally calcining at 600°C for 2h. $Ni/CeO_2$, $Ni/UO_3$, $Ni/MoO_3$ and $Ni/B_2O_3$ catalysts (Table 2.1.1) were prepared by thoroughly mixing nickel nitrate with ammonium cerium (IV) nitrate or uranyl acetate or ammonium molybdate or boric acid, and drying and calcining the mixed salt at 600°C for 2h in static air. Ni/HZSM-5, Ni/Si-MCM-41, Ni/H-Mordenite, Ni/Hâ, Ni/NaY and Ni/Ce(72)NaY catalysts (Table 2.1.2) were prepared by impregnating nickel nitrate on HZSM-5, (Si/Al=40) or Si-MCM-41 or H-Mordenite or Hâ or NaY or CeNaY, using the incipient wetness technique, followed by drying and calcining in air at 500°C for 4h. All the above catalysts were powdered, pressed and crushed to particles of 30-52 mesh size.

The experimental procedure for the methane decomposition and carbon gasification reactions over the catalysts, has already been discussed (section 1.2.3.1 and Fig. 1.2.4). The reactions were carried out in two parallel stainless steel fixed bed reactors, each containing 0.4g catalyst. The two reactors had different feeds but a common outlet. A flow switchover valve was connected to inlets of the two reactors to switch the two different gaseous feeds between the two reactors. One feed (called as Feed-A) was a mixture of methane and nitrogen, and the other one (called as Feed-B) was a mixture of steam and nitrogen, as has been shown in Fig. 1.2.4. The two feeds were switched between the two reactors at a fixed interval of time (called as

feed switch over time). Before carrying out the reactions, the catalyst in both the reactors was reduced in a flow of $H_2$ - $N_2$ mixture (50 mol% hydrogen) at 500°C for 4h. The reaction temperature in both the reactors was controlled by Cr-Al thermocouple located in the catalyst bed. The reactor effluent gases were cooled to about 2°C using a coiled condenser immersed in the ice-water slurry to remove the water from the product gases. The product gases were collected in a collapsible plastic bag for a reaction period of 2h and then analyzed by a gas chromatograph with TCD detector, using Porapak Q and Spherocarb columns. Also in the separate experiments, the product gases at a constant flow rate (35 $cm^3.min^{-1}$) were passed through the TCD and FID detectors connected in series (without any gas chromatographic column) using nitrogen as a carrier gas, for continuously measuring the concentration of hydrogen (by TCD) and also of methane (by FID) present in the product gases as a function of reaction time (time-on-stream).

At the reaction conditions employed in the present investigation, no formation of carbon monoxide in the cyclic process over all the catalysts was observed.

### 2.1.3. Results and Discussion

Results of a representative experiment for the cyclic stepwise steam reforming of methane (at 500°C) over the $Ni/ZrO_2$ catalyst in the two parallel reactors operated in cyclic manner with a feed switch over time of 10 min are presented in Fig. 2.1.1. In this case, the combined feed streams (without steam) and the combined gaseous product streams (after the removal of water from them) are directly passed through the TCD and FID detectors connected in series. The frontal chromatograms obtained by the FID (Fig. 2.1.1a,b) show the relative concentration of methane in the combined feed streams and in the combined product streams. The chromatogram (Fig. 2.1.1b) indicates a steady conversion of methane (19.6%, after correcting for a change in the gas flow rate due to the reaction) in the process. The observed downward spikes, which are due to a momentary change in flow rate, correspond to switch over of the Feed-A and Feed-B between the two reactors (Figs. 1.2.4 and 2.1.1). The frontal chromatograms obtained by the TCD (Figs. 2.1.1c,d) indicate the formation of hydrogen in the process; the detector response for the product stream is higher because of the higher thermal conductivity of $H_2$ present in the products, as compared to the components in the feed. Because of the detector's high sensitivity towards a

small change in the gas flow rate, which results from the feed switch over between the two reactors, the upward spikes and the up and down steps in the chromatogram (Fig. 2.1.1d) are observed. Nevertheless, the results (Fig. 2.1.1) clearly shows that $H_2$ can be produced continuously almost at the same rate and also without affecting the feed flow rates by carrying out the methane decomposition (reaction 1) and the carbon gasification by steam (reaction 2) simultaneously in the two separate reactors operated parallely, while switching the methane containing feed (Feed-A) and the steam containing feed (Feed-B) between the two reactors at a predecided interval of time.

**Table 2.1.1.** Results of the cyclic stepwise steam reforming of methane over different Ni-containing metal oxide (Ni/M = 1.0) catalysts (pre-reduced by $H_2$ at 500°C for 4h) [Reaction conditions: Feed A = 18.2 mol% $CH_4$ in $N_2$; GHSV of Feed-A = 7100 $cm^3g^{-1}h^{-1}$; Feed B = 20.5 mol% steam in $N_2$; GHSV of Feed B = 7290 $cm^3g^{-1}h^{-1}$; temperature = 500°C and feed switch over time = 10 min].

| Catalyst | Surface area ($m^2.g^{-1}$) | No. of feed switch over | TOF ($mmol.g^{-1}.h^{-1}$) | $H_2$ produced per mole of $CH_4$ converted (mol) | Pressure drop (atm) | |
|---|---|---|---|---|---|---|
| | | | | | Initial[a] | Final[b] |
| $Ni/ZrO_2$ | 62.8 | 36 | 11.3 | 3.8 | 0.02 | 0.02 |
| Ni/MgO | 33.0 | 12 | 7.9 | 3.6 | 0.02 | 0.02 |
| $Ni/ThO_2$ | 59.0 | 10 | 9.5 | 2.9 | 0.02 | 0.21 |
| $Ni/UO_3$ | 6.0 | 12 | 8.7 | 3.1 | 0.02 | 0.16 |
| $Ni/CeO_2$ | 43.0 | 10 | 8.8 | 3.0 | 0.02 | 0.18 |
| $Ni/B_2O_3$ | 37.4 | 12 | 7.7 | 3.2 | 0.02 | 0.08 |
| $Ni/MoO_3$ | 11.4 | 12 | 6.4 | 3.5 | 0.02 | 0.04 |
| Ni-$Co/ZrO_2$[c] | 31.1 | 14 | 8.0 | 3.7 | 0.02 | 0.03 |

[a,b] pressure drop across the catalyst bed for the methane decomposition step at the start of first cycle and at the end of the last cycle, respectively.

[c] Ni : Co : Zr = 1:1:2

The amount of carbon formed in the methane decomposition for the total reaction period of 6h (36 cycles) is estimated as 0.82g per gram of catalyst. Whereas, the carbon left over on the catalyst after the reaction (at the end of $36^{th}$ cycle) was 0.044g per gram catalyst. This shows that almost 95% of the carbon formed in the process was gasified in the steam treatment cycles and hence there was no increase in the pressure drop across the catalyst bed in both the parallel reactors. However, when the carbon formed in the methane decomposition was not removed intermittently by its gasification with steam, there was an appreciable and continuous increase in the pressure drop with the increase in the time-on-stream, particularly about the reaction period of 30 min.

**Table 2.1.2.** Results of the step-wise steam reforming of methane over different Nickel (10 wt%) impregnated zeolite catalysts (pre-reduced at 500°C for 4h) [Reaction conditions: same as that given in Table 2.1.1].

| Catalyst | Surface area ($m^2.g^{-1}$) | No. of feed switch overs | TOF ($mmol.g^{-1}.h^{-1}$) | $H_2$ produced per mole of $CH_4$ converted (mol) | Pressure drop (atm) | |
|---|---|---|---|---|---|---|
| | | | | | Initial[a] | Final[b] |
| Ni/H-ZSM-5 | 266.0 | 12 | 9.6 | 3.7 | 0.03 | 0.04 |
| Ni/Si-MCM-41 | 786.0 | 12 | 8.7 | 3.7 | 0.03 | 0.04 |
| Ni/H-Mordenite | 319.7 | 18 | 6.9 | 3.6 | 0.03 | 0.04 |
| Ni/H-beta zeolite | 408.0 | 10 | 10.8 | 3.4 | 0.03 | 0.15 |
| Ni/NaY | 450.0 | 12 | 9.6 | 3.3 | 0.03 | 0.20 |
| Ni/Ce (72)NaY | 341.8 | 12 | 10.7 | 3.6 | 0.03 | 0.05 |

[a,b]pressure drop across the catalyst bed for the methane decomposition step at the start of first cycle and at the end of the last cycle, respectively

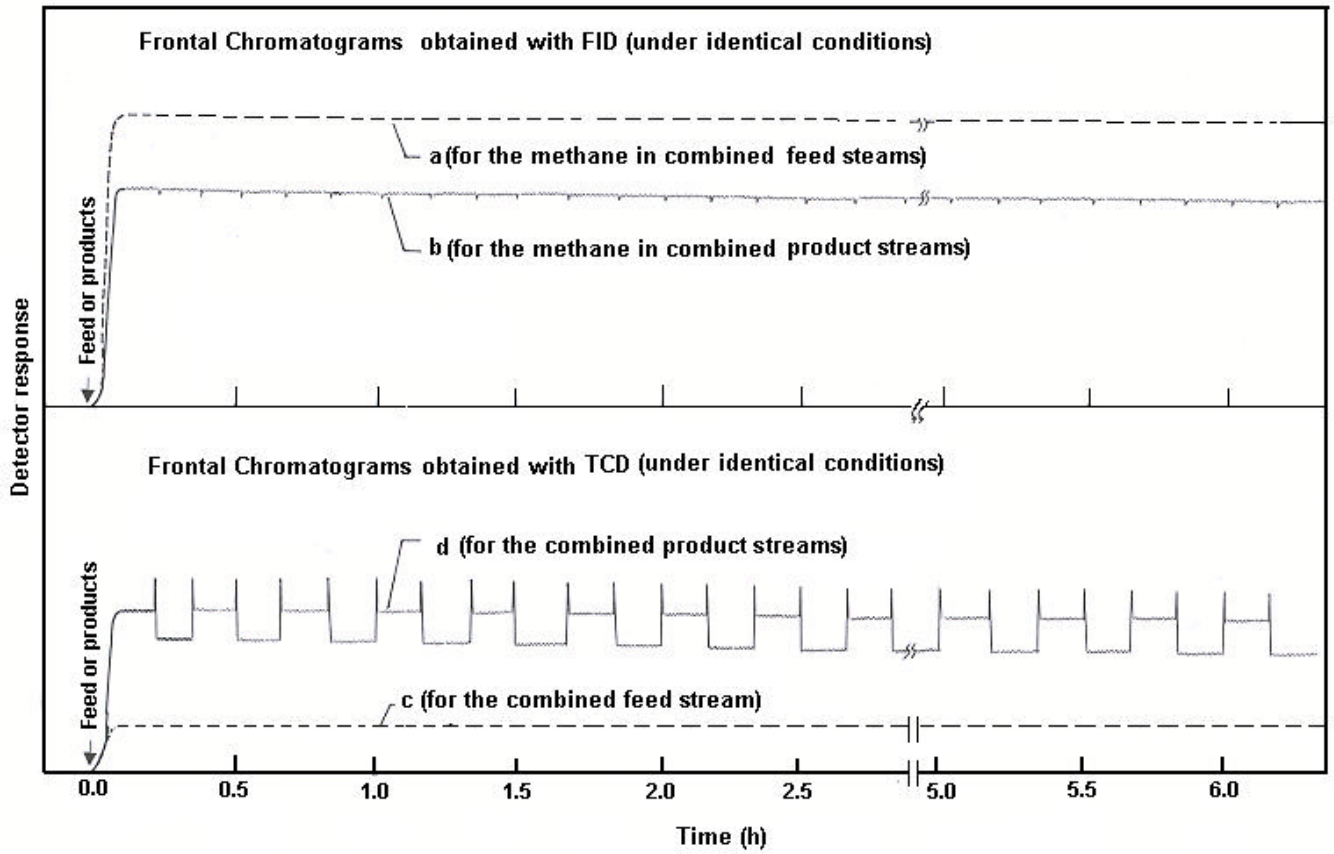


**Fig. 2.1.1.** Representative frontal chromatograms obtained with the FID and TCD for the combined feed streams and the combined product streams of the stepwise steam reforming of methane carried out in two parallel reactors, each containing the same catalyst ($Ni/ZrO_2$), at 500°C and with a feed switch over time of 10 min [Feed-A = 18.2 mol% $CH_4$ in $N_2$; Feed-B = 20.5 mol% steam in $N_2$; GHSV of Feed-A = 7100 $cm^3g^{-1}h^{-1}$; GHSV of Feed-B = 7290 $cm^3g^{-1}h^{-1}$]

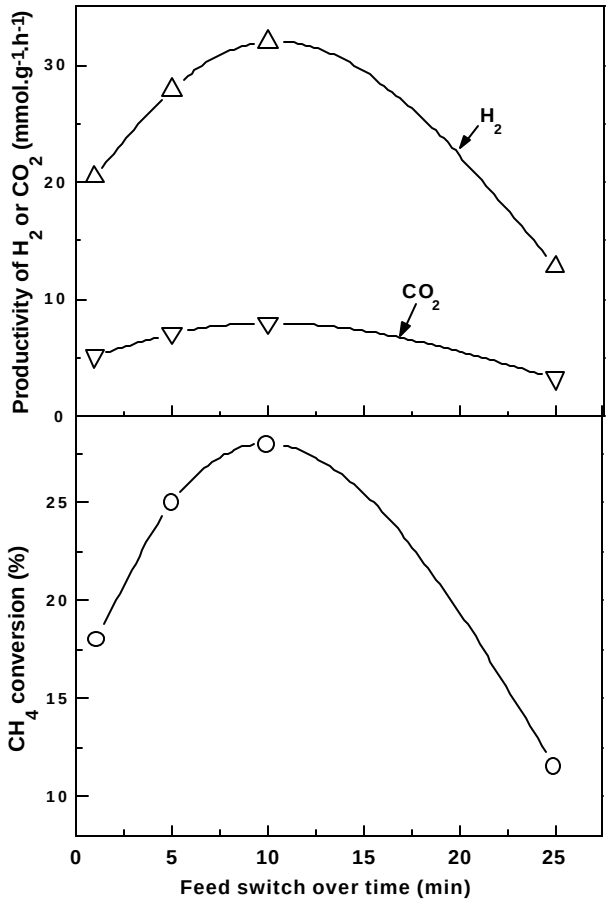


**Fig. 2.1.2.** Effect of feed switch over time on the process performance using $Ni/ZrO_2$ (Ni/Zr = 1.0) catalyst [Feed A = 20 mol% $CH_4$ in $N_2$; Feed B = 80.9 mol% steam in $N_2$; GHSV = 3225 (feed A) and 6770 (feed B) $cm^3.g^{-1}.h^{-1}$; temperature in both the reactors = 500°C].

It may also be noted that, the catalyst did not show a sign of deactivation in the process for a sufficiently long period (Fig. 2.1.1). However, when the methane decomposition was carried out alone (without the cyclic operation) over the same catalyst under the similar conditions continuously for a period of 2h, a steady conversion of methane (19.6 $\pm$ 0.2%) was observed, even though there was a continuous build up of carbon (estimated as 0.27g per gram at the end of the run) on the catalyst. The pressure drop across the catalyst bed was increased continuously

from its initial value of 0.02 atm to 0.12 atm. A steady methane conversion in the decomposition of methane for a long period was also observed earlier for the $Ni/SiO_2$ catalyst [1] and Ni (or Co)/$Al_2O_3$ [4] catalysts. However, a need for the intermittent removal of carbon from the catalyst by its gasification by steam is necessary to avoid the undesirable large pressure drop across the catalyst due to formation of excessive carbon between the catalyst particles. Moreover, the removal of carbon from the catalyst is more and more difficult at the higher and higher surface coverage of carbon [3]. The aging of carbon during the methane decomposition process is also expected to cause a change in the nature and/or form of the carbon deposited on the catalyst, making removal of the carbon increasingly difficult. Moreover, the aging may lead to a permanent deactivation of the catalyst or reduce drastically the catalyst regenerability.

Results showing the influence of the feed switch over time on the process performance are presented in Fig. 2.1.2. Both the methane conversion and the $H_2$ productivity, and consequently the $CO_2$ produced in the process, are passed through a maximum (at a feed switch over time of about 10 min) with increasing the feed switch over time from 1.0 min to 25.0 min. The amount of $H_2$ produced per mole of the methane converted was $3.9 \pm 0.05$, which is very close to the stoichiometric amount (4.0) expected to be formed in the cyclic process. The results clearly show that there is an optimum value for the feed switch over time; it is 10 min for the $Ni/ZrO_2$ catalyst at the specified reaction conditions. However, the optimum value may vary with the reaction conditions for the same catalyst and it may also differ from catalyst to catalyst. Further studies are required for knowing the carbon retained on the catalyst after each successive cycle (i.e. the methane decomposition followed by the carbon gasification) and its dependence on the different process conditions.

The observed lower methane conversion and consequently the lower $H_2$ productivity, at the high switch over time (25 min), is certainly due to a larger amount of carbon deposited on the catalyst. However, the observed lower methane conversion for the shorter feed switch over time (1 min and 5 min) than that at the optimum switch over time (10 min) is unusual. At the very short feed switch over time (1.0 min), the carbon deposited on the catalyst is expected to be much smaller and hence a higher methane conversion is expected. The observed higher methane conversion at the intermediate feed switch over time indicates a beneficial effect of the presence of carbon species at an optimum concentration on the surface of the catalyst for it to be

more active in the methane decomposition. A further detailed investigation is required for understanding the observed optimum feed switch over time in the process of this investigation.

Results on a few more Ni-containing metal oxides and zeolite catalysts for the stepwise steam reforming of methane (at 500°C) operated in the cyclic manner in the two parallel reactors with a feed switch over time of 10 min for a time-on-stream of 2h are presented in Tables 2.1.1 and 2.1.2. TOF was estimated as the amount of methane converted per unit mass of catalyst per unit time. The initial and final pressure drops across the catalyst bed were measured for the methane decomposition step in the cyclic process.

Among the Ni-containing metal oxide catalysts (Table-2.1.1), the $Ni/ZrO_2$ showed the best performance in the cyclic process. Whereas, among the Ni-containing zeolite catalysts (Table-2.1.2), the Ni/Ce(72)NaY showed the best performance. Though the Ni/Hâ showed methane conversion activity comparable to that of Ni/Ce(72)NaY, the former one produced less $H_2$ per mole of methane converted and also a larger amount of carbon accumulated on the catalyst resulting in undesirable pressure drop across the catalyst bed. The $Ni/UO_3$, $Ni/ThO_2$, $Ni/CeO_2$, $Ni/B_2O_3$ and Ni/NaY catalysts also showed high pressure drop across the catalyst bed; the pressure drop was found to increase exponentially with increasing the reaction period (or number of cycles). The observed high pressure drop for these catalysts was resulted mainly due to the formation of filamentous carbon blocking the inter-particle voids in the catalyst bed. This was confirmed by observing a drastic reduction in the pressure drop, approaching to its initial value, due to an air oxidation of the catalyst at 500°C. Because of the larger amount of carbon accumulated on these catalysts, the $H_2$ produced per mole of the methane converted was appreciably lower than the expected theoretical value (4.0). For the cyclic process, the $Ni/ZrO_2$ catalyst, however, showed the best performance - highest TOF (methane conversion activity), highest moles of $H_2$ (3.8) produced per mole of $CH_4$ converted and almost no pressure drop across the catalyst bed, even when operated for a much larger number of cycles.

In their earlier cyclic pulse studies, Choudhary and Goodman [2,3] obtained 1.0 to 1.3 mol $H_2$ per mole of methane consumed in the methane decomposition step over $Ni/ZrO_2$ catalyst at 375°C. However, in the present cyclic process the $H_2$ produced is almost close to the stoichiometric amounts. This is expected most probably because of the fact that, unlike the cyclic pulse process, the present process

operates under or very close to a steady state and also involves the reforming by steam of partially hydrogenated carbon species (produced in the methane decomposition step) into $CO_2$ and $H_2$ in the steam treatment step.

### 2.1.4. Conclusions

The above results lead to the following important conclusions:

(i) It is possible to produce continuously hydrogen at a constant rate and also close to stoichiometric amounts by the cyclic stepwise steam reforming of methane at a low temperature ($500^oC$), by carrying out the catalytic methane decomposition and the gasification of carbon deposited on the catalyst during the methane decomposition separately in two parallel catalytic reactors, containing the same catalyst, operated in cyclic manner by switching methane containing feed and steam containing feed between the two reactors at a known interval of time.

(ii) The feed switch over time has an optimum value for achieving the best performance in the process.

(iii) The $Ni/ZrO_2$ and Ni/Ce(72)NaY are promising catalysts for the cyclic stepwise steam reforming of methane to hydrogen and $CO_2$ at a low temperature ($500^oC$).

### 2.1.5. References


1. T. Zhang and M. D. Amiridis, Appl. Catal A: Gen., 167 (1998) 161.
2. T. V. Choudhary and D. W. Goodman, Catal. Lett., 59 (1999) 93.
3. T. V. Choudhary and D. W. Goodman, J. Catal., 192 (2000) 316.
4. L. B. Avdeeva, D. I. Kochubey and Sh. K. Shaikhutdinov, Appl. Catal A: Gen., 177 (1999) 43.

# CHAPTER 2.2

# HYDROGEN FROM STEP-WISE STEAM REFORMING OF METHANE OVER $Ni/ZrO_2$: FACTORS AFFECTING CATALYTIC METHANE DECOMPOSITION AND GASIFICATION BY STEAM OF CARBON FORMED ON THE CATALYST

## 2.2.1. Earlier Work/Background and Objective of Present Work

The demand for carbon monoxide-free hydrogen required for proton exchanged membrane (PEM) fuel cells is increasing day by day. CO-free $H_2$ can be obtained from the catalytic decomposition of methane. Hence efforts are being made to produce CO-free $H_2$ from low temperature catalytic step-wise steam reforming of methane [1-4] involving the following reactions in consecutive steps:

$$CH_4 \rightleftharpoons C + 2H_2 \quad [1]$$

$$C + 2H_2O \rightleftharpoons CO_2 + 2H_2 \quad [2]$$

In the previous chapter (chapter 2.1), a possibility of the continuous production of $H_2$ at a low temperature (500°C) by carrying out the two reactions simultaneously in two parallel catalytic reactors (containing the same catalyst) operated in cyclic manner has been reported. The cyclic operation was accomplished by switching a methane containing feed (18.2 mol% $CH_4$ in $N_2$) and a steam containing feed (20.5% steam in $N_2$) between the two reactors at a predecided interval of time.

Both the above reactions are thermodynamically favored at higher temperatures. The methane decomposition reaction (reaction 1) is also favored at lower pressure (or at lower concentration) of methane. In the methane decomposition (reaction 1), there is a continuous accumulation of carbon, which is deposited on the catalyst. Hence, the reaction equilibrium is shifted towards the reactant side, putting a more thermodynamic limitation on the forward reaction. Whereas, in case of the gasification by steam of carbon from the catalyst, the products of the gasification are continuously removed from the reaction zone by the incoming gaseous reactant (steam), thus reducing the thermodynamic limitation on the gasification reaction. It is therefore very interesting to study the influence of methane concentration and temperature on the performance of catalytic step-wise steam reforming of methane for producing CO-free $H_2$. The present investigation was undertaken for this purpose. The

methane decomposition over $Ni/ZrO_2$ catalyst followed by the gasification by steam of the carbon formed on the catalyst in the same reactor for the same period and also at the same temperature was carried out at the atmospheric pressure. The influence of methane concentration (2 – 75% $CH_4$ in $N_2$) in the feed and temperature on the methane conversion and pressure drop across the catalyst (due to filamentous carbon formation) in the methane decomposition and also on the degree of carbon removal in the carbon gasification has been investigated for a better understanding of the factors affecting the cyclic process.

### 2.2.2. Experimental

$Ni/ZrO_2$ catalyst (Ni/Zr mole ratio = 1.0) was prepared by the procedure given earlier (section 1.2.1.1). The catalyst was characterized for its surface area and carbon monoxide chemisorption at 40°C (using a GC pulse technique) (section 1.2.2.8 and Fig. 1.2.2).

The surface area of the catalyst before and after reduction (at 600°C for 2h) was found to be 66.9 and 62.7 $m^2g^{-1}$, respectively. The amount of CO-chemisorbed (at 40°C) on the reduced catalyst was 0.16 $mmol.g^{1}$. The catalyst before and after the reduction was also characterized for its relative surface concentration of Ni and Zr by XPS.

The methane decomposition reaction over the catalyst (0.4 g) was carried out in a continuous flow stainless steel fixed bed reactor (i.d. 4.5 mm) kept in a tubular furnace for a time-on-stream of 1h at different reaction conditions (feed = 2 –75 mol% $CH_4$ in $N_2$, temperature = 450 – 600°C, space velocity = 6450 $cm^3g^{-1}h^{-1}$, measured at NTP). The experimental set-up is same as that used in the previous study (section 2.1) and has been described earlier (section 1.2.3.1 and Fig. 1.2.4). The pressure drop across the catalyst bed was measured as a function of the time-on-stream. A small portion of the gaseous product stream was passed through TCD and FID connected in series for continuously analyzing the concentration of $H_2$ (by TCD) and methane (by FID). The gaseous products for the total reaction period (1 h) were also collected in a collapsible plastic bag and then analyzed by GC (with TCD), using a spherocarb column.

For every methane decomposition experiments, a fresh $Ni/ZrO_2$ catalyst (which was pre-reduced in situ by $H_2$ at 600°C for 2h) was used. After each methane

decomposition experiment, the carbon formed on the catalyst was gasified by its reaction with steam by passing a steam-$N_2$ mixture (50 mol% steam at a space velocity of 7740 $cm^3g^{-1}h^{-1}$, measured at NTP) over the catalyst for the same period (1h) and at the same temperature employed in the methane decomposition experiment.

The gasification products, after removing the water by condensation at about 2$^oC$, were collected in a plastic bag and then analyzed for CO, $CO_2$ and $CH_4$ by the GC (with a TCD detector), using a spherocarb column. The formation of methane in the gasification step was found to be negligibly small. No formation of carbon monoxide in the gasification, except at 600$^oC$, was detected; at 600$^oC$ the $CO/CO_2$ ratio in the gasification products was <0.01. In order to determine the amount of carbon remained ungasified in the gasification step, the catalyst after the gasification was oxidized in a flow of air at 600$^oC$ for a sufficiently long period and the $CO_2$ formed in the combustion of the ungasified carbon was measured quantitatively by absorbing it in an aqueous barium hydroxide solution and measuring the $BaCO_3$ formed gravimetrically. The degree of carbon gasification in the gasification step was evaluated as follows:

Degree of gasification (%) = [(A – B)/A] x 100

where, A = the amount of carbon formed in the methane decomposition (which was obtained from the knowledge of the conversion in the methane decomposition) and, B = the amount of carbon retained on the catalyst after the gasification (i.e. ungasified carbon).

In order to study the nature and location of carbon formed in the decomposition step, the catalyst after the decomposition step was characterized by XPS. Since the carbon from the catalyst is not removed completely during the gasification step, the catalyst after the gasification step was also characterized by XPS.

### 2.2.3. Results

#### *2.2.3.1. Effect of methane concentration*

Results showing the effect of methane concentration in the feed on the conversion in the methane decomposition over the $Ni/ZrO_2$ catalyst and also on the pressure drop across the catalyst, depending upon the time-on-stream, are presented in Figs. 2.2.1 and 2.2.2, respectively. Data showing the maximum achievable conversion of methane at the reaction equilibrium for the different $CH_4$ concentrations are also included in Fig. 2.2.1. Whereas, Fig. 2.2.3 shows effect of the methane concentration on the amount of carbon formed on the catalyst in the methane decomposition and also on the carbon gasified in the gasification step after the methane decomposition. Both the methane decomposition and carbon gasification steps were carried out at the same temperature ($500^oC$).

From the above results following important observations can be made:

- The methane decomposition reaction (at $500^oC$) is strongly influenced by the concentration of methane in the feed; lower the concentration, higher is the methane conversion. The observed conversion is much lower than that achievable at the equilibrium (Fig. 2.2.1).

- Depending upon the concentration of methane, an increase in the pressure drop across the catalyst in the methane decomposition step is negligibly small in the initial period (ranging from 10 to 60 min), but it is sharply increased with increasing the time-on-stream. Higher the concentration of methane, lower is the reaction period from which the pressure drop increase starts and also higher is the rate of increase in the pressure drop.

- The removal of carbon in the carbon gasification step is strongly influenced by the methane concentration used in the methane decomposition; higher the methane concentration, lower is the extent of carbon (which is formed in the methane decomposition step) gasified in the gasification step. The extent of carbon gasified is decreased with increasing the amount of carbon present on the catalyst.

### *2.2.3.2. Effect of temperature*

Figure 2.2.4 shows the effect of temperature on both the observed and equilibrium conversion of methane in the methane decomposition for the same methane concentration (14% $CH_4$ in $N_2$) in the feed and space velocity (6450 $cm^3.g^{-1}.h^{-1}$). The variation of pressure drop across the catalyst with the time-on-stream in the methane decomposition at different temperatures is shown in Fig. 2.2.5. Whereas, Fig. 2.2.6 shows the effect of temperature on the amount of carbon formed on the catalyst in the methane decomposition step and also on the extent of carbon gasified in the gasification step. It may be noted that both the methane decomposition and carbon gasification steps were carried out at the same temperature.

The above results show a strong influence of temperature on both the methane decomposition and carbon gasification steps, as follows:

- The observed methane conversion in the decomposition step is sharply increased with increasing the temperature and its increase is consistent with the increase in the equilibrium conversion.

- Upto a time-on-stream of 60, 45, 30 and 20 min for the temperature of 450°, 500°C, 550° and 600°C, respectively, there was no significant change in the pressure drop across the catalyst bed in the methane decomposition step. However, a further increase in the time-on-stream has caused an increase in the pressure drop, depending upon the temperature. Higher the temperature, lower is the time-on-stream for which there is no significant increase in the pressure drop and also higher is the pressure drop increase rate.

- Both the amount of carbon formed in the methane decomposition step and extent of the carbon gasified in the gasification step are increased sharply with increasing the temperature. At 600°C, the extent carbon gasification was close to 100%.

Results in Fig. 2.2.7 show that the formation of carbon upto about 10 $mmol.g^{-1}$ on the catalyst in the methane decomposition at 500°C (for the different methane concentrations) or at the different temperatures (for the same methane concentration, 14% $CH_4$ in $N_2$) causes a negligibly small increase in the pressure drop. However, a

further increase in the carbon formation causes an exponential increase in the pressure drop, depending upon the methane decomposition conditions.

After the carbon gasification in all the cases, the pressure drop across the catalyst is reduced to its initial value (i.e. the pressure drop observed at the start of the methane decomposition step).

#### *2.2.3.3. XPS of the catalysts*

The surface Ni/Zr ratio obtained from the Ni ($2p_{3/2}$) and Zr ($3d_{5/2}$) XPS spectra of the catalyst before and after its reduction (by $H_2$ at $600^oC$ for 2h) and also after the methane decomposition and carbon gasification steps (at $600^oC$) are presented in Table 2.2.1. (The XPS spectra of the above have been shown in Appendices 2.1-2.4).

The surface Ni/Zr atom ratio for the catalyst before the reduction is almost same as its bulk Ni/Zr ratio (1.0). However after the reduction, the surface Ni/Zr ratio is decreased (from 1.02 to 0.45), indicating dissolution of a part of the Ni in the $ZrO_2$. After the methane decomposition (at $600^oC$) over the reduced catalyst, the surface Ni/Zr ratio is further decreased to 0.17. However, after the carbon gasification (at $600^oC$), the surface Ni/Zr ratio is increased from 0.17 to 0.41.

The carbon present on the catalyst after the methane decomposition step and also the one retained on the catalyst after the gasification step were characterized for their $C_{1s}$ XPS spectra. For studying the effect of temperature on the nature or type of carbon present on the catalyst, the methane decomposition followed by the carbon gasification at the same temperature was carried out at two different temperatures ($500^o$ and $600^oC$). The XPS spectra for the catalyst samples obtained at $500^oC$ and $600^oC$ are presented in Figs. 2.2.8 and 2.2.9, respectively. The XPS spectra were deconvoluted.

From the XPS spectra (Figs. 2.2.8 and 2.2.9) following important observations can be made:

- All the XPS spectra show multiple peaks indicating the presence of carbon in different forms.

- The binding energies, 280, 282.4 and 284.9 eV, observed for the carbon formed in the methane decomposition at 500$^{o}$C indicate the presence of carbidic, semi-carbidic/semi-graphitic and graphitic species, respectively; the order of their concentration is semi-carbidic/semi-graphitic > graphitic > carbidic. However, after the carbon gasification at the same temperature, the number of carbon species is increased from 3 to 4. The additional (4$^{th}$) carbon species with the binding energy of 290.1 eV corresponds to carbonate species ($CO_3^{2-}$). The relative concentration of the carbidic (280.2 eV), semi-carbidic/semi-graphitic (283.6 eV) and graphitic (285.3 eV) species is also changed, particularly the concentration of carbidic species relative to that of semi-carbidic/semi-graphitic species is increased appreciably (Fig. 2.2.8).

- In case of the carbon formed in the methane decomposition at 600$^{o}$C, no presence of carbidic species is observed; the observed carbon species are semi-carbidic/semi-graphitic (283.2 eV), graphitic (284.6 eV) and carbonate (289.8 eV) species. However, after the carbon gasification at the same temperature, the carbidic species (279.2 eV) appeared along with the semi-carbidic/semi-graphitic (283.9 eV), graphitic (285.6 eV) and carbonate (289.7 eV) species.

**Table 2.2.1.** XPS Data for the Catalyst before and after Reduction, after Methane Decomposition (at 600$^{o}$C) and also after the Gasification (at 600$^{o}$C)

| Catalyst | Ni ($2p_{3/2}$)/Zr ($3d_{5/2}$) area ratio | Surface Ni/Zr atom ratio |
|---|---|---|
| Before reduction | 2.95 | 1.02 |
| After reduction | 1.30 | 0.45 |
| After the methane decomposition (at 600$^{o}$C) | 0.50 | 0.17 |
| After the carbon gasification (at 600$^{o}$C) | 1.17 | 0.41 |

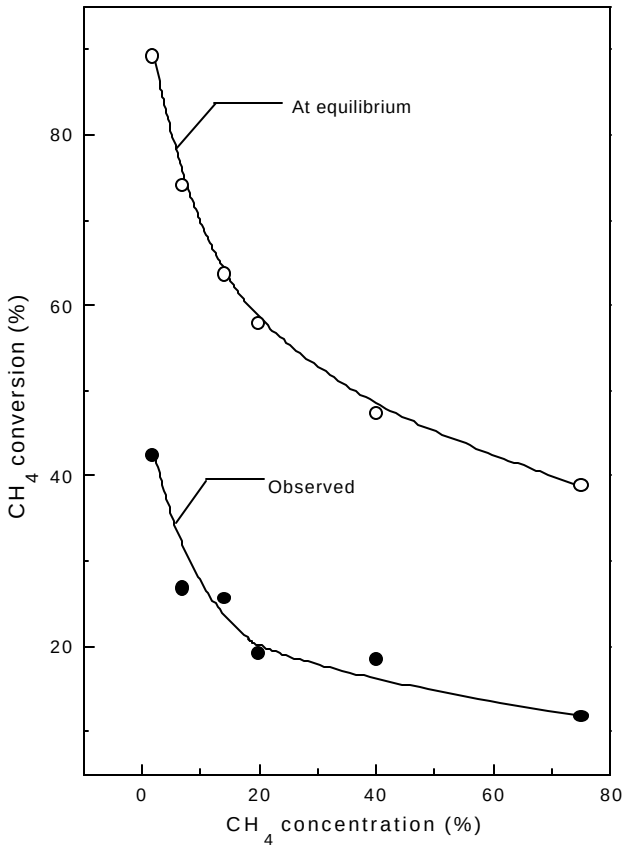


**Figure 2.2.1.** Effect of methane concentration in the feed on the methane conversion in the methane decomposition step at 500°C (space velocity = 6450 $cm^3g^{-1}h^{-1}$).

### 2.2.4. Discussion

In the cyclic process described earlier for the continuous production of $H_2$ from step-wise steam reforming of methane [5], the methane decomposition (reaction 1) and carbon gasification (reaction 2) steps are carried out simultaneously in two parallel catalytic reactors containing the same catalyst at the same temperature by switching the two feeds (one methane containing feed and second steam containing feed) between the two reactors at a predecided interval of time. For a successful operation of the catalytic process, the pressure drop across the catalyst (which is increased because of the formation of filamentous carbon between the catalyst particles in the methane decomposition step) should be as low as possible. The methane decomposition (reaction 1) is thermodynamically favored at higher

temperatures and lower pressures (or concentration of methane). The carbon gasification (reaction 2) is also favored at the higher temperatures (538 – 1038°C) (7). The present investigation was undertaken to know the influence of the methane concentration (in the feed used for the methane decomposition) and temperature on the methane conversion and pressure drop across the catalyst in the methane decomposition step and also on the extent of carbon removed from the catalyst in the carbon gasification step. Immediately after the methane decomposition reaction, the carbon gasification reaction was carried out at the temperature same as that used in the methane decomposition for obtaining the desired information.

The results (Figs. 2.2.1-2.2.6) show that the conversion and pressure drop across the catalyst in the methane decomposition step and also the extent of carbon removal in the gasification step are strongly influenced by both the methane concentration (in the feed) and temperature.

#### *2.2.4.1. Effect of the methane concentration and temperature on the methane conversion*

In the methane decomposition step, the methane conversion is decreased sharply with increasing the methane concentration at the same temperature (500°C). But it is increased very markedly with increasing the temperature for the same methane concentration (14% $CH_4$ in $N_2$). In both the cases, the observed methane conversion is lower than that expected at the reaction equilibrium and also the variation with the methane concentration or temperature of the observed methane conversion is consistent with that of the equilibrium methane conversion (Figs. 2.2.1 and 2.2.4). These observations clearly show that the methane decomposition reaction (at 450° – 600°C) is limited thermodynamically. A very high methane conversion is therefore possible only when the methane concentration in the feed is very low for the reaction at the lower temperature or when the reaction temperature is high enough (≥ 600°C) for the higher concentration of methane in the feed.

In the cyclic process [5], if a highly diluted methane is used as a feed in the methane decomposition, the process economics will be controlled by the cost of separation of the inert diluent from the products, making the process economically not feasible. Hence, it is of great practical importance to use methane without dilution in

the cyclic process. However, because of the limitation imposed by the thermodynamics, the methane decomposition is to be carried out at higher temperatures. Values of the reaction equilibrium constant ($K_p$) and maximum possible methane conversion (i.e. methane conversion at the equilibrium) at different temperatures for the use of undiluted methane in the methane decomposition are given below:

| | | | | | | |
|---|---|---|---|---|---|---|
| Temperature ($^oC$) | : 400 | 500 | 600 | 700 | 800 | 900 |
| $K_p$ | : 0.08 | 0.57 | 2.62 | 8.68 | 23.02 | 51.71 |
| $CH_4$ conversion (at equilibrium) | : 14.0 | 35.3 | 62.9 | 82.7 | 92.3 | 96.3 |

(The detailed calculation has been given in Appendix 2.5).

It may be noted that all the values of methane conversion at the equilibrium were obtained from the equilibrium constant ($K_p$) based on the partial pressure of the reacting species, assuming zero pressure for the carbon species formed and also assuming the carbon is in graphitic form. In the present case only a part of the carbon formed on the catalyst is graphitic one and also the carbon formed in the methane decomposition reaction is accumulated on the catalyst. Hence the estimated values for equilibrium methane conversion are not the real ones, these values, however, provide an idea about the thermodynamic limitation imposed on the methane decomposition reaction.

#### *2.2.4.2. Effect of the methane concentration and temperature on the pressure drop*

The results in Figs. 2.2.2 and 2.2.5 provide information about the initial reaction period during which there is no substantial increase in the pressure drop (due to the carbon formation) across the catalyst in the methane decomposition at the different reaction conditions. This initial reaction period can be considered as the induction period for the increase in the pressure drop due to the formation of carbon between the catalyst particles. The results indicate that the induction period is decreased markedly with increasing the $CH_4$ concentration or the reaction temperature. It is also interesting to note that, after the induction period, the increase in the pressure drop with the time-on-stream is more sharper for the higher methane concentration and also for the higher reaction temperature.

Pressure drop across the catalyst bed is considered as one of the most important process operating parameters to be controlled; the lower pressure drop is preferred in the practice. The induction period observed at the different reaction conditions thus provides an information about the maximum feed switch-over time to be used at a particular set of reaction conditions in the cyclic process [5].

The results in Fig. 2.2.7 indicate that upto the carbon formation of about 10 mmol per gram of the catalyst, the increase in the pressure drop is negligible or very small. However, after a further increase in the carbon formation, the trend for the increase in the pressure drop in the methane decomposition at 500°C is different from that observed at the higher temperatures. This indicates a possibility of formation of carbon in different forms, depending upon the reaction conditions.

#### *2.2.4.3. Effect of temperature on the carbon species formed in the methane decomposition*

A comparison of the $C_{1s}$ spectra of the catalyst after the methane decomposition at 500°C and 600°C (Figs. 2.2.8a and 2.2.9a) shows that (i) the carbidic species are formed at 500°C but not at 600°C, (ii) the concentration of semi-carbidic/semi-graphitic species relative to that of graphitic species is much higher at the lower temperature (500°C), (iii) the carbonate species are observed only at the higher temperature (600°C). At the lower temperature, the formation of semi-carbidic/semi-graphitic species is favored over the formation of both the carbidic and graphitic species. Whereas, at the higher temperature, there is no formation of carbidic species and the formation of graphitic species is favored over the formation of semi-carbidic/semi-graphitic species.

The absence of carbonate species in the catalyst after the methane decomposition at 500°C indicate that the carbonate species observed at the higher temperature cannot be due to chemical absorption of $CO_2$ from the atmosphere, as both the catalyst samples were handled under identical conditions. The presence of carbonate species may therefore be attributed to the formation of small amount of $CO_2$ by reaction between an active carbon species with the lattice oxygen of the catalyst at the higher temperature. The $CO_2$ as soon as formed is expected to be chemisorbed on basic sites of the zirconia. No firm conclusion can however be drawn for the above from this investigation.

### *2.2.4.4. Effect of the methane concentration and temperature on the carbon gasification*

The carbon gasification (at the temperature same as that used in the methane decomposition) is very strongly influenced by both the methane concentration and temperature used in the gasification step (Figs. 2.2.3 and 2.2.6). The degree of carbon gasification is sharply decreased with increasing the methane concentration, but it is increased very markedly with increasing the temperature. Thus the use of higher temperature in the cyclic process is favorable not only for getting higher conversion in the methane decomposition step but also for achieving the higher degree of carbon removal from the catalyst in the gasification step.

Carbon gasification step (reaction 2) is also limited by its thermodynamics; it is increasingly favored at the higher temperature. The estimated values of $K_p$ and carbon conversion at the reaction equilibrium (estimated assuming carbon in graphitic form) at the different temperatures are as follows:

| | | | | | |
|---|---|---|---|---|---|
| Temperature ($^oC$) | : | 500 | 600 | 700 | 800 |
| $K_p$ | : | 0.258 | 0.825 | 2.56 | 7.94 |
| Carbon conversion (%): | | 43.6 | 61.9 | 75.2 | 83.7 |

(The detailed calculation procedure has been shown in Appendix 2.6). However, in the present carbon gasification step, the reaction products are removed continuously and hence the reaction equilibrium is shifted towards the side of the products. Moreover a part of the carbon formed on the catalyst is non-graphitic one, which is easier to gasify by steam. Hence, the observed degree of carbon gasification (Fig. 2.2.2b) is higher than that estimated for the reaction equilibrium. Nevertheless, the observed degree of carbon gasification is increased with increasing the temperature as expected from the reaction thermodynamics.

No formation of carbon monoxide was detected in the gasification reaction at or below $550^oC$. However, a small amount of CO formation relative to $CO_2$ formation was observed at $600^oC$. According to the reverse water-gas shift reaction,

$$CO_2 + H_2 \rightleftharpoons CO + H_2O \qquad [3]$$

which favors at higher temperatures, a substantial amount of CO formation is expected even at the lower temperatures ($\leq 550^oC$) [$K_p$ (for reaction-3) $\approx$ 0.13 ($450^oC$), 0.20 ($500^oC$), 0.28 ($550^oC$) and 0.38 ($600^oC$)] [7]. The failure to detect the

CO formation in significant amounts in the gasification, particularly at the lower temperatures (≤ 550°C) may be attributed to the CO disproportionation reaction (called Boudouard reaction),

$$2\,CO \rightleftharpoons C + CO_2 \qquad [4]$$

and/or CO hydrogenation reaction,

$$CO + H_2 \rightleftharpoons C + H_2O \qquad [5]$$

Both the above reactions are favored at the lower temperatures and are catalyzed by the nickel [7]

. (The free energy change of some chemical reactions involving CO, $CO_2$, $H_2$ and $H_2O$ at different temperature has been supplied in Appendix 2.7).

It is interesting to note that, after the carbon gasification, the relative concentration of the different carbon species (viz. carbidic, semi-carbidic/semi-graphitic, graphitic and carbonate species) on the catalyst is drastically changed (Figs. 2.2.8 and 2.2.9). After the gasification at 550°C, the concentration of carbidic species relative to that of semi-carbidic/semi-graphitic or graphitic species is increased. Whereas, after the gasification at 600°C, the carbidic species, which were absent before the gasification, make their presence very significantly in the carbon retained on the catalyst. This may be attributed to the formation of carbidic species by the Boudouard and/or CO-hydrogenation reactions (reaction 4 and 5) in the gasification step. The presence of carbonate species after the gasification at both the temperatures is attributed to the reaction of $CO_2$ (formed in the gasification) with the basic surface hydroxide groups of the zirconia from the catalyst.

#### *2.2.4.5. Location of carbon formed on the catalyst*

The XPS results (Table 2.2.1) reveal that the surface Ni/Zr ratio of the catalyst is drastically reduced after the methane decomposition. After the carbon gasification, the surface Ni/Zr ratio is increased, approaching close to its initial value. These observations show that a very large part of the Ni surface is covered by the carbon formed in the methane decomposition. From this study, it is, however, not possible to discard the presence of carbon on the $ZrO_2$ of the catalyst. However, if it is present, it is expected to be much smaller than that on the Ni.

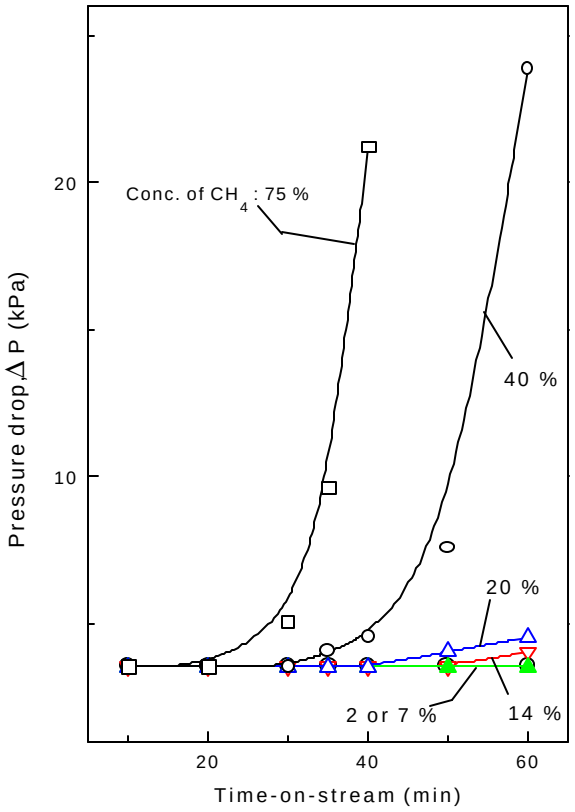


**Figure 2.2.2.** Variation of pressure drop across the catalyst with time-on-stream in the methane decomposition for the feed containing methane at different concentrations (at 500$^{o}$C and space velocity = 6450 $cm^3g^{-1}h^{-1}$).

It is interesting to note from the results in Fig. 2.2.7 that, upto a certain amount of carbon formed on the catalyst in the methane decomposition, there was no significant increase in the pressure drop across the catalyst. However, a further build-up of the carbon causes an exponential increase in the pressure drop, depending upon the process conditions. This observation indicates that the carbon formation in the initial methane decomposition period (Figs. 2.2.2 and 2.2.4) occurs on the internal surface of the catalyst and the carbon formed is mainly non-filamental type. However, at the higher methane decomposition periods, after the build-up of carbon above about 10 $mmol.g^{-1}$, the further carbon build-up occurs most probably by the formation of filamentous carbon on the external surface of the catalyst particles, gradually reducing the inter-particle space/voids. Very recently, Ermakova [8] have demonstrated that in the methane decomposition over a Fe-based catalyst, filamentous carbon does not

form below 680°C. However, the formation of filamentous carbon in the methane decomposition over Ni-catalyst even at the lower temperature (550°C) was observed earlier [1].

#### *2.2.4.6. Comments on the use of undiluted methane in the cyclic process*

As mentioned earlier, practically it is more important to use undiluted methane as a feed in the methane decomposition step. From the above discussion, it is clear that, for using the undiluted methane, the cyclic process must be operated at the higher temperature (≥ 600°C) to achieve methane conversion of practical interest and also to achieve a very high degree of carbon removal so as to make the cyclic operation of the process technically feasible. However, at the higher temperature operation, a significant amount of CO is also expected to be formed in the gasification step. Hence in order to produce CO-free $H_2$ continuously by the cyclic process operated at the higher temperature (≥ 600°C), the product streams received from the two steps are to be collected/processed separately (as shown in Fig. 1.2.5). The high temperature cyclic process would provide a continuous production of CO-free hydrogen from the methane decomposition step. Preliminary results for the operation of such a cyclic process for 1h at 600°C using pure methane (without any dilution) as a feed (space velocity = 3280 $cm^3g^{-1}h^{-1}$) for the decomposition step and using 80% steam in $N_2$ as a feed (space velocity = 8360 $cm^3g^{-1}h^{-1}$) for the gasification step and switching the two feeds between the two parallel reactors (each containing the $Ni/ZrO_2$ catalyst) and also switching the two product streams between the two gas collectors/product processing units simultaneously at an interval of 5 min (as shown in Fig. 2.2.10) are as follows: The methane decomposition step provided a continuous production of CO-free $H_2$ at a methane conversion of 45.4%. In the carbon gasification step, the $CO/CO_2$ ratio in the product was 0.1. These preliminary results show a high promise for the high temperature cyclic process for the production of CO-free $H_2$ from the methane decomposition step.

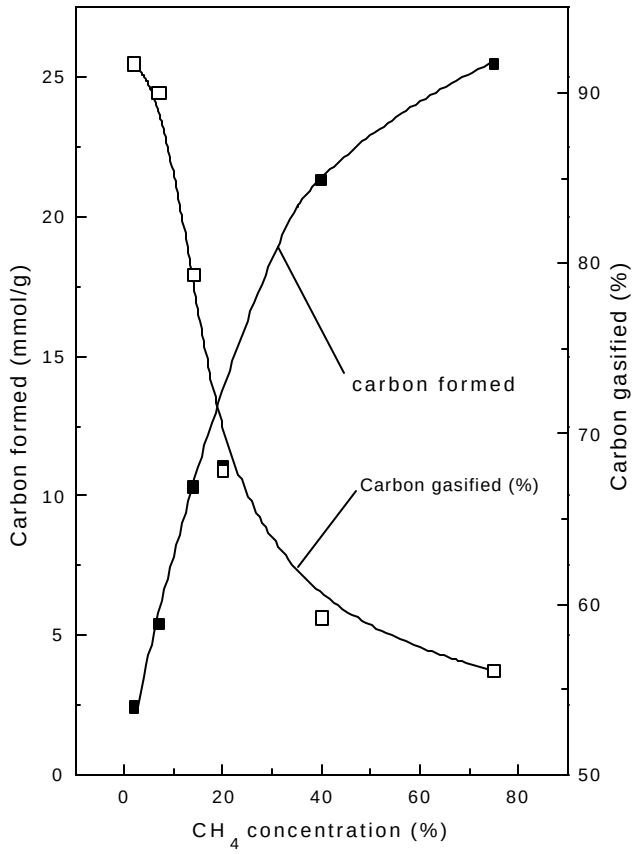


**Figure 2.2.3.** Effect of methane concentration in the feed used in the methane decomposition at 500°C (space velocity = 6450 $cm^3g^{-1}h^{-1}$) on a) the amount of carbon formed in the decomposition step and b) the extent of carbon gasified in the gasification step at 500°C (feed=50% steam in $N_2$ and space velocity=7740 $cm^3g^{-1}h^{-1}$)

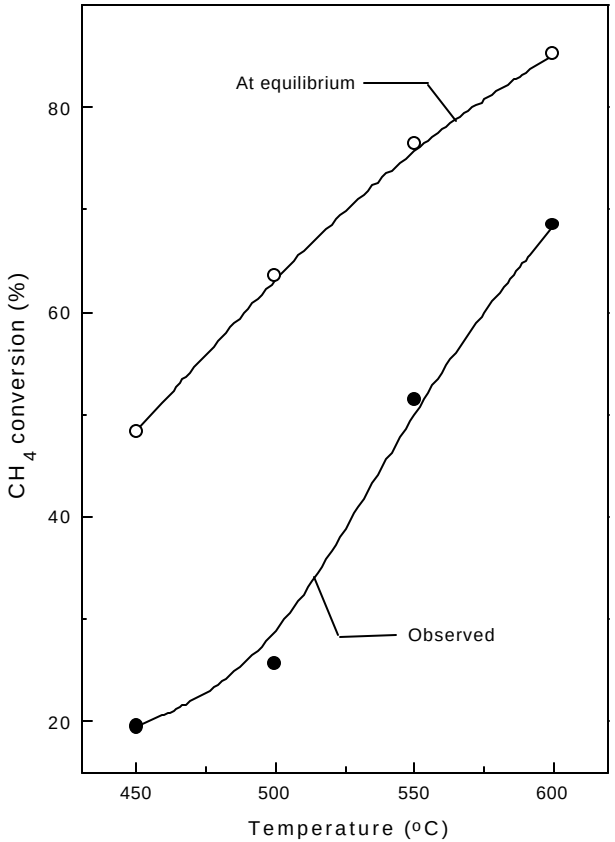


**Figure 2.2.4.** Effect of temperature on the methane conversion in the methane decomposition step (feed = 14% $CH_4$ in $N_2$ and space velocity = 6450 $cm^3g^{-1}h^{-1}$).

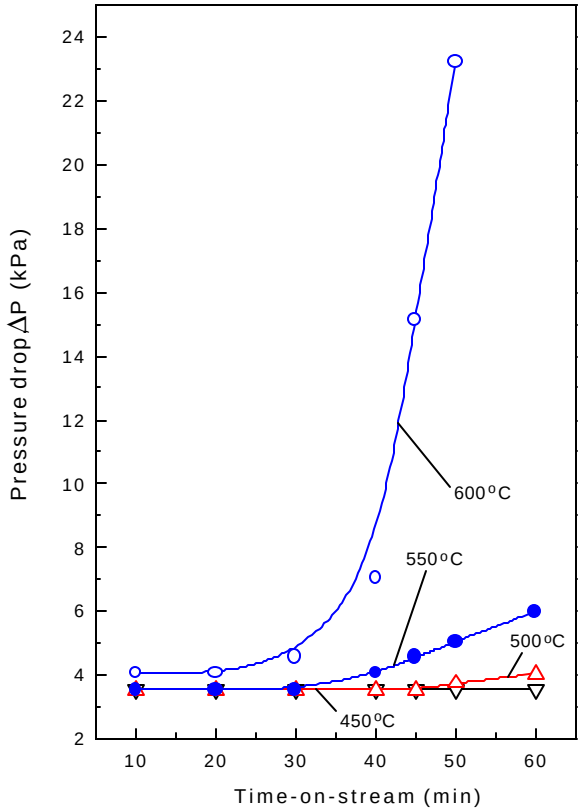


**Figure 2.2.5.** Variation of pressure drop across the catalyst with time-on-stream in the methane decomposition (feed = 14% $CH_4$ in $N_2$ and space velocity = 6450 $cm^3g^{-1}h^{-1}$) at different temperatures.

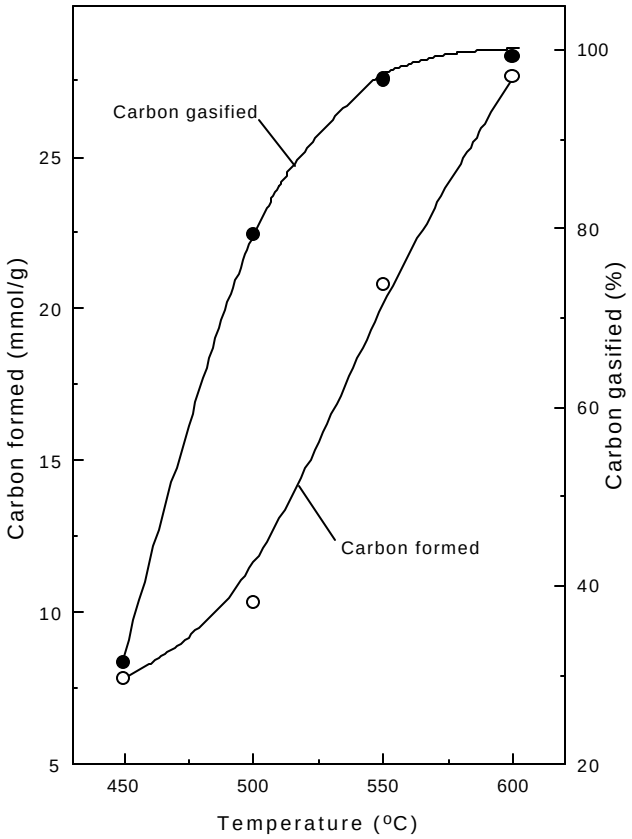


**Figure 2.2.6.** Effect of temperature on (a) the amount of carbon formed in the methane decomposition step (feed = 14% $CH_4$ in $N_2$ and space velocity = 6450 $cm^3g^{-1}h^{-1}$) and (b) the extent of carbon gasified in the gasification step (feed = 50% steam in $N_2$ and space velocity = 7740 $cm^3g^{-1}h^{-1}$).

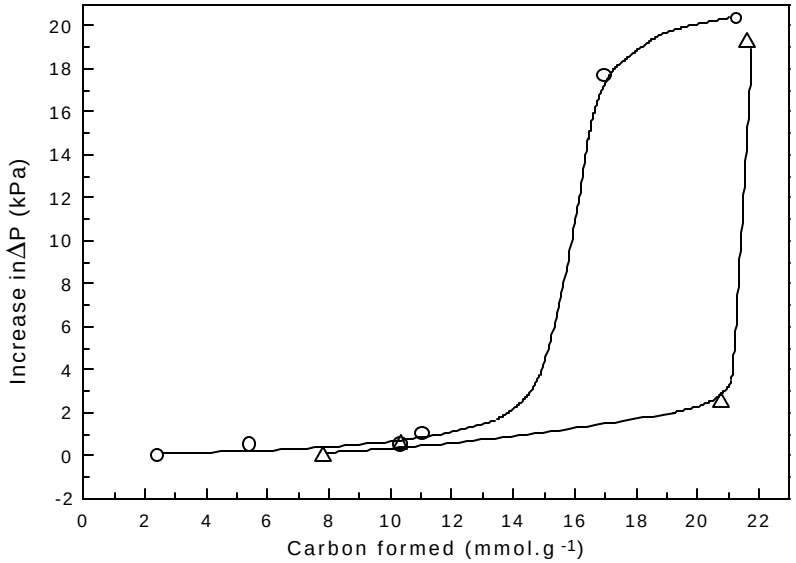


**Figure 2.2.7.** Increase in the pressure drop (ΔP) across the catalyst vs. amount of carbon formed on the catalyst in the methane decomposition [Δ - data for different concentration of methane in feed at 500°C and ○ - data for different temperature using a feed of 14% $CH_4$ in $N_2$]

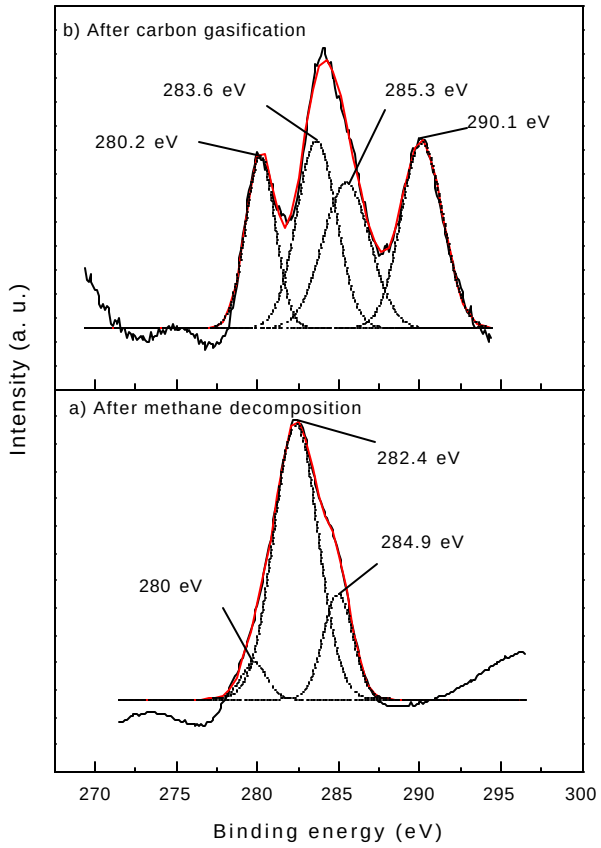


**Figure 2.2.8.** XPS $C_{1s}$ spectra (a) for the carbon formed on the catalyst in the methane decomposition at 500°C and (b) for the carbon retained on the catalyst after the gasification at 500°C.

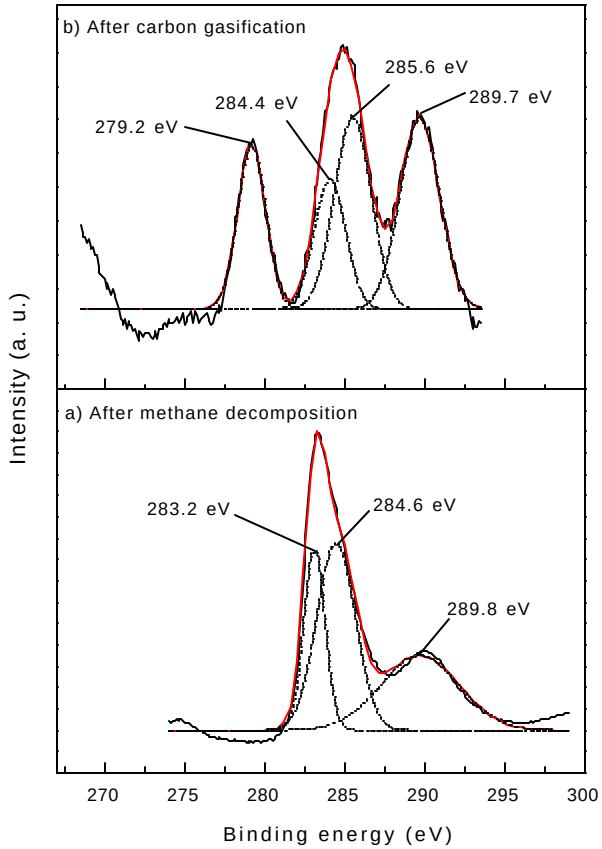


**Figure 2.2.9.** XPS $C_{1s}$ spectra (a) for the carbon formed on the catalyst in the methane decomposition at 600°C and (b) for the carbon retained on the catalyst after the gasification at 600°C.

### 2.2.5. Conclusions

From the present studies on the low temperature step-wise steam reforming of methane to hydrogen, involving the methane decomposition reaction over $Ni/ZrO_2$ (for different methane concentrations at $500^oC$ or for the same methane concentration at different temperatures), followed by the gasification of carbon from the catalyst by steam at the same temperature, following important conclusions have been drawn:

1. Both the methane conversion and degree of carbon gasification are decreased sharply with increasing the methane concentration. However, the two are increased sharply with increasing the temperature. For using undiluted methane as a feed in the cyclic process, involving the two reactions in consecutive steps, the process needs to be carried out at a higher temperature ($\geq 600^oC$).

2. At the higher temperature, a significant amount of CO is formed in the carbon gasification step. Hence, in the cyclic process operated at the higher temperature, CO-free $H_2$ can be produced only in the methane decomposition step. Thus for producing CO-free $H_2$ by the high temperature cyclic process, the product streams of the two steps must be processed separately.

3. For the pressure drop increase across the catalyst due to carbon formation in the methane decomposition, there is an induction period, which is strongly influenced by both the methane concentration and reaction temperature. After the induction period, the pressure drop is increased exponentially with increasing the carbon formation, depending upon the methane concentration and/or reaction temperature; higher the concentration or temperature, sharper is the pressure drop rise.

4. The relative concentration of the different carbon species (viz. carbidic, semi-carbidic/semi-graphitic, graphitic and carbonate species) formed on the catalyst in the methane decomposition is strongly influenced by the reaction temperature. After the carbon gasification, the relative concentration of the carbon species is changed very substantially. In the methane decomposition, an appreciable part of the Ni surface is covered by the carbon. However, after the gasification, the Ni surface is cleared off the carbon.

### 2.2.6. References


1. T. Zhang and M. D. Amiridis, Appl. Catal.A. 167 (1998) 161.
2. T. V. Choudhary and D. W. Goodman, Catal. Lett. 59 (1999) 93.
3. T. V. Choudhary and D. W. Goodman, J. Catal. 192 (2000) 316.
4. L. B. Avdeeva, D. I. Kochubey and Sh. K. Shaikhutdinov, Appl. Catal. A: Gen. 177 (1999) 43.
5. V. R. Choudhary, S. Banerjee and A. M. Rajput, J. Catal. 198 (2001) 136.
6. D. Panjala, N. Shah and G. P. Hoffman, Prepr.-Am. Chem. Soc. Fuel Chem. Div. 46 (2001) 18.
7. H. F. Rase, "Handbook of Commercial Catalysts: heterogeneous Catalysts", pp 403. CRC Press, USA, 2000.
8. M. A. Ermakova, D. Y. Ermakov, A. L. Chuvilin and G. G. Kuvshinov, J. Catal. 201 (2001) 183.

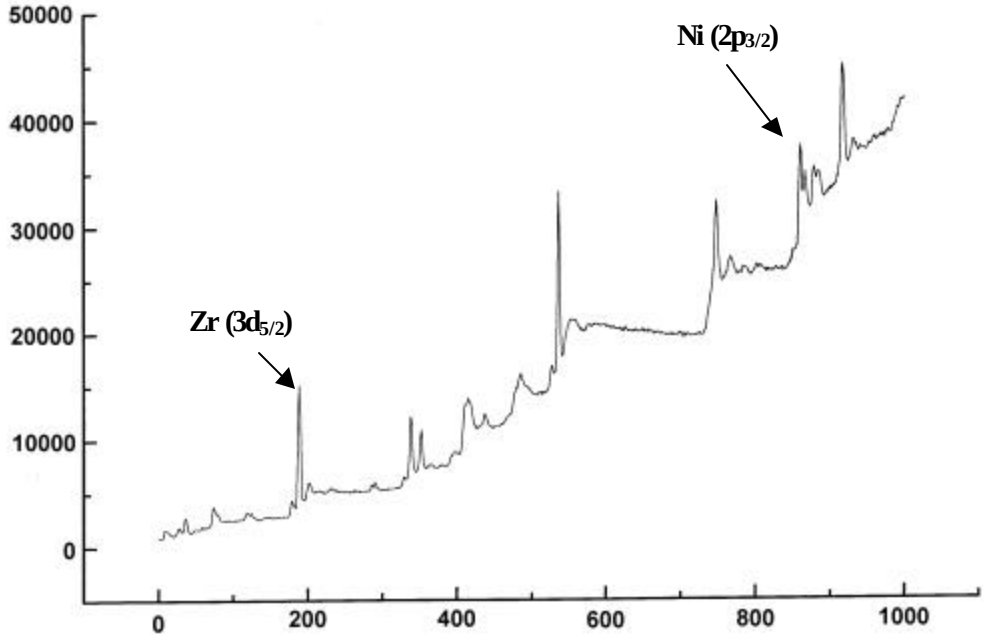


**Appendix 2.1.** XPS spectra of $Ni/ZrO_2$ calcined at 600°C for 2h (as synthesized)

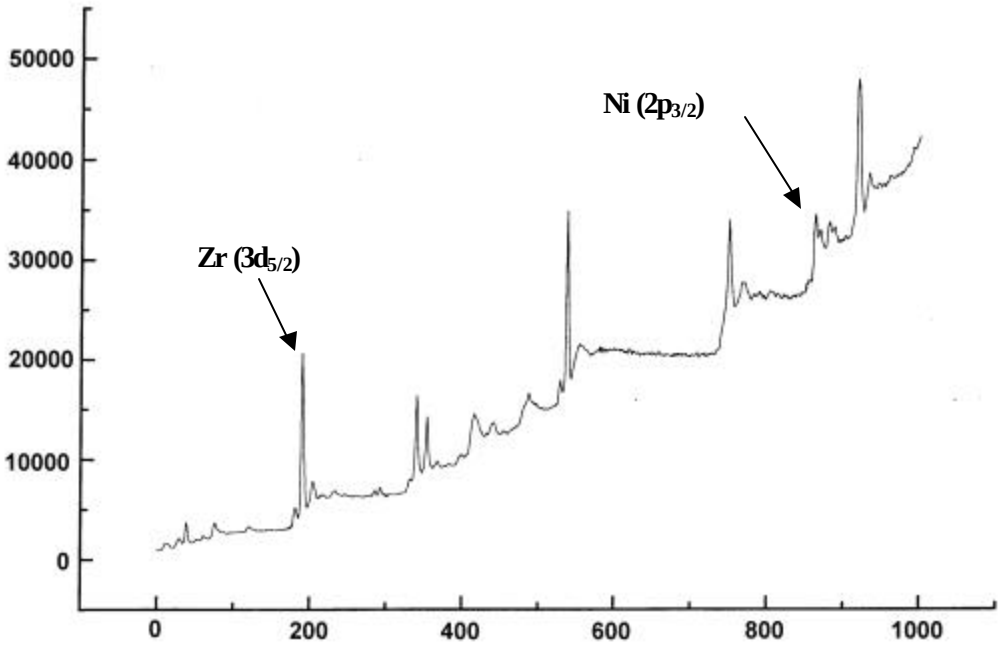


**Appendix 2.2.** XPS spectra of $Ni/ZrO_2$ after reduction at 600°C for 2h

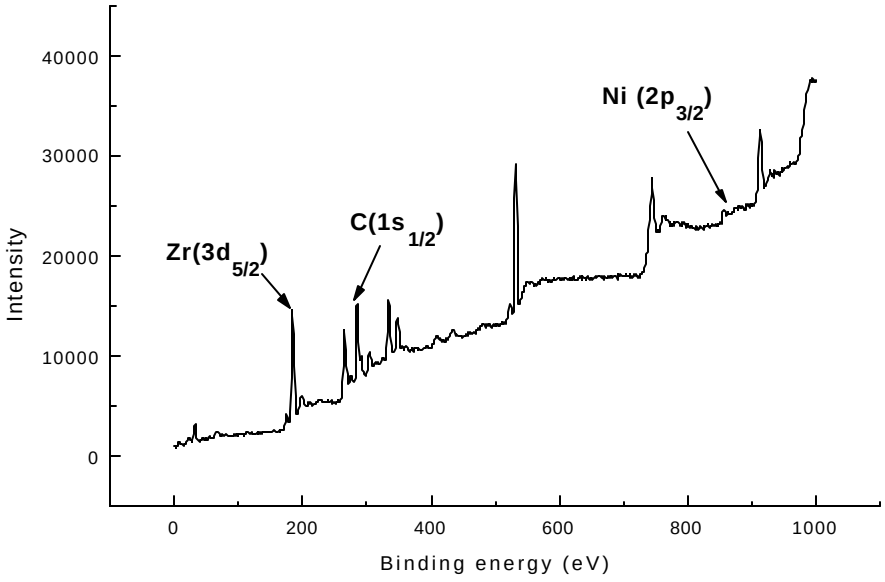


**Appendix 2.3.** XPS spectra of $Ni/ZrO_2$ after $CH_4$ decomposition at 600°C

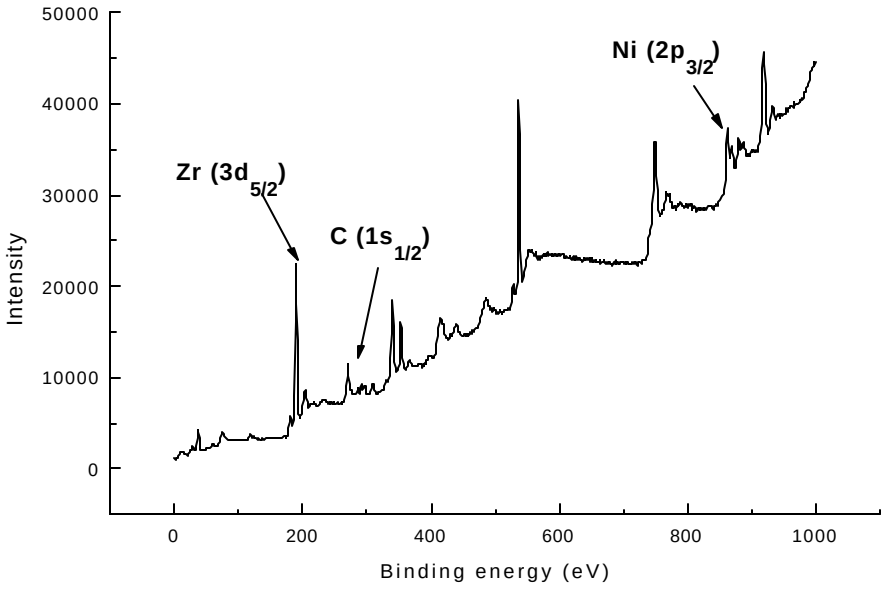


**Appendix 2.4.** XPS spectra of $Ni/ZrO_2$ after gasification of carbon by steam at 600°C

**Appendix 2.5:** Some thermodynamic calculations for determining equilibrium constant ($K_p$) and equilibrium conversion of some chemical reactions.

Reaction: $CH_4 \rightleftharpoons C_{(s)} + 2H_2$ (1)

Equilibrium constant, $K_p = P_{H2}^2 / P_{CH4}$ (i) [where, $P_{H2}$ = partial pressure of hydrogen at equilibrium and $P_{CH4}$ = partial pressure of methane at equilibrium]

But, $P_{H2} = [2x/(1+x)] * P$ and $P_{CH4} = [(1-x)/(1+x)]*P$, where x = extent of the conversion and P = total pressure (= 1 atm.)

So, the equation (i) becomes,

$x = [K_p/(K_p +4)]^{1/2}$ and also we know that $K_p = e^{-\Delta G/RT}$ ($\Delta G$ is the free energy change for the reaction at a particular temperature)

So, knowing the value of $K_p$ (using the standard $\Delta G$ value), one can calculate the extent of reaction at equilibrium and the equilibrium conversion of the reaction.

Below the free energy change ($\Delta G$) of reaction – 1, $K_p$, x and equilibrium conversion for reaction-1 has been presented in a tabular form as a function of temperature.

| Temperature ($^oC$) | Free energy change ($\Delta G$), J/mol | $K_p$ | x | Equilibrium conversion (%) |
|---|---|---|---|---|
| 400 | 14092 | 0.0811 | 0.14 | 14.1 |
| 500 | 3600 | 0.5710 | 0.35 | 35.3 |
| 600 | -6980 | 2.62 | 0.629 | 62.9 |
| 700 | -17480 | 8.68 | 0.827 | 82.7 |
| 800 | -27980 | 23.02 | 0.923 | 92.3 |
| 900 | -38480 | 51.71 | 0.963 | 96.3 |

**Appendix 2.6:** Some thermodynamic calculations for determining equilibrium constant ($K_p$) and equilibrium conversion of some chemical reactions.

Reaction: $C_{(s)} + 2H_2O \rightleftharpoons CO_2 + 2H_2$ (2)

Equilibrium constant, $K_p = [(P_{CO2} * P_{H2}^2) / P_{H2O}^2]$ (ii) [where, $P_{CO2}$, $P_{H2}$ and $P_{H2O}$ are the partial pressure of carbon dioxide, hydrogen and steam, respectively, at equilibrium]

But, $P_{H2} = [2x/(2+x)] * P$; $P_{CO2} = [x/(2+x)]*P$ and $P_{H2O} = [(2-2x)/(2+x)]*P$, where x = extent of the conversion and P = total pressure (= 1 atm.)

So, the equation (ii) becomes,

$K_p = [x^3/(2 - 3x + x^3)]$ and also we know that $K_p = e^{-\Delta G/RT}$ ($\Delta G$ is the free energy change for the reaction at a particular temperature)

So, knowing the value of $K_p$ (using the standard $\Delta G$ value), one can calculate the extent of reaction at equilibrium and the equilibrium conversion of the reaction.

Below the free energy change ($\Delta G$) of reaction – 1, $K_p$, x and equilibrium conversion for reaction-2 has been presented in a tabular form as a function of temperature.

| Temperature ($^oC$) | Free energy change ($\Delta G$), kJ/mol | $K_p$ | x | Equilibrium conversion (%) |
|---|---|---|---|---|
| 527 | 11.444 | 0.179 | 0.49 | 49.0 |
| 627 | 0.458 | 0.941 | 0.66 | 66.1 |
| 727 | -10.659 | 3.60 | 0.78 | 78.0 |
| 827 | -21.88 | 10.85 | 0.85 | 85.0 |

**Appendix 2.7 :** Free energy changes ($\Delta G_r$) in some reactions at different temperatures

| Reactions | Free energy change ($\Delta G_r$), kJ.mol$^{-1}$ | | | | | | |
|---|---|---|---|---|---|---|---|
| | 327°C | 427°C | 527°C | 627°C | 727°C | 827°C | 927°C |
| $2\,CO \rightleftharpoons CO_2 + C$ | - 66.192 | -48.341 | -30.57 | -12.89 | +4.697 | +22.184 | +39.499 |
| $CO + H_2 \rightleftharpoons C + H_2O$ | -49.528 | -35.301 | -21.007 | -6.674 | +7.678 | +22.032 | +36.379 |
| $CO + H_2O \rightleftharpoons CO_2 + H_2$ | -16.664 | -13.04 | -9.563 | -6.216 | -2.981 | +0.152 | +3.12 |
| $C + 2\,H_2O \rightleftharpoons CO_2 + 2H_2$ | +32.864 | +22.261 | +11.444 | +0.458 | -10.659 | -21.88 | -33.259 |
| $C + H_2O \rightleftharpoons CO + H_2$ | +49.528 | +35.301 | +21.007 | +6.674 | -7.678 | -22.032 | -36.379 |

# PART - III

## AROMATIZATION OF LOWER OLEFINS

**CHAPTER 3.1: AROMATIZATION OF DILUTE ETHYLENE OVER Ga-MODIFIED ZSM-5 TYPE ZEOLITE CATALYST**

**CHAPTER 3.2: INFLUENCE OF TEMPERATURE AND SPACE VELOCITY ON THE PRODUCT SELECTIVITY AND DISTRIBUTION OF AROMATICS AND $C_8$ AROMATIC ISOMERS IN THE CONVERSION OF DILUTE ETHYLENE OVER H-GALLOALUMINOSILICATE (ZSM-5 TYPE) ZEOLITE**

**CHAPTER 3.3: AROMATIZATION OF PROPENE AND n-BUTENE OVER H- GALLOALUMINOSILICATE (ZSM-5 TYPE) ZEOLITE CATALYST**

# CHAPTER 3.1

# AROMATIZATION OF DILUTE ETHYLENE OVER Ga-MODIFIED ZSM-5 TYPE ZEOLITE CATALYSTS

## 3.1.1. Earlier Work/Background and Objectives of Present Work

Oxidative coupling of methane (OCM) to ethane and ethylene has been widely investigated catalytic process for the past 15 years [1,2]. This process is of great practical importance for the effective utilization of natural gas by the conversion of methane, which is most inert among the hydrocarbons, into value added products, such as ethylene and higher hydrocarbons. However, one of the serious limitations of the OCM process is the very high cost of the separation of ethylene at very low concentrations (about 5 mole%) from the product stream of the process. The available literatures which addresses this problem has been reviewed in the earlier chapter (section 1.1.2). One promising way to overcome this limitation of the OCM process is to convert directly the dilute ethylene present in the OCM product streams into much less volatile products, such as aromatics and/or gasoline range hydrocarbons, which can be easily separated [3,4,5]. Hence, there is a great need of a highly active and selective ethylene aromatization catalyst useful for converting ethylene at very low concentrations or partial pressures into aromatics and other liquid hydrocarbons.

Available literatures which have reported the aromatization of ethylene over H-ZSM-5 [6,7,8], ZSM-5 zeolite impregnated with oxides of zinc [9,10], copper [11] or gallium [12,13] and H-ferrisilicate zeolite [14] have already been reviewed (section 1.1.2). A very recent study [12] showed that Ga/H-ZSM-5 is an effective catalyst for the conversion of dilute ethylene into aromatics at 500°-550°C. Zn- or Ga-oxide containing H-ZSM-5 catalysts showed much better performance and on-stream stability than the parent zeolite [10]. Unlike Ga/H-ZSM-5 zeolite catalyst, in case of pentasil H-gallosilicate (H-GaMFI) and H-galloaluminosilicate (H-GaAlMFI) zeolites, their non-framework Ga-oxide species are formed due to degalliation of the framework gallium and hence, the Ga-oxide species are distributed uniformly in the zeolite channels. It is, therefore, very interesting to study the aromatization of ethylene at low concentration over H-GaMFI and H-GaAlMFI.

The present investigation was, therefore, undertaken for investigating thoroughly the aromatization of dilute ethylene (5 mole% in nitrogen) at atmospheric

pressure and 400°C over H-ZSM-5, Ga/H-ZSM-5 with different Ga loading, H-GaMFI and H-GaAlMFI (with different Si/Al and Si/Ga ratios) at different space velocities. The catalysts have been compared for their performance (viz. activity, selectivity and product distribution) in the ethylene aromatization.

### 3.1.2 Experimental

H-GaMFI (Si/Ga=30.1), H-GaAlMFI (Si/Ga=15.3 - 46.6 and Si/Al=17.7 - 49.6), ZSM-5 (Si/Al=35.0) zeolites have been synthesized by their hydrothermal crystallization from a gel consisting of Na-trisilicate (Fluka), gallium nitrate (Aldrich) and/or aluminum nitrate (BDH), TPA-Br (Aldrich), sulfuric acid and demineralized water in a stainless steel autoclave. The detailed procedure of the synthesis of different types of zeolites has been already described in the earlier section (section 1.2.1.2).

The MFI structure of the zeolite was confirmed by XRD and FTIR. The incorporation of Ga in the framework of GaMFI and GaAlMFI was confirmed by the $^{71}$Ga MAS NMR peak at +156 ppm. The framework (FW) Si/Ga and Si/Al ratios were obtained from the $^{29}$Si MAS NMR peaks, Si (0Ga or Al) at about -112 ppm and Si (1Ga or Al) at about -104 ppm by the method described earlier [15]. The $^{71}$Ga, $^{29}$Si and $^{27}$Al MAS NMR was obtained using Bruker MSL 300MHz NMR instrument. The crystal size and morphology of the zeolite was studied by SEM (using JOEL Scanning Electron Microscope). The zeolite bulk chemical composition was determined by the chemical analysis of Ga, Al, Si and Na. Strong acid sites of the zeolite were measured in terms of the pyridine chemisorbed at 400°C, using the GC adsorption/desorption method [16], as has been described previously (section 1.2.2.5).

Ethylene aromatization reaction over the catalysts was carried out at 400°C and atmospheric pressure, in a continuous flow quartz reactor (13mm i.d.) (Fig. 1.2.1a) provided with a Chromel-Alumel thermocouple in the center of the catalyst bed (containing 0.2g zeolite catalyst diluted uniformly by an inert solid, the total volume being 1ml), using a ethylene-nitrogen mixture (5 mole% ethylene) as feed. The conversion and selectivity data (at 400°C) at different space velocities (3,100 – 24,600 $cm^3g^{-1}h^{-1}$), measured at 0°C and 1 atm pressure in the absence of catalyst deactivation, were obtained by a square pulse technique by passing the reaction mixture over a fresh catalyst bed for a short period (2-5 min) under steady state condition and then replacing the reactant mixture by a stream of pure $N_2$ during the

period of product analysis. At the end of the square pulse, the reaction products were sampled using a heated gas sampling valve and analyzed by a GC with FID, using Porapak-Q (3mm X 3m), Benton-34 (5%) and dinonylphthalate (5%) on Chromosorb-W (3mm X 5m) columns. The reaction set-up used for the ethylene aromatization has been shown schematically in Fig. 1.2.6 and described in earlier section (section 1.2.3.2). The absence of catalyst deactivation in the step pulse experiments was confirmed by repeating the first experiment.

The ethylene aromatization (at 400°C and GHSV = 3100 $cm^3g^{-1}h^{-1}$) over all the zeolite catalysts which were pre-poisoned by pyridine (by its chemisorption at 400°C) was also studied as above.

### 3.1.3. Results

#### *3.1.3.1. Catalyst characterization*

The Ga-modified ZSM-5 type catalysts were characterized for their bulk and framework compositions, crystal size and morphology, concentration of non-framework (non-FW) Ga-oxide species in their channels and also for their strong acid sites, measured in terms of the pyridine chemisorbed on them at 400°C. The catalyst characterization data are presented in Table 3.1.1. The Na/(Al and/or Ga) ratio in all the zeolites was from 0.01 to 0.03.

A comparison of the bulk and framework (FW) composition of the H-GaMFI and H-GaAlMFI (I - III) zeolites shows the presence of appreciable amounts of non-FW Ga in their channels. The FW Si/Al (for ZSM-5), Si/Ga (for GaMFI) and Si/(Ga+Al) (for GaAlMFI) ratios were determined from the $^{29}$Si-MAS NMR. However, for the GaAlMFI zeolites, their individual FW Si/Al and Si/Ga ratios were estimated from the FW Si/(Ga+Al), octahedral (non-FW) Al, determined from $^{27}$Al MAS NMR, and bulk concentration of Al in the respective zeolite. It may be noted that the T-sites of ZSM-5 type zeolites are not crystallographically identical and hence, the determination of FW Si/Ga and Si/Al ratios from $^{29}$Si MAS NMR is not very accurate [17].

The Ga(4.7)/H-ZSM-5 and H-GaAlMFI (II) zeolites have nearly the same bulk compositions and FW Si/Al ratio. However, all the catalysts differ markedly in their strong acidity and non-FW Ga.

### *3.1.3.2. Ethylene aromatization*

The aromatization of dilute ethylene (5 mole% ethylene in $N_2$) over the different zeolite catalysts was studied under steady state using a square pulse technique in a continuous flow reactor at 400°C but at different space velocities. The ethylene conversion and product selectivity data at different space velocities for the ethylene aromatization over the different catalysts are presented in Figs. 3.1.1-3.1.3. The distribution of aromatics and also of xylenes in the ethylene aromatization over the different catalysts at the different space velocities is presented in Figs. 3.1.4 - 3.1.6 and Figs. 3.1.7 – 3.1.9, respectively. The data is also presented in Appendices 3.1-3.7. The catalysts are compared for their activity, product selectivity, aromatics distribution and shape selectivity (p-X/m-X product ratio) at the ethylene iso-conversion (60% and 90%) in Table 3.1.2.

The results in Figs. 3.1.1-3.1.3 show following general trends for the selectivity of different products formed in the ethylene aromatization over the different zeolite catalysts with increasing the GHSV:

- For all the catalysts, the aromatics selectivity is decreased markedly; the decrease in case of the H-GaAlMFI (II) is, however, much smaller.
- For all the catalysts the selectivity for propylene is increased markedly.
- The propane and $C_{4+}$ hydrocarbons selectivity trends differ from catalyst to catalyst. For example, the propane selectivity is almost unchanged for the H-GaAlMFI (I - III), but it is increased fast for the H-ZSM-5 and Ga(4.7)/H-ZSM-5 and decreased slowly for the H-GaMFI and Ga(1.4)/H-ZSM-5. The selectivity for $C_{4+}$ hydrocarbons remains almost unchanged for the Ga(1.4)/H-ZSM-5. It shows an appreciable decrease for the H-ZSM-5 and Ga(4.7)/H-ZSM-5. But it shows a small increase for H-GaMFI and an appreciable increase for the H-GaAlMFI (I - III).

The results in Figs. 3.1.4 – 3.1.6 indicate that the catalysts do not follow general trends for the formation of the different aromatics (viz. benzene, toluene, $C_8$ and $C_{9+}$ aromatics) in the ethylene aromatization over them. The trends of the formation of the different aromatics over the catalysts with increasing the space velocity are summarized in Table 3.1.3. The order of the formation of the different aromatic hydrocarbons for all the catalysts is in general the same ($C_8$ aromatics >

toluene > $C_{9+}$ aromatics > benzene) except at very low and/or very high space velocity for some catalysts (Figs. 3.1.4 – 3.1.6). In all the cases, the concentration of ethyl benzene in the $C_8$-aromatics was quite small (< 10%).

The results in Figs. 3.1.7-3.1.9 show that for all the catalysts, the concentration of p-X, m-X and o-X in the xylenes formed in the ethylene aromatization is increased, decreased and increased, respectively, very markedly with increasing the space velocity. The order for the formation of different xylene isomers for most of the catalysts depends strongly on the space velocity, as follows:

| | |
|---|---|
| H-ZSM-5 | : p-X > m-X > o-X (at all GHSV) |
| H-GaMFI | : m-X > p-X > o-X (at low GHSV); |
| | p-X > m-X > o-X (at high GHSV) |
| Ga(1.4)/H-ZSM-5 | : m-X > p-X > o-X (at low GHSV) |
| | p-X > o-X > m-X (at high GHSV) |
| Ga(4.7)/H-ZSM-5 | : p-X ≥ m-X > o-X (at low GHSV) |
| | p-X > o-X > m-X (at high GHSV) |
| H-GaAlMFI (I) | : m-X > p-X > o-X (at all GHSV) |
| H-GaAlMFI (II) | : m-X > p-X > o-X (at all GHSV) |
| H-GaAlMFI (III) | : m-X > p-X > o-X (at low GHSV) |
| | p-X > m-X > o-X (at high GHSV) |

From the comparison of the results in Table 3.1.2, the Ga-modified ZSM-5 type zeolite catalysts can be arranged in the order of their catalytic activity (ethylene conversion activities), aromatics selectivity and shape selectivity (in terms of p-X/m-X ratio) at the ethylene iso-conversion (60%), as follows:

| | |
|---|---|
| For catalytic activity | H-GaAlMFI (I) > H-GaAlMFI (II) > H-GaAlMFI (III) > H-GaMFI ≈ Ga(1.4)/H-ZSM-5 > Ga(4.7)/H-ZSM-5. |
| For aromatics selectivity | H-GaMFI > H-GaAlMFI (III) > H-GaAlMFI (II) > Ga(1.4)/H-ZSM-5 > Ga(4.7)/H-ZSM-5 > H-GaAlMFI (I) |
| For shape selectivity | H-GaAlMFI (III) > H-GaAlMFI (II) > > H-GaAlMFI (I) > Ga(4.7)/H-ZSM-5 > H-GaMFI > Ga(1.4)/H-ZSM-5 |

### *3.1.3.3. Influence of acidity and non-FW Ga*

Results showing the influence of strong acidity (measured in terms of pyridine chemisorbed at 400$^{o}$C) of the Ga-modified ZSM-5 type zeolite catalysts on their turn over rate (TOR) [at the iso-conversion of ethylene (60%)] for the ethylene conversion to all products and ethylene-to-aromatics conversion in the ethylene aromatization are presented in Fig. 3.1.10. Whereas, Fig. 3.1.11 shows the influence of strong acidity and non-FW Ga of all the zeolite catalysts on their aromatics selectivity at the iso-conversion of ethylene (60%). Influence of the poisoning of all the strong acid sites of the zeolite catalysts by the pyridine chemisorbed at 400$^{o}$C on the ethylene aromatization is shown in Table 3.1.4 .

The observed continuous and very appreciable increase in the TOR for ethylene conversion [or the ethylene conversion (Figs. 3.1.1-3.1.3 and Table 3.1.1)] with increasing the strong acidity (Fig. 3.1.10a) reveals a strong dependence of the ethylene conversion activity of the zeolite catalysts on their strong acidity. The poisoning of all the strong acid sites of the zeolite catalysts results in almost a total deactivation of the catalysts for the ethylene conversion (Table 3.1.4). Both the observations indicate a direct relationship between the acidity and the ethylene conversion activity of the zeolite catalysts. The observed catalyst deactivation after blocking the strong acid sites by pyridine cannot be attributed just to the increased diffusional limitations of reaction species due to the chemisorbed pyridine. Our earlier studies on the aromatization of methanol over H-ZSM-5 and H-GaMFI [18] indicated that unlike H-ZSM-5, H-GaMFI shows appreciable aromatization activity even after the poisoning of its strong acid sites by pyridine chemisorption; both the poisoned zeolites showed high methanol dehydration activity. In the present case, the olefin precursor (ethylene) is different from that involved in the methanol-to-aromatics conversion and hence the pyridine poisoned zeolite catalysts showed little or no activity.

However, the ethylene-to-aromatics conversion activity is not increased continuously, it is passed through a maximum, with increasing the strong acid sites on the zeolite catalysts (Fig. 3.1.10b). It is also interesting to note that the aromatics selectivity (at the iso-conversion of ethylene, 60%) in the ethylene aromatization shows direct dependence neither on the strong acidity nor on the non-FW Ga of the zeolite catalysts. Results in Fig. 3.1.12 however show a strong influence of the non-

FW Ga/strong acid sites ratio on the aromatics selectivity and also on the $H_2$ produced per mole of ethylene converted. Both the aromatics selectivity and $H_2$ produced passed through a maximum, having almost the same value ($\approx$ 1.0), with increasing the ratio.

### 3.1.4. Discussion

#### *3.1.4.1. Comparison of Ga-modified ZSM-5 type zeolite catalysts*

The results in Figs. 3.1.1-3.1.9 show the strong influence of the space velocity on the product selectivity, aromatic distribution and also on the xylenes distribution. Since the ethylene conversion is decreased markedly with increasing the space velocity, the product selectivity and the aromatics and xylene distributions show a strong dependence on the conversion. Hence, the zeolite catalysts are compared for their product selectivity and also for their aromatics and xylenes distributions at the iso-conversion of ethylene (Table 3.1.2).

For the Ga(1.4)/H-ZSM-5 and Ga (4.7)/H-ZSM-5 zeolites, the distribution of Ga-species throughout the zeolite crystals is not uniform. Since these catalysts are prepared by adding externally gallium oxide by impregnation method to the H-ZSM-5, only a part of the total gallium oxide species are expected to be present in the zeolite channels and the remaining ones at the external surface of the zeolite crystals. Moreover, the Ga-oxide species present in the zeolite channels are not expected to be distributed uniformly throughout the zeolite channels. On the contrary, in the case of H-GaMFI and H-GaAlMFI zeolite crystals, their non-FW Ga-species are expected to be distributed uniformly and located at the channel intersections in close proximity to the zeolitic protons, in the zeolite channels, because these are derived from the framework gallium by the degalliation of the respective zeolite.

From a comparison of the Ga-modified ZSM-5 type zeolite catalysts having at least one similar bulk or surface property, following interesting observations can be made:

The Ga (4.7)/H-ZSM-5 and H-GaAlMFI (II) have more or less the same bulk compositions, but the two differ widely in their ethylene conversion activity, product selectivity/distribution and shape selectivity (Tables 3.1.1 and 3.1.2). The H-GaAlMFI (II) catalyst shows much more activity and aromatics selectivity. Also, the Ga (1.4)/H-ZSM-5 and H-GaMFI have comparable non-FW Ga and strong acidity.

This two catalysts show similar ethylene conversion activity, but the H-GaMFI zeolite show appreciably higher aromatics selectivity. The observed higher aromatics selectivity of the H-GaAlMFI and H-GaMFI zeolite is attributed to their higher dehydrogenation activity resulting from the uniformly distributed non-FW Ga species in close proximity to the zeolitic protons, as discussed later.

Among the Ga-modified ZSM-5 type zeolite catalysts, the H-GaAlMFI zeolite catalysts show much higher ethylene conversion activity and shape selectivity. Their higher ethylene conversion activity is attributed to their higher acidity as the ethylene conversion activity is increased with increasing the acidity (Fig. 3.1.10a). The observed higher shape selectivity of these zeolite catalysts (Table 3.1.2) is attributed to both their higher acidity (which causes more interactions between the diffusing aromatic species and acid sites) and their non-FW Ga-species (which causes more hindrance for the diffusion of aromatic species in the zeolite channels by reducing the effective channel diameter) present in the zeolite channels [19,20]. The shape selectivity is increased with increasing the non-FW Ga, in spite of an appreciable decrease in the acidity (Tables 3.1.1 and 3.1.2). This shows that the influence of non-FW Ga-species on the zeolite shape selectivity is stronger than that of the acidity.

The ethylene conversion activity shows a strong dependence on the acidity (Fig. 3.1.10a) indicating a direct relationship between the acidity and the activity of the Ga-modified zeolite catalysts. However, although the ethylene-to-aromatics conversion activity is influenced by both the acidity and the non-FW Ga of the zeolite catalysts (Table 3.1.2), the aromatics selectivity and/or the ethylene-to-aromatics conversion activity show a direct dependence neither on the acidity nor on the non-FW Ga (Figs. 3.1.10b and 3.1.11). This is also the case even for the H-GaMFI and H-GaAlMFI zeolite catalysts for which the distribution of non-FW Ga in the zeolite channel is expected to be uniform. These observations suggest that the aromatics selectivity and also the ethylene-to-aromatics conversion activity depend essentially on a combined effect produced by the acidity and the non-FW Ga-species in the zeolite channels. It is interesting to note that both the aromatics selectivity and the hydrogen produced per mole of ethylene converted are increased but passes thorough a maximum with increasing the ratio of the non-FW Ga-species (present in the zeolite channels) to the strong acid sites of the H-GaMFI and H-GaAlMFI zeolite catalysts (Fig. 3.1.12); the maximum occurs at the non-FW Ga/strong acid sites ratio of about 1.0. Thus there is an optimum ratio of non-FW Ga species to the strong acid sites for

obtaining high aromatics selectivity and/or high dehydrogenation in the ethylene aromatization over the Ga-modified zeolites.

#### *3.1.4.2. Active sites and reaction path for the ethylene aromatization*

For the Ga-modified ZSM-5 type zeolite catalysts to be highly active and at the same time highly selective for the ethylene aromatization, it should have both the high acidity and the optimum non-FW Ga/strong acid sites ratio (close to 1.0). Among the catalysts, the H-GaAlMFI (II) showed the best performance - the highest ethylene-to-aromatics conversion activity (Fig. 10) because of its high acidity (strong acid sites $\approx$ 0.46 mmol.g$^{-1}$) and the non-FW Ga to the strong acid sites ratio (0.7) not far from the optimum one (1.0)

In the ethylene aromatization, a number of reactions involving oligomerization, cracking, H-transfer, dehydrogenation and dehydrocyclization reactions followed by aromatics interconversion reactions are expected to occur in a complex sequence. The ethylene oligomerization reaction occurs on the zeolitic protonic sites and the observed direct dependence of ethylene conversion activity on the zeolitic acidity (Fig. 3.1.10a) is consistent with this. The other acid catalyzed reactions involved in the overall ethylene aromatization process are cracking, cyclization, hydrogen transfer and aromatics interconversion reactions (e.g. isomerization, disproportionation and dealkylation / alkylation reactions). An acid catalyzed dehydrogenation reaction is slow. Hence, although the high acidity of the zeolite catalysts impart high ethylene conversion activity to the catalysts, it alone is not enough for obtaining high aromatics selectivity or yield in the ethylene aromatization.

Like in the aromatization of lower alkanes [21-23], the role of Ga-species in the zeolite channels is to drastically enhance the dehydrogenation activity of the catalyst and thereby to increase drastically the aromatics selectivity and/or ethylene-to-aromatics conversion activity of the catalyst in the ethylene aromatization. From this investigation, it is however not possible to know the nature of the Ga-species present in the channels of the Ga-modified ZSM-5 type zeolite catalysts. However, for the H-GaMFI and H-GaAlMFI zeolites, the Ga-species (G) having Lewis acid character are expected to be formed by the degalliation of the framework gallium and hence are likely to be located at the zeolitic channel intersections in a close vicinity of the framework Al or Ga (i.e. zeolitic protons). The observed optimum non-FW

Ga/strong acid sites ratio (close to 1.0) for obtaining high aromatics selectivity indicates that for the high aromatics selectivity, each zeolitic protonic acid site should be accompanied by one gallium species (G), thus forming a protonic ($H^+$) acid site and Lewis (G) acid site pairs at the channel intersections. The measured strong acidity of the zeolite catalysts (Table 3.1.1) is essentially Bronsted (protonic) acidity because the Lewis acid of ZSM-5 (or ZSM-8) type zeolite are not accessible for the chemisorption of pyridine [24-26].

Following reaction path and elementary reaction steps, based on the above observations and also on the dependence of the product distribution on the conversion or space velocity (i.e. contact time), for the ethylene aromatization over the Ga-modified ZSM-5 type zeolite catalyst, containing both Lewis (extra framework Ga-species, G) and Bronsted (zeolitic protons) acid sites in a close vicinity of each other are proposed.

The main reactions responsible for the formation of observed products in the ethylene aromatization seem to follow a reaction sequence similar to that given in Fig. 3.1.13. The proposed reaction path, however, provides a simplified picture of the highly complex network of a large number of hydrocarbon conversion reactions occurring in the overall ethylene-to-aromatics conversion process. The product selectivity and the distribution of aromatics and xylenes and their variation with the space velocity indicated that p-xylene and o-xylene (p-X» o-X) are primary aromatic products and the propylene selectivity is very high, particularly at the higher space velocities (or lower conversions). In this case, propylene can not form directly from ethylene and hence the former cannot be a precursor for aromatics. The concentration of benzene in the aromatics is decreased with increasing the space velocity (Figs. 3.1.4 – 3.1.6). This suggests that benzene is not a primary aromatic hydrocarbon, but it is formed in the aromatics inter-conversion reactions. The propylene formation is expected mostly due to a symmetrical scission of $C_6$ olefin. The formation of xylenes in the order: p-X » o-X » m-X, particularly at higher space velocity is consistent with the steric hindrance of the respective xylene isomer for its diffusion in the zeolite channels; an order for the diffusivity of xylene isomers in ZSM-5 type zeolite is p-X » o-X > m-X [27]. The final (observed) distribution of aromatics is however controlled by their interconversion reactions, viz. isomerization, disproportionation and dealkylation (hydrodealkylation)/alkylation reactions occurring on the zeolitic acid sites, depending upon the contact time. The selectivity for the formation of

methane and ethane in the ethylene aromatization is relatively low for all the Ga-modified zeolite catalysts. The methane formation is expected mainly by the hydrodealkylation of methyl aromatics. Whereas the $C_2$ - $C_4$ alkanes are formed mostly by the hydrocracking of ethylene oligomers and/or by the H-transfer reactions of $C_2$-$C_4$ alkenes with naphthenes or ethylene oligomers.

In the ethylene aromatization, the main role played by the zeolitic proton is to catalyze the ethylene oligomerization, cyclization of dehydrogenated ethylene oligomer, H-transfer reactions and aromatics interconversion reactions. However, the dehydrogenation of ethylene oligomer, which is essential for cyclization of the ethylene oligomer to occur by the zeolitic proton and other dehydrogenation reactions are facilitated by the Ga-species (G) in the presence of zeolitic protons, as follows:

Ethylene oligomerization

$$C_2H_4 + H^+ \bullet C_2H_5^+ \underset{+C_2H_4}{\overset{-C_2H_4}{\bullet}} C_4H_9^+ \underset{+C_2H_4}{\overset{-C_2H_4}{\bullet}} C_6H_{13}^+ \underset{+C_2H_4}{\overset{-C_2H_4}{\bullet}} C_8H_{17}^+ \underset{-H^+}{\overset{+H^+}{\bullet}} C_8H_{16} \quad (1)$$

Dehydrogenation of ethylene oligomer

$$C_8H_{16} + G \bullet C_8H_{15}^+ + GH^{-1} \quad (2)$$

$$GH^- + H^+ \bullet G + H_2\uparrow \quad (3)$$

or

$$G + C_8H_{17}^+ \bullet GH^- + C_8H_{16}^{2+} \rightarrow G + C_8H_{15}^+ + H_2 \quad (4)$$

$$C_8H_{15}^+ \bullet C_8H_{14} + H^+ \quad (5)$$

Dehydrocyclization to aromatic hydrocarbons

$$C_8H_{15}^+ \rightarrow C_8H_{10} \text{ (mostly p-X and/or o-X)} + H^+ + 4H_{(ad)} \quad (6)$$

$$H_{(ad)} + G \leftrightarrow H\text{-}G \quad (7)$$

$$2\,H\text{-}G \leftrightarrow 2\,G + H_2\uparrow \quad (8)$$

A successive dehydrogenation of the $C_8H_{15}^+$ carbonium ion leads to the formation of aromatic hydrocarbon, while releasing proton and adsorbed H-atoms on the catalyst surface. The desorption of $H_{(ad)}$ atoms from the zeolite surface as molecular hydrogen, which control the formation of aromatic hydrocarbons and hence the aromatics selectivity, is facilitated by their spill over to the gallium sites followed by recombinative desorption [28,29]. The observed very high aromatics selectivity in the ethylene aromatization for the H-GaMFI and H-GaAlMFI (II and III) zeolite catalysts

is attributed to the presence of well dispersed non-FW Ga-species in a close vicinity of the zeolitic protons.

For the dehydrogenation of ethylene oligomer (Reactions 2 - 5), the required ratio of G to $H^+$ is 1.0, which is consistent with that actually observed (Fig. 3.1.12). The optimum ratio of G to the strong zeolitic acidity for obtaining highest aromatics selectivity is also found to be close to 1.0 (Fig. 3.1.12). This indicates that the aromatics selectivity in the ethylene aromatization is controlled by the dehydrogenation of ethylene oligomers.

### 3.1.5 Conclusions

From the present investigation on the ethylene aromatization (400°C) over the Ga/H-ZSM-5, H-GaMFI and H-GaAlMFI zeolite catalysts following important conclusions have been drawn:

1. Among the Ga-modified ZSM-5 type zeolite catalysts, the H-GaAlMFI (II) zeolite catalyst (having 0.46 $mmol.g^{1}$ strong acid sites and non-FW Ga/strong acid sites ratio of 0.70) shows highest ethylene-to-aromatics conversion activity. It is a highly promising catalyst for the aromatization of dilute ethylene with high conversion and aromatics selectivity (≥ 90% ethylene conversion with ≥ 80% aromatics selectivity at a space velocity of 6150 $cm^3g^{-1}h^{-1}$).
2. The product selectivity and the distribution of aromatics and xylene isomers in the ethylene aromatization are strongly dependent upon the ethylene conversion; higher the conversion, higher is the selectivity for aromatics. The p- and o-xylenes are the primary aromatics formed in the aromatization process and the aromatics and xylenes distributions are controlled by the aromatics interconversion reactions viz. isomerization, disproportionation and dealkylation/alkylation.
3. A direct correlation exists between the ethylene conversion activity and strong acidity (measured in terms of the pyridine chemisorbed at 400°C) of the Ga-modified ZSM-5 type zeolite catalysts. However the aromatics selectivity or ethylene-to-aromatics conversion activity of the catalyst shows no direct dependence upon their strong acidity alone or upon their non-FW Ga alone. It shows dependence on a combination of the two; there is an optimum non-

FW/strong acid sites ratio, which is close to 1.0, for achieving highest aromatics selectivity in the ethylene aromatization.

The H-GaMFI and H-GaAlMFI zeolites having their non-FW / strong acid sites ratio close to the optimum one, show high selectivity for aromatics because of the uniform distribution of their non-FW Ga species (which are formed by the degalliation of the framework Ga) throughout the zeolite channels and also in a close vicinity of the zeolitic protonic sites. The presence of non-FW Ga and zeolite protons in a close vicinity of each other is essential for the high dehydrogenation activity and consequently for the aromatization activity/selectivity of the Ga-modified ZSM-5 type zeolite catalysts for the ethylene aromatization.

**Table 3.1.1:** Bulk and surface properties of H-ZSM-5 and Ga-modified ZSM-5 type zeolite catalysts.

| Catalysts | Bulk composition | | | Framework composition | | | Crystal size (μm) | Crystal morphology | Non-FW Ga ($mmol.g^{-1}$) | Strong acidity ($mmol.g^{-1}$) |
|---|---|---|---|---|---|---|---|---|---|---|
| | Si/Al | Si/Ga | Si/(Ga + Al) | Si/Al | Si/Ga | Si/(Al+Ga) | | | | |
| H-ZSM-5 | 35 | - | 35 | 36 | - | 36 | 6.7 ± 2 | Hexagonal | 0.0 | 0.24 |
| Ga(1.4)/H-ZSM-5 | 35 | 80.4 | 24.4 | 36 | - | 36 | 6.7 ± 2 | Hexagonal | 0.20 | 0.21 |
| Ga(4.7)/H-ZSM-5 | 35 | 24.1 | 14.6 | 36 | - | 36 | 6.7 ± 2 | Hexagonal | 0.67 | 0.15 |
| H-GaMFI | - | 30.1 | 30.1 | - | 48.5 | 48.5 | 6.0 ± 2 | Spherical | 0.21 | 0.25 |
| H-GaAlMFI (I) | 17.7 | 46.6 | 12.8 | 25.0 | 88.6 | 19.5 | 3.5 ± 0.5 | Spherical hexagonal | 0.16 | 0.54 |
| H-GaAlMFI (II) | 37.5 | 24.3 | 14.7 | 40.3 | 49.9 | 22.3 | 5.5 ± 1.5 | Spherical hexagonal | 0.32 | 0.46 |
| H-GaAlMFI (III) | 49.6 | 15.3 | 11.7 | 54.1 | 44.8 | 24.5 | 3.7 ± 1 | Spherical hexagonal | 0.65 | 0.41 |

**Table 3.1.2:** Comparison of the Ga-modified ZSM-5 type zeolite catalysts for their activity, product selectivity/distribution and shape selectivity in the aromatization of ethylene at iso-conversion of ethylene.

| Catalyst | TOR ($\mu mol.g^{-1}.s^{-1}$) | | Selectivity | | | | | | Aromatics distribution (wt%) | | | | p-X/m-X ratio |
|---|---|---|---|---|---|---|---|---|---|---|---|---|---|
| | Ethylene conversion | Ethylene-to-aromatics conversion | Aromatics | $CH_4$ | $C_2H_6$ | $C_3H_8$ | $C_3H_6$ | $C_{4+}$ | B | T | $C_8$ | $C_{9+}$ | |
| a) For ethylene iso-conversion of 60% | | | | | | | | | | | | | |
| Ga(1.4)/H-ZSM-5 | 1.41 | 0.61 | 43.4 | 0.5 | 1.1 | 3.9 | 28.4 | 22.6 | 5.5 | 26.0 | 50.0 | 18.5 | 0.55 |
| Ga(4.7)/H-ZSM-5 | 1.12 | 0.41 | 37.3 | 0.12 | 0.08 | 2.5 | 30.9 | 29.1 | 5.3 | 29.8 | 52.5 | 12.4 | 0.96 |
| H-GaMFI | 1.41 | 0.94 | 67.3 | 0.13 | 0.08 | 2.1 | 18.0 | 12.4 | 8.4 | 28.6 | 49.0 | 14.0 | 0.62 |
| H-GaAlMFI (I)[a] | 16.8 | 3.20 | 19.0[b] | 0.01 | 0.01 | 3.1 | 35.9 | 42.0 | 0.5 | 26.0 | 58.9 | 14.6 | 1.26 |
| H-GaAlMFI (II)[a] | 12.7 | 7.70 | 60.9 | 0.01 | 0.6 | 0.7 | 16.3 | 21.5 | 3.3 | 25.2 | 58.1 | 13.4 | 1.35 |
| H-GaAlMFI (III)[a] | 9.8 | 6.30 | 63.8 | 0.7 | 0.7 | 3.1 | 15.2 | 16.5 | 7.8 | 31.2 | 54.1 | 6.9 | 1.53 |
| b) For ethylene iso-conversion of 90% | | | | | | | | | | | | | |
| H-GaAlMFI (I) | 2.3 | 1.61 | 70.1 | 1.4 | 0.7 | 8.8 | 5.4 | 13.7 | 11.5 | 37.4 | 41.8 | 9.3 | 0.38 |
| H-GaAlMFI (II) | 2.2 | 1.72 | 78.1 | 2.6 | 1.2 | 7.8 | 4.0 | 6.3 | 10.9 | 31.7 | 37.5 | 19.9 | 0.39 |
| H-GaAlMFI (III) | 1.2 | 0.97 | 81.0 | 3.4 | 1.5 | 4.7 | 3.9 | 5.5 | 17.6 | 35.2 | 36.3 | 10.9 | 0.41 |

[a]For these catalysts the data presented were obtained from extrapolation of the experimental data (Figs. 3.1.3, 3.1.6 and 3.1.9)
[b]For the lower iso-conversion levels, the aromatics selectivity for the H-GaAlMFI (I) would be much more favorable

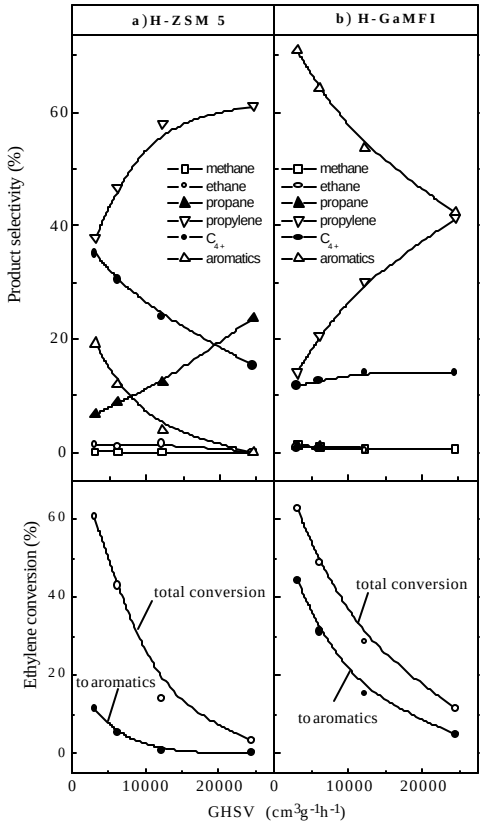


**Figure 3.1.1.** Variation with the space velocity of the conversion and product selectivity in the ethylene aromatization over ZSM-5 and H-GaMFI zeolites

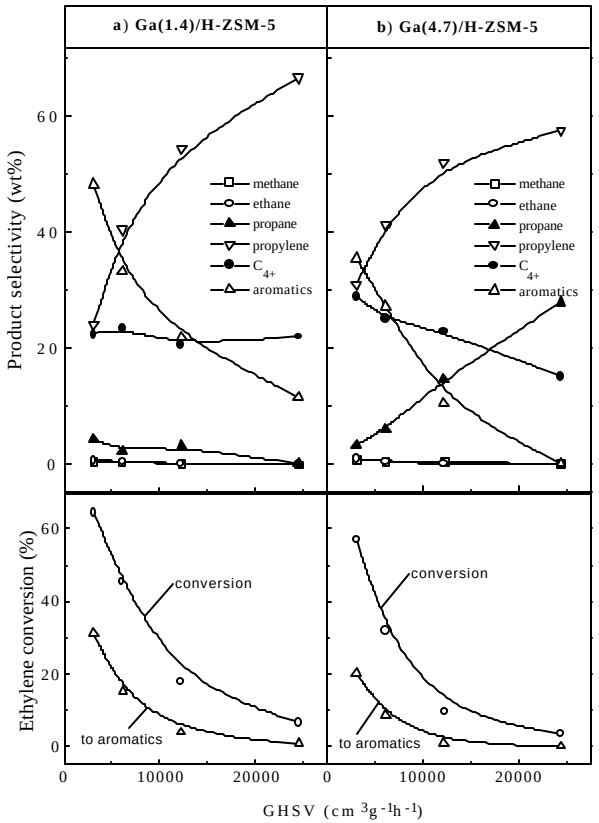


**Figure 3.1.2.** Variation with the space velocity of the conversion and product selectivity in the ethylene aromatization over Ga(1.4)/ZSM-5 and Ga(4.7)/ZSM-5 zeolites.

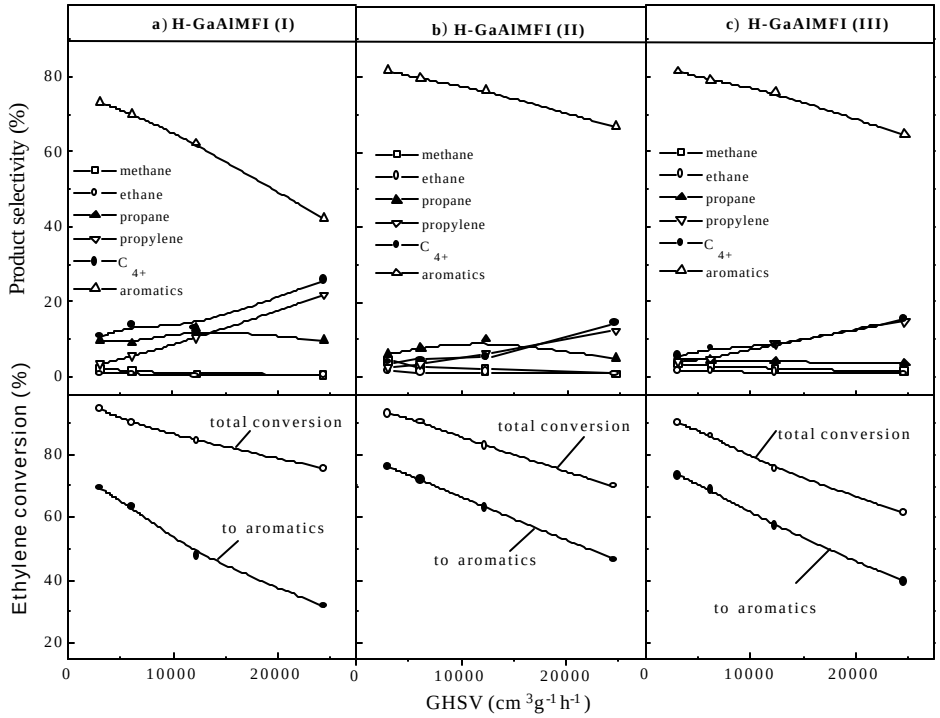


**Figure 3.1.3**. Variation with the space velocity of the conversion and product selectivity in the ethylene aromatization over H-GaAlMFI(I), (II) and (III) zeolites.

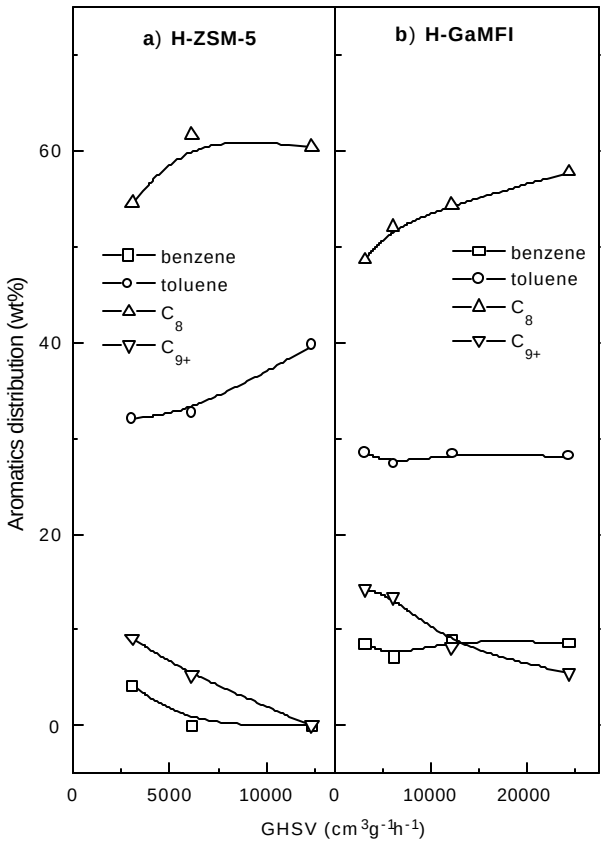


**Figure 3.1.4**. Dependence on the space velocity of the distribution of aromatics formed in the ethylene aromatization over H-ZSM-5 and H-GaMFI zeolites

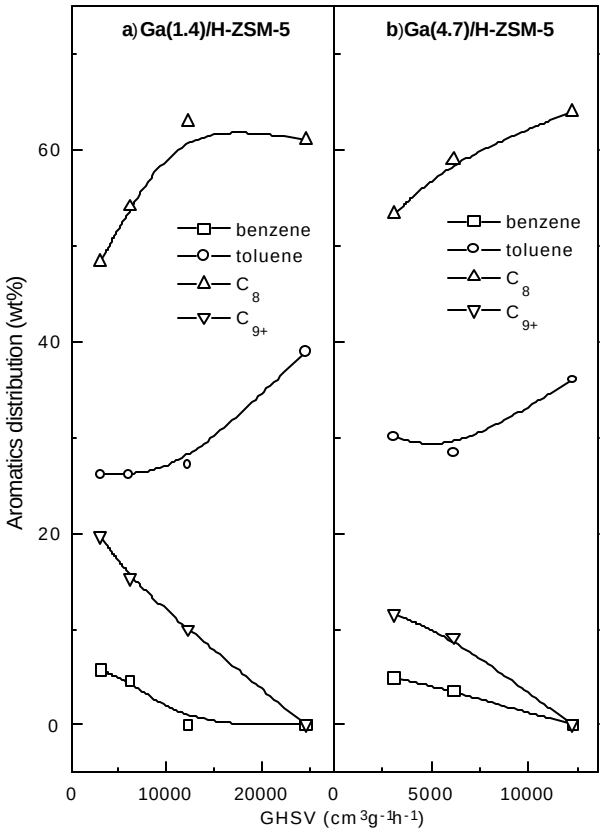


**Figure 3.1.5.** Dependence on the space velocity of the distribution of aromatics formed in the ethylene aromatization over Ga(1.4)/ZSM-5 and Ga(4.7)/ZSM-5 zeolites.

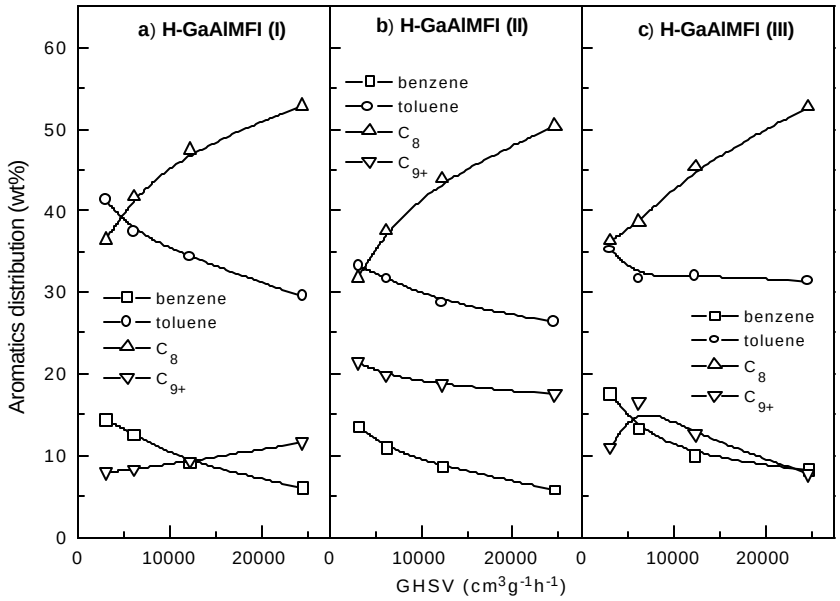


**Figure 3.1.6.** Dependence on the space velocity of the distribution of aromatics formed in the ethylene aromatization over H-GaAlMFI (I), (II) and (III) zeolites.

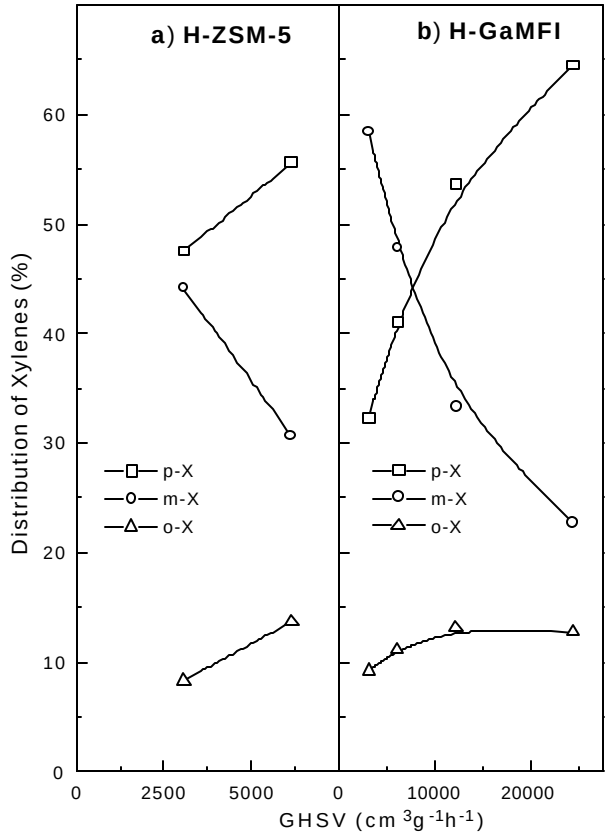


**Figure 3.1.7.** Effect of space velocity on the distribution of xylenes formed in the ethylene aromatization over H-ZSM-5 and H-GaMFI zeolites

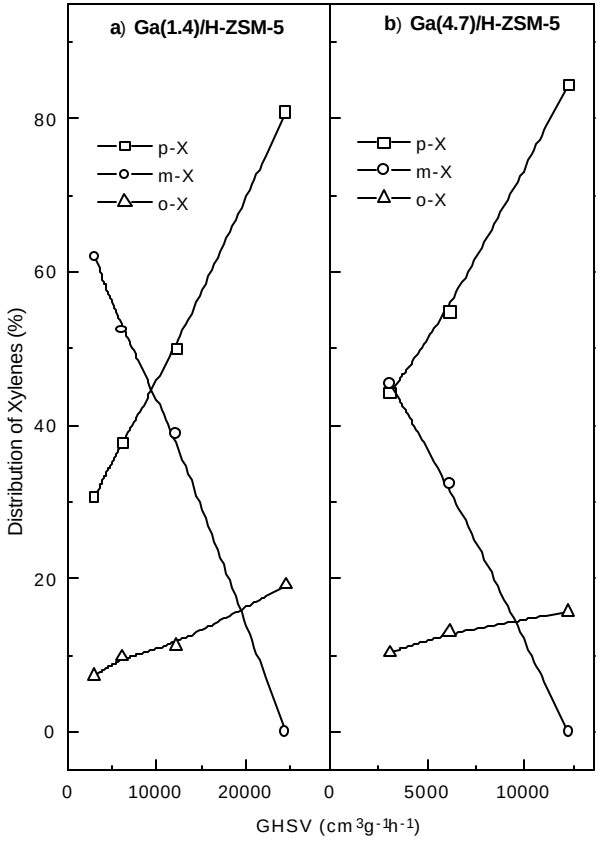


**Fig. 3.1.8.** Effect of space velocity on the distribution of xylenes formed in the ethylene aromatization over Ga(1.4)/ZSM-5 and Ga(4.7)/ZSM-5 zeolites

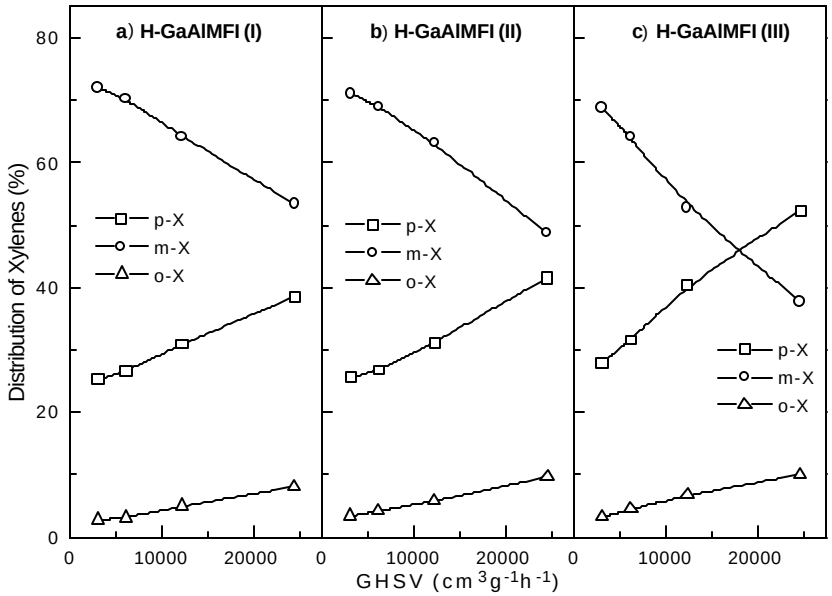


**Figure 3.1.9**. Effect of space velocity on the distribution of xylenes formed in the ethylene aromatization over H-GaAlMFI (I), (II) and (III) zeolites

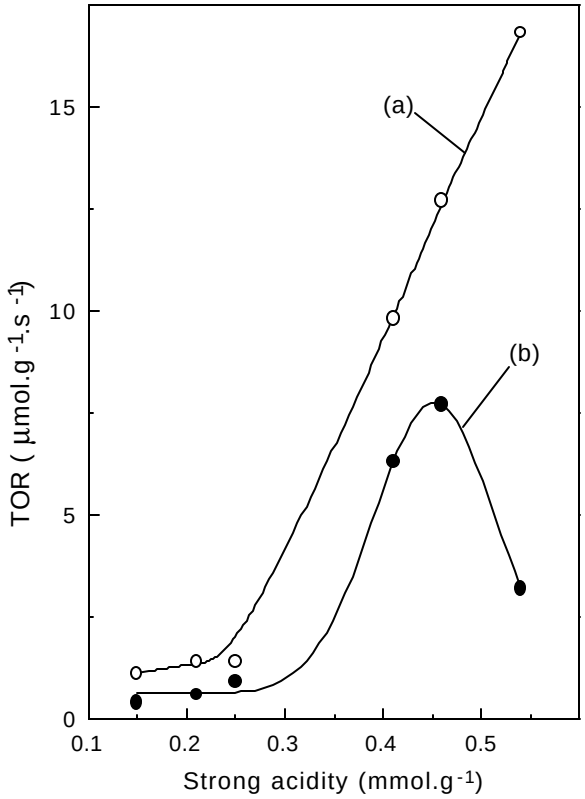


**Figure 3.1.10.** Dependence of TOR for (a) ethylene conversion and (b) ethylene-to-aromatics conversion in the ethylene aromatization over the Ga-modified ZSM-5 type zeolites at the ethylene iso-conversion of 60% on their strong acidity

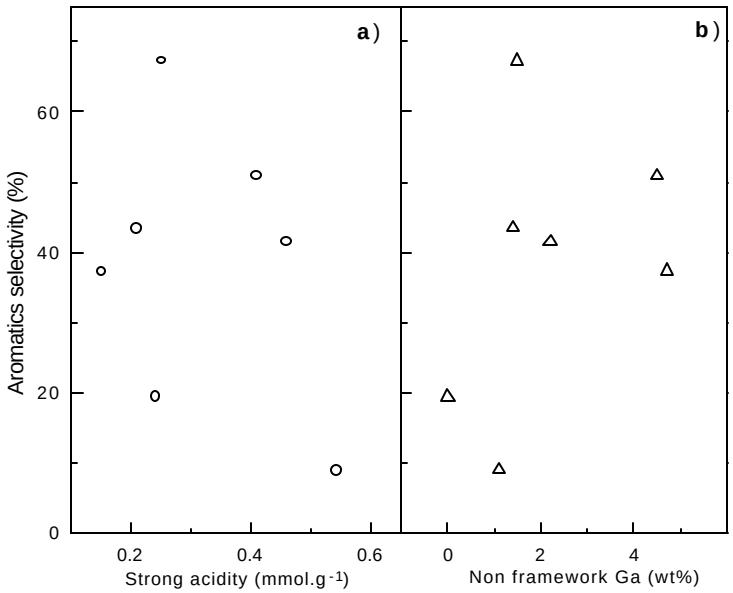


**Figure 3.1.11.** Variation of the selectivity for aromatics in the ethylene aromatization for the ethylene iso-conversion of 60% with the strong acidity and the non-FW Ga of the Ga-modified ZSM-5 type zeolites

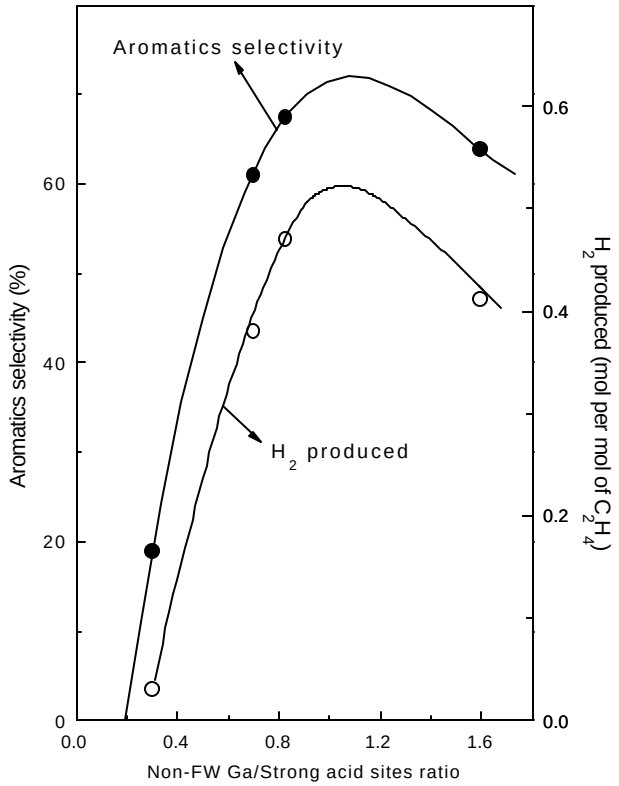


**Figure 3.1.12**. Dependence on the non-FW Ga/strong acid sites ratio of the aromatics selectivity and $H_2$ produced in the aromatization of ethylene over the H-GaMFI and H-GaAlMFI (I-III) zeolites at iso-conversion of ethylene (60%)

**Table 3.1.3:** Summary of the trends for the formation of different aromatic hydrocarbons in the ethylene aromatization over the zeolite catalysts.

| Zeolite catalyst | Trend for the aromatic product formation with increasing space velocity | | | |
|---|---|---|---|---|
| | Benzene (B) | Toluene (T) | $C_8$ aromatics | $C_{9+}$ aromatics |
| H-ZSM-5 | Decreases | increases | passes through a maximum | decreases |
| H-GaMFI | increases slowly | unchanged | Increases | decreases |
| Ga(1.4)-H-ZSM-5 | Decreases | increases | passes through a maximum | decreases |
| Ga(4.7)-H-ZSM-5 | Decreases | passes through a minimum | Increases | decreases |
| H-GaAlMFI (I) | Decreases | decreases | Increases | increases slowly |
| H-GaAlMFI (II) | Decreases | decreases | Increases | decreases slowly |
| H-GaAlMFI (III) | Decreases | decreases | Increases | passes through a maximum |

**Table 3.1.4:** Results of the aromatization of ethylene (at 400°C and GHSV of 3100 $cm^3.g^{-1}.h^{-1}$) over the zeolite catalyst pre-poisoned by the chemisorbed pyridine at 400°C.

| Zeolite catalyst | Without the catalyst poisoning | | With the catalyst poisoning | |
|---|---|---|---|---|
| | Conversion of ethylene (%) | Aromatics yield (%) | Conversion of ethylene (%) | Aromatics yield (%) |
| H-ZSM-5 | 60.4 | 11.5 | < 0.5 | 0 |
| Ga(1.4)/H-ZSM-5 | 64.6 | 31.1 | < 0.5 | 0 |
| Ga(4.7)/H-ZSM-5 | 57.2 | 20.3 | < 0.5 | 0 |
| H-GaMFI | 62.6 | 44.4 | < 0.5 | 0 |
| H-GaAlMFI (I) | 94.2 | 69.0 | 7.5 | < 1.0 |
| H-GaAlMFI (II) | 93.1 | 76.1 | 4.0 | < 1.0 |

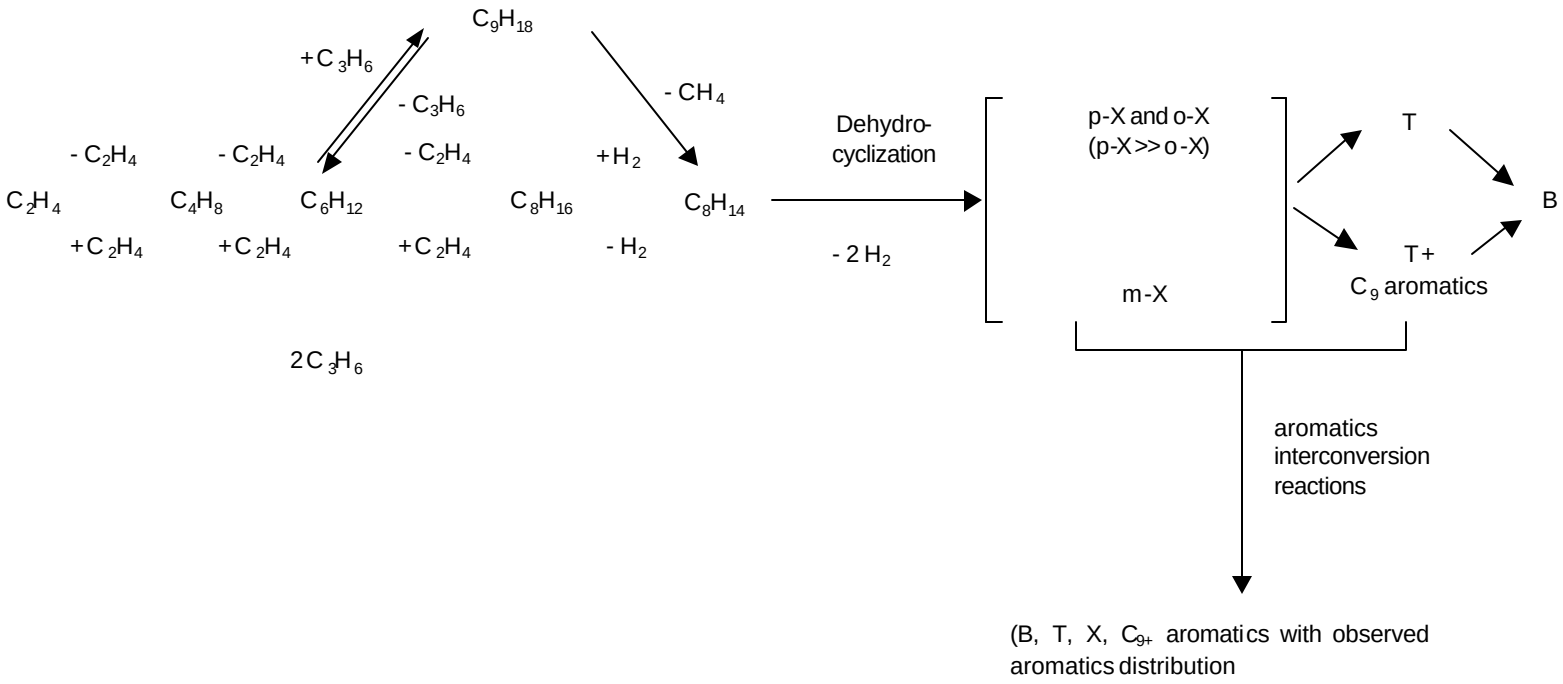


**Fig. 3.1.13.** Simplified reaction path for the ethylene aromatization over Ga-modified ZSM-5 type zeolite catalysts

### 3.1.6. References


1. J. H. Lunsford, Angew. Chem. Int. Ed. Engl., 34 (1995) 970.
2. L. Guczi, R. A. Van Santen, K. V. Sarma, Catal. Rev.-Sci. Eng., 38 (1996) 249.
3. V. R. Choudhary, S. D. Sansare, A. M. Rajput, US Patent 5,306,854 (April 26, 1994).
4. V. R. Choudhary, S. D. Sansare, S. T. Chaudhari, US Patent 5,336,825 (August 9, 1994).
5. P. Qiu, J. H. Lunsford, M. P. Rosynek, Catal. Lett. 48 (1997) 11.
6. V. S. Nayak, V. R. Choudhary, Appl. Catal. 9 (1984) 251.
7. D. B. Lukyanov, Stud. Surf. Sci. Catal. 122 (1999) 299.
8. E. G. Derouane, C. Lefebvre, J. B. Nagy, J. Mol. Catal. 38 (1986) 387.
9. R. Cao, H. Zhao, M-J, Cheng, Y-S, Yang, Gaodeng Xuexiao Huaxue Xuebao, 17 (1996) 102.
10. R. Le VanMao, Kh. Dufresne, J. Yao, Y. Yu, Appl. Catal. A, 164 (1997) 81.
11. K. Arishtirova, Kh. Dimitrov, K. Dyrek, K. H. Hallmeier, Z. Popova, S. Witkowski, Appl. Catal. A. 81 (1992) 15.
12 P. Qiu, J. H. Lunsford, M. P. Rosynek, Catal. Lett. 52 (1998) 37.
13. D. B. Lukyanov, N. S. Gnep, M. R. Guisnet, Ind. Eng. Chem. Res. 32 (1994) 223.
14. O. V. Bragin, L. M. Kustov, T. V. Vasina, E. G. Khelkovskaya-Sergeeva, V. B. Kazanskii, Kinet. Katal. 29 (1988) 1393.
15. X-S, Lin, J. Klinowski, J. Phys. Chem. 96 (1992) 3403.
16. V. R. Choudhary, V. S. Nayak, Appl. Catal., 4 (1982) 31.
17. J. M. Thomas, X-S, Lin, J. Phys. Chem., 90 (1986) 4843.
18. V. R. Choudhary and A. K. Kinage, Zeolites, 15 (1995) 732.
19. V. R. Choudhary, K. R. Srinivasan, J. Catal., 102 (1986) 328.
20. V. R. Choudhary, A. S. Mamman, AIChEJ, 36 (1990) 1577.
21. M. Guisnet, N. S. Gnep, F. Alario, Appl. Catal., 89 (1992) 1.
22. Y. Ono, Catal. Rev. Sci. Eng., 34 (1992) 179.
23. G. Giannetto, R. Monque, R. Galiasso, Catal. Rev. Sci. Eng., 36 (1994) 271.
24. V. S. Nayak, V. R. Choudhary, J. Catal., 81 (1983) 26.

25. V. R. Choudhary, D. B. Akolekar, J. Catal., 105 (1987) 416.
26. V. R. Choudhary, C. Sivadinarayana, P. Devadas, A. K. Kinage, M. Guisnet, Appl. Catal. A: Gen., 136 (1996) 125.
27. V. R. Choudhary, V. S. Nayak, T. V. Choudhary, Ind. Eng. Chem. Res., 36 (1997) 1812.
28. O. P. Keipert, D. Wolf, P. Schulz, M. Baerns, Appl. Catal. A: Gen., 131(1995) 347.
29. E. Iglesia, J. E. Baumgartner, G. L. Price, J. Catal., 134 (1992) 549.

# CHAPTER 3.2

# INFLUENCE OF TEMPERATURE SPACE VELOCITY ON THE PRODUCT SELECTIVITY AND DISTRIBUTION OF AROMATICS AND $C_8$ AROMATIC ISOMERS IN THE CONVERSION OF DILUTE ETHYLENE OVER H-GALLOALUMINOSILICATE (ZSM-5 TYPE) ZEOLITE

## 3.2.1. Earlier Work/Background and Objective of the Present Work

In the previous chapter (chapter 3.1), the aromatization of dilute ethylene over the H-ZSM-5 and Ga-modified ZSM-5 type zeolites (viz. Ga-impregnated H-ZSM-5, H-gallosilicate and H-galloaluminosilicate zeolites) has been described. It was found that the most effective catalyst for this process is a H-galloaluminosilicate (MFI) zeolite. The high ethylene aromatization activity of this zeolite catalyst is attributed to the uniformly distributed Ga-oxide species (which are formed insitu due to degalliation of the framework gallium of the zeolite) in the zeolite channels and also to the high acidity of the zeolite.

Present work was undertaken with the objective of thoroughly investigating the influence of temperature ($300^o$ – $500^oC$) [at different space velocities (3100 – 49500 $cm^3g^{-1}h^{-1}$)] on the product selectivity/distribution in the aromatization of dilute ethylene (5 mol% ethylene in $N_2$) over H-galloaluminosilicate (MFI) zeolite having high concentration of both zeolitic acidity and non-framework Ga-oxide species, and also for finding a most probable reaction path in the process.

## 3.2.2. Experimental

The H-galloaluminosilicate (ZSM-5 type) or H-GaAlMFI zeolite used in the present work is the same zeolite [H-GaAlMFI (II)] whose chemical properties and composition has already been described in the earlier chapter (chapter 3.1, in Table 3.1.1).

Aromatization of ethylene over the H-galloaluminosilicate zeolite catalyst was carried out in the same way as has already been described earlier (section 1.2.3.2 and Fig. 1.2.6), using 5 mol% ethylene in $N_2$ as a feed. The conversion and selectivity data at different temperatures (300-500$^oC$) and space velocities (3100-49,500 $cm^3g^{-1}h^{-1}$, measured at $0^oC$ and 1 atm pressure) were obtained in the same way as that has been

described earlier (section 3.1.2) by a square pulse technique. The reaction products were sampled using a heated gas sampling valve and analyzed by a GC with FID, using Porapak-Q (3mm X 3m), Benton-34 (5%) and dinonylphthalate (5%) on Chromosorb-W (3mm X 5m) columns. The absence of catalyst deactivation in the step pulse experiments was confirmed by repeating the first experiment.

### 3.2.3. Results and Discussion

Representative results showing a strong influence of ethylene conversion on the product selectivity and the distribution of aromatics and $C_8$-isomers in the aromatization of dilute ethylene over the zeolite catalyst at 350$^oC$ are presented in Fig. 3.2.1.

Because of the observed strong influence of conversion (Fig. 3.2.1), it is essential to compare the product selectivity/distribution at the same conversion (i.e. iso-conversion) for knowing a true effect of the reaction temperature on the product selectivity/distribution. Hence, the ethylene aromatization data for each temperature were collected at different space velocities and from these results the data on the product selectivity/distribution at three different iso-conversion levels (40%, 60% and 80%) were obtained. Some data are also presented as a function of space velocity (at different temperatures) to show the influence of space velocity and temperatures. Results showing the influence of temperature on the product selectivity, the $H_2$ produced per mole of ethylene converted to aromatics, $H_2$ produced per mole of aromatics formed, the $C_2$-$C_6$ alkanes/aromatics mole ratio, the distribution of aromatics and $C_8$ isomers and the p-xylene/m-xylene and p-xylene/o-xylene ratios at different iso-conversion levels, are presented in Figs. 3.2.2 - 3.2.8.

#### *3.2.3.1. Effect of temperature on product selectivity*

From the results in Fig. 3.2.2, following important observations on the temperature dependence of the product selectivity at the three different iso-conversion levels can be made:

When the temperature is increased,

- The aromatics selectivity is increased very markedly
- The selectivities for $C_4$, $C_{5\text{-}6}$ and propylene are decreased; the decrease of the $C_4$ hydrocarbon selectivity is very appreciable.

- The selectivities for ethane and methane are increased but the increase is small.
- The propane selectivity at the high conversion levels is affected but only to a small extent.

The above observations show a strong influence of temperature on the selectivity of aromatics. The formation of aromatics is more and more favored at the higher temperatures.

It is interesting to note from the results in Fig. 3.2.3, that the $H_2$ formed in the ethylene-to-aromatics conversion is increased very markedly with increasing the temperature. The $H_2$ produced per mole of aromatics formed as a function of space velocity at four different temperatures has been shown in Fig. 3.2.4. Since $H_2$ is formed by the dehydrogenation of hydrocarbons, the $H_2$ produced in the ethene aromatization provides a measure of the dehydrogenation reactions involved in the aromatization. The observed very small amount of $H_2$ formed at 300$^o$C indicates that the ethylene aromatization at this temperature involves mainly hydrogen transfer reactions (catalyzed by the zeolitic acid sites) leading to the formation of alkanes from olefins, with almost no dehydrogenation reactions. On the contrary, at $\geq$ 400$^o$C the $H_2$ produced in the aromatization is quite large, indicating the occurrence of dehydrogenation reactions catalyzed by the non-framework Ga-oxide species in combination with the zeolitic acid sites. At the intermediate temperature (350$^o$C), both the hydrogen transfer and dehydrogenation reactions seem to play important role in the aromatization.

The high aromatics selectivity at the higher temperatures ($\geq$ 400$^o$C) is attributed to the high dehydrogenation activity of the catalyst at the higher temperature. At the lower temperature (300$^o$C), the catalyst showed little or no dehydrogenation activity. The formation of aromatics is thus controlled by hydride transfer reactions at the lower temperatures (300$^o$C), by dehydrogenation reactions at the higher temperatures ($\geq$400$^o$C) and by both the reactions at the intermediate temperatures.

This is also evident from the Fig. 3.2.5, which illustrates the dependence on the space velocity of ethylene conversion (both total and to aromatics) and also of alkanes formed per mole of aromatics formed in the ethylene aromatization at different temperatures (300$^o$ – 500$^o$C). The results in Fig. 3.2.5 indicate that the

involvement of hydrogen transfer reactions in the ethylene aromatization is strongly influenced by both the process parameters (viz. temperature and space velocity). It is evident from Fig. 3.2.5 that at all the temperatures, both the total ethene conversion and ethene-to-aromatics conversion are decreased with increasing the space velocity. However, the decrease is more pronounced at the lower temperatures. This shows that the influence of space velocity on the conversion is stronger at the lower temperatures. It is also evident that the $C_2 - C_6$ alkanes/aromatics mole ratio in the products is much larger at the lower temperatures. Moreover, it is strongly influenced by the space velocity, particularly at the lower temperatures ($\leq 400^oC$); it is increased with increasing the space velocity. However, at the higher temperature ($500^oC$), it is quite small ($0.15 \pm 0.02$) and almost unaffected by the space velocity.

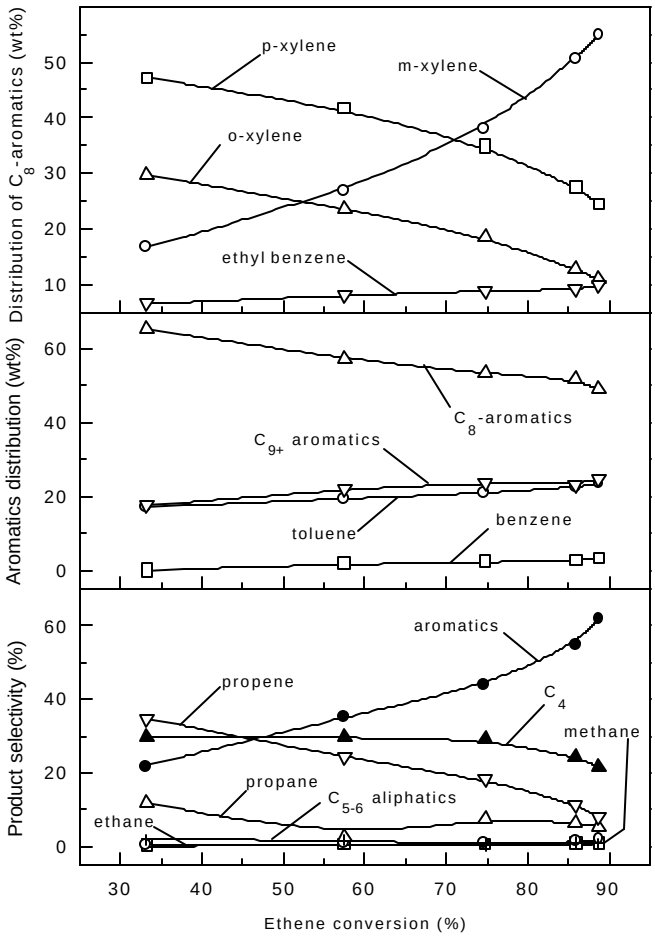


**Figure 3.2.1.** Dependence of product selectivity and distribution of aromatics and $C_8$ aromatics isomers on the conversion in the ethylene aromatization (at $350^oC$).

The results on the alkane/ aromatics ratio (Fig. 3.2.4) and the $H_2$ produced per mole of aromatics formed (Fig. 3.2.5) are complementary to each other. They also show that, depending upon the process conditions, both the hydrogen transfer and dehydrogenation reactions occur simultaneously in the ethene aromatization; the $H_2$ transfer reactions are favored at the lower temperatures and/or at higher space velocities and the dehydrogenation ones at the higher temperatures and/or lower space velocities.

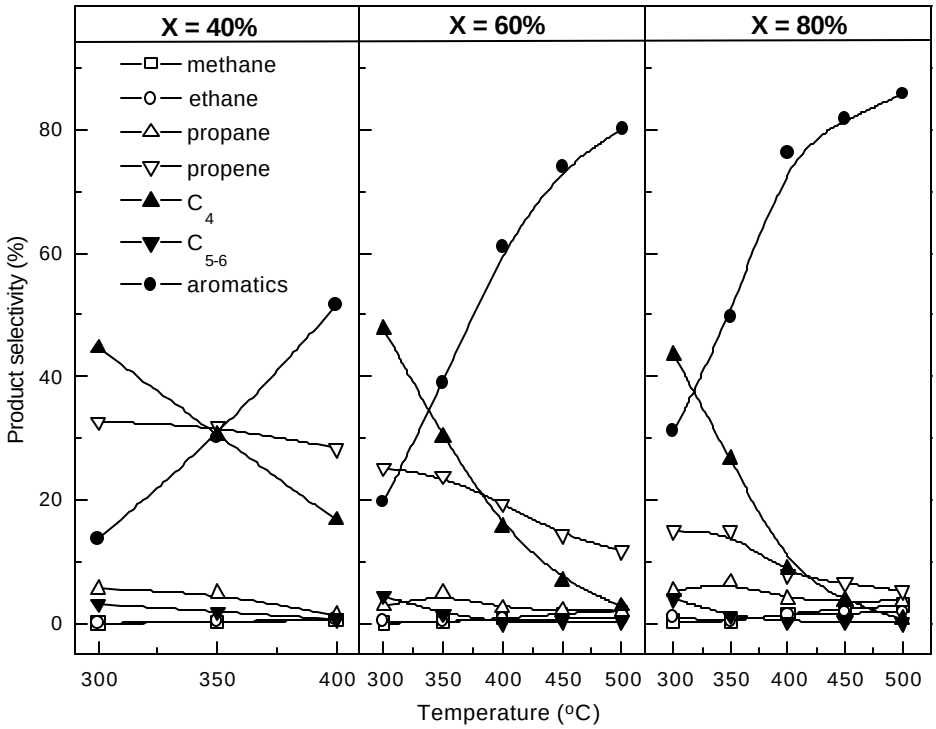


**Figure 3.2.2.** Effect of temperature on the product selectivity in the ethylene aromatization at three different iso-conversions.

The formation of propylene to an appreciable extent is expected mostly by the symmetrical scission of $C_6$-oligomer and that of propane by the hydride transfer reaction of propylene with ethylene oligomers/naphthenes. $C_4$ hydrocarbons are formed with high selectivity at the lower temperatures, mostly by the dimerization of ethylene and hydride transfer reactions of the ethylene dimers (butenes) with oligomers/naphthenes. With increasing the temperature, the selectivity for propane and $C_4$ hydrocarbons is decreased due to a decrease in the hydride transfer reactions and also because of their transformation into aromatics at the higher temperatures.

The formation of $C_{5-6}$ hydrocarbons is quite small and moreover observed only at the lower temperatures (< 400°C). This is expected because of the high reactivity of $C_{5-6}$ hydrocarbons over the catalyst at the higher temperatures. The formation of methane is very small and observed only at the higher temperatures mostly due to dealkylation of aromatics and cracking of ethylene oligomers.

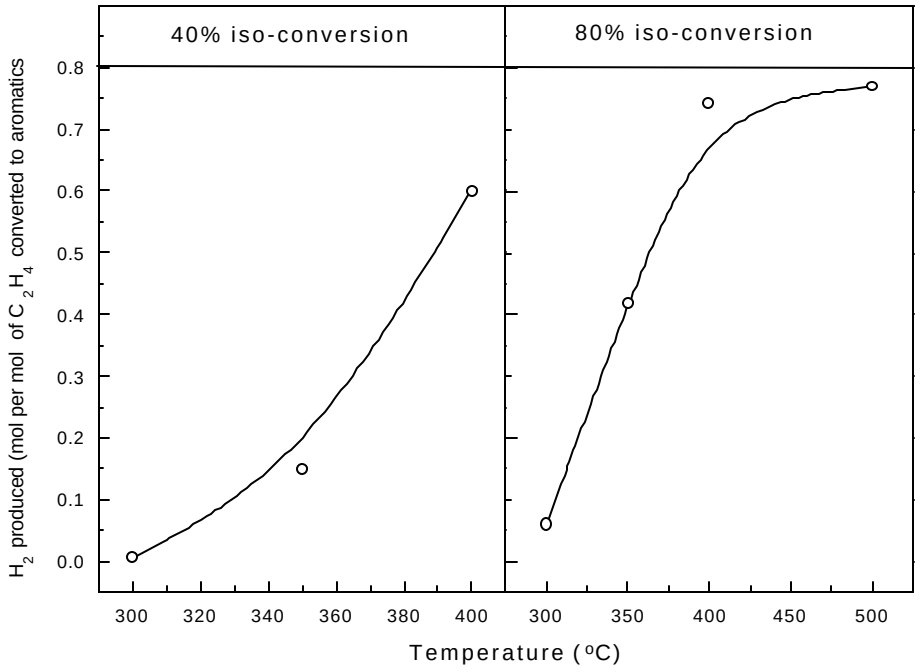


**Figure 3.2.3.** Effect of temperature on the $H_2$ produced per mole of ethylene converted to aromatics in the ethylene aromatization at two different iso-conversions.

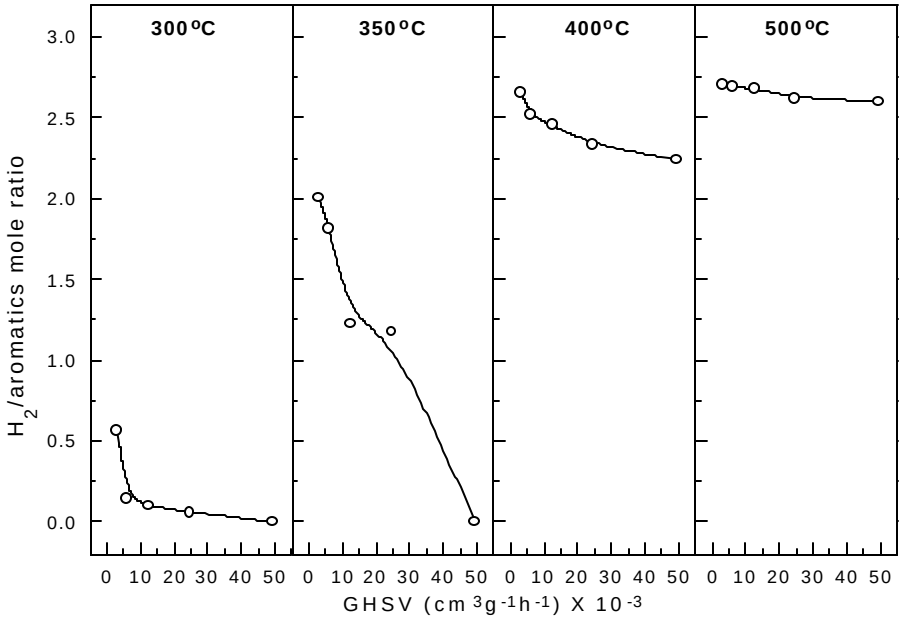


**Figure 3.2.4.** Effect of space velocity on the $H_2$/aromatics mole ratio in the ethylene aromatization at different temperatures

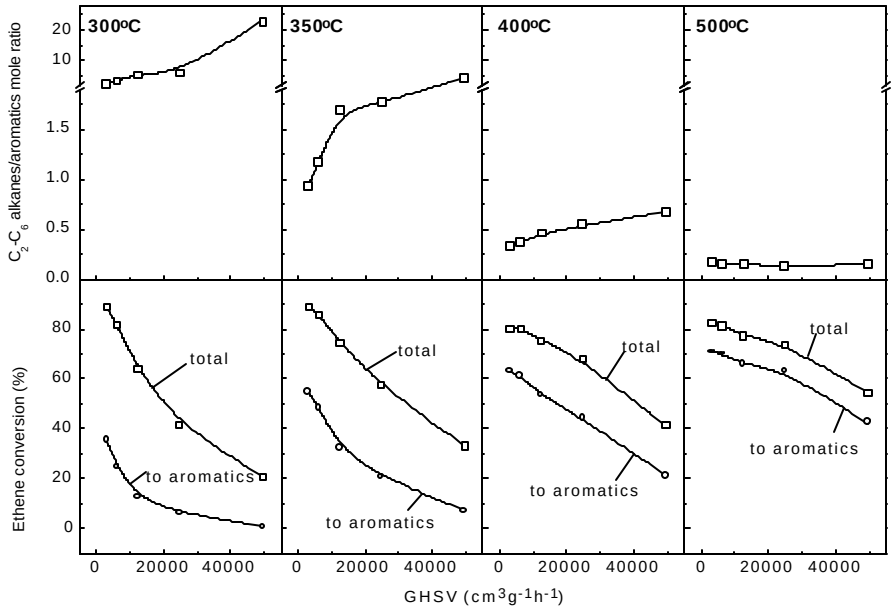


**Figure 3.2.5.** Effect of space velocity on the ethylene conversion and $C_2$-$C_6$ alkanes /aromatics mole ratio in the aromatization of ethylene at different temperatures.

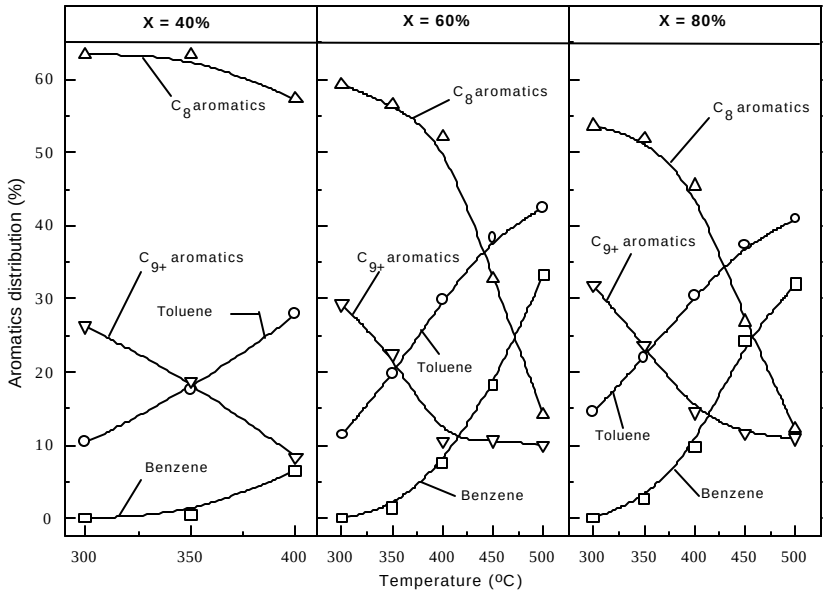


**Figure 3.2.6.** Effect of temperature on the distribution of aromatics in the ethylene aromatization at three different iso-conversions.

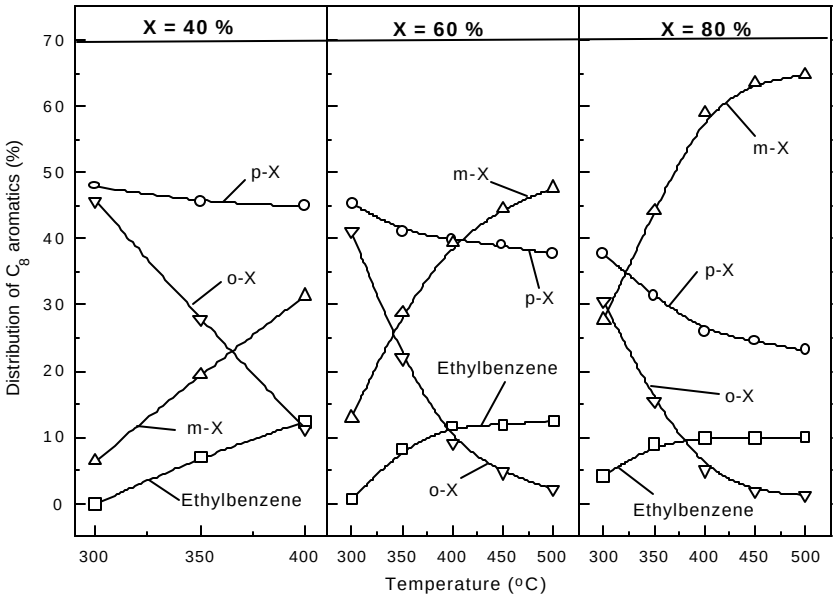


**Figure 3.2.7.** Effect of temperature on the distribution of $C_8$ aromatic isomers in the ethylene aromatization at three different iso-conversions

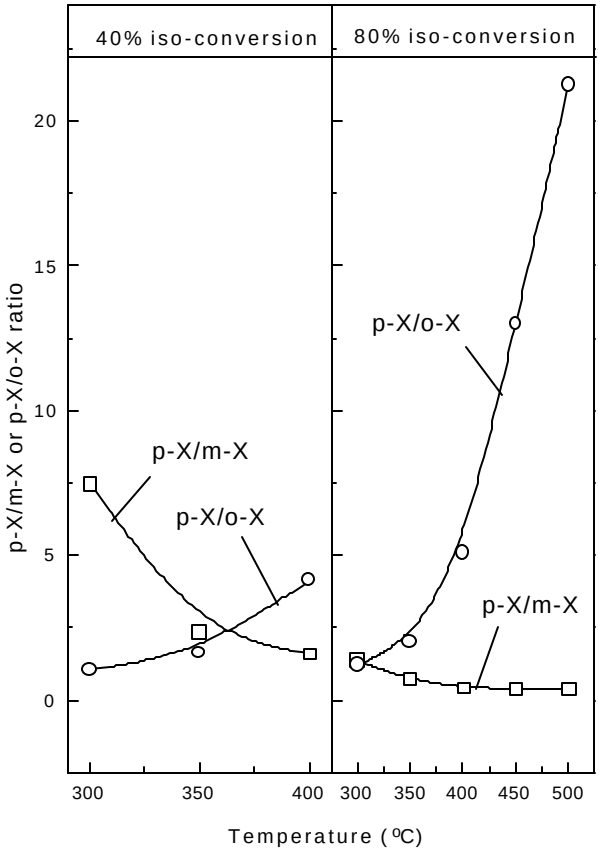


**Figure 3.2.8.** Effect of temperature on the p-xylene/m-xylene and p-xylene/o-xylene ratios in the ethylene aromatization at three different iso-conversions

### *3.2.3.2. Effect of temperature on aromatics distribution*

Results in Fig. 3.2.6 show a strong influence of the temperature on the aromatics distribution at the three different iso-conversion levels.

When the temperature is increased, the concentration of different aromatics in the total aromatics formed in the ethylene aromatization is changed as follows:

- The formation of $C_8$-aromatics is decreased; the decrease is very sharp at the higher temperatures (> 400$^o$C).
- The concentration of $C_{9+}$ aromatics is also decreased; the decrease is however pronounced at the lower temperatures.
- The concentration of toluene is increased markedly.
- The concentration of benzene is increased exponentially.

The order of the formation of different aromatics at the lowest and highest temperatures are as follows:

At 300°C: $C_8$-aromatics >> $C_{9+}$-aromatics > toluene >> benzene

At 500°C: toluene > benzene > $C_8$-aromatics ≥ $C_{9+}$-aromatics

The observed more and more formation of benzene and toluene at higher and higher temperatures is expected mostly because of the increased dealkylation of $C_8$ and $C_{9+}$ aromatics with increasing the temperature. The results thus indicate that the aromatics distribution, particularly at the higher temperatures is controlled mostly by the aromatics transformation reactions, particularly by the dealkylation of alkylbenzenes.

#### *3.2.3.3. Effect of temperature on the distribution of $C_8$-aromatics*

The relative concentration of the p-xylene, o-xylene, m-xylene and ethylbenzene are strongly influenced by the reaction temperature (Figs. 3.2.7 and 3.2.8). With increasing the temperature, the concentrations of p-, o- and m-xylenes and ethylbenzene in the $C_8$ aromatics are influenced as follows:

- The concentration of p-xylene is decreased appreciably
- The concentration of o-xylene is also decreased but the decrease is very sharp.
- The concentration of m-xylene is increased very markedly.
- The concentration of ethylbenzene is also increased upto the temperature of 400°C and then leveled-off.
- The p-xylene/m-xylene ratio is decreased but p-xylene/o-xylene ratio is increased very sharply.

The temperature dependence of the distribution of $C_8$ aromatics is quite complex. At 300°C, the concentration of all the four $C_8$ aromatics (except ethylbenzene for the iso-conversion of 80%) is far away from that expected at the thermodynamic equilibrium. The equilibrium concentration of ethylbenzene, p-xylene, m-xylene and o-xylene is 5, 23, 51 and 21%, respectively, at 300°C and 10, 21, 46 and 23%, respectively at 500°C [1].

The increase of the ethylbenzene concentration with the ethylene conversion (Fig. 3.2.1) and temperature (Fig. 3.2.5) indicates that ethylbenzene is not formed as a

primary aromatic hydrocarbon from $C_8$-oligomer; it is formed most probably by the ethenation of benzene.

At 300°C, the order for the formation of xylene isomers is as follows: p-xylene > o-xylene > m-xylene. This order is same as that for the diffusivity of the xylene isomers in H-ZSM-5 [2]. Because of the presence of non-FW Ga oxide species in the zeolitic channel, as compared to H-ZSM-5, the H-GaAlMFI zeolite is expected to show a stronger effect on the diffusivity of xylene isomers. The observed trend for the formation of xylene isomers indicates a strong influence of steric hindrance for the formation of xylene isomers, particularly on the formation of m-xylene, in the zeolite channels at 300°C. However, the influence of steric hindrance is reduced with increasing the temperature, allowing the isomerization of p- and o-xylenes to m-xylene. It is, however, very interesting to note that, the concentration of m-xylene is increased from 27.7% to 65.6% (which is above the thermodynamic equilibrium value, 46%) and that of o-xylene is decreased from 30.6% to 1.2% (which is much below the thermodynamic value, 23%), with increasing the temperature from 300°C to 500°C (Fig. 3.2.7c). This shows that the formation of m-xylene is mostly by the isomerization of p- and o-xylenes and it is controlled kinetically, particularly at the higher temperatures.

#### *3.2.3.4. Reaction path*

Based on the above observations a simplified reaction path for the aromatization of ethylene over the H-GAlMFI zeolite is presented in Fig. 3.2.9. The ethylene oligomerization, cracking, dehydrocyclization involving hydrogen transfer and the aromatic transformation reactions (viz. isomerization, alkylation/dealkylation and disproportionation reactions) are catalyzed by the zeolitic acid sites (which are large in numbers and also have high strength). Whereas, the dehydrocyclization involving dehydrogenation reactions are catalyzed by the non framework Ga-oxide species in combination with the zeolitic protonic acid sites, as has been discussed in the earlier section (section 3.1).

### 3.2.4. Conclusions

From the present studies on the temperature dependence of the product selectivity and distribution of aromatics and $C_8$ aromatic isomers at different iso-

conversion levels in the aromatization of dilute ethylene over H-GaAlMFI zeolite, following important conclusions have been drawn:

1. The product selectivity, particularly the selectivity for aromatics, propylene and $C_4$ hydrocarbons and also the distribution of aromatics are strongly influenced by the temperature.
2. In the aromatization, hydride transfer reactions are predominant at the lower temperatures (below $400^oC$). But at the higher temperatures the dehydrogenation reaction becomes predominant, producing an appreciable amount of $H_2$.
3. The distribution of $C_8$ aromatic hydrocarbons is also very strongly influenced by the temperature. It is controlled mostly by the steric factors at the lower temperatures, but it is controlled kinetically at the higher temperatures ($500^oC$).

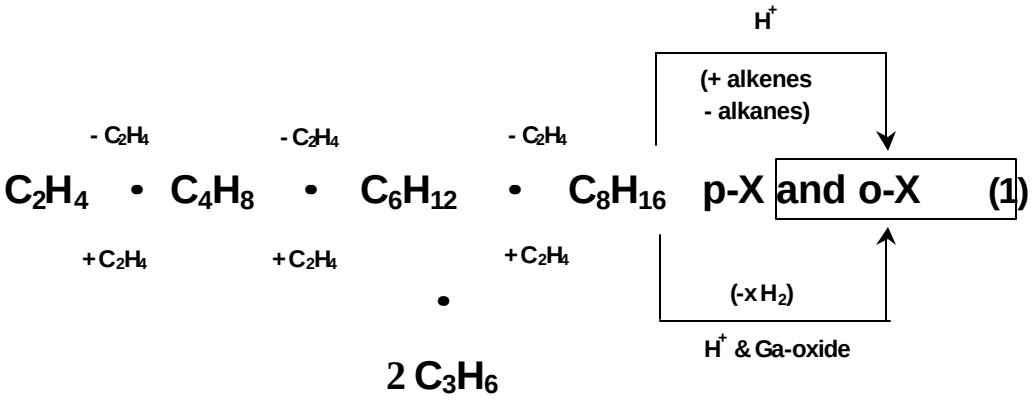


o-xylene • p-xylene and m-xylene (2)

p-xylene • m-xylene (3)

$$\text{o-, m- or p-xylene} \xrightarrow{(+H_2)} \text{Toluene} + CH_4 \quad (4)$$

$$\text{2 Xylene} \longrightarrow \text{Toluene} + C_{9+}\text{ aromatics} \quad (5)$$

$$\text{Toluene} \xrightarrow{+H_2} \text{Benzene} + CH_4 \quad (6)$$

$$\text{Benzene} \xrightarrow[(+H_2,\ -C_2H_6)]{(+C_2H_4)} \text{Ethylbenzene} \quad (7)$$

**Figure 3.2.9** Simplified reaction path showing the formation of primary aromatics and the involvement of acid catalyzed aromatics inter-conversion reactions in the aromatization of ethylene over H-GaAlMFI.

### 3.2.5. References


1. D. R. Stull, E. F. Westrum Jr. and G. C. Sinke, *in* "Chemical Thermodynamics of Organic Compounds", John Wiley & Sons. Inc., New York (1969).
2. V. R. Choudhary, V. S. Nayak and T. V. Choudhary, Ind. Eng. Chem. Res., 36 (1997) 1812.

# CHAPTER 3.3

# AROMATIZATION OF PROPENE AND n-BUTENE OVER H-GALLOALUMINOSILICATE (ZSM-5 TYPE) ZEOLITE

## 3.3.1 Earlier Work/ Background and Objectives of Present Work

Because of its high protonic acidity and unique shape-selective behavior, ZSM-5 zeolite has been proved to be a highly active and stable (against coke formation in the zeolite channels) catalyst for the oligomerization [at low temperature ($200^{o}$-$300^{o}$C) and high pressures (30-100 bar)] and aromatization [at the higher temperatures and lower pressures] of light olefins [1-6]. Further studies showed that the performance of H-ZSM-5 zeolite in the aromatization of light olefins ($C_2$-$C_4$ olefins) is greatly improved when it is ion-exchanged with $Ga^{3+}$ [7,8], $Zn^{2+}$[7,9,10], Cu [10,11] or $Ag^{+}$ [12] and/or impregnated with metal oxides such as $Ga_2O_3$ [13,14], ZnO [15,16] or $Ag_2O$ [15]. The observed improved performance of the modified ZSM-5 zeolite is attributed to the respective metal cation or metal oxide, having high hydrocarbon dehydrogenation activity.

In the earlier studies by Choudhary et al., H-GaAlMFI (H-galloaluminosilicate of ZSM-5 type) showed much better performance in the aromatization of propane [17,18]. In the earlier sections (section 3.1 and 3.2), it was shown to be highly active for aromatization of ethylene compared to Ga-impregnated H-ZSM-5 zeolite. The observed better performance of H-GaAlMFI zeolite is attributed to the uniform distribution in the zeolite channels of non-framework Ga-oxide species formed due to degalliation of the zeolite during its calcination and/or pretreatment. It is therefore interesting to study the aromatization of lower olefins over a highly acidic H-GaAlMFI zeolite. The present work was undertaken to study the conversion of propene and n-butene (at a concentration of 33-mole% in $N_2$) to aromatics over this zeolite catalyst at $400^{o}$C for different space velocities at atmospheric pressure. The effect of space velocity on the product selectivity and also on the distribution of aromatics and xylene isomers in the aromatization of propene and n-butene has been investigated.

### 3.3.2 Experimental

H-GaAlMFI (Si/Al = 37.5; Si/Ga = 24.3) zeolite was same or that used for aromatization of dilute ethylene (section 3.2) and was synthesized by its hydrothermal crystallization, using the same process as already described in section 1.2.1.2. The zeolite was pretreated in a flow of hydrogen (1030 $cm^3.g^{-1}.h^{-1}$) at 600°C for a period of 1h and then in a flow of air for 30 min.

Aromatization of propene and n-butene over the zeolite catalyst was carried out at 400°C and atmospheric pressure, in a continuous flow quartz reactor (13mm i.d.) as already described in section 1.2.3.2 and Fig. 1.2.6, using an olefin (propene or n-butene) - nitrogen mixture (33 mole%) as feed. The conversion and selectivity data (at 400°C) at different space velocities (measured at 0°C and 1 atm pressure) in the absence of catalyst deactivation, were obtained by a square pulse technique by passing the reaction mixture over a fresh catalyst bed for a short period (2-5 min) under steady state conditions and then replacing the reactant mixture by a stream of pure $N_2$ during the period of product analysis. At the end of the square pulse experiment, the reaction products were sampled using a heated gas sampling valve and analyzed by a GC with FID, using Porapak-Q (3mm X 3m), Benton-34 (5%) and dinonylphthalate (5%) on Chromosorb-W (3mm X 5m) columns. The absence of catalyst deactivation in the step pulse experiments was confirmed by repeating the first experiment.

### 3.3.3. Results and Discussion

#### *3.3.3.1. Catalyst characterization*

The H-GaAlMFI zeolite was the same [HGaAlMFI (II)] used in the aromatization of dilute ethylene (Section 3.1 and 3.2). It was characterized for its bulk and framework compositions, crystal size and morphology, concentration of non-framework (non-FW) Ga-oxide species in its channels and also for its strong acid sites, measured in terms of the pyridine chemisorbed on the zeolite at 400°C. The characterization data of the zeolite has already been presented in Table 3.1.1.

Comparison of the bulk and framework (FW) compositions of the H-GaAlMFI catalyst shows the presence of appreciable amounts of non-FW Ga within its channels. The FW Si/(Ga + Al) ratio was determined from the $^{29}Si$ MAS NMR. The FW Si/Al and Si/Ga ratios were estimated from the FW Si/(Ga + Al) and octahedral

(i.e. non-FW) Al, measured from $^{27}$Al MAS NMR and bulk concentration of Al in the zeolite. It may be noted that the T-sites of ZSM-5 type zeolites are not crystallographically identical and hence, the determination of FW Si/Ga and Si/Al ratios from the $^{29}$Si MAS NMR are not very accurate [19].

#### *3.3.3.2. Aromatization of propene*

Results showing the influence of space velocity on the conversion and product selectivity in the propene aromatization over the H-GaAlMFI zeolite at 400°C are presented in Fig. 3.3.1. Data on the distribution of aromatics and xylene isomers formed in the propene aromatization at different space velocities are presented in Fig. 3.3.2 and 3.3.3, respectively. The data is also presented in Appendix 3.8.

When the space velocity was increased from 3100 to 24,600 $cm^3g^{-1}h^{-1}$, the propene conversion (total and to aromatics), the selectivity for aromatics and different aliphatic hydrocarbons, and the distribution of aromatics and xylene isomers formed in the propene aromatization were influenced as follows:

*Effect of space velocity on conversion and product selectivity (Fig. 3.3.1)*

- The total conversion of propene and also its conversion to aromatics (i.e. aromatics yield) decreased with increasing the space velocity as expected, but the decrease of the total propene conversion was quite small.
- The trend for the aromatics selectivity was similar to that for the propene-to-aromatics conversion (or aromatics yield).
- The selectivities for methane, ethane, ethylene and $C_{5-6}$ aliphatics were very low and these were influenced only to a small extent by the space velocity.
- The selectivity for propane was quite appreciable (about 15%) and it was not influenced significantly by the space velocity.
- The selectivity for the $C_4$-hydrocarbons was also quite appreciable and it was increased with increasing the space velocity.

*Effect of space velocity on the distribution of aromatics (Fig. 3.3.2)*

- With increasing the space velocity, the formation of benzene and toluene was decreased (the decrease in the case of toluene was however quite small), that of $C_8$-aromatics was increased but that of $C_{9+}$ aromatics was passed through a maximum.

*Effect of space velocity on the distribution of xylenes (Fig. 3.3.3)*

- With increasing the space velocity, the formation of p-xylene and o-xylene was increased, but that of m-xylene was decreased. The changes in all the cases were very pronounced.

The order for the selectivity of different products and that for the distribution of different aromatic hydrocarbons and xylene isomers formed in the propene aromatization (at the space velocities employed) were as follows:

For the product selectivity

Aromatics > $C_4$-hydrocarbons > propane > ethylene > $CH_4$, $C_2H_6$ and $C_{5-6}$ aliphatics

For distribution of aromatics

$C_8$ aromatics >> toluene > $C_{9+}$ aromatics >> benzene

For distribution of xylene isomers

m-xylene >> p-xylene > o-xylene (at lower space velocity)

p-xylene >> m-xylene > o-xylene (at the highest space velocity)

It may be noted that the aromatics yield obtained in the present case is much higher than that obtained over HZSM-5 even at higher temperatures (> 400$^oC$) [6].

### *3.3.3.3. Aromatization of n-butene*

The influence of space velocity on the conversion and product selectivity in the aromatization of n-butene at 400$^oC$ over the HGaAlMFI zeolite is shown in Fig. 3.3.4. The distribution of aromatics and xylene isomers at different space velocities are shown in Fig. 3.3.5 and 3.3.6, respectively. The data is also presented in Appendix 3.9.

The increase in the space velocity from 3100 to 58100 $cm^3g^{-1}h^{-1}$ caused following effects on the n-butene conversion (total and to aromatics), the product (aromatics and aliphatic hydrocarbons) selectivity and the distribution of aromatics and xylene isomers formed in the n-butene aromatization:

*Effect of space velocity on conversion and product selectivity (Fig. 3.3.4)*

- The variation of n-butene conversion with the space velocity was unusual; the butene conversion was increased significantly with increasing the space velocity.
- The n-butene-to-aromatics conversion (aromatics yield) and the aromatics selectivity were, however, decreased markedly with increasing the space velocity.
- The propene selectivity increased but the propane selectivity decreased markedly with increasing the space velocity; at the lowest space velocity, propene selectivity << propane selectivity, but at the highest space velocity, propene selectivity >> propane selectivity.
- The selectivity of $C_4$ alkanes was in general higher as compared to that of other aliphatic hydrocarbons and it increased with increasing the space velocity, similar to that observed in case of the propene aromatization.
- The selectivities of methane, ethane, ethylene and $C_{5-6}$ aliphatics were quite small. The selectivity of ethylene and $C_{5-6}$ aliphatics increased, that of ethane remained almost unchanged and that of methane decreased with increasing the space velocity.

*Effect of space velocity on the distribution of aromatics (Fig. 3.3.5)*

- The formation of benzene and toluene decreased, while that of $C_8$ and $C_{9+}$ aromatics increased with increasing the space velocity.

*Effect of space velocity on the distribution of xylene isomers (Fig.3.3.6)*

- The distribution of xylene isomers was influenced by the space velocity in the same way as that observed in the case of propene aromatization. The formation of m-xylene decreased and that of p-xylene and o-xylene increased with increasing the space velocity.

The order of selectivity of the different products and that of the distribution of aromatics and xylene isomers in the aromatization of n-butene at the different space velocities were as follows:

For product selectivity

At low space velocity (3,100 $cm^3g^{-1}h^{-1}$) : Aromatics > $C_4$-alkanes > propane >> propene > $CH_4$ > ethylene > $C_2H_6$ > $C_{5-6}$ aliphatics

At high space velocity (58,100 $cm^3g^{-1}h^{-1}$) : $C_4$-alkanes > aromatics > propene >> propane > ethylene > $C_{5-6}$ aliphatics > $C_2H_6$ > $CH_4$

For distribution of aromatics

$C_8$ aromatics > toluene > $C_{9+}$ aromatics > benzene (at all the space velocities)

For distribution of xylene isomers

At low space velocity (3100 $cm^3g^{-1}h^{-1}$) : m-xylene >> p-xylene > o-xylene

At high space velocity (58,100 $cm^3g^{-1}h^{-1}$) : p-xylene > o-xylene ≥ m-xylene

In the earlier studies, the aromatics yield in butene aromatization over H-ZSM-5 [6,9,20] and Zn/H-ZSM-5 [9] at 400°C was much lower than that obtained over the H-GaAlMFI used in the present case.

#### *3.3.3.4. Role of non-framework Ga-species and zeolitic protons and reaction path*

The H-GaAlMFI zeolite catalyst used in the present case contains two different types of active sites: zeolitic protons (measured in terms of the pyridine chemisorbed at 400°C) and the non-framework Ga-species (created due to the degalliation during the pretreatment of the zeolite catalyst), which are expected to be distributed uniformly in the zeolite channels. The observed high propene/butene aromatization activity of this zeolite catalyst is attributed to the presence of a large number of strong protonic acid sites in combination with the non-framework Ga-species (Table 3.3.1). The role of these active sites and the reactions involved in the aromatization of propene and butene have been illustrated in a simplified reaction scheme/pathway [based on the product selectivity/distribution at different space velocities (Figs. 3.3.1-3.3.6)] for the aromatization in Fig. 3.3.7.

The olefin aromatization is initiated with the oligomerization of olefin catalyzed by the zeolitic protons. The formation of an appreciable amount of $C_2$ and $C_4$ hydrocarbons in the propene aromatization and the $C_2$ and $C_3$ hydrocarbons in the

butene aromatization (Figs. 3.3.1 and 3.3.4) indicates the occurrence of olefin disproportionation and/or oligomer interconversion reactions. Among the aromatics, the formation of $C_8$ aromatics is highest and it is increased with increasing the space velocity (i.e. decreasing the contact time). This suggests that the predominant oligomer (which is formed in the oligomerization and/or oligomer interconversion reactions) involved in the aromatization consists essentially of 8 carbon atoms.

An appreciable amount of lower alkanes viz. $C_3$ and $C_4$ alkanes are formed in both the propene and butene aromatization reactions (Figs. 3.3.1 and 3.3.4). This suggests that the hydride transfer mechanism involving protonic acid sites in the conversion of olefin to aromatics hydrocarbons, proposed by Poustma [21], is operative in the aromatization process. However, the alkane/aromatics mole ratio observed in both the cases, particularly at the high aromatics yield (i.e. at lower space velocities), is < 1.0, which is much less than the alkane/aromatics ratio (3.0) required for satisfying the Poustma's mechanism. This observation leads to the conclusion that the formation of aromatics in the propene or n-butene aromatization also occurs by the direct dehydrocyclization essentially over the Ga-species, most probably in combination with the zeolitic protons. The Ga-species in the present case are expected to be formed by the degalliation of framework gallium and hence are likely to be located at the zeolitic channel intersections in a close vicinity of framework Al or Ga (i.e. zeolitic protons). Non- framework Ga-species in combination with protonic acid sites in Ga-modified ZSM-5 type zeolites are well known for their high dehydrogenation activity [22-24]. In the earlier sections (section 3.1 and 3.2) the study of the ethylene aromatization over H-ZSM-5 and different Ga-modified ZSM-5 type zeolites indicated that large number of both acid sites and non-framework Ga-species, particularly with an optimum ratio of non-framework Ga to strong acid sites (measured in terms of pyridine chemisorbed at 400°C), are required for obtaining high aromatic yields.

The distribution of aromatics and xylene isomers and their variation with space velocity (Figs. 3.3.2, 3.3.3, 3.3.5 and 3.3.6) suggest that p-xylene is likely to be a primary aromatic hydrocarbon formed, at least among the $C_8$-aromatics, in the aromatization of both propene and n-butene. This is also consistent with the steric hindrance to the respective xylene isomer in the zeolite channels. The diffusivity of xylene isomers in ZSM-5 zeolites is found to be in the following order: p-xylene >> o-xylene > m-xylene [25]. In case of the H-GaAlMFI, the steric hindrance is expected

to be much more because of the presence of Ga-species in the zeolite channels [26]. The observed distribution of aromatics (Figs. 3.3.2 and 3.3.5) is however controlled by their interconversion reactions, such as isomerization, disproportionation and dealkylation/alkylation, catalyzed by the zeolitic protons, depending upon the contact time. The formation of methane (the selectivity of which is relatively very low) is expected to be mostly by the hydrodealkylation of methyl aromatics. This is consistent with the increase in the formation of benzene (which is expected mostly from the dealkylation of toluene) with increasing the contact time (Figs. 3.3.2 and 3.3.5).

The proposed reaction path (Fig. 3.3.7) is, however, a simplified picture of a highly complex network of a large number of hydrocarbon conversion reactions occurring simultaneously in the overall propene or butene aromatization process over the H-GaAlMFI zeolite. Nevertheless, it provides a probable explanation for most of the product distributions in the propene or n-butene aromatization.

### 3.3.4. Conclusions

From the studies on the aromatization of propene and n-butene over the H-GaAlMFI catalyst, following important conclusions can be drawn:

1. The HGaAlMFI zeolite catalyst is a highly promising catalyst for the aromatization of propene and butenes. Its high olefin aromatization activity is attributed to the presence of non-framework Ga-species and strong protonic acid sites, both in large numbers.
2. The product selectivity and the distribution of aromatic hydrocarbons and xylene isomers found in both the propene and butene aromatization processes are strongly influenced by the space velocity (i.e. contact time).
3. In both the propene and butene aromatization processes, the distribution of aromatics and xylene isomers and their dependence on the space velocity are more or less similar but this is not the case for the aliphatic hydrocarbons.
4. The propene or n-butene aromatization processes involve both the hydride transfer reaction catalyzed by the zeolitic protons and the direct dehydrogenation reactions catalyzed by the non-framework Ga-species, probably in combination with the zeolitic protons. Among the aromatics, the formation of $C_8$-aromatics in both the processes is highest and it is increased with decreasing the contact time. The primary aromatic hydrocarbon formed

in both the processes seems to be p-xylene and the aromatics distribution is essentially controlled by the inter-aromatics transformation reactions (viz. isomerization, alkylation/dealkylation and disproportionation), depending upon the contact time.

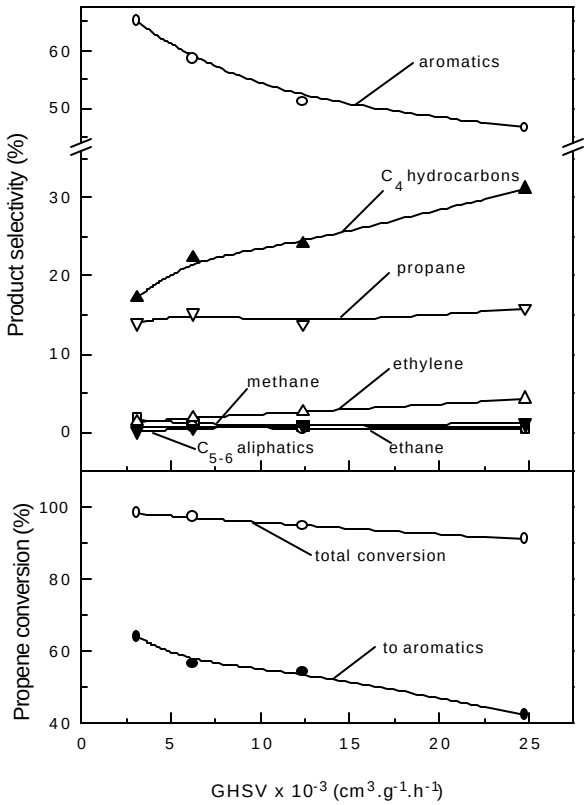


**Figure 3.3.1**. Variation with the space velocity of propene conversion (total and to aromatics) and product selectivity in the propylene aromatization.

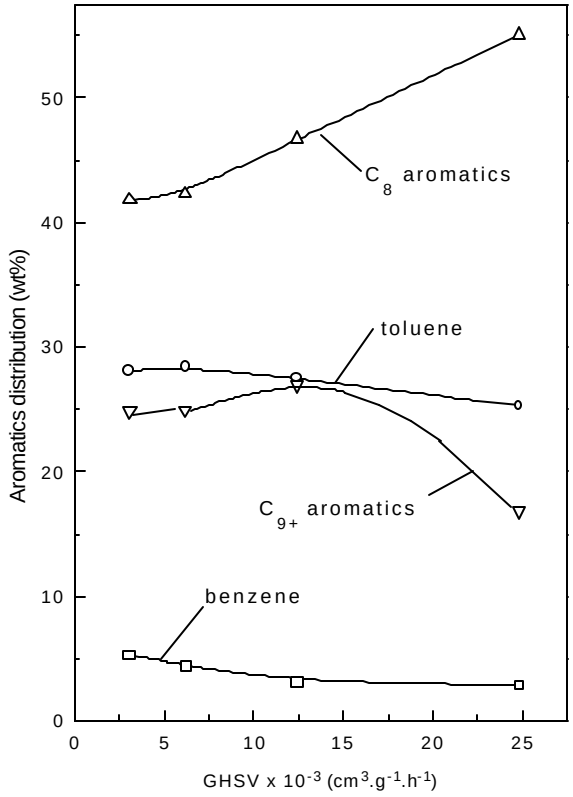


**Figure 3.3.2**. Dependence on the space velocity of the aromatics formed in the propylene aromatization.

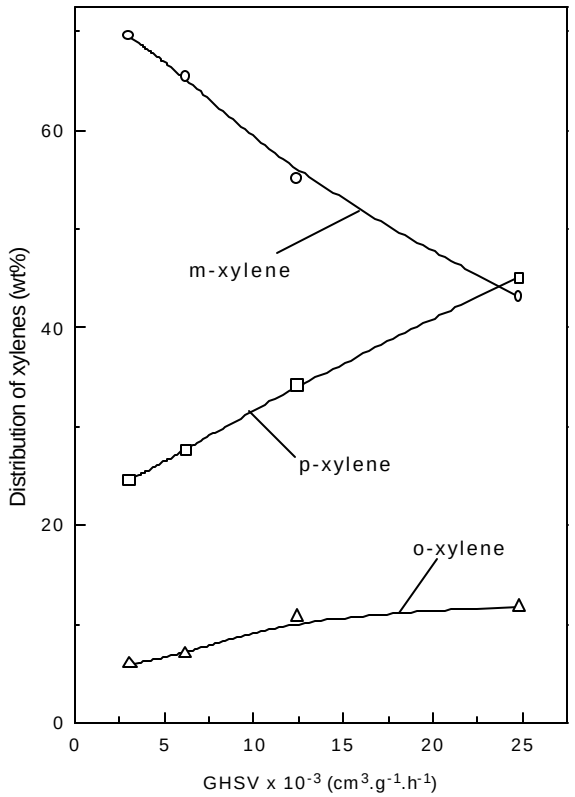


**Figure 3.3.3.** Dependence on the space velocity of the distribution of xylene isomers formed in the propene aromatization.

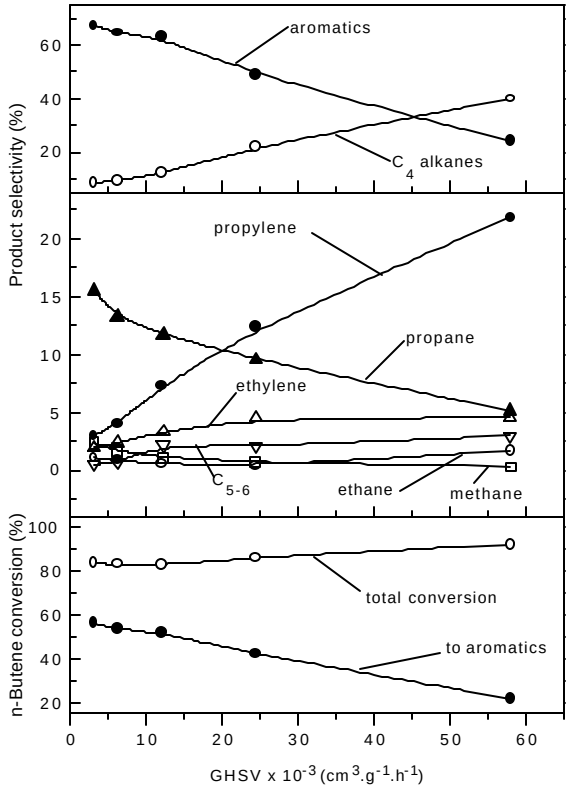


**Figure 3.3.4.** Variation with the space velocity of n-butene conversion (total and to aromatics) and product selectivity in the n-butene aromatization.

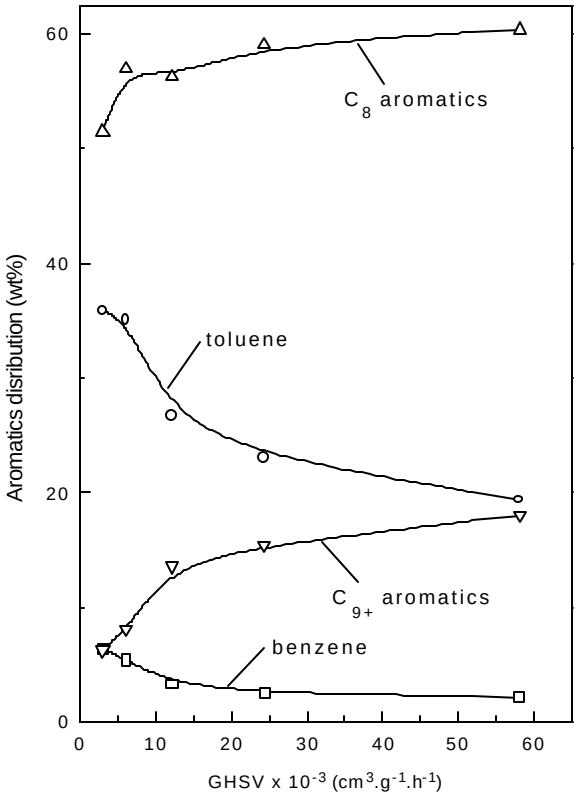


**Fig. 3.3.5** Dependence on the space velocity of the aromatics formed in the n-butene aromatization.

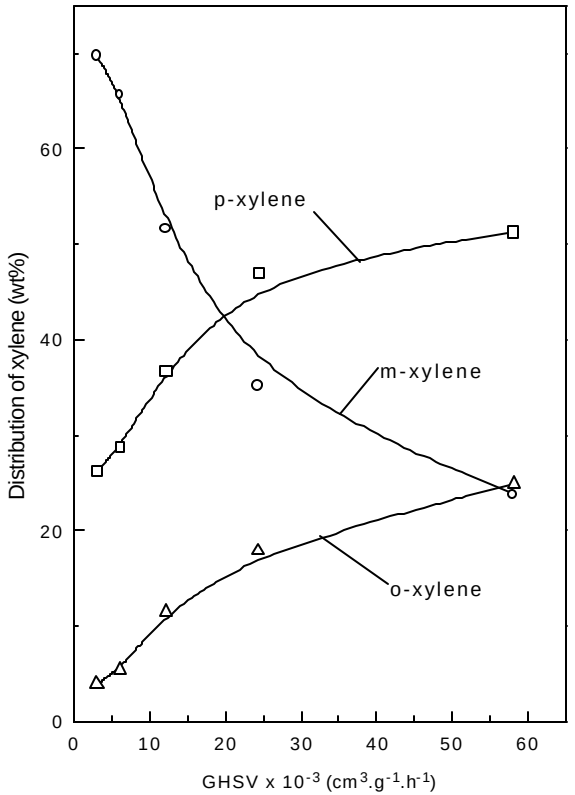


**Fig. 3.3.6**. Dependence on the space velocity of the distribution of xylene isomers formed in the n-butene aromatization.

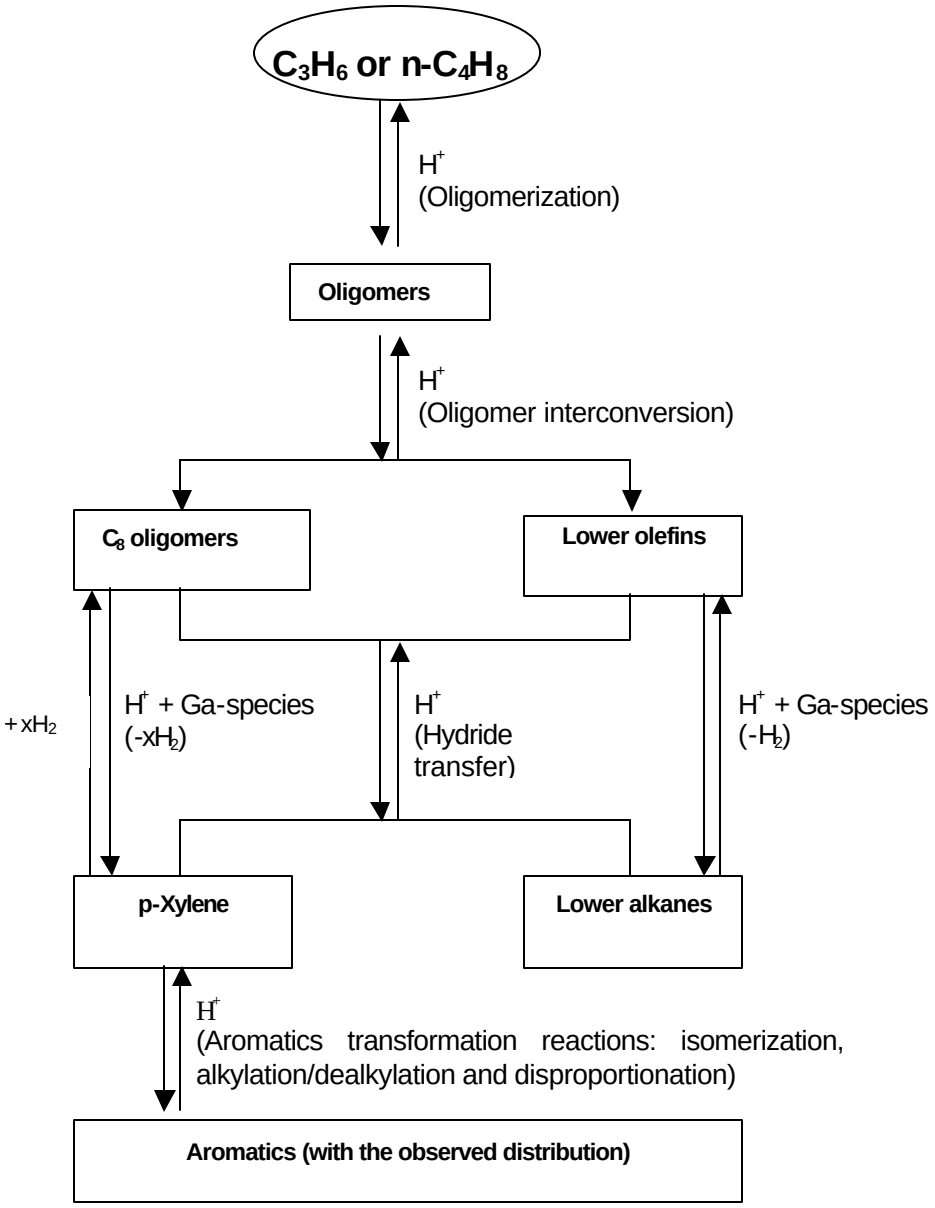


**Figure 3.3.7.** Simplified reaction scheme/pathway for the aromatization of propene or n-butene over H-GaAlMFI zeolite.

### 3.3.5. References


1. E. G. Derouane, J. P. Gilson and J. B. Nagy, J. Mol. Catal. 10 (1981) 331.
2. E. G. Derouane, J. P. Gilson and J. B. Nagy, Zeolite, 2 (1982) 42.
3. E. G. Derouane, C. Lefebvre and J. B. Nagy, J. Mol. Catal., 38 (1986) 387.
4. V. S. Nayak and V. R. Choudhary, Appl. Catal., 9 (1984) 251.
5. R. J. Quann, L. A. Green, S. A. Tabak, and F. J. Krambeck, Ind. Eng. Chem. Res., 27 (1988) 565.
6. G. W. Norval, M. J. Phillips, K. S. Virk and R. V. Simons, Can. J. Chem. Eng., 67 (1989) 521.
7. M. Shibata, H. Kitagawa, Y. Sendoda and Y. Ono, Stud. Surf. Sci. Catal., 28 (1986) 717.
8. D. B. Lukyanov, N. Gnep and M. R. Guisnet, Ind. Eng. Chem. Res., 33 (1994) 223.
9. Y. Ono, H. Kitagawa and Y. Sendoda, J. Chem. Soc. Faraday. Trans. 1, 83 (1987) 2913.
10. Z. Popova, K. Aristirova and Kh. Dimitrov, React. Kinet. Catal. Lett., 41 (1990) 369.
11. K. Arishtirova, Kh. Dimitrov, K. Dyrec, K. H. Hallmeier, Z. Popova and S. Witkowski, Appl. Catal. A:Gen., 81 (1992) 15.
12. G-J. Kim, K-H. Kim, W-S. Ko and Y. Ono, Kongop. Hwahak., 5 (1994) 957.
13. E. Angelescu, V. Parvulescu, G. Musca, F. Constantinescu, V. Dima, G. Gheorghe and G. Possa, Prog. Catal., 1 (1993) 32.
14. P. Qiu, J. H. Lunsford and M. P. Rosynek, Catal. Lett., 52 (1998) 37.
15. E. Angelescu, R. Stanescu, A. Cruceanu, G. Pop and F. Constantinescu, Prog. Catal., 4 (1995) 25.
16. R. Le VanMao, L. A. Dufresne, A. Louise, J. Yao and Y. Yu, Appl. Catal. A, 164 (1997) 81.
17. V. R. Choudhary, A. K. Kinage, C. Sivadinarayana and M. Guisnet, J. Catal., 158 (1996) 23.
18. V. R. Choudhary, A. K. Kinage and T. V. Choudhary, Appl. Catal. A: Gen., 162 (1997) 239.
19. J. M. Thomas and X-S. Lin, J. Phys. Chem., 90 (1986) 4843.

20. D. Bhattacharya and S. Sivasanker, Catal. (Pap. Natl. Symp.) 12th, Meeting Date 1994 (N. M. Gupta and D. K. Chakrabarty, Eds.), p. 191, Narosa, New Delhi, India, (1996).
21. M. I. Poustma, in "Zeolite Chemistry and Catalysis". (J. A. Rabo, Ed.), ACS Monograph 171, p. 437, American Chemical Society, Washington D. C., (1976).
22. M. Guisnet, N. S. Gnep and F. Alario, Appl. Catal., 89 (1992) 1.
23. Y. Ono, Catal. Rev. Sci. Eng., 34 (1992) 179.
24. G. Giannetto, R. Monque and R. Galiasso, Catal. Rev. Sci. Eng., 36 (1994) 271.
25. V. R. Choudhary, V. S. Nayak and T. V. Choudhary, Ind. Eng. Chem. Res., 36 (1997) 1812.
26. V. R. Choudhary and A. S. Mamman, AIChEJ, 36 (1990) 1577.

# PART IV

## COMPLETE COMBUSTION OF LOWER ALKANES

# CHAPTER 4.1

# ACTIVATION BY HYDROTHERMAL TREATMENT OF LOW SURFACE AREA $ABO_3$-TYPE PEROVSKITE OXIDE CATALYSTS

## 4.1.1. Earlier Work/ Background and Objectives of Present Work

$ABO_3$ type perovskite oxides (A= rare earth element with or without its partial substitution by alkaline earth element, and B= transition element such as Co, Mn, Ni, Fe, etc., with or without its partial substitution by other transition element) have high potential for their use as catalysts in a number of catalytic reactions [1-5]. The classical ceramic solid-solid reaction and coprecipitation methods, commonly used for the synthesis of perovskite-type oxide, involve high reaction temperature (>900°C) and hence yield perovskite-type oxides with a low surface area (< $2 m^2 g^{-1}$) due to their sintering [1]. The perovskite-type oxides are also deactivated due to sintering or crystal growth during their continuous use in high temperature processes. The catalytic performance of the perovskite-type oxides is well known to depend on their specific surface area [1,2,6], and hence it is of great practical interest to activate low surface area perovskite oxides, which are prepared by the high temperature synthesis methods and/or sintered during their use, by some means. Perovskite-type oxides, having surface areas up to about 20 $m^2 g^{-1}$ could be prepared by spray drying and freeze drying processes, using mutually soluble compounds. Such processes achieve good chemical homogeneity for perovskite precursors, which are then fired at low temperatures [1-3]. These aspects have been discussed earlier (section 1.1.3). However, the processes need special equipment and are limited to mutually soluble compounds.

The present work was undertaken with the objective of activating low surface area $LaCoO_3$ and $LaMnO_3$ perovskite-type oxides, synthesized by the conventional carbonate precipitation method, by their hydrothermal treatment and test their catalytic activity for the complete combustion of methane.

## 4.1.2. Experimental

The $LaCoO_3$ (surface area SA=0.9 $m^2 g^{-1}$) and $LaMnO_3$ (SA=1.7 $m^2 g^{-1}$) perovskite-type oxides were prepared by carbonate coprecipitation method involving calcination at 925°C. The detailed synthesis procedure of the perovskites has already

been described earlier (section 1.2.1.3). The hydrothermal treatment to the perovskite-type oxide with water under autogeneous pressure was carried out in a closed stainless steel bomb, using 1.6 ml water per gram of perovskite-type oxide, at different temperatures for 4h. The hydrothermal treatment to the $LaCoO_3$ with steam at atmospheric pressure was carried out in a conventional quartz reactor by passing a mixture of steam and $N_2$ (60 mol% steam) at a space velocity of 5100 $cm^3g^{-1}h^{-1}$. After the hydrothermal treatment, the perovskite-type oxides were calcined at 600°C for 1h.

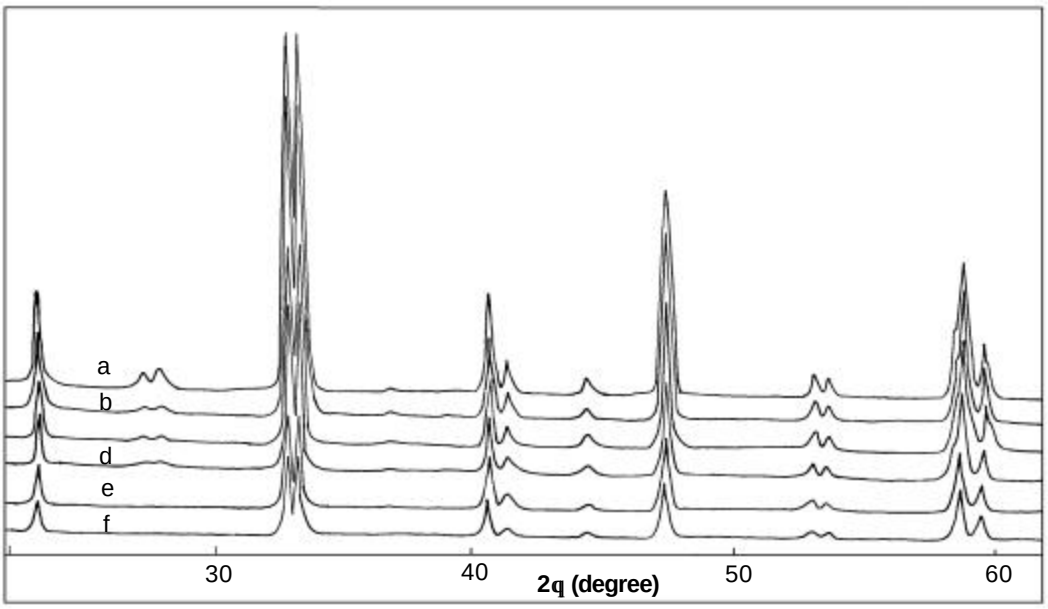


**Figure 4.1.1**. XRD spectra of $LaCoO_3$ [ without treatment (a), treated with water at 125°C (b), 175°C (c), 275°C (d) and with steam at 350°C (e) and 800°C (f)].

The perovskite-type oxides before and after the hydrothermal treatments were characterized by XRD, XPS, SEM and surface area.

The catalytic activity of the perovskite-type oxides in a complete combustion of methane was measured by passing continuously a methane (2.5 mole%)-air mixture at a space velocity of 51,000 $cm^3g^{-1}h^{-1}$ (measured at 0°C and atmospheric pressure) over a 0.1 g catalyst diluted uniformly with 0.4g inert solid particles in a quartz reactor (Figure

1.2.1a) at different temperatures and analyzing the reaction products by an on-line gas chromatograph. The reaction set-up has been described earlier (section 1.2.3.3 and Fig. 1.2.8).

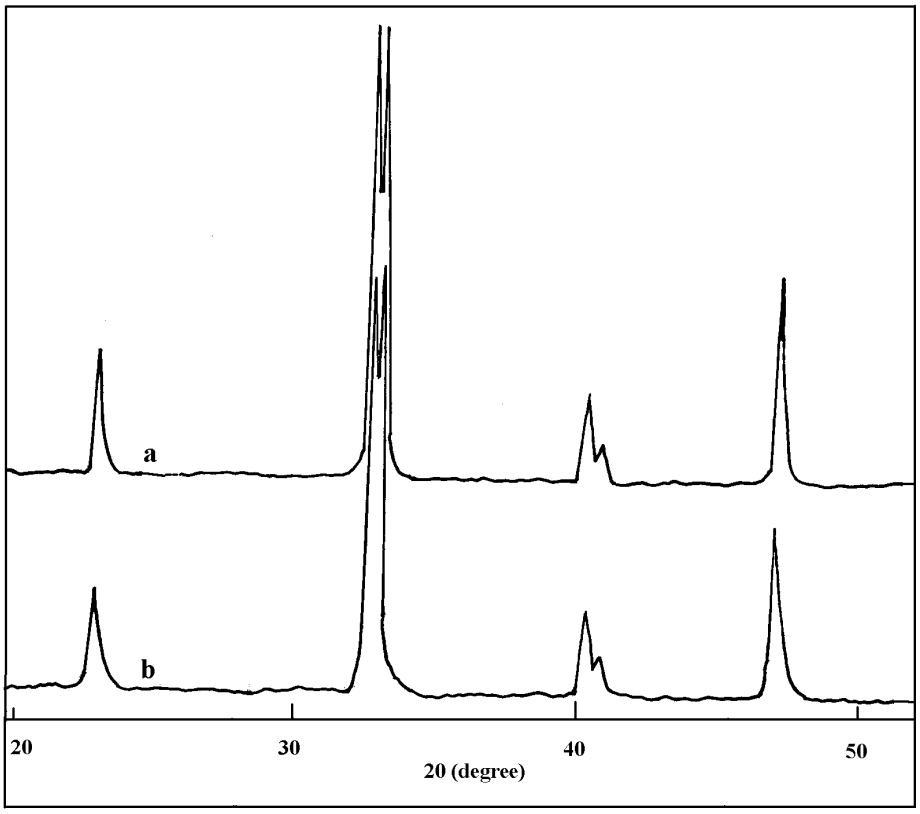


**Figure.4.1.2.** XRD spectra of $LaMnO_3$ [without treatment (a), treated with water at 225$^oC$ (b)].

### 4.1.3. Results and Discussion

The XRD spectra of $LaCoO_3$ and $LaMnO_3$ perovskite-type oxides with or without hydrothermal treatment are shown in Figs. 4.1.1 and 4.1.2. The scanning electron micrographs of $LaCoO_3$ and $LaMnO_3$ perovskite oxides with or without hydrothermal treatment are shown in Figs. 4.1.3 and 4.1.4. Results showing the influence of temperature on the conversion of methane in its complete combustion over hydrothermally treated $LaCoO_3$ and $LaMnO_3$ perovskite oxides are presented in Figs. 4.1.5 – 4.1.7. The $LaCoO_3$ and $LaMnO_3$ perovskites with or without hydrothermal

treatment are compared for their surface area, crystal size, surface La/(Co or Mn) atomic ratio and turn over frequency (TOF) at 600°C in Tables 4.1.1 and 4.1.2.

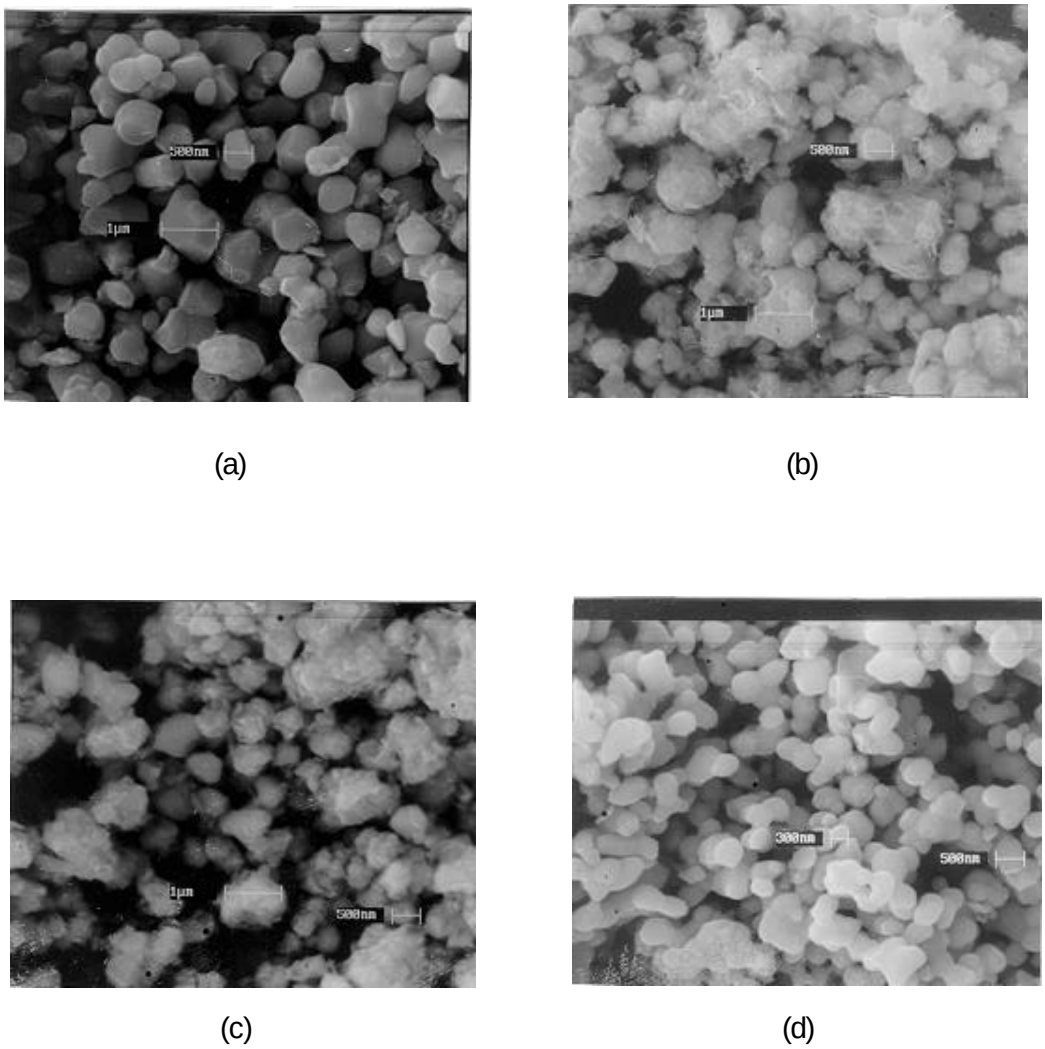


(a) (b)

(c) (d)

**Figure 4.1.3.** Scanning Electron Micrograph of $LaCoO_3$ without water treatment (a), treated with water at 175°C (b) and at 225°C (c), treated with steam at 800°C (d).

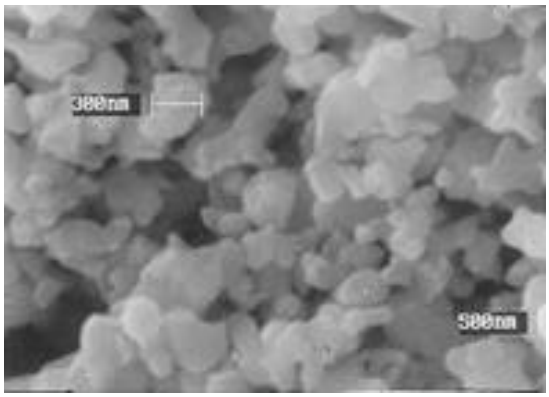

(a)

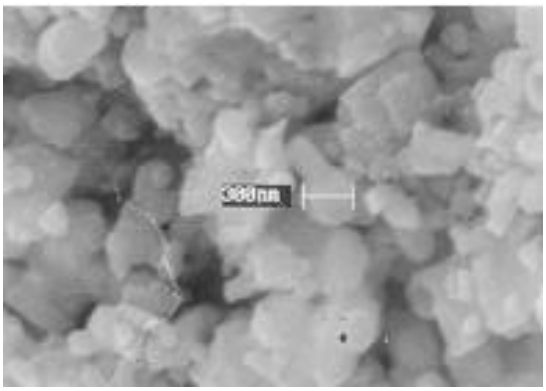

(b)

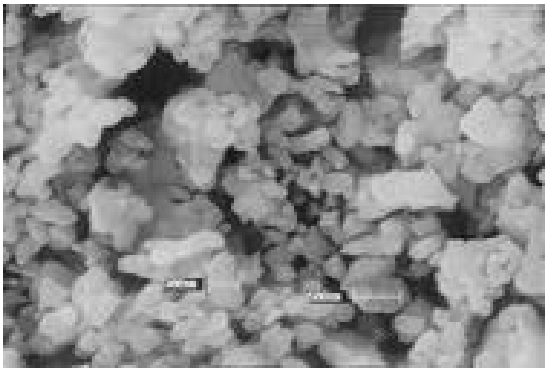

(c)

**Figure 4.1.4.** Scanning Electron Micrograph of $LaMnO_3$ without water treatment (a), treated with water at 225°C (b) and at 300°C (c).

**Table 4.1.1.** Results of the activation of $LaCoO_3$ and $LaMnO_3$ perovskite oxides by their water treatment under autogeneous pressure.

| Perovskite oxide | Water treatment tempera-ture ($^oC$) | Surface area ($m^2g^{-1}$) | Crystal size ($\mu m$) | Surface La/(Co or Mn) ratio | Methane conversion at 600$^oC$ (%) | TOF at 600$^oC$ ($\mu mol.m^{-2}s^{-1}$) |
|---|---|---|---|---|---|---|
| $LaCoO_3$ | Without treatment | 0.9 | 1.1 | 0.98 | 20.0 | 3.51 |
| | 125 | 7.8 | - | - | 42.1 | 0.85 |
| | 175 | 14.3 | 0.7 | - | 43.5 | 0.48 |
| | 225 | 16.0 | 0.6 | 1.30 | 64.0 | 0.63 |
| $LaMnO_3$ | Without treatment | 1.7 | 0.5 | 1.08 | 15.1 | 1.40 |
| | 175 | 3.0 | - | - | 26.4 | 1.38 |
| | 225 | 3.9 | 0.45 | 1.11 | 36.7 | 1.49 |
| | 300 | 4.5 | 0.4 | 1.20 | 39.9 | 1.40 |

**Table 4.1.2.** Results of the activation of $LaCoO_3$ by its steam treatment at atmospheric pressure.

| Steam Treatment temperature ($^oC$) | Surface area ($m^2g^{-1}$) | Crystal size ($\mu m$) | Surface La/Co ratio | Methane conversion at 600$^oC$ (%) | TOF at 600$^oC$ ($\mu mol.m^{-2}s^{-1}$) |
|---|---|---|---|---|---|
| Without treatment | 0.9 | 1.1 | 0.98 | 20.0 | 3.5 |
| 350 | 1.4 | - | - | 34.1 | 3.9 |
| 500 | 1.5 | - | - | 35.0 | 3.7 |
| 600 | 1.7 | - | - | 37.3 | 3.5 |
| 700 | 1.9 | - | - | 39.1 | 3.3 |
| 800 | 2.3 | 0.4 | 1.08 | 41.2 | 2.8 |

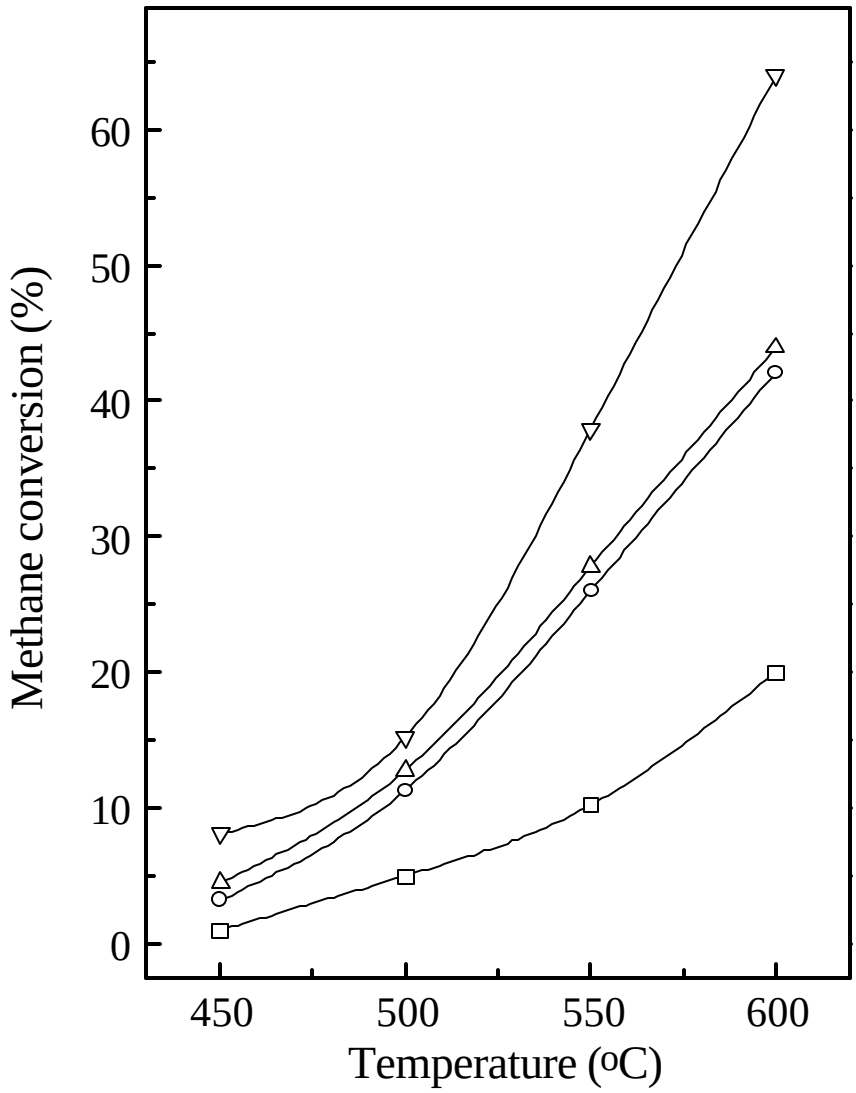


**Figure 4.1.5.** Effect of temperature on the conversion of methane in its complete combustion over $LaCoO_3$ treated with water at 125°C (○), 175°C (Δ), 225°C (∇) and without water treatment ( ).

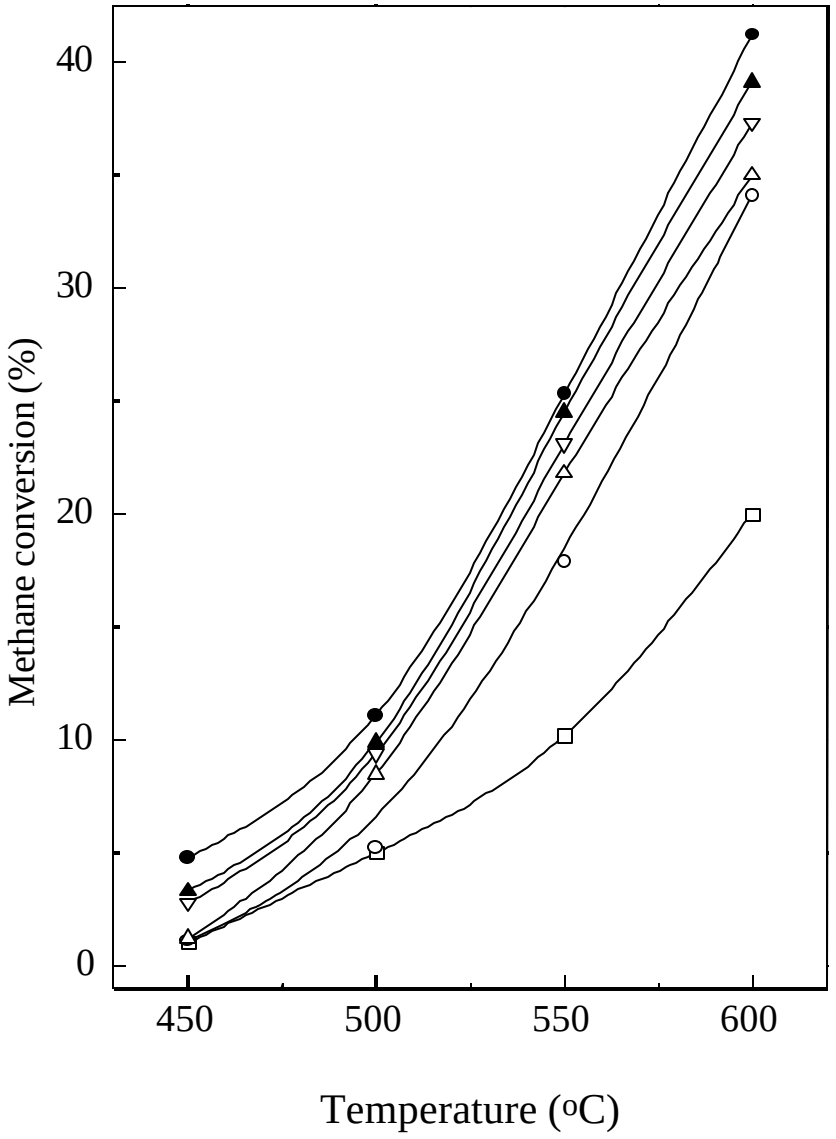


**Figure 4.1.6.** Effect of temperature on the conversion of methane in its complete combustion over $LaCoO_3$ treated with steam at 350°C (○), 500°C (Δ), 600°C (▽), 700°C ( ), 800°C (●) and without water treatment ( ).

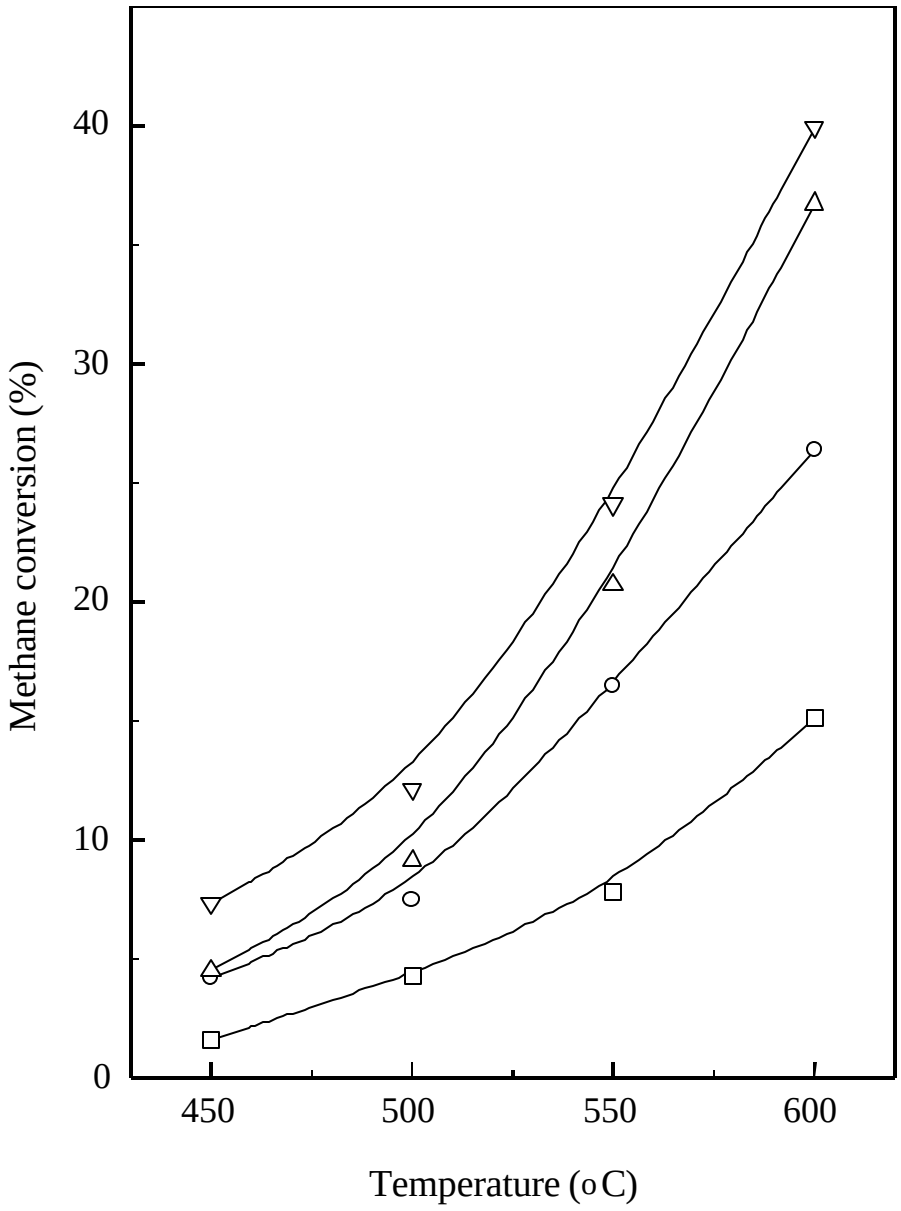


**Figure 4.1.7.** Effect of temperature on the conversion of methane in its complete combustion over $LaMnO_3$ treated with water at 175°C (o), 225°C (Δ), 300°C (∇) and without water treatment ( ).

The following observations are made from the results (Figs. 4.1.1-4.1.7 and Tables 4.1.1-4.1.2) of the water treatment to $LaCoO_3$ and $LaMnO_3$ perovskites and steam treatment to $LaCoO_3$ perovskite oxide:

- Both the water and steam treatments (at different temperatures) have no significant effect on the structure of perovskite oxides (Figs. 4.1.1 - 4.1.2).
- The hydrothermal treatments result in a very significant increase in surface area for $LaCoO_3$ perovskite oxide, but for $LaMnO_3$ perovskite, the increase in surface area is relatively less.
- The steam treatment of $LaCoO_3$ perovskite results in a small increase in its surface area.
- In case of $LaCoO_3$, there is a very significant change in the crystal size and morphology due to the hydrothermal treatment (Fig. 4.1.3), depending upon its severity. However, in case of $LaMnO_3$, the observed changes in the crystal size and morphology after the hydrothermal treatment are relatively very small (Fig. 4.1.4).
- The surface La/Co (or Mn) ratio of the perovskite oxides is increased with increasing the severity (i.e. temperature) of the hydrothermal treatment.
- The methane combustion activity of all the water and steam treated catalysts are higher than that of the untreated one. As compared to $LaMnO_3$, the increase in the catalytic activity of $LaCoO_3$ due to the hydrothermal treatments is larger.

These observations clearly indicate a beneficial effect of the hydrothermal treatments and steam treatment to the perovskite-type oxides for their activation or reactivation. This approach may also be employed for activating other low surface area or sintered perovskite-type oxides.

The increase in the surface area of the perovskite-type oxides and the observed decrease in the crystal size by the steam treatment at $350^oC$ - $800^oC$ are expected because of the recrystallization during the high temperature hydrothermal treatment depending upon the steam treatment temperature. Whereas, in the water treatment at autogeneous pressure (at $125^oC$ - $300^oC$), the perovskite-type oxides are expected to be hydrolyzed, at least partially, and recrytallized during the calcination at $600^oC$, leading to a large increase in their surface area. The hydrolysis followed by the recrystallization may have caused a larger change in the surface area and crystal size in case of the water treatment.

The observed increase in the surface La/Co (or Mn) ratio with increasing the severity of the hydrothermal treatment in both the water and steam treatment also indicate the recrystallization of the perovskite-type oxide causing redistribution of La and Co (or Mn).

The methane combustion activity, when expressed per unit mass of the perovskite-type oxide catalyst, is increased due to the hydrothermal pretreatment. However, the catalytic activity, when expressed per unit surface is decreased appreciably (Table 4.1.1), particularly due to water treatment and this is consistent with the increase in the surface La/Co (or Mn) ratio or with the decrease in the surface concentration of Co or Mn (which is responsible for the combustion activity of the catalyst.

### 4.1.4. Conclusions

Surface area and catalytic activity (in the methane combustion for methane emission control) of low surface area (or sintered) $LaCoO_3$ and $LaMnO_3$ perovskite type oxides can be increased markedly by hydrothermal treatment of the perovskites with water (under autogeneous pressure) or steam. In the hydrothermal treatments, there is little or no influence on the structure of the perovskite oxide, but its crystal size and surface La/Co (or Mn) ratio are changed significantly; the former is decreased and the later is increased with increasing the severity of hydrothermal treatment.

### 4.1.5. References


1. R. J. H. Voorhoeve, D. W. Johnson Jr., J. P. Remeika and P.K. Gallagher, Science, 195 (1977) 827.
2. L. G. Tejuca, J. L. G. Fierro and J. M. D. Tascon Adv. Catal, 36 (1989) 237.
3. L. G. Tejuca and J. L. G. Fierro (Eds) *in* "Properties and Applications of Perovskite-type oxides", Marcel Dekker Inc., New York, 1993.
4. T. Seiyama, Catal. Rev. Sci. Eng., 34 (1992) 281.
5. J. G. McCurry and H. Wise, Catal. Today, 8 (1990) 175.
6. N. Yamazoe and Y. Teraoka, Catal. Today, 8 (1990) 175.

# CHAPTER 4.2

# LOW TEMPERATURE COMPLETE COMBUSTION OF DILUTE PROPANE OVER Mn-DOPED $ZrO_2$ (CUBIC) CATALYST

## 4.2.1. Earlier Work/Background and Objectives of Present Work

Because of its cleaner combustion, liquefied petroleum gas (LPG), which is a mixture of propane and butanes, is used as a petrol substitute for automobiles in metropolitan cities. The reactivity of propane is less than that of butanes, and hence the concentration of propane in the unburned hydrocarbons in the auto-exhaust gases is much higher. For controlling the hydrocarbon emission from the LPG-fuelled automobiles, an efficient catalyst for the complete combustion of propane at low concentration (<1%) is essential.

A number of studies have been reported earlier on the catalytic combustion of propane over different noble metals and transition metal oxide catalysts, such as Pt or Pd/glass fiber [1], $Pt/TiO_2$ [2], $Pd/SiO_2$-$Al_2O_3$ [3], $Pt/Al_2O_3$ [4], Cu, Pd or Pt modified ZSM-5 [5,6], single or mixed transition metal oxides [7-10] and transition metal oxides supported on silica fiber [11]. Recent literatures have been briefly reviewed in earlier section (section 1.1.4). However, the studies on the complete combustion of dilute propane are scarce. Recently Taylor and O'Leary [12] reported oxidative destruction of $C_1$-$C_4$ hydrocarbons over uranium oxide based catalysts. They observed that the oxidation activity of $U_3O_8$ is increased by its modification by Cr, which causes an increase in the defect structure of the oxide.

Noble metal-based catalysts have in general high hydrocarbon combustion activity but they are quite costly and more prone to deactivation by poisoning [13,14]. Whereas, transition metal oxide based catalysts are generally less active but more resistant towards catalyst poisoning and also their cost is much lower. In the earlier literatures, the high activity of Mn-doped $ZrO_2$ in its cubic form for the combustion of butane [15] and dilute methane (1% in air) [16], comparable to that of noble metal catalysts, have been reported.

This work was undertaken for studying in details the complete combustion of dilute propane (0.9% propane in air) over Mn-doped $ZrO_2$ (cubic) catalysts. Influence of various catalyst parameters (catalyst preparation and composition) and process parameters (temperature and space velocity) on the propane combustion have been

investigated. Involvement of lattice oxygen from the catalyst in the combustion has also been studied.

### 4.2.2. Experimental

The Mn-doped $ZrO_2$ catalyst was prepared by mixing aqueous solutions of zirconyl nitrate and manganese acetate (Mn/Zr mole ratio varied from 0.05 to 0.67), coprecipitating metal hydroxides from the solution using tetramethyl ammonium hydroxide (25%) (TMAOH). The details of catalyst synthesis have been discussed earlier (section 1.2.1.3). Other Mn-doped $ZrO_2$ catalysts having Mn/Zr ratio 0.25 were prepared by coprecipitating the mixed metal hydroxides from mixed aqueous solution of respective metal nitrates, using different precipitating agents e.g. tetramethyl ammonium hydroxide (25%) (TMAOH), tetraethyl ammonium hydroxide (25%) (TEAOH), tetrapropyl ammonium hydroxide (25%) (TPAOH), tetrabutyl ammonium hydroxide (25%) (TBAOH) and ammonium hydroxide (30%), by the same way. The Mn-doped $ZrO_2$ having Mn/Zr ratio 0.11 was calcined at different temperature (500°C - 800°C) for 8h. The Mn- impregnated $ZrO_2$ (Mn/Zr =0.25) was prepared by impregnating $ZrO_2$ with Mn- acetate by incipient wetness method and calcining at 500°C for 8h.

The catalysts were characterized for their surface area and for their crystalline phases by XRD.

The propane combustion activity of all the catalysts was measured at atmospheric pressure in a continuous fixed bed quartz-microreactor. (i. d. 10 mm) containing 0.1 g catalyst (22-30 mesh size particles), mixed uniformly with 0.4 g inert $\alpha$-$Al_2O_3$ particles (22 - 30 mesh size), at different process conditions (temperature: 300° – 500°C and space velocity: 25000 – 100,000 $cm^3.g^{-1}.h^{-1}$, measured at NTP) using 0.9 mol % propane in air as a feed .The reaction set-up has already been described in section 1.2.3.3b and Fig. 1.2.8.

The pulse reaction of propane (at 500°C) over the catalyst in the absence of $O_2$ as a function of pulse number was carried out in a quartz pulse micro-reactor connected to the GC, using He (30 $cm^3.min^{-1}$) as a carrier gas, following the procedure described elsewhere [17,18]. The products of the pulse reaction were analyzed using a Spherocarb column and thermal conductivity detector. The experimental set-up has been described in earlier section (section 1.2.3.3a and Fig. 1.2.7).

**Table 4.2.1.** Surface area and crystalline phases of the Mn-doped $ZrO_2$ catalysts (Mn/Zr = 0.05 – 0.67) prepared by using different precipitating agents and calcined at different temperatures.

| Mn/Zr ratio in Mn-doped $ZrO_2$ | Precipitating agent used in the catalyst preparation | Calcination temperature ($^oC$) | Surface area ($m^2g^{-1}$) | Crystalline phases |
|---|---|---|---|---|
| 0.05 | TMAOH | 500 | 74 | Cubic $ZrO_2$ (major) and monoclinic $ZrO_2$ (minor) |
| 0.11 | TMAOH | 500 | 86 | Cubic $ZrO_2$ |
| 0.25 | TMAOH | 500 | 105 | Cubic $ZrO_2$ |
| 0.43 | TMAOH | 500 | 91 | Cubic $ZrO_2$ |
| 0.67 | TMAOH | 500 | 73 | Cubic $ZrO_2$ |
| 0.11 | TMAOH | 600 | 72 | Cubic $ZrO_2$ |
| 0.11 | TMAOH | 700 | 25 | Cubic $ZrO_2$ |
| 0.11 | TMAOH | 800 | 11 | Cubic $ZrO_2$, monoclinic $ZrO_2$ and $MnO_2$ |
| 0.25 | TEAOH | 500 | 134 | Amorphous |
| 0.25 | TPAOH | 500 | 65 | Amorphous |
| 0.25 | TBAOH | 500 | 45 | Cubic $ZrO_2$ (major) and monoclinic $ZrO_2$ (minor) |
| 0.25 | $NH_4OH$ | 500 | 122 | Cubic $ZrO_2$ (major) and monoclinic $ZrO_2$ (minor) |

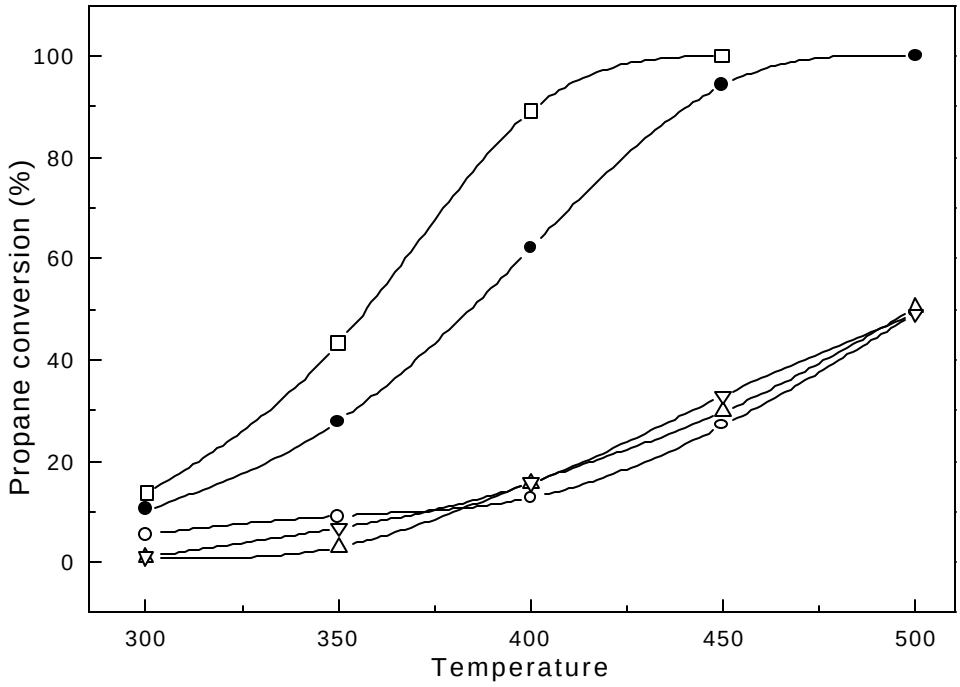


**Figure 4.2.1.** Temperature dependence of the propane conversion in the combustion of propane (GHSV = 51,000 $cm^3g^{-1}h^{-1}$) over Mn-doped $ZrO_2$ (Mn/Zr = 0.25) catalyst (calcined at 500°C) prepared using different precipitating agents [TMAOH (□), TEAOH (○), TPAOH (Δ), TBAOH (▽) and $NH_4OH$ (●)].

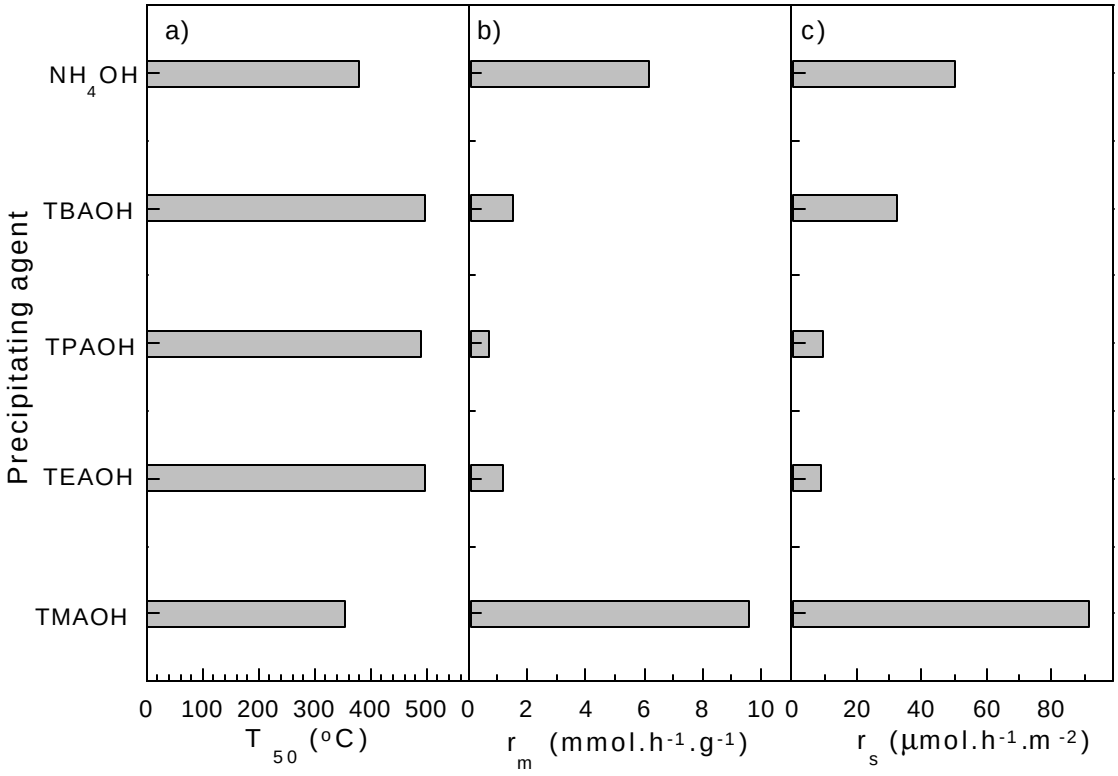


**Figure 4.2.2.** Effect of the precipitating agent used for the preparation of Mn-doped $ZrO_2$ (Mn/Zr = 0.25) catalyst (calcined at 500°C) on (a) the temperature required for 50% ($T_{50}$) conversion of propane, (b) propane conversion rate (at 350°C) based on the mass of catalyst ($r_m$) and (c) propane conversion rate (at 350°C) based on the surface area of catalyst ($r_s$) in the combustion of propane (space velocity: 51,000 $cm^3.g^{-1}.h^{-1}$).

### 4.2.3. Results and Discussion

#### *4.2.3.1. Characterization of Mn-doped $ZrO_2$ catalysts*

The Mn-doped $ZrO_2$ catalysts (with different Mn/Zr ratios) prepared using different precipitating agents and calcined at different temperatures have been characterized for their surface area and crystalline nature. The catalyst characterization data are given in Table 4.2.1. From a comparison of the data,

following important observations for the effect of the precipitating agent used, and the Mn/Zr ratio and calcination temperature of the catalyst on its surface and bulk properties can be made.

- The use of TEAOH or TPAOH as the precipitating agent leads to the catalyst amorphous in nature. Whereas, when TMAOH, TBAOH and $NH_4OH$ are used as the precipitating agents, the $ZrO_2$ of the resulting catalyst is at least partly in cubic form. The use of TBAOH and $NH_4OH$ results in the catalyst (with Mn/Zr = 0.25) in both cubic (major) and monoclinic (minor) forms. However, a pure cubic form of the catalyst (with Mn/Zr = 0.11 – 0.67) is obtained when TMAOH is used as the precipitating agent.
- The cubic form of the catalyst (with Mn/Zr =0.11) remains intact upto the catalyst calcination temperature of 700°C; at 800°C a small part of the cubic $ZrO_2$ is transformed into monoclinic $ZrO_2$.
- The surface area of the catalyst is also strongly influenced by the Mn/Zr ratio, precipitating agent and calcination temperature. It is decreased with increasing the calcination temperature but passed through a maximum with increasing the Mn/Zr ratio. The order of the surface area of the catalysts (with Mn/Zr ratio = 0.25, and calcined at 500°C) prepared using the different precipitating agents is as follows: TEAOH > $NH_4OH$ > TMAOH > TPAOH > TBAOH.

#### *4.2.3.2. Catalytic combustion of propane*

***4.2.3.2.1. Effect of precipitating agent:*** Results showing the influence of the precipitating agent used in the preparation of Mn-doped $ZrO_2$ (with Mn/Zr = 0.25, and calcined at 500°C) on the propane combustion are presented in Figs. 4.2.1 and 4.2.2.

Results in Fig. 4.2.1 show a strong influence of the precipitating agent on the propane conversion activity at different temperatures of the Mn-doped catalyst. The temperature required for half the propane combustion reaction (i.e. 50% conversion of propane) is lowest for the catalyst prepared using TMAOH (Fig. 4.2.2a). The rate of propane conversion in the combustion reaction when expressed in terms of the amount of propane converted per hour per unit mass or per unit surface area of the

catalyst is also highest for the catalyst prepared using TMAOH. The order of preference for the different precipitating agents is as follows:

Order based on the rate per unit mass: TMAOH > $NH_4OH$ > TBAOH > TEAOH > TPAOH

Order based on the rate per unit surface area: TMAOH > $NH_4OH$ > TBAOH > TPAOH ≥ TEAOH

The results clearly show that the most preferred precipitating agent for the preparation of the catalyst, which shows highest propane combustion activity, is TMAOH and the next preferred precipitating agent is $NH_4OH$.

It is interesting to note from the results (Fig 4.2.2b,c and Table 4.2.1) that the catalyst, which showed highest propane combustion activity, is in a pure cubic form. Whereas, the catalysts, which showed very low propane combustion activity, are in amorphous form and those showed intermediate performance are in both the cubic and monoclinic forms.

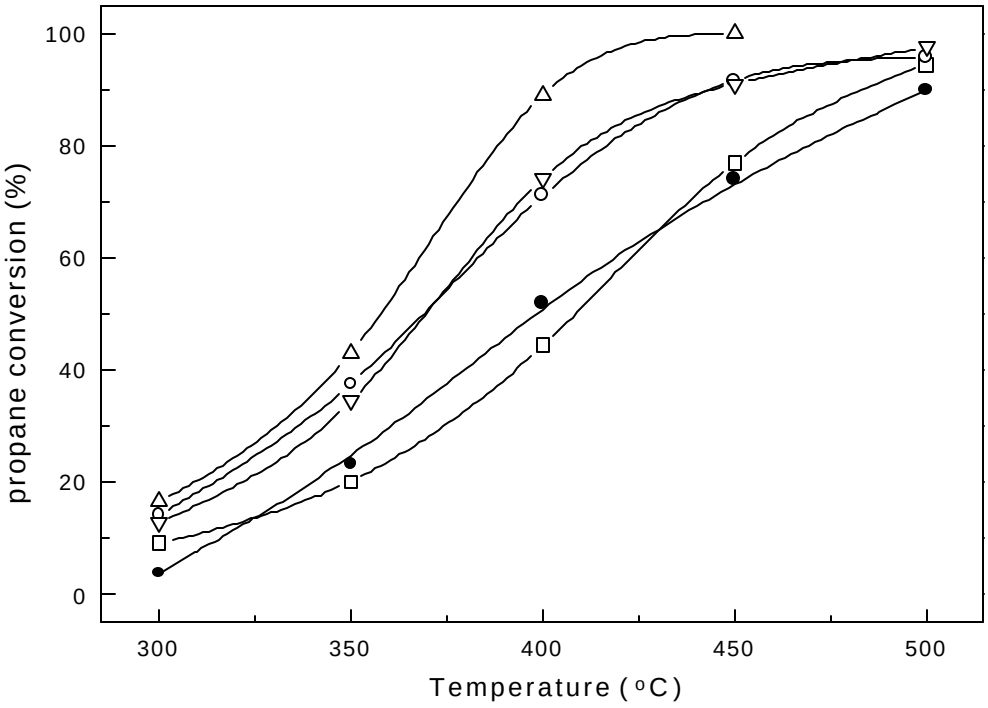


**Figure 4.2.3.** Temperature dependence of the propane conversion in the combustion of propane (GHSV = 51,000 $cm^3g^{-1}h^{-1}$) over Mn-doped $ZrO_2$ catalyst (prepared using TMAOH and calcined at 500°C) with different Mn/Zr ratios [Mn/Zr = 0.05 ( ), 0.11 (O), 0.25 (Δ), 0.43 (∇) and 0.67 (●)].

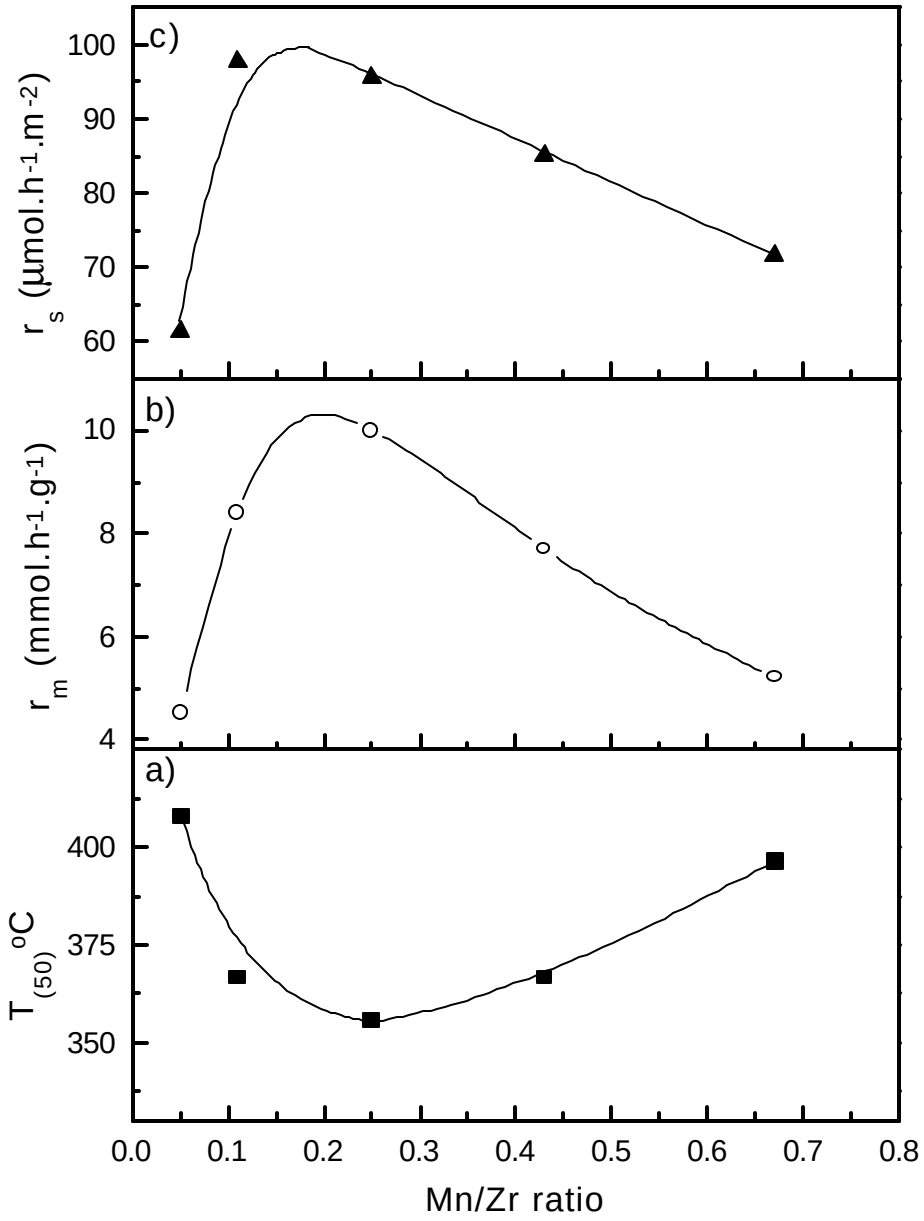


**Figure 4.2.4.** Effect of the Mn/Zr ratio of Mn-doped $ZrO_2$ catalyst (prepared using TMAOH) and calcined at 500°C) on (a) the temperature required for 50% ($T_{50}$) conversion of propane, (b) propane conversion rate (at 350°C) based on the mass of catalyst ($r_m$) and (c) propane conversion rate (at 350°C) based on the surface area of catalyst ($r_s$) in the combustion of propane.

***4.2.3.2.2. Effect of Mn/Zr ratio:*** Results showing the temperature dependence of propane conversion in the combustion reaction over the Mn-doped $ZrO_2$ catalyst (prepared using TMAOH and calcined at 500°C) with different Mn/Zr ratios are presented in Fig. 4.2.3. Dependence of the temperature required for half the reaction and also of the propane combustion activity upon the Mn/Zr ratio of the catalyst (prepared using TMAOH and calcined at 500°C) is shown in Fig. 4.2.4.

The results show a strong influence of the Mn/Zr ratio on the catalytic performance of the Mn-doped $ZrO_2$ catalyst in the propane combustion. When the Mn/Zr is increased, the activity of the catalyst, expressed in terms of the temperature required for half the propane combustion reaction or the propane conversion rate, is passed through a maximum at the Mn/Zr ratio of about 0.2 (Fig. 4.2.4).

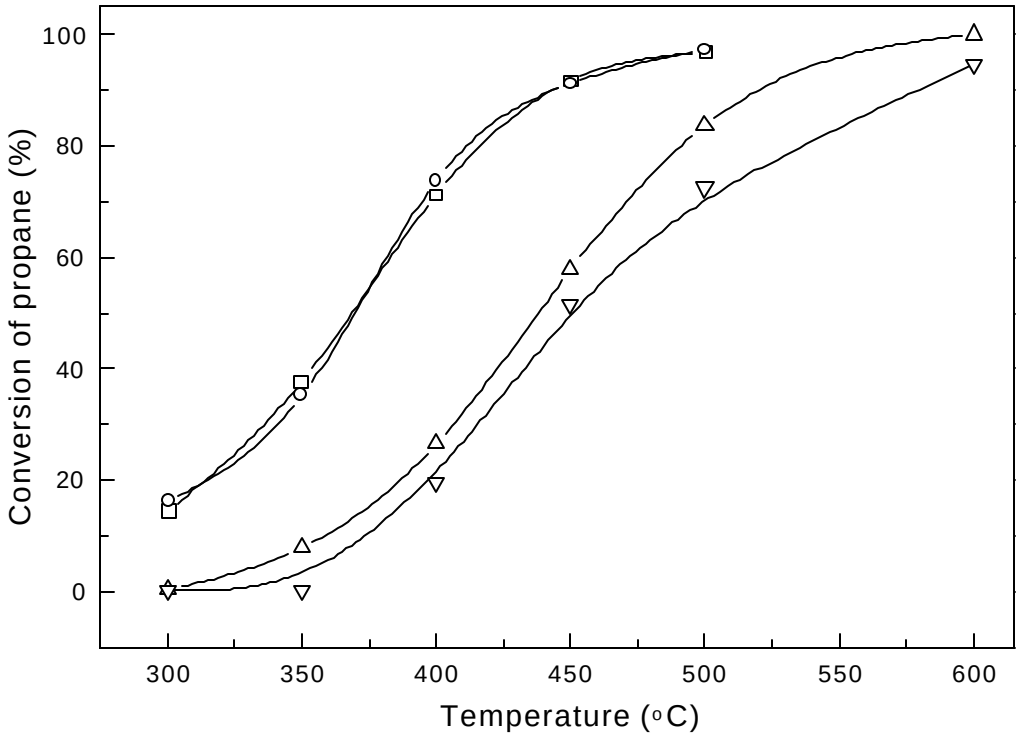


**Figure 4.2.5.** Temperature dependence of the propane conversion in the combustion of propane (GHSV = 51,000 $cm^3g^{-1}h^{-1}$) over Mn-doped $ZrO_2$ (Mn/Zr = 0.11) catalyst (prepared using TMAOH) calcined at different temperatures [500°C ( ), 600°C (O), 700°C (Δ) and 800°C (∇)].

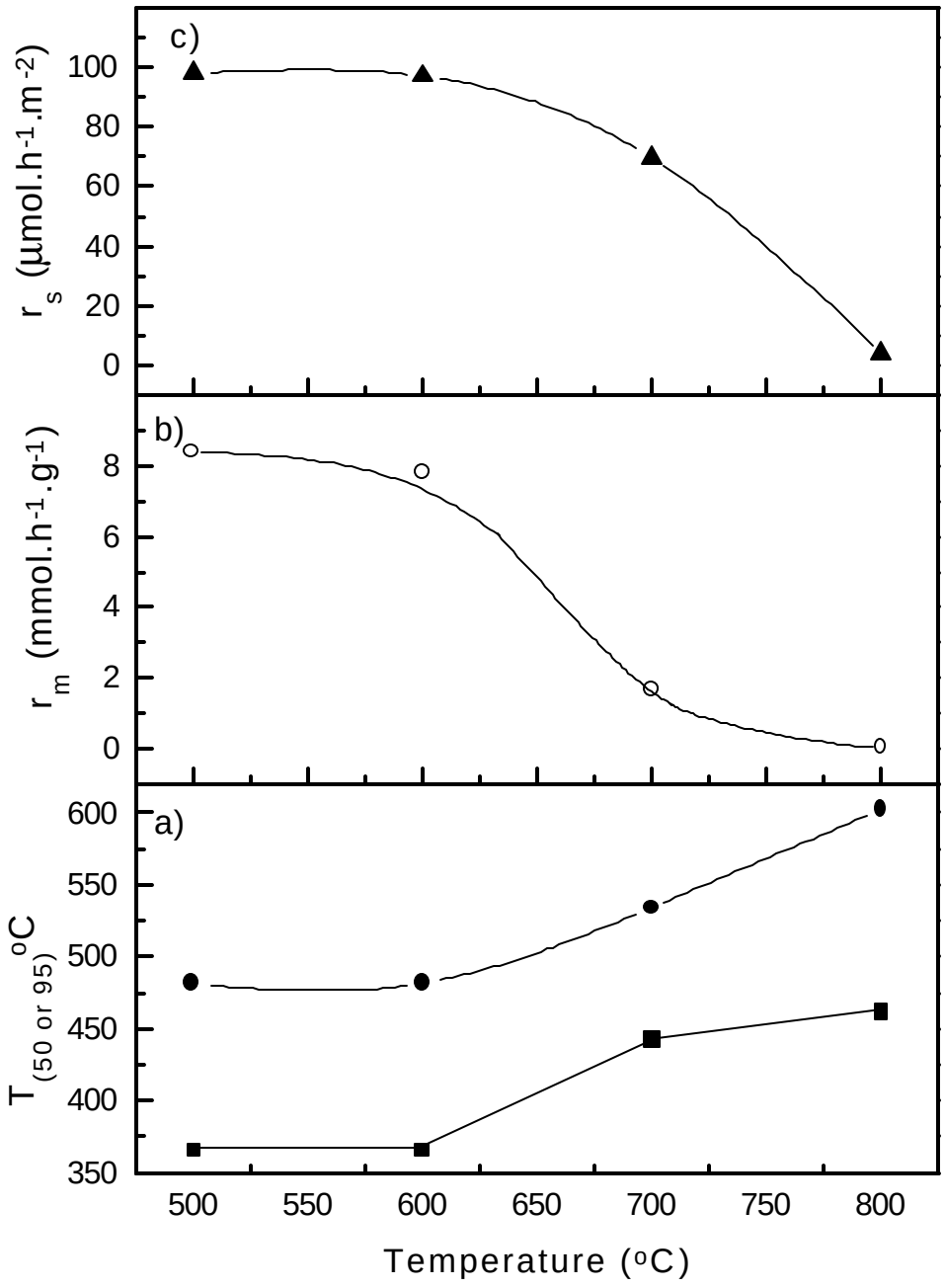


**Figure 4.2.6.** Effect of the calcination temperature of Mn-doped $ZrO_2$ (Mn/Zr = 0.11) catalyst (prepared using TMAOH) on (a) the temperature required for 50% ($T_{50}$) and 95% ($T_{95}$) conversion of propane, (b) propane conversion rate (at 350°C) based on the mass of catalyst ($r_m$) and (c) propane conversion rate (at 350°C) based on the surface area of catalyst ($r_s$) in the combustion of propane (space velocity: 51,000 $cm^3.g^{-1}.h^{-1}$).

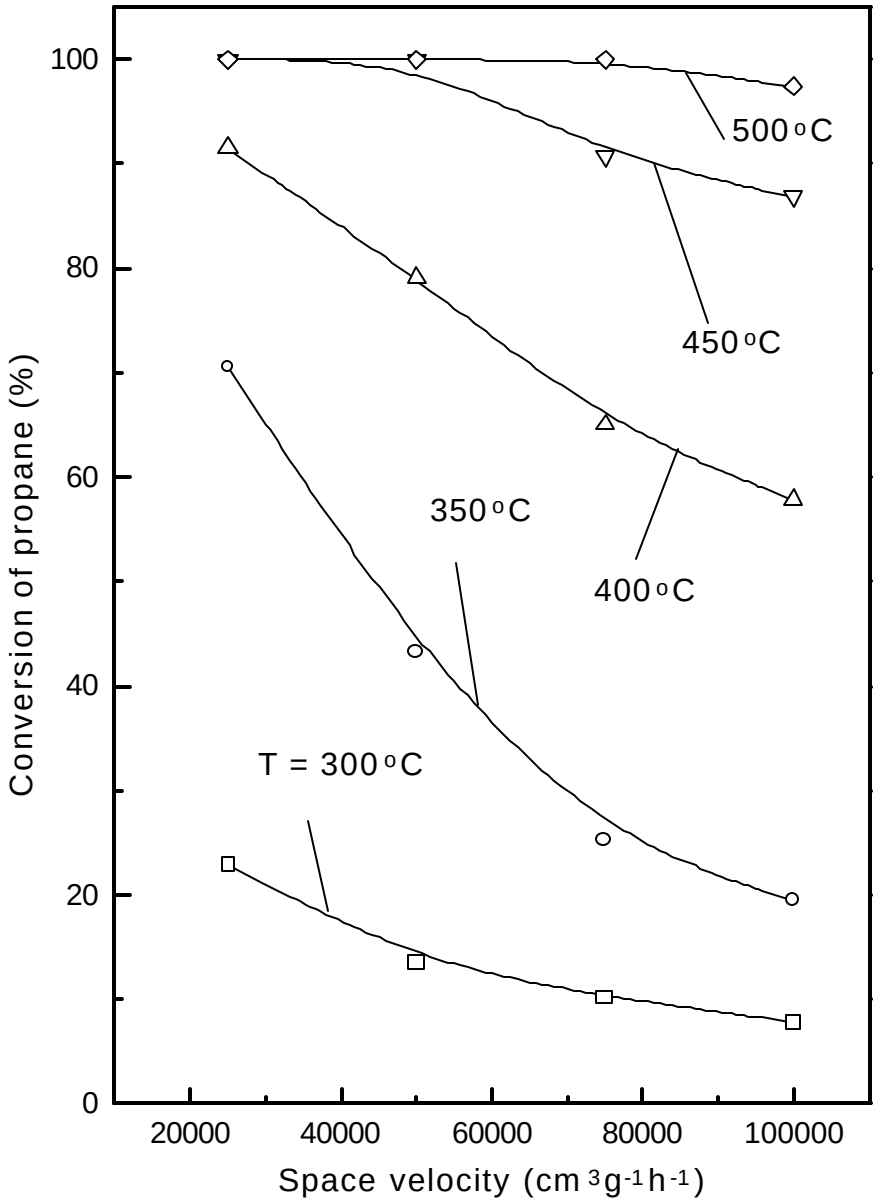


**Figure 4.2.7.** Effect of the space velocity on propane conversion in the propane combustion over Mn-doped $ZrO_2$ (Mn/Zr = 0.25) catalyst (prepared using TMAOH and calcined at $500^oC$)

***4.2.3.2.3. Effect of catalyst calcination temperature:*** Results in Figs. 4.2.5 and 4.2.6 show a strong effect of the catalyst calcination temperature, particularly above the calcination temperature of 600°C, on the propane combustion activity of the Mn-doped catalyst (Mn/Zr = 0.11). The increase in the calcination temperature from 500°C to 600°C has no significant effect on the catalytic activity. However, a further increase in the temperature above 600°C results in a sharp decrease in the catalytic activity. The observed very small activity (at 350°C) of the catalyst calcined at 800°C (Fig. 4.2.6b) is not just because of the sintering of the catalyst at the higher temperature but also because of the structural transformation of the catalyst producing monoclinic $ZrO_2$ and $MnO_2$ phases (Fig. 4.2.6c and Table 4.2.1).

***4.2.3.2.4. Effect of space velocity:*** Results showing the effect of space velocity on the propane conversion at different temperatures in the propane combustion over the Mn-doped catalyst (Mn/Zr = 0.25) prepared using TMAOH and calcined at 500°C are presented in Fig. 4.2.7. The space velocity effect shows a strong dependence upon the reaction temperature; the effect being more and more pronounced at the lower and lower temperatures.

### *4.2.3.3. Pulse reactions of propane*

In order to study a possibility of involvement of the lattice oxygen of the catalyst in the propane combustion, a pulse reaction of propane in the absence of free-$O_2$ over the Mn-doped $ZrO_2$ (Mn/Zr = 0.25) was carried out. A number of pulses of pure propane were passed one after another at a fixed interval of time (8 min) over the catalyst at 500°C and the conversion of propane was measured as a function of pulse number. A similar pulse reaction of propane was also carried out in case of the Mn-impregnated $ZrO_2$ catalyst (Mn/Zr = 0.25) for a purpose of comparing the reactivity of the lattice oxygen of both the catalysts. The results of the pulse reaction over the two catalysts are presented in Fig. 4.2.8.

From the results, following important observations can be made:

- Among the two catalysts, the initial propane conversion activity (i.e. the propane conversion in the first pulse) of the Mn-doped $ZrO_2$ is much higher.

- For both the catalysts, the propane conversion is sharply decreased with increasing the pulse number because of the consumption of lattice oxygen at or close to the catalyst surface.
- After the 12$^{th}$ pulse, when the Mn-doped $ZrO_2$ catalyst is aged at 500$^{o}$C for 1h in the flow of pure He and then the pulse experiments are continued, there is a sharp increase in the propane conversion for the 13$^{th}$ pulse, after which the propane conversion is sharply decreased with increasing the pulse number. Whereas, in case of the Mn-impregnated $ZrO_2$ catalyst, no sharp increase but a continuous decrease in the propane conversion, even for the 13$^{th}$ pulse, is observed.
- After the 16$^{th}$ pulse, when the Mn-doped $ZrO_2$ catalyst is reoxidized by air at 500$^{o}$C for 1h and then the pulse experiments are continued, the catalyst is found to regain its initial activity for the 17$^{th}$ pulse. However, for the subsequent pulses, the propane conversion over the catalyst is sharply decreased with increasing the pulse number. A similar behavior is also shown by the Mn-impregnated catalyst.

The observed sharp decrease in the propane conversion with increasing the pulse number and a complete regeneration of the catalyst, gaining its initial activity, clearly indicate that the propane combustion over both the catalysts involves redox mechanism (Mars and van Krevelen cycle), involving following reactions:

$$C_3H_8 + 10(O_L) \longrightarrow 3\,CO_2 + 4\,H_2O + 10\,(\square) \quad (1)$$

$$10\,(\square) + 5\,O_2 \longrightarrow 10\,(O_L) \quad (2)$$

where $\square$ is the anion vacancy and $O_L$ is the lattice oxygen.

The observed somewhat higher propane conversion activity of both the reoxidized catalysts may be due to a small amount of oxygen adsorbed on the catalysts during the reoxidation.

The two catalyst however differ very markedly in their initial propane conversion activity (i.e. the reactivity of their lattice oxygen) and also in their reactivation by the thermal aging treatment. The deactivated (due to the consumption of the lattice oxygen at or close to the surface) Mn-doped $ZrO_2$ catalyst is partially reactivated by the thermal aging treatment but such a reactivation is not observed in case of the Mn-impregnated $ZrO_2$ catalyst. The observed reactivation of the Mn-doped $ZrO_2$ catalyst is attributed to the transfer of sub-surface lattice oxygen to the catalyst surface during the thermal treatment. This clearly shows that the mobility of

lattice oxygen in case of the Mn-doped $ZrO_2$ catalyst is much larger than that in case of the Mn-impregnated $ZrO_2$. In the earlier literatures, it is shown that the methane combustion activity of the Mn-doped $ZrO_2$ is much higher than that of the Mn-impregnated $ZrO_2$ [16]. This work clearly shows that the mobility of lattice oxygen in $ZrO_2$ is increased because of the Mn-doping.

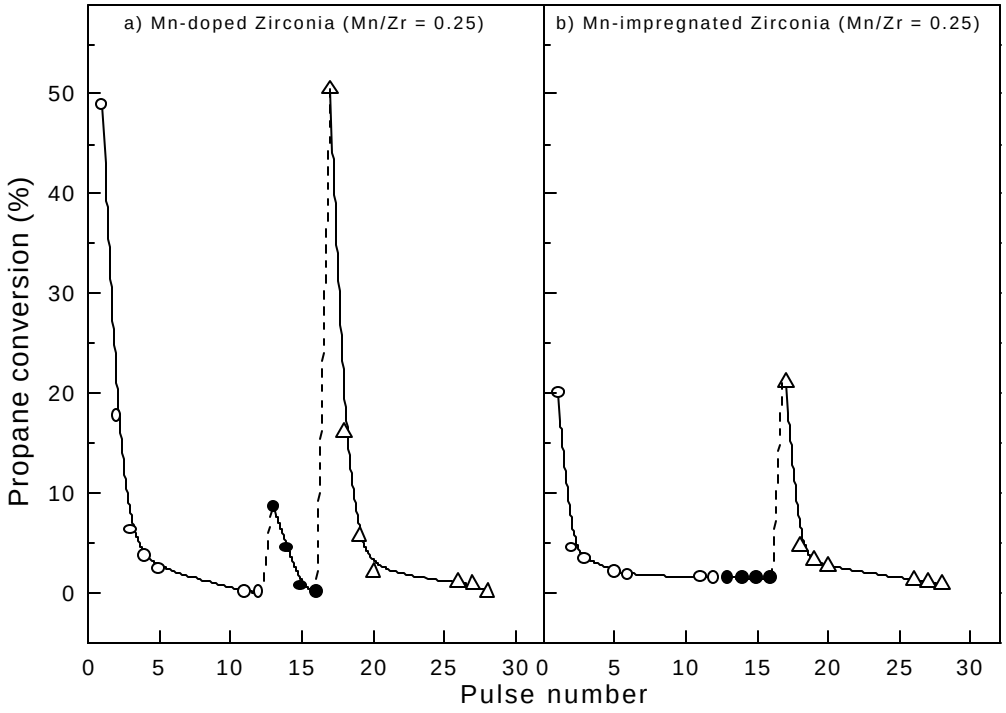


**Figure 4.2.8.** Variation of propane conversion (at 500°C) with pulse number in the reaction of pure propane (in the absence of free-$O_2$) with (a) Mn-doped $ZrO_2$ (Mn/Zr = 0.25) catalyst (prepared using TMAOH and calcined at 500°C) and (b) Mn-impregnated $ZrO_2$ (Mn/Zr = 0.25) catalyst (calcined at 500°C) in a pulse micro-reactor [for the fresh catalyst (○), after aging the deactivated catalyst under He at 500°C for 1.0 h (●) and after reoxidizing the deactivated catalyst by air at 500°C for 1.0 h and flushing with pure He for 0.5 h (Δ)].

### 4.2.4. Conclusions

The Mn-doped $ZrO_2$ (cubic) is a promising catalyst for the combustion of dilute propane and hence for controlling the propane emissions from the LPG-fuelled vehicles. The propane combustion activity of this catalyst is strongly influenced by the precipitating agent used in the catalyst preparation, Mn/Zr ratio of the catalyst and also by the calcination temperature of the catalyst. The catalyst prepared using TMAOH as a precipitating agent, having the Mn/Zr mole ratio of about 0.2 and calcined at $500^{o}$-$600^{o}$C is found to show the best performance in the propane combustion. The propane combustion over the catalyst involves redox (Mars and van Krevelen) mechanism. The doping of Mn in $ZrO_2$ greatly enhances the mobility of lattice oxygen in the Mn-doped $ZrO_2$ catalyst.

### 4.2.5. References


1. L. Kiwi-Minsker, I. Yuranov, E. Slavinskaia, V. Zaikovskii, A. Renken, Catal. Today 59 (2000) 61.
2. K. Ruth, M. Hayes, R. Burch, S. Tsubota, M. Haruta, Appl. Catal. B: Environ. 24 (2000) L133.
3. Y. Yazawa, H. Yoshida, S-I. Komai, A. Satsuma, T. Hattori, Appl. Catal. B: Environ. 19 (1998) 261.
4. A. Chiba, M. Komoda, T. Kosumi, T. Nanba, N. Azuma, A. Ueno, Chem. Lett. 8 (1999) 801.
5. A. Kalantar Neyestanaki, N. Kumar, L.-E. Lindfors, Appl. Catal. B: Environ. 7 (1995) 95.
6. A. Kalantar Neyestanaki, N. Kumar, L.-E. Lindfors, Fuel, 74 (1995) 690.
7. R. Prasad, L. A. Kennedy, E. Ruckenstein, Combust. Sci. Technol. 22 (1980) 271.
8. G. Busca, M. Daturi, E. Finocchio, V. Lorenzelli, G. Ramis, R. J. Willey, Catal. Today 33 (1997) 239.
9. M. Baldi, E. Finocchio, F. Milella, G. Busca, Appl. Catal. B: Environ. 16 (1998) 43.

10. M. Baldi, V. S. Escribano, J. M. G. Amores, F. Milella, G. Busca, Appl. Catal. B: Environ. 17 (1998) L175.
11. A. Kalantar Neyestanaki, L.-E. Lindfors, Combust. Sci. Technol. 110/111 (1995) 303.
12. S. H. Taylor, S. R. O'Leary, Appl. Catal. B: Environ. 25 (2000) 137.
13. J. J. Spivey, Ind. Eng. Chem. Res. 26 (1987) 2165.
14. M. F. M. Zwinkels, S. G. Jaras, P. G. Menon, Catal. Rev. Sci. Eng. 35 (1993) 319.
15. A. Keshavaraja, A. V. Ramaswamy, Appl. Catal. B: Environ. 8 (1996) L1.
16. V. R. Choudhary, B. S. Uphade, S. G. Pataskar, A. Keshavaraja, Angew. Chem. Int. Ed. Engl. 35 (1996) 2393.
17. V. R. Choudhary, V. H. Rane, J. Catal. 135 (1992) 310.
18. V. R. Choudhary, A. S. Mamman, S. G. Pataskar, S. Banerjee, Prepr. – Am. Chem. Soc. Fuel. Chem. Div. 46 (2001).

# CHAPTER 4.3

# COMBUSTION OF DILUTE PROPANE OVER TRANSITION METAL-DOPED $ZrO_2$ (CUBIC) CATALYSTS

## 4.3.1. Earlier Work/Background and Objectives of Present Work

In the earlier chapter (chapter 4.2), studies on the complete combustion of propane on Mn-doped $ZrO_2$ catalyst have been described. The Mn-doped $ZrO_2$ showed very good performance in the propane combustion. Hence it is interesting to compare the performance of different transition metal doped $ZrO_2$ (cubic) catalysts in the combustion of dilute propane. The present investigation was therefore undertaken for studying in details the complete combustion of dilute propane (0.9 mol% propane in air) over different transition metal (viz. Mn, Co, Cr, Fe and Ni)-doped $ZrO_2$ (cubic) catalysts at different process conditions. Pulse reaction of pure propane, in the absence of $O_2$, over the fresh catalyst and also over the reoxidized catalyst (used in the pulse reaction) as a function of pulse number have also been studied.

## 4.3.2. Experimental

The Mn-, Co-, Cr-, Fe- and Ni-doped $ZrO_2$ (cubic) catalysts were prepared by mixing aqueous solutions of zirconyl nitrate and the respective transition metal nitrate (transition metal/Zr mole ratio = 0.25), coprecipitating the metal hydroxide from the solution with aqueous tetramethyl ammonium hydroxide (25%) (TMAOH). The detail preparation procedure has been given earlier (section 1.2.1.3). Co-doped $ZrO_2$ catalysts having different Co/Zr ratios (0.11 – 0.43) were also prepared in the same way. The Co- impregnated $ZrO_2$ (Co/Zr =0.25) was prepared by impregnating $ZrO_2$ with cobalt nitrate by incipient wetness method and calcining at $500^oC$ for 8h. The $ZrO_2$ was prepared by precipitating $Zr(OH)_4$ from an aqueous solution of zirconyl nitrate by ammonium hydroxide by the procedure similar to that described above.

The catalysts were characterized for their BET surface area and for their crystalline phases by XRD. The catalyst was also characterized by its temperature programmed reduction (TPR) by $H_2$ from $100^oC$ to $600^oC$ with a linear heating rate of $10^oC.min^{-1}$ in a flow of $H_2$ – Ar (3.7 mol% in $H_2$) mixture (space velocity = 30,600 $cm^3.g^{-1}.h^{-1}$) in a quartz reactor (i. d. 4 mm) having a low dead volume. The hydrogen

consumed in the TPR of the catalysts was measured quantitatively by a thermal conductivity detector (TCD). Before the TPR, the catalyst was pretreated in a flow of nitrogen (30 $ml.min^{-1}$) at 600°C for 1h. The experimental procedure is given in the earlier section (section 1.2.2.9 and Fig. 1.2.3).

The propane combustion activity of all the catalysts was measured at atmospheric pressure in a continuous fixed bed quartz-microreactor. (i. d. 10 mm) (Fig. 1.2.1a) containing 0.1 g catalyst (22-30 mesh size particles) mixed uniformly with 0.4 g inert $\alpha$-$Al_2O_3$ particles (22-- 30 mesh size), at different process conditions (temperature: 300° – 500°C and space velocity: 25,000 – 100,000 $cm^3.g^{-1}.h^{-1}$, measured at NTP) using 0.9 mol % propane in air as a feed. The reaction procedure is given earlier (section 1.2.3.3b and Fig. 1.2.8). No partial combustion product (e.g. carbon monoxide) was detected in the propane combustion over either of the catalysts.

The pulse reaction of propane (at 500°C) over the catalyst in the absence of $O_2$ as a function of pulse number was carried out in a quartz pulse micro-reactor connected to the GC, using He (30 $cm^3.min^{-1}$) as a carrier gas, following the procedure described elsewhere [1,2] and also in section 1.2.3.3a and Fig. 1.2.7. The products of the pulse reaction were analyzed using a Spherocarb column and thermal conductivity detector.

### 4.3.3. Results

#### *4.3.3.1. Catalyst characterization*

XRD spectra of the transition metal doped $ZrO_2$ catalysts (Fig. 4.3.1) show the presence of only cubic $ZrO_2$ phase; no crystalline transition metal oxide phase is detected.

The transition metal doped $ZrO_2$ catalysts were further characterized for their temperature programmed reduction (TPR) by $H_2$ from 100° to 600°C at the heating rate of $10°C.min^{-1}$. The TPR spectra of the catalyst are presented in Fig. 4.3.2. Data on the temperature of the TPR peaks, the amount of $H_2$ consumed in the TPR and that expected to be consumed for the complete reduction of respective transition metal oxides [viz. Co(II) → Co(0); Mn(IV) → Mn(III); Cr(III) → Cr(II); Fe(III) → Fe(II) or Fe(0) and Ni(II) → Ni(0)] have been presented in Table 4.3.1. Estimated values of the

degree of reduction according to the transition metal oxide reduction reactions are also included in Table 4.3.1.

In the TPR of all the catalysts, the observed degree of reduction of the respective transition metal oxides for the indicated reduction reactions is very low (Table 4.3.1). This observation also indicates the incorporation of the transition metals in the zirconia lattice.

For all the catalysts, the reduction of transition metal oxides occurs in two steps, as shown by two TPR peaks - a large $H_2$ consumption peak and a small $H_2$ consumption peak or hump (Fig. 4.3.2). In the TPR of the Co-doped $ZrO_2$, the small hump (at the lower temperature side) is followed by a large peak. Whereas, in case of the other transition metal-doped $ZrO_2$ catalysts, the large TPR peak (at the lower temperature side) is followed by a small peak (for Mn-, Cr-, Fe-doped $ZrO_2$) or hump (Ni-doped $ZrO_2$). The order for the main (i.e. large) TPR peak temperature is as follows: Co-doped $ZrO_2$ (545$^oC$) > Ni-doped $ZrO_2$ (477$^oC$) > Fe-doped $ZrO_2$ (422$^oC$) > Mn-doped $ZrO_2$ (365$^oC$) > Cr-doped $ZrO_2$ (341$^oC$).

#### *4.3.3.2. Combustion of propane over transition metal-doped $ZrO_2$ catalysts*

The combustion of dilute propane (0.9 mol% $C_3H_8$ in air) over the transition metal-doped $ZrO_2$ catalysts was studied, covering a wide range of temperature (200$^o$ – 500$^o$C) and space velocity (25,000 – 100,000 $cm^3g^{-1}h^{-1}$). Results showing the influence of temperature on the propane conversion over the different catalysts at a space velocity of 51,000 $cm^3g^{-1}h^{-1}$ are presented in Fig. 4.3.3. Figure 4.3.4 shows the dependence of the temperature required for half the combustion reaction (i.e. for 50% propane conversion in the combustion) upon the space velocity for the different catalysts. The catalysts are also compared for their propane combustion activity, measured in terms of the rate of propane combustion at the same conversion (viz. 50% conversion) per unit mass or per unit surface of the catalyst at different temperatures. The results are presented in Fig. 4.3.5 and Table 4.3.2. Figure 4.3.5 also shows the Arrhenius type temperature dependence of the propane combustion rate at the isoconversion for the different catalysts. The activation energy and frequency factor data for the different catalysts are presented in Table 4.3.3.

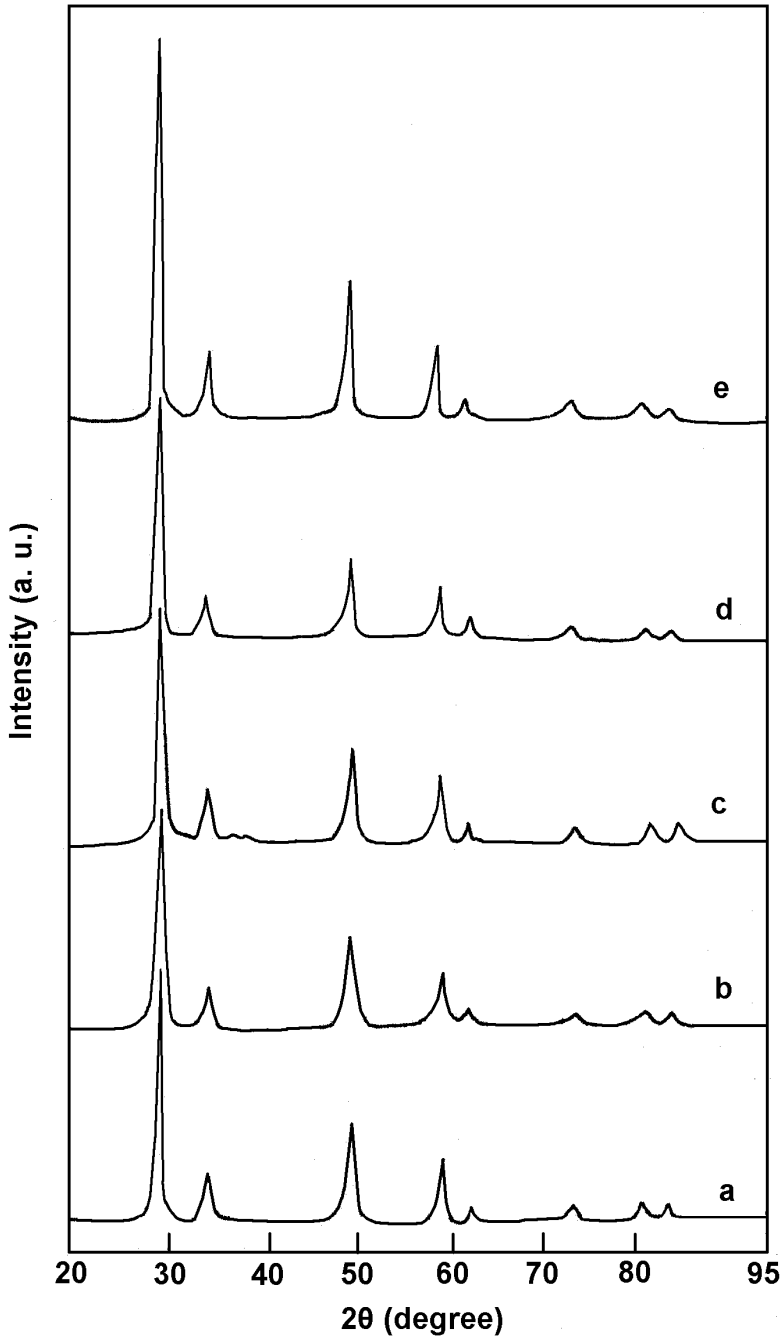


**Figure 4.3.1.** XRD spectra of the transition metal-doped (transition metal/Zr = 0.25) catalysts (a) Co-doped $ZrO_2$, (b) Mn-doped $ZrO_2$, (c) Cr-doped $ZrO_2$, (d) Fe-doped $ZrO_2$ and (e) Ni-doped $ZrO_2$.

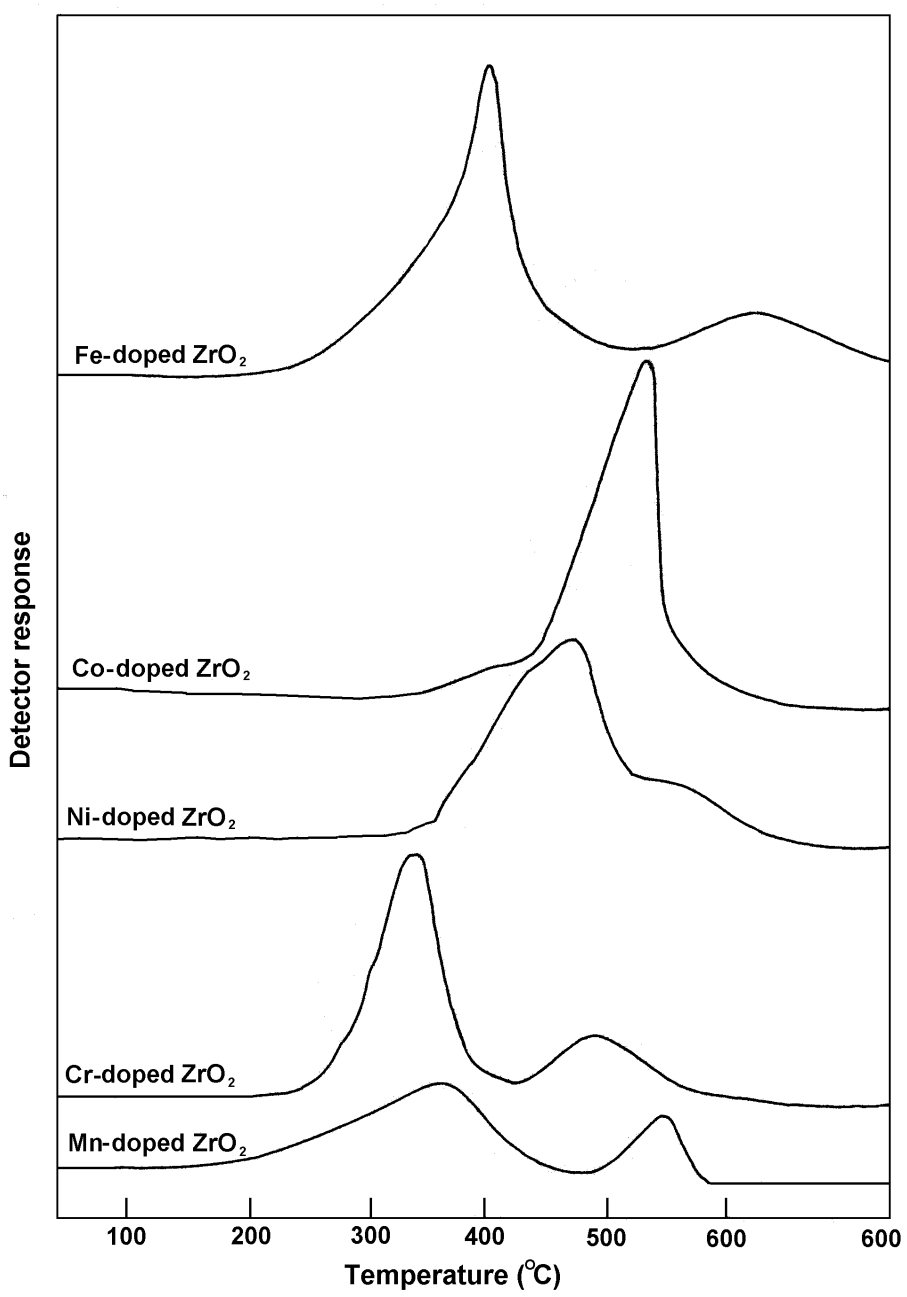


**Figure 4.3.2.** Temperature programmed reduction (TPR) by $H_2$ of the transition-metal doped $ZrO_2$ catalysts (transition metal/Zr = 0.25).

From the above results, following important observations for comparing the propane conversion performance of the transition metal-doped $ZrO_2$ catalyst can be made:

- For their "light-off" temperature, the catalysts can be ordered as follows: Co-doped $ZrO_2$ < Cr-doped $ZrO_2$ < Mn-doped $ZrO_2$ < Fe-doped $ZrO_2$ < Ni-doped $ZrO_2$.
- The catalysts differ widely in their propane combustion activity. When their propane combustion activity is measured in terms of the temperature required for half the combustion reaction at the same space velocity or in terms of the propane combustion rate expressed per unit mass or per unit surface area, the catalysts have following order for their performance in the propane combustion: Co-doped $ZrO_2$ > Mn-doped $ZrO_2$ > Cr-doped $ZrO_2$ > Fe-doped $ZrO_2$ > Ni-doped $ZrO_2$.
- For the Ni-doped $ZrO_2$, both the activation energy and frequency factor are lowest. Because of its very low frequency factor, this catalyst is the least preferred one. Whereas, for the Fe-doped $ZrO_2$, both the activation energy and frequency factor have highest value. This catalyst is also less preferred because of the very high activation energy. Among the Co-, Mn- and Cr-doped $ZrO_2$ catalysts, which showed better performance in the propane combustion, the Co-doped $ZrO_2$ catalyst is the most preferred one because for this catalyst the activation energy is lowest and the frequency factor is highest.

Thus the above comparative results clearly show that, among the transition metal-doped $ZrO_2$ catalysts, the Co-doped $ZrO_2$ is the best catalyst for the combustion of dilute propane.

Figure 4.3.6 shows the influence of Co/Zr ratio in the Co-doped $ZrO_2$ catalyst on its performance in the propane combustion. The results show that the propane combustion activity, measured in terms of the temperature required for 50% or 90% propane conversion in the combustion (space velocity = 51,000 $cm^3g^{-1}h^{-1}$), passes through a maximum when the Co/Zr ratio is increased from 0.11 to 0.43. The optimum Co/Zr ratio for the catalyst to be most active is found to be about 0.25.

**Table 4.3.1.** Comparison of the $H_2$ consumed in the TPR with the theoretical one required for reduction of the transition metal-doped $ZrO_2$ (transition metal/Zr = 0.25) catalysts

| Catalyst | TPR peak temperature (°C) | | $H_2$ consumed in TPR ($mmol.g^{-1}$) | Theoretical amount of $H_2$ required for reduction ($mmol.g^{-1}$) | Estimated degree of reduction (%) |
|---|---|---|---|---|---|
| | First peak | Second peak | | | |
| Co-doped $ZrO_2$ | 410 (hump) | 545 (large) | 0.14 | 1.76[a] | 8.0[a] |
| Mn-doped $ZrO_2$ | 365 (large) | 550 (small) | 0.09 | 0.86[b] | 10.5[b] |
| Cr-doped $ZrO_2$ | 341 (large) | 489 (small) | 0.12 | 0.88[c] | 13.6[c] |
| Fe-doped $ZrO_2$ | 422 (large) | > 600 (small) | 0.18 | 0.87[d], 2.63[e] | 20.6[d], 6.8[e] |
| Ni-doped $ZrO_2$ | 477 (large) | 565 (hump) | 0.13 | 1.76[f] | 7.4[f] |

[a] for $CoO + H_2 \rightarrow Co + H_2O$; [b] for $2\ MnO_2 + H_2 \rightarrow Mn_2O_3 + H_2O$; [c]for $Cr_2O_3 + H_2 \rightarrow 2CrO + H_2O$; [d]for $Fe_2O_3 + H_2 \rightarrow 2\ FeO + H_2O$; [e]for $Fe_2O_3 + 3\ H_2 \rightarrow 2\ Fe + 3\ H_2O$; [f]for $NiO + H_2 \rightarrow Ni + H_2O$

#### *4.3.3.3. Pulse reactions of propane over Co-doped $ZrO_2$ catalysts*

In order to study the reactivity and mobility of the lattice oxygen of the Co-doped $ZrO_2$ (Co/Zr = 0.25) catalyst in the propane combustion, experiment involving pulse reaction of pure propane in the absence of oxygen over this catalyst and also over the Co-impregnated $ZrO_2$ (Co/Zr = 0.25) catalyst have been carried out under identical conditions, as follows. Over the fresh catalyst, a number of pulses of pure propane were passed one after another in a flow of pure He at a fixed interval of time (8 min) at 500°C and the conversion of propane was measured as a function of pulse number. After the 12th pulse, the catalyst was thermally aged at 500°C for 1h and then the pulse experiments were continued as above. After the 16th pulse, the catalyst was oxidized by $O_2$ at 500°C for 2h. After the catalyst reoxidation and removing the reversibly adsorbed oxygen from the catalyst, again the pulse experiments were

continued as above. The results of the pulse experiments over both the catalysts are presented in Fig. 4.3.7.

From the results, following important observations can be made:

- Among the two catalysts, the initial propane conversion activity (i.e. the propane conversion in the first pulse) of the Co-doped $ZrO_2$ is higher.
- For both the catalysts the propane conversion is sharply decreased with increasing the pulse number because of the consumption of their lattice oxygen at or close to the surface.
- After the $12^{th}$ pulse, when the Co-doped $ZrO_2$ catalyst is aged at $500^oC$ for 1h in the flow of pure He and then the pulse experiments are continued, there is a sharp increase in the propane conversion for the $13^{th}$ pulse, after which the propane conversion is sharply decreased with increasing the pulse number. Whereas, in case of the Co-impregnated $ZrO_2$ catalyst, no sharp increase but a continuous decrease in the propane conversion, even for the $13^{th}$ pulse, is observed.
- After the $16^{th}$ pulse, when the Co-doped $ZrO_2$ catalyst is reoxidized by air at $500^oC$ for 1h and then the pulse experiments are continued, the catalyst is found to regain its original initial activity for the $17^{th}$ pulse. However, for the subsequent pulses, the propane conversion over the catalyst is sharply decreased with increasing the pulse number. A similar behavior is also shown by the Co-impregnated $ZrO_2$ catalyst.

### 4.3.4. Discussion

#### *4.3.4.1. TPR of transition metal doped $ZrO_2$ catalysts*

The observed very low degree of reduction of the transition metal oxide from the catalysts, even for their first stage of reduction (Table 4.3.1), indicates a deep penetration of the respective transition metal cations in the bulk structure of $ZrO_2$, forming a solid solution of the corresponding transition metal oxide with $ZrO_2$. The first TPR peak in each case (Fig. 4.3.2) is expected because of the reduction of transition metal oxide (viz. $Co^{2+} \rightarrow Co^o$; $Mn^{4+} \rightarrow Mn^{3+}$; $Cr^{3+} \rightarrow Cr^{2+}$; $Fe^{3+} \rightarrow Fe^{2+}$ and $Ni^{2+} \rightarrow Ni^o$) at or close to the surface of the catalyst. However, the second TPR peak (which appear at the higher temperature) is attributed mostly to the hydrogen

consumed in the reaction with sub-surface lattice oxygen which is migrated (at the higher temperatures) from the interior to the surface of the catalyst. The second TPR peak, except for the Co-doped $ZrO_2$, is smaller than the first one.

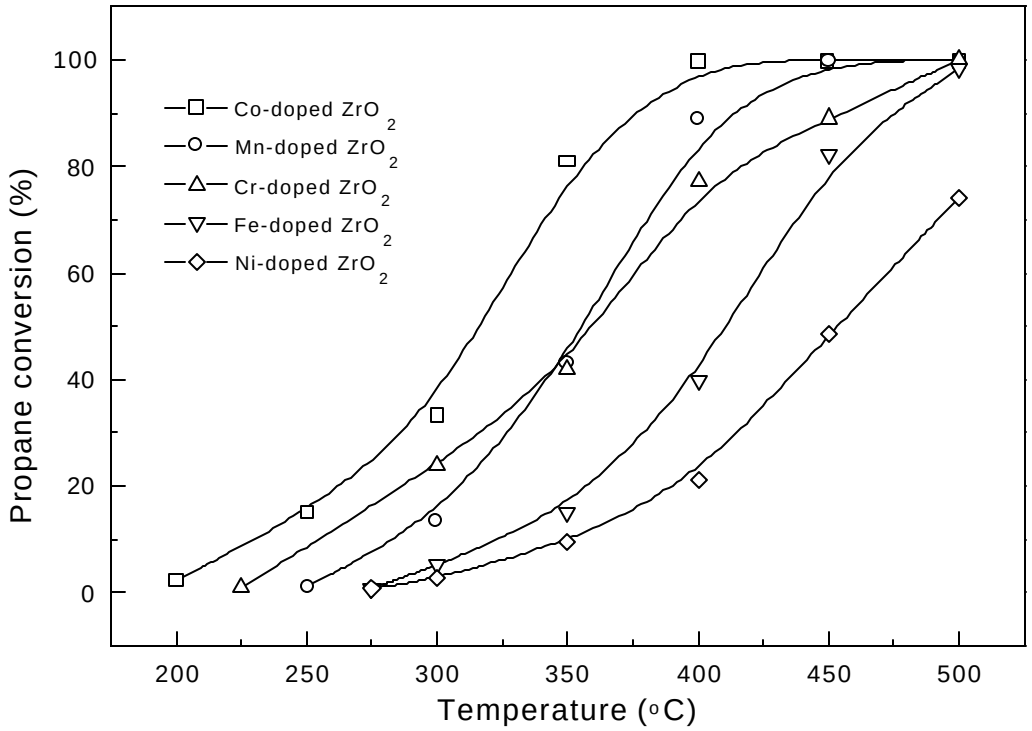


**Figure 4.3.3.** Temperature dependence of the propane conversion in the combustion of propane over different transition metal-doped $ZrO_2$ catalysts [TM (transition metal)/Zr mole ratio = 0.25] at a space velocity of 51,000 $cm^3.g^{-1}.h^{-1}$.

**Table 4.3.2.** Comparison of the transition metal-doped $ZrO_2$ catalysts (transition metal/Zr = 0.25) for their propane combustion activity at different temperatures

| Catalyst | Rate of propane combustion (at 50% conversion), $r_S \times 10^6$ ($mol.m^{-2}.h^{-1}$) | | | | |
|---|---|---|---|---|---|
| | 300°C | 350°C | 400°C | 450°C | 500°C |
| Co-doped $ZrO_2$ | 0.47 | 2.51 | 8.60 | 12.2 | - |
| Mn-doped $ZrO_2$ | - | 0.95 | 3.13 | 7.38 | 18.4 |
| Cr-doped $ZrO_2$ | - | 0.75 | 3.03 | 6.67 | 16.1 |
| Fe-doped $ZrO_2$ | - | - | 0.34 | 2.05 | 4.66 |
| Ni-doped $ZrO_2$ | - | - | 0.44 | 0.92 | 1.88 |

The reduction of transition metal oxides at or close to the catalyst surface may not be restricted only to the first stage of their reduction. Particularly in case of the Mn- and Fe-doped $ZrO_2$ catalysts, the reductions may occur in two steps: i.e. $Mn^{4+} \rightarrow Mn^{3+} \rightarrow Mn^{2+}$ and $Fe^{3+} \rightarrow Fe^{2+} \rightarrow Fe^{o}$. However, from this investigation no firm conclusion about this can be drawn. Nevertheless, the XRD and TPR results clearly show the formation of solid solution between the respective transition metal oxide and $ZrO_2$ in the catalysts, stabilizing their $ZrO_2$ into cubic form.

The temperature of first TPR peak of the catalyst is expected to provide information on the relative reactivity of their lattice oxygen; lower the peak temperature, higher is the reactivity. The reactivity in the reaction with hydrogen of the lattice oxygen for the catalysts is in the following order: Cr-doped $ZrO_2$ > Mn-doped $ZrO_2$ > Co-doped $ZrO_2$ > Fe-doped $ZrO_2$ > Ni-doped $ZrO_2$ (Table 4.3.1). Whereas, the second TPR peak is expected to provide an information on the relative mobility of the lattice oxygen; lower the peak temperature higher is the mobility. From this consideration, the mobility of lattice oxygen of the catalysts is in the

following order: Cr-doped $ZrO_2$ > Co-doped $ZrO_2$ > Mn-doped $ZrO_2$ > Ni-doped $ZrO_2$ > Fe-doped $ZrO_2$.

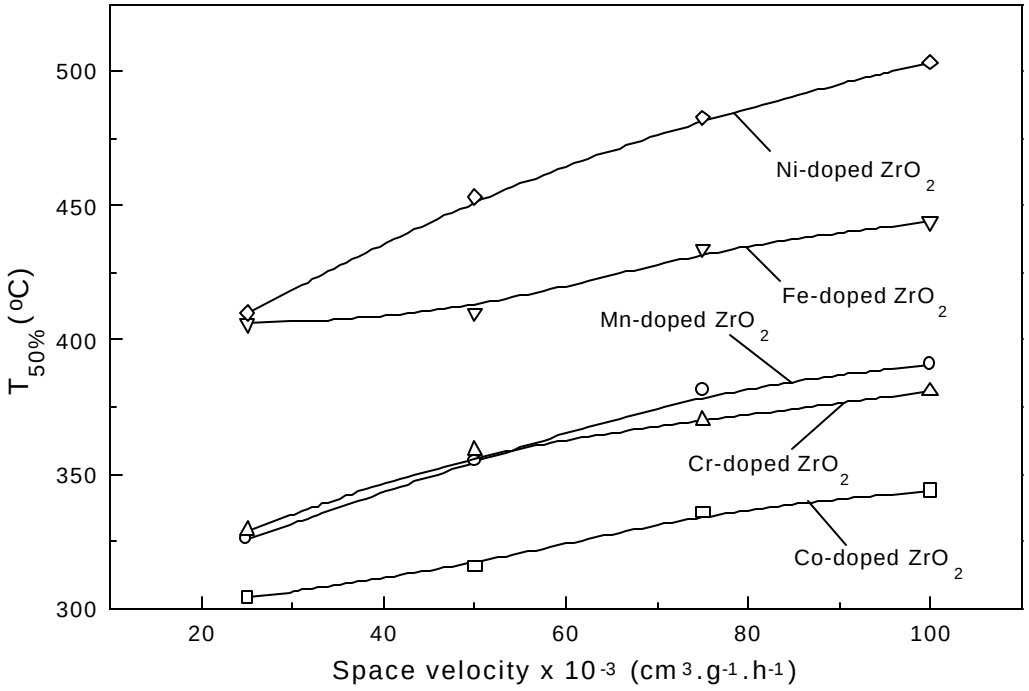


**Figure 4.3.4.** Temperature required for half the propane combustion reaction over different transition metal-doped $ZrO_2$ catalysts (transition metal/Zr mole ratio = 0.25) at different space velocities.

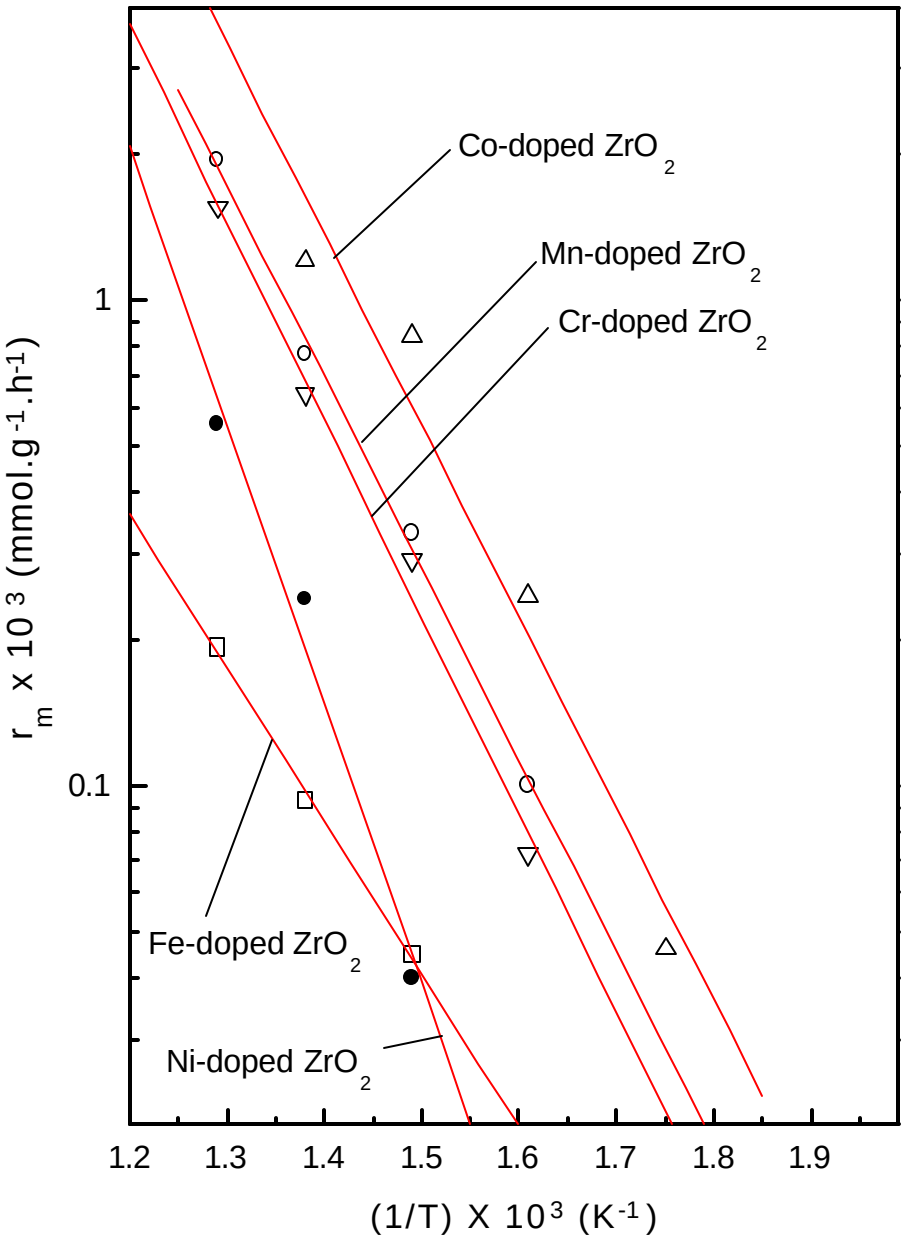


**Figure 4.3.5.** Arrhenius plots [log (propane combustion rate, $r_m$ at 50% conversion) vs. 1/T plots] for the combustion of propane over Co-doped $ZrO_2$ (Δ), Mn-doped $ZrO_2$ (○), Cr-doped $ZrO_2$ (▽), Fe-doped $ZrO_2$ (□) and Ni-doped $ZrO_2$ ( ) (TM/Zr = 0.25).

**Table 4.3.3.** Comparison of the transition metal-doped $ZrO_2$ catalyst for the Arrhenius parameters (activation energy and frequency factor) in the propane combustion.

| Catalyst | Activation energy, E ($kJ.mol^{-1}$) | Frequency factor, A ($mol.g^{-1}.h^{-1}$) |
|---|---|---|
| Co-doped $ZrO_2$ | 65.9 | 448 |
| Mn-doped $ZrO_2$ | 66.1 | 235 |
| Cr-doped $ZrO_2$ | 68.1 | 280 |
| Fe-doped $ZrO_2$ | 96.2 | 16076 |
| Ni-doped $ZrO_2$ | 52.7 | 2.2 |

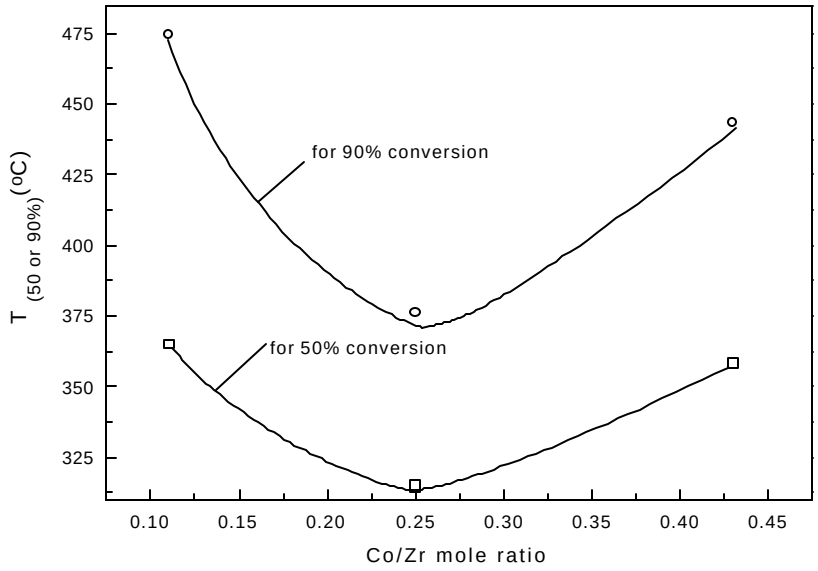


**Figure 4.3.6.** Effect of Co/Zr ratio on the temperature required for 50 and 90% conversion of propane in the propane combustion over Co-doped $ZrO_2$ catalyst (space velocity = 51,000 $cm^3g^{-1}h^{-1}$).

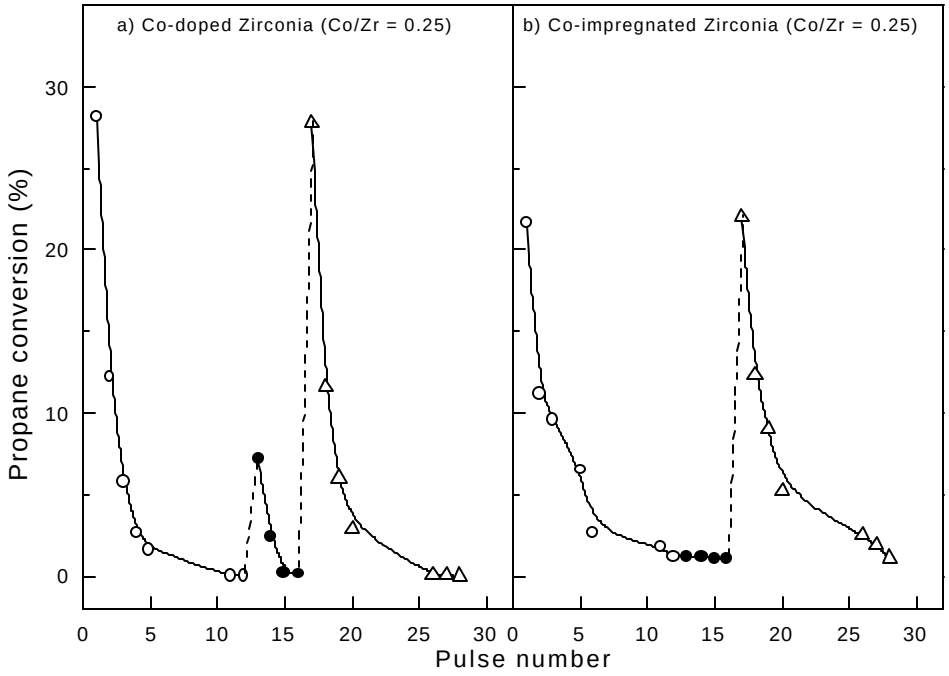


**Figure 4.3.7.** Variation of propane conversion with pulse number in the pulse reaction of propane over (a) Co-doped $ZrO_2$ (Co/Zr = 0.25) and (b) Co-impregnated $ZrO_2$ (Co/Zr = 0.25) catalysts in the absence of oxygen at 500$^oC$ [○ - for fresh catalyst; - after aging the deactivated catalyst under He at 500$^oC$ for 1.0 h, and Δ - after reoxidation].

### *4.3.4.2. Propane combustion activity of the catalyst*

The results (Figs. 4.3.4, 4.3.5 and Table 4.3.2) clearly indicate that among the catalysts, Co-doped $ZrO_2$ shows the best performance in the combustion of dilute propane. However, in our earlier studies on the combustion of dilute methane over the same catalysts, the Mn-doped $ZrO_2$ was found to be the most active catalyst for the methane combustion [3]. The order of the catalyst for their performance in the methane combustion (Mn-doped $ZrO_2$ > Co-doped $ZrO_2$ > Fe-doped $ZrO_2$ > Cr-doped $ZrO_2$ > Ni-doped $ZrO_2$) was also different.

It is intersting to note that among the Co-, Mn- and Cr-doped $ZrO_2$ catalysts (which show better performance in the propane combustion), for the Co-doped $ZrO_2$ catalyst not only the activation energy is lowest but also the frequency factor is

highest (Table 4.3.3). Thus the Co-doped $ZrO_2$ is the best choice for the combustion of dilute propane. However, the best performance is shown by this catalyst when its Co/Zr ratio is optimum (about 0.25) (Fig. 4.3.6).

The results of the pulse reactions of propane in the absence of oxygen over the Co-doped $ZrO_2$ catalyst show that the propane conversion over the fresh catalyst is decreased sharply with increasing the pulse number. This is expected because of the consumption of lattice oxygen at or close to the surface in the reaction:

$$C_3H_8 + 10\,(O_L) \rightarrow 3\,CO_2 + 4\,H_2O + 10\,(\square) \qquad (1)$$

where $\square$ is the anion vacancy.

However, the reoxidation of the catalyst (used in the pulse experiments) results in filling of the anion (or oxygen) vacancies by the reaction:

$$2\,(\square) + O_2 \rightarrow 2\,(O_L) \qquad (2)$$

and thereby the catalyst regains its original activity (Fig. 4.3.7). This suggests that the lattice oxygen from the catalyst plays a significant role in the propane combustion involving Mars and van Krevelen type redox mechanism.

#### *4.3.4.3. Enhanced mobility of lattice oxygen due to the Co-doping*

As discussed earlier, the high temperature TPR peak ($2^{nd}$ peak) is expected mostly because of the migration of deeper oxygen anions towards the catalyst surface. This was further confirmed by carrying out the propane pulse experiments over the Co-doped $ZrO_2$ and Co-impregnated $ZrO_2$ catalysts in the absence of oxygen (Fig. 4.3.7). The thermal aging (at $500^oC$ for 1h) of Co-impregnated $ZrO_2$ catalyst deficient in oxygen has produced no siginificant effect on the propane conversion but that of the Co-doped $ZrO_2$ has resulted in a large increase in the propane conversion (from almost zero to 8%). The latter effect is attributed to the migration of sub-surface oxygen to the catalyst surface. These results clearly show that under the experimental conditions prevailing in both the cases, the lattice oxygen in the Co-impregnated catalyst is immobile, whereas, that in the Co-doped $ZrO_2$ is mobile. Thus, it can be concluded that the doping of Co in $ZrO_2$ causes a significant increase in the mobility of its lattice oxygen.

### 4.3.5. Conclusions

From the studies on the TPR by $H_2$ and combustion of dilute propane (0.9% propane in air) over the Co-, Mn-, Cr-, Fe- and Ni-doped $ZrO_2$ catalysts at the

different process conditions and pulse reaction of pure propane (in the absence of $O_2$) over the Co-doped $ZrO_2$ and Co-impregnated $ZrO_2$ catalysts, following important conclusions can be drawn:

- For all the transition metal doped $ZrO_2$ catalysts (transition metal/Zr mole ratio of 0.25), the dgree of reduction in the TPR is very low, confirming the formation of transition metal oxides – $ZrO_2$ solid solution in each of the catalysts. The second TPR peak (which appears at the higher temperatures) of the catalysts can be attributed to the migration of the deeper lattice oxygen to the catalyst surface.
- Among the transition metal doped $ZrO_2$ catalysts, Co-doped $ZrO_2$ is the most promising catalyst for the combustion of dilute propane, the choice of the catalyst being in the following order: Co-doped $ZrO_2$ > Mn-doped $ZrO_2$ > Cr-doped $ZrO_2$ > Fe-doped $ZrO_2$ > Ni-doped $ZrO_2$. For the best catalytic performance in the propane combustion, the Co/Zr mole ratio in the Co-doped $ZrO_2$ has an optimum value (about 0.25).
- The pulse reaction of propane (in the absence of $O_2$) reveal a possibility of the involvement of redox mechanism (Mars and van Krevelen type) in the propane combustion over the Co-doped $ZrO_2$ catalyst.
- The doping of Co in $ZrO_2$ causes a very significant increase in the mobility of the lattice oxygen in the Co-doped $ZrO_2$ catalyst.

### 4.3.6. References


1. V. R. Choudhary and V. H. Rane, J. Catal., 135 (1992) 310.
2. V. R. Choudhary, A. S. Mamman, S. G. Pataskar and S. Banerjee, Prepr. – Am. Chem. Soc. Fuel. Chem. Div., 46 (2001) 83.
3. V. R. Choudhary, B. S. Uphade, S. G. Pataskar and A. Keshavaraja, Angew. Chem. Int. Ed. Engl., 35 (1996) 2393.

# CHAPTER 4.4

# PULSE REACTION OF METHANE IN THE PRESENCE OR ABSENCE OF $O_2$ OVER Pd (OR PdO)/$Al_2O_3$ OXIDIZED (OR REDUCED) TO DIFFERENT EXTENTS

## 4.4.1. Earlier Work/Background and Objectives of Present Work

Catalytic combustion of methane is of great practical importance [1-4]. It is essential for controlling methane (which is a greenhouse gas and produces a much more green house effect than carbon dioxide) emissions from natural gas fuelled vehicles. It is also seriously considered for replacing the conventional thermal combustion in the gas turbine combustors to reduce the combustion temperature and thereby eliminate the $NO_x$ formation in the power plants. Among the catalysts used for the methane combustion, the supported Pd has been found to be the most active catalyst [1]. The methane oxidation over Pd catalysts have been found to be structure sensitive [5-10]. The structure sensitivity has been attributed to the different reactivities of the adsorbed oxygen on the Pd surface [5,9]. There are contradicting views for the nature of the active surface Pd- species involved in the combustion. Oh et al. [11] proposed that a thin layer of PdO on metallic Pd is the active form of the catalyst, but bulk PdO is inactive in the methane combustion. Whereas, Burch and Urbano [12] and Carstens et al. [13] have observed high catalytic activity of PdO/$Al_2O_3$ and PdO/$ZrO_2$, respectively, in the methane combustion. In both the cases [12,13], the methane combustion activity is increased with increasing the degree of Pd oxidation forming PdO until 3-4 ML of O for Pd/$Al_2O_3$ and 6-7 ML of O for Pd/$ZrO_2$. Thus, oxidized Pd form or PdO skin over Pd is considered as the most active state of the supported Pd catalysts [12-15]. Garbowski and Primet [16] proposed a redox mechanism involving surface Pd and surface PdO. They claimed that for a catalyst to be active, a total oxidation of its Pd is not essential. These aspects have been discussed earlier in detail (section 1.1.5).

Pulse methane combustion reaction over a supported Pd catalyst, pretreated under different conditions, carried out by passing a small pulse of reactants over the catalyst in a micro-reactor connected to a gas chromatograph, can provide the initial activity of the catalyst [17]. The initial catalytic activity could very well be correlated to the bulk and surface properties of the catalyst as there is little or no change in these properties during the pulse reaction. It is, therefore, interesting to study the initial

activity by the pulse reaction technique of $Pd/Al_2O_3$ catalyst (a commonly used catalyst for the combustion of hydrocarbon) in its different forms, such as the metallic Pd from the $Pd/Al_2O_3$ catalyst oxidized to different degrees (0 to 100%) and PdO from the $PdO/Al_2O_3$ catalyst reduced to different extents (0 to 100%), for a better understanding of the most active form of the catalyst. This investigation was undertaken for this purpose.

### 4.4.2. Experimental

$Pd/Al_2O_3$ catalyst (Pd loading of 5 wt%) was obtained from Lancaster, UK. The surface area of the catalyst was $153 m^2.g^{-1}$. The dispersion of Pd in the catalyst (measured by the CO chemisorption on the reduced catalyst at $25^oC$) was 11.2%.

The oxidation – reduction cycles of the catalyst was carried out as follows. The completely oxidized catalyst ($PdO/Al_2O_3$) was obtained by oxidizing the $Pd/Al_2O_3$ catalyst in a flow of pure oxygen at $600^oC$ for 2h. The completely reduced catalyst ($Pd^o/Al_2O_3$) was obtained by reducing the $PdO/Al_2O_3$ in a flow of pure hydrogen at $600^oC$ for 2h. The initial methane combustion activity of the reduced ($Pd^o/Al_2O_3$) or oxidized ($PdO/Al_2O_3$) catalyst was determined in a pulse micro-reactor (made up of quartz, i.d. = 4.0 mm) connected to a G. C. (with a thermal conductivity detector) containing 0.1g catalyst by passing a 0.1 ml pulse of methane-air mixture (7.9% methane) over the catalyst in a flow (30 $cm^3.min^{-1}$ at NTP) of pure He (which is used as a carrier gas) at 338 kPa pressure. The reaction products were analyzed by the G.C. using a 0.2 cm X 100 cm Spherocarb column. The pulse could be introduced in the GC column with or without bypassing the micro-reactor. Detailed description of the pulse micro-reactor and its operation are given elsewhere [18,19] and also in earlier section (section 1.2.3.3a and Fig. 1.2.7). The initial activity of the catalyst was measured at different temperatures ($160^oC$ to $280^oC$).

In order to study the activation of methane over the reduced or oxidized catalyst, a number of pulses of pure methane (pulse size = 0.1 ml) one after another at an interval of 5 min were passed over the catalyst at $250^oC$ and the conversion of methane over the catalyst as a function of pulse number was measured.

The methane conversion in all the pulse reactions was estimated as follows: Methane conversion (%) = 100 [(A – B)/A]; where A = counts of methane when the

reactor was by-passed and B = counts of methane in the products i.e. when the reactor was not by-passed.

The oxidation or reduction of the catalyst was carried out in the micro-reactor in situ. During the oxidative or reductive pretreatment to the catalyst, the reactor could be by-passed from the GC (Fig. 1.2.7). The oxidation of $Pd^o/Al_2O_3$ to different extents for having a skin of PdO over metallic Pd with different $PdO/Pd^o$ ratios was carried out by injecting a controlled number of pulses of pure $O_2$ over the $Pd^o/Al_2O_3$ at $600^oC$. Similarly, the reduction of $PdO/Al_2O_3$ to different extent for having a skin of metallic Pd over PdO with different $Pd^o/PdO$ ratios was carried out by injecting a controlled number of pulses of pure $H_2$ over the $PdO/Al_2O_3$ catalyst at $600^oC$. For measuring the concentration of PdO in the partially oxidized and reduced catalysts, separate reduction-oxidation experiments under identical conditions were carried out. The PdO content of each of the partially reduced or oxidized catalyst was determined by passing a number of pulses of pure $H_2$ over the catalyst using a pure $N_2$ as a carrier gas (flow rate: $30cm^3.min^{-1}$ at NTP) for the GC and measuring the amount of $H_2$ required for completely reducing the catalyst at $600^oC$, as follows: % of PdO (in Pd-PdO) = [100(X/Y)], where X is the amount of $H_2$ required for completely reducing the partially reduced or oxidized catalyst, and Y is the amount of $H_2$ required for completely reducing the $PdO/Al_2O_3$ catalyst.

### 4.4.3. Results and Discussion

#### *4.4.3.1. Methane combustion over $Pd^o/Al_2O_3$ and $PdO/Al_2O_3$*

Results in Fig. 4.4.1 show the influence of reduction, oxidation and oxidation-reduction cycle (upto 3 cycles) of the catalyst on its initial methane combustion activity at the different temperatures ($160^oC$ – $280^oC$).

The results clearly show that the catalyst in its oxidized form ($PdO/Al_2O_3$) is much more active in the methane combustion and the oxidation-reduction cycle has a small effect on the combustion activity of the catalyst in its both the forms.

In order to study the methane activation over the reduced and oxidized catalysts, the pulse reaction of methane in the absence of $O_2$ was carried out over the $Pd^o/Al_2O_3$ and $PdO/Al_2O_3$ catalysts at $250^oC$. The results showing the variation of methane conversion with the pulse number for both the catalysts are presented in Fig. 4.4.2.

The methane conversion over both the catalysts is decreased with increasing the pulse number (Fig. 4.4.2). However, the initial activity of the $PdO/Al_2O_3$ catalyst could be regained by reoxidizing (at 600°C) the catalyst, after the last (i.e. $7^{th}$) pulse experiment. However, when the two catalysts are compared for the initial methane conversion (i.e. the conversion of methane in the first pulse), the methane reactivity over the reduced catalyst was found to be much lower than that over the oxidized catalyst. The methane reactivity over the oxidized catalyst, however, approaches to that of the reduced catalyst after $5^{th}$ pulse. It is also interesting to note that, the thermal treatment (at 600°C for 1h) to the oxidized catalyst after the $5^{th}$ pulse causes an appreciable increase in the reactivity of methane (from 9% conversion in $5^{th}$ pulse to 22% conversion in the $6^{th}$ pulse) over this catalyst.

The conversion of methane over the reduced catalyst is expected due to the methane decomposition over metallic Pd [20,21], as follows:

$$CH_4 \xrightarrow{-H} CH_3 \xrightarrow{-H} CH_2 \xrightarrow{-H} CH \xrightarrow{-H} C \qquad [1]$$

Whereas, the methane conversion over the oxidized catalyst is expected to involve a gas-solid reaction (in a first few pulses), resulting in the catalyst reduction,

$$CH_4 + PdO \longrightarrow CO_2, H_2O \text{ and } Pd^o \qquad [2]$$

and also the methane decomposition over the $Pd^o$ formed in reaction-2 in the later pulses. The observed sharp decrease in the methane conversion over the oxidized catalyst with increasing the pulse number is because of the decrease in the concentration of PdO, at or close to the catalyst surface, by reaction-2. The increase in the methane conversion for the $6^{th}$ pulse (Fig. 4.4.2b) indicates the migration of lattice oxygen from sub-surface PdO to the surface of the catalyst by its diffusion during the high temperature (600°C) thermal treatment. In case of the reduced catalyst, the decrease in the methane conversion is, however, can be attributed to the formation of carbon and/or $CH_x$ species in reaction-1, causing a catalyst deactivation for the methane decomposition.

The observed much higher methane conversion over the $PdO/Al_2O_3$ catalyst in the first few pulses of pure methane in the absence of $O_2$ indicates that the activation of methane on the $PdO/Al_2O_3$ is much easier than that on the $Pd^o/Al_2O_3$. This observation contradicts the earlier claim that methane is dissociatively adsorbed on metallic Pd, but it is not readily activated on PdO at low temperature [22].

In the methane combustion over the $Pd^o/Al_2O_3$ catalyst, Eley-Rideal mechanism is expected to prevail [23], involving following steps:

$$2Pd^o + O_2 \longrightarrow 2\,(Pd = O) \quad [3]$$

$$4\,(Pd = O) + CH_4 \longrightarrow CO_2 + 2H_2O + 4Pd^o \quad [4]$$

Whereas, the methane combustion over the $PdO/Al_2O_3$ is expected to follow the redox (Mars and van Krevelen) mechanism (which is supported by the results in Fig. 4.4.2b), involving following two simplified steps:

$$CH_4 + 4(Pd\text{-}O) \longrightarrow CO_2 + H_2O + 4\,(Pd - \delta) \quad [5]$$

$$2\,(Pd - \delta) + O_2 \longrightarrow 2\,(Pd - O) \quad [6]$$

(where $\delta$ is the anion vacancy)

The observed high methane combustion activity of $PdO/Al_2O_3$ catalyst (Fig. 4.4.1) is consistent with the fact that the Pd – O bond strength in PdO is much lower than the strength of chemisorbed oxygen on the metallic Pd [24].

Table 4.4.1. Effect of the concentration and position of PdO (in the outer skin or in the inner core) in the partially reduced or oxidized catalyst on the methane combustion at different temperatures

| Concentration of PdO(%) in the catalyst | Position of PdO in the catalyst | Methane conversion (%) | | | |
|---|---|---|---|---|---|
| | | 180°C | 200°C | 220°C | 240°C |
| 20 | Inner core | 4.5 | 8.6 | 15.6 | 28.2 |
| 20 | Outer skin | 6.9 | 14.3 | 21.4 | 32.1 |
| 50 | Inner core | 8.3 | 16.1 | 27.9 | 42.8 |
| 50 | Outer skin | 11.7 | 23.5 | 50.0 | 58.7 |
| 80 | Inner core | 12.0 | 25.0 | 46.6 | 75.5 |
| 80 | Outer skin | 13.1 | 30.4 | 63.1 | 83.8 |

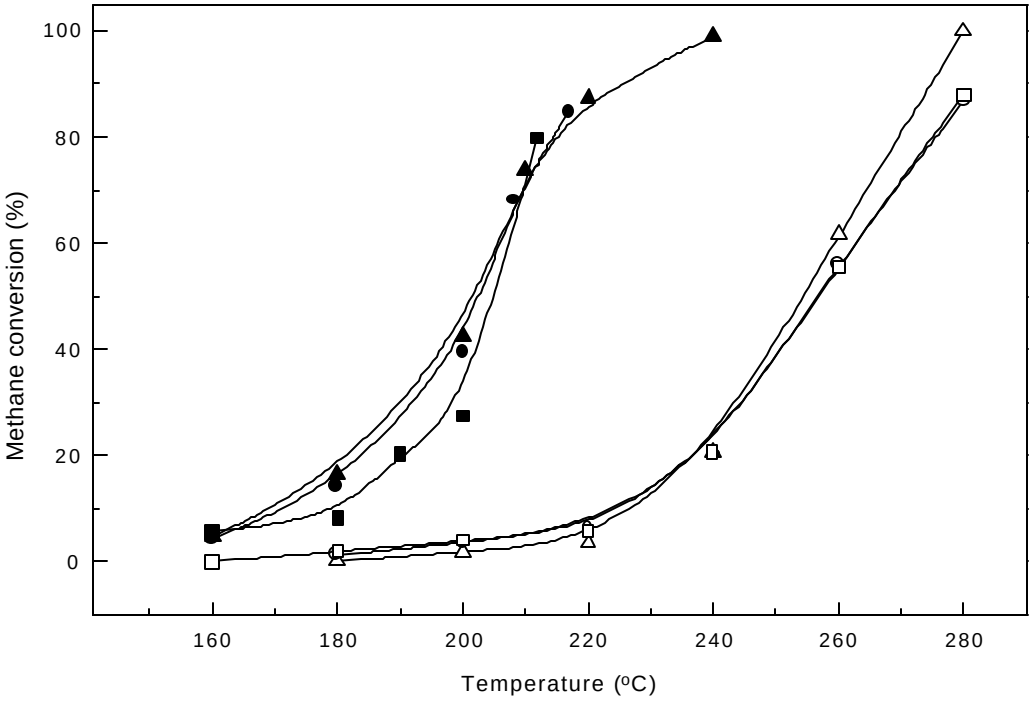


**Figure 4.4.1.** Effect of oxidation-reduction cycles on the methane combustion over the $Pd/Al_2O_3$ catalyst at different temperatures [Δ - $Pd/Al_2O_3$(I) [fresh catalyst]; ▲ - $PdO/Al_2O_3$(I) obtained from oxidation of $Pd/Al_2O_3$(I) by $O_2$ at 600°C for 2h; ○ -$Pd/Al_2O_3$(II) obtained from reduction of $PdO/Al_2O_3$(I) by $H_2$ at 600°C for 2h; ● - $PdO/Al_2O_3$(II) obtained from oxidation of $Pd/Al_2O_3$(II) by $O_2$ at 600°C for 2h; □ - $Pd/Al_2O_3$(III) obtained from reduction of $PdO/Al_2O_3$(II) by $H_2$ at 600°C for 2h; ■ - $PdO/Al_2O_3$(III) obtained from oxidation of $Pd/Al_2O_3$(III) by $O_2$ at 600°C for 2h.

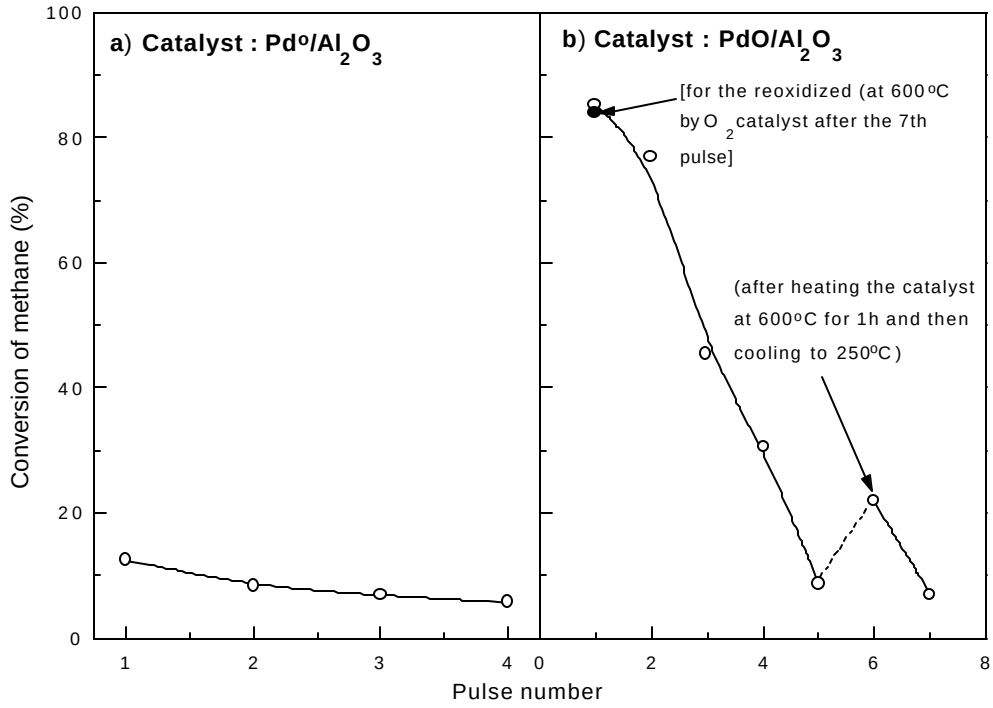


**Figure 4.4.2.** Variation of methane conversion (at 250°C) over the $Pd/Al_2O_3$ (a) and $PdO/Al_2O_3$ (b) catalysts in the absence of oxygen with the pulse number (Pulse: 0.1ml of pure methane).

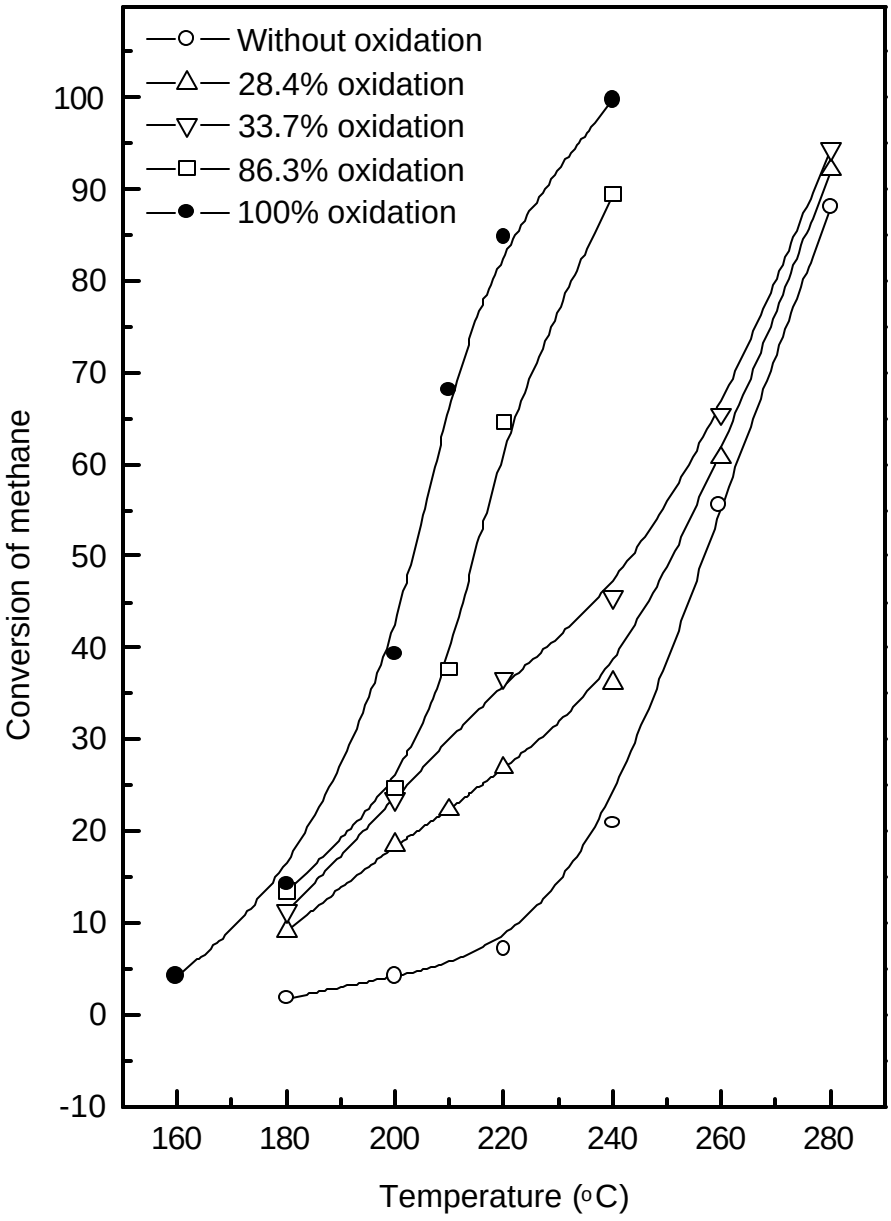


**Figure 4.4.3.** Temperature dependence of the methane combustion activity of $Pd^{o}/Al_2O_3$ catalyst oxidized to different extents by $O_2$ at $600^{o}C$.

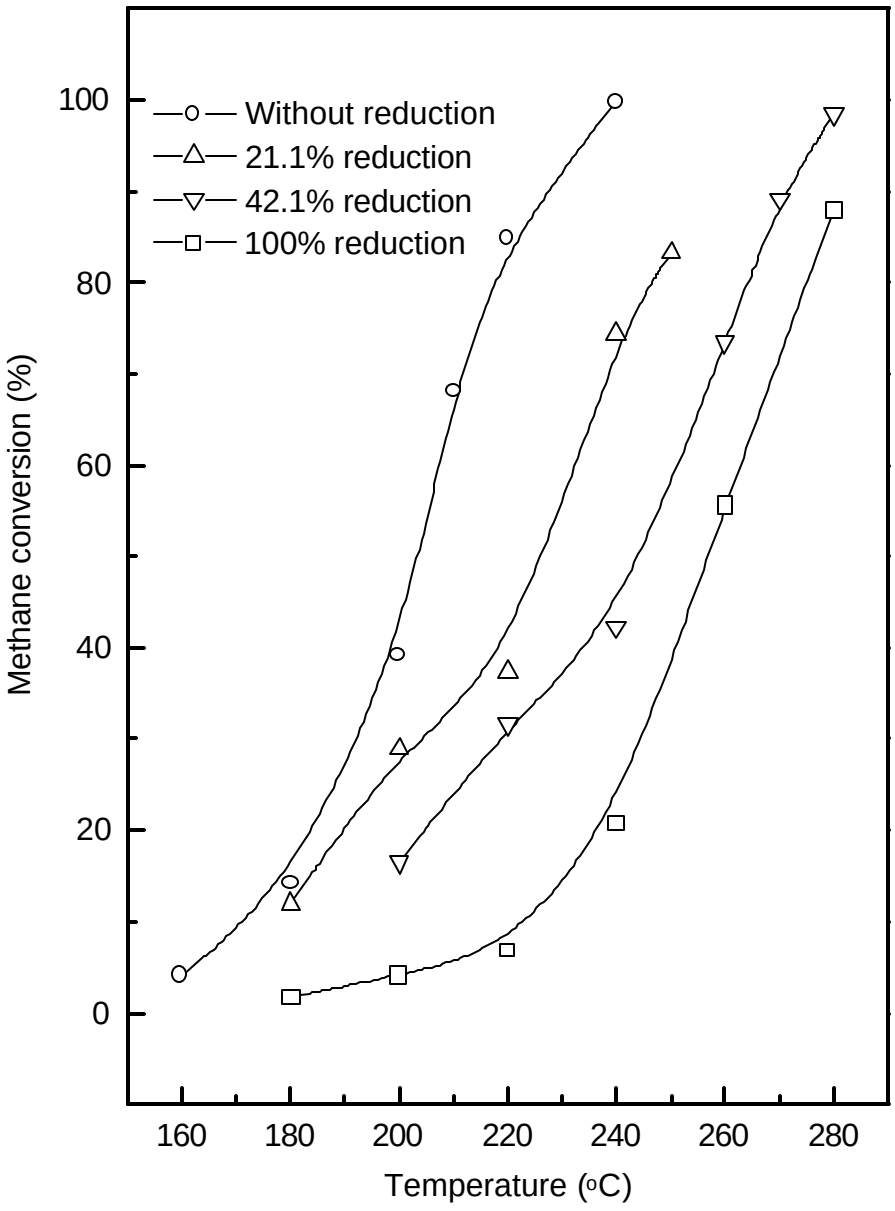


**Figure 4.4.4.** Temperature dependence of the methane combustion activity of $PdO/Al_2O_3$ catalyst reduced to different extents by $H_2$ at 600°C.

#### *4.4.3.2. Influence of relative concentration and position of $Pd^o$ and PdO in the catalyst*

Under the operating conditions, the presence of metallic Pd or PdO species and their relative concentration and/or positions (a skin of PdO on metallic Pd or vice versa) are expected to vary depending upon the catalyst pretreatment and the combustion process conditions, particularly temperature and $O_2$ to $CH_4$ ratio. It is, therefore, interesting to study the initial methane combustion activity of the $Pd^o/Al_2O_3$ and $PdO/Al_2O_3$, oxidized and reduced, respectively, to different extents. Results of such studies are presented in Figs. 4.4.3 and 4.4.4.

Figure 4.4.3 shows that, at all the temperatures, the methane combustion activity is increased with increasing the degree of the catalyst oxidation. Since the oxidation is expected to proceed gradually from the surface to the inner core following the shrinking core model for gas-solid reactions [25], a skin of PdO over the metallic Pd is formed in the catalyst oxidation. Thus the increase in the degree of Pd oxidation corresponds to an increase in the thickness of a skin of PdO over the metallic Pd. The results thus clearly show a strong dependence of the methane combustion activity on the thickness of the PdO skin. Burch and Urbano [12] and Carstens et al. [21] have also observed an increase in the methane combustion activity with increasing the degree of Pd oxidation but only upto 3-4 and 5-6 ML (monolayer) of PdO respectively. However, in the present case, the increase in the initial methane combustion activity is observed for the entire Pd-oxidation range.

It is interesting to note that an exactly opposite trend for the dependence of the initial methane combustion activity on the degree of PdO reduction (Fig. 4.4.4) is observed to that for the variation of the initial activity with the degree of Pd-oxidation (Fig. 4.4.3).

The initial activity of the reduced $PdO/Al_2O_3$ catalyst is decreased with increasing the degree of PdO reduction at all the temperatures and consequently with increasing the skin thickness of metallic Pd over the PdO (Fig. 4.4.4). The PdO reduction is also expected to follow the shrinking core model [25].

Results showing the influence of the position of the PdO (i.e. PdO as a inner core or as a outer skin) and its concentration in the Pd-PdO of the catalyst on the initial activity in the methane combustion are presented in Table 4.4.1. It is interesting to note that, for the same Pd-concentration, the activity at all the temperatures is strongly influenced by the position of PdO in the catalyst. The catalyst having the

PdO in the outer skin over the metallic Pd showed appreciably higher methane combustion activity. This indicates that not only the PdO concentration relative to that of metallic Pd but also the position of the PdO (as an inner core or outer skin) plays important role in deciding the methane combustion activity of the catalyst.

Surface restructuring and/or change in the surface composition of a oxidation catalyst during hydrocarbon oxidation reactants are commonly observed phenomenon. Restructuring of Pd catalyst during the methane combustion has also been observed earlier [1,26]. Hence it is really not possible to obtain reliable information on the influence of the position and concentration of PdO on the methane combustion activity by carrying out the reaction under steady state, as the bulk and surface properties of the Pd catalyst are expected to vary with the process time conditions, viz. temperature and $O_2$ - or methane-rich atmosphere over the catalyst. However, in the case of pulse reaction carried out using a small pulse of reactants, almost no change in the catalyst properties is expected and the results (initial catalytic activity) obtained are much more reliable for finding the correlation between the known surface and bulk property and the catalytic activity.

### 4.4.4. Conclusions

From the present pulse reaction studies on the methane conversion in the presence or absence of $O_2$ over $Pd/Al_2O_3$ catalyst in its different reduced or oxidized forms, following important conclusions can be drawn:

1. The initial methane combustion activity of the oxidized catalyst ($PdO/Al_2O_3$) is much higher than that of the reduced one ($Pd^o/Al_2O_3$). The activity of the respective catalyst is almost unaffected by oxidation-reduction cycles.
2. The reactivity of methane in the absence of $O_2$ over the reduced catalyst is much smaller than that over the fresh catalyst. The methane combustion over the oxidized catalyst involves the redox mechanism.
3. The methane combustion activity of the partially reduced and oxidized catalysts is strongly influenced by the degree of PdO reduction and the Pd oxidation, respectively; it is decreased with increasing the degree of PdO reduction but increased with the degree of Pd oxidation.
4. For the partially reduced or oxidized catalysts, having the same relative concentration of $Pd^o$ and PdO, the catalyst with its PdO in outer skin over the

metallic Pd shows higher methane combustion activity than the one having its PdO in the inner core and metallic Pd in the outer skin.

5. The methane combustion activity is controlled essentially by both the relative concentration and position of metallic Pd and PdO in the catalyst and not only by its surface properties.

### 4.4.5. References


1. Y-H. Chin and D. E. Resasco *in* "Catalysis – A specialist periodical report", vol. 14, pp. 1-39, Royal Society of Chemistry, (1999).
2. M. F. M. Zwinkels, S. G. Jaras, and P. G. Menon, Catal. Rev. – Sci. Eng., 35 (1993) 319.
3. E. M. Johansson, D. Papadias, P. O. Thevenin, A. G. Ersson, R. Gabrielsson, P. G. Menon, P. H. Bjornbom, and S. G. Jaras, *in* "Catalysis – A specialist periodical report", vol. 14, pp. 183-235, Royal Society of Chemistry, (1999).
4. V. R. Choudhary, S. Banerjee and R. E. Babcock, 6th Annual Int. Petroleum Environment Conference, Nov. 16-19, 1999, Houston, Texas.
5. R. F. Hicks, H. Qi, M. L. Young, and R. G. Lee, J. Catal., 122 (1990) 280.
6. P. Briot and M. Primet, Appl. Catal., 68 (1991) 301.
7. L. P. Haack, and K. Otto, Catal. Lett., 34 (1995) 31.
8. C. A. Muller, M. Maciejewski, R. A. Koeppel, and A. Baiker, Catal. Today, 47 (1999) 245.
9. H. Widjaja, K. Sekizawa, K. Eguchi, and H. Arai, Catal. Today, 35 (1997) 197.
10. K-I. Fujimoto, F. H. Ribeiro, M. Avalos-Borja and E. Iglesia, J. Catal., 179 (1998) 431.
11. S. H. Oh, P. J. Mitchell, and R. M. Siewert, J. Catal. 146 (1994) 537.
12. R. Burch and F. J. Urbano, Appl. Catal. A, 124 (1995) 121.
13. S. C. Su, J. N. Carstens and A. T. Bell, J. Catal. 176 (1998) 136.
14. R. Burch, Catal. Today, 35 (1997) 27.
15. R. J. Farrauto, J. K. Lampert, M. C. Hobson and E. M. Waterman, Appl. Catal.B 6 (1995) 263.
16. E. Garbowski, and M. Primet, Appl. Catal. 125 (1995) 185.

17. V. R. Choudhary and L. K. Doraiswamy, Ind. Eng. Chem. Prod. Res. Dev., 10 (1971) 218.
18. V. R. Choudhary and V. H. Rane, J. Catal., 135 (1992) 310.
19. V. R. Choudhary, S. D. Sansare, A. M. Rajput, and D. B. Akolekar, Appl. Catal. 69 (1991) 187.
20. Y-N Wang, R. G. Herman, and K. Klier, Surf. Sci. 279 (1992) 33.
21. J. N. Carstens, S. C. Su and A. T. Bell, J. Catal., 176 (1998) 136.
22. F. Solymosi, J. Erdohelyi, J. Cserenyi and A. Felvegi, J. Catal., 147 (1994) 272.
23. S. Seimanieds and M. Stoukides, J. Catal., 98 (1986) 540.
24. G. D. Zakumbaeva and S. V. Artamonov, React. Kinet. Catal. Lett., 10 (1979) 183.
25. O. Levenspiel, Chemical Reaction Engineering ,John Wiley, 1962.
26. E. Garbowski, C. Feumi-Jantou, N. Mouaddib and M. Primet, Appl. Catal. A, 109 (1994) 277.

# CHAPTER 4.5

# HIGH TEMPERATURE COMBUSTION OF METHANE OVER THERMALLY STABLE CoO-MgO CATALYST FOR CONTROLLING METHANE EMISSIONS FROM OIL/GAS-FIRED FURNACES

## 4.5.1. Earlier Work/Background and Objectives of Present Work

As compared to carbon dioxide, methane causes a much larger green house effect and hence the control of methane emission is essential. An appreciable amount of methane is produced in the combustion of hydrocarbons, which is practised on a very large scale in chemical and other industries and also in the power plants for producing energy. Gas or oil-fired furnaces are commonly used for this purpose. The furnace effluent gases are generally at high temperature (upto about 1300$^{o}$C) and contain an appreciable amount of methane along with uncombusted other hydrocarbons. Since methane is most inert among hydrocarbons, its destruction by combustion is difficult and hence requires an active combustion catalyst. Hence for the complete combustion of methane from the hot furnace effluent gases, a high temperature stable combustion catalyst is essential.

A number of catalysts, such as those based on noble metals, perovskites, zeolites and single or mixed transition metal oxides have been reported for the complete combustion of hydrocarbons [1-4]. A detailed discussion regarding high temperature combustion catalysts has already been made in the earlier section (section 1.1.6). It is now evident, most of these catalysts were not found to be suitable for the high temperature methane combustion [1]. In the recent studies, metal stabilized cubic $ZrO_2$ [5] and Ag-doped $LaCoO_3$ [6] or $LaFe_{0.5}Co_{0.5}O_3$ [7] catalysts showed high activity in the low temperature complete combustion of methane. However, these catalysts have low thermal stability and hence not suitable for methane combustion at high temperatures ($\geq 900^{o}$C).

The main problem associated with the use of any catalyst at high temperatures are as follows: 1) structural collapse and/or sintering with a drastic reduction in the surface area, 2) evaporation of catalytically active components and 3) solid-solid reactions of the active components of the catalysts among themselves or with reactive components of the catalyst support, ultimately deactivating the catalyst. Cobalt and magnesium oxides are very high melting compounds. At high temperatures, they do

not undergo solid-solid reaction but form a solid solution at a wide concentration range [8] Hence, it is interesting to investigate the catalytic activity of CoO-MgO calcined at high temperatures ($900^{o}$-$1400^{o}$C) in the total combustion of very dilute methane at high temperatures for controlling the methane emissions from oil/gas-fired furnaces. The present work was undertaken for this purpose.

### 4.5.2. Experimental

CoO-MgO (with Co/Mg mole ratio = 0.5 and 1.0) catalyst was prepared from mixed nitrates of cobalt (II) and magnesium by the procedure described already in earlier section (section 1.2.1.3). The catalyst was calcined at different temperatures ($900^{o}$-$1400^{o}$C) under static air in an electric furnace for 4h. The catalysts were characterized by powder X-ray diffraction, by XPS and also for their surface area.

For comparing the catalysts (calcined at different temperatures) for the reduction of their cobalt oxide, pulses of pure $H_2$ (pulse size = 0.2 $cm^3$) one after another were passed over the catalyst at different temperatures ($150^{o}$C - $900^{o}$C) in a micro-reactor connected to a gas chromatograph with a thermal conductivity detector using pure argon as a carrier gas.

The combustion of dilute methane over the catalysts was carried out in a quartz reactor (i.d. = 4.0 mm) (Fig. 1.2.1b) packed with 0.154 $cm^3$ catalyst particles (0.2-0.3 mm size) at the following reaction conditions: feed=0.5 vol% methane in air, gas hourly space velocity (GHSV), measured at $0^{o}$C and 1atm = 15000 - 120000 $h^{-1}$; temperature = $600^{o}$-$1100^{o}$C and pressure = 1.1 $\pm$ 0.05 atm. The detailed experimental procedure has been discussed earlier (section 1.2.3.3b and Fig. 1.2.8). The dead volume in the reactor was reduced by inserting quartz rods (4.0 mm diameter) below and above the catalyst bed in the reactor, as has been shown in Figure 1.2.1b. The concentration of methane in the feed and reactor effluent gases was measured by the flame ionization detector. The combustion of methane was complete; there was no formation of carbon monoxide in the catalytic combustion of methane.

The pulse reaction of pure methane over the catalysts at $800^{o}$C for studying the involvement of lattice oxygen in the methane combustion was carried out in a pulse micro-reactor connected to a gas chromatograph with thermal conductivity detector, using pure helium as a carrier gas, as described earlier [6,10] and also shown in detail earlier (section 1.2.3.3 and Fig. 1.2.7).

### 4.5.3. Results And Discussion

#### *4.5.3.1. Catalyst characterization*

XRD spectra of the CoO-MgO catalyst (Co/Mg = 0.5 and 1.0) calcined at different temperatures (900°C and 1200°C or 1400°C) are shown in Fig. 4.5.1. The spectra indicates that there is no presence of any separate phase of cobalt oxide even for the catalyst calcined at 900°C.

Results in Fig. 4.5.2 show the influence of calcination temperature on the reduction of cobalt oxide from the catalyst at different temperatures. The reduction was carried out by passing a pulse of pure $H_2$ over the catalyst as a function of temperature and measuring quantitatively the $H_2$ consumed in the catalyst reduction. Upto about 400°C, there was little or no reduction of the catalyst calcined at both the temperatures. However, at the higher temperatures (>400°C) the catalyst calcined at 900°C showed much higher reducibility than that observed for the catalyst calcined at the higher temperature (1200°C or 1400°C).

Co ($2p_{3/2}$) XPS spectra of the CoO-MgO catalyst (Co/Mg = 0.5) calcined at 900°C and 1400°C are presented in Fig. 4.5.3. The spectra were obtained under identical conditions. It is interesting to note that while for the catalyst calcined at 900°C, the XPS peak at 780 eV for Co ($2p_{3/2}$) is quite distinct, a similar peak for the catalyst calcined at 1400°C is negligibly small. This suggests that the surface concentration of cobalt in the latter case is much smaller.

The above results indicate that the CoO-MgO catalyst calcined at 900°C or at the higher temperatures exists as a solid solution of the oxides of Co and Mg. The observed lower reducibility of the catalyst calcined at higher temperature is expected mostly because of the catalyst sintering causing a reduction in the surface area (Table 4.5.1) and/or the lower concentration of cobalt in the outer layers of the catalyst.

The catalysts surface area is decreased markedly with increasing the calcination temperature and/or the Co/Mg ratio of the catalyst (Table 4.5.1).

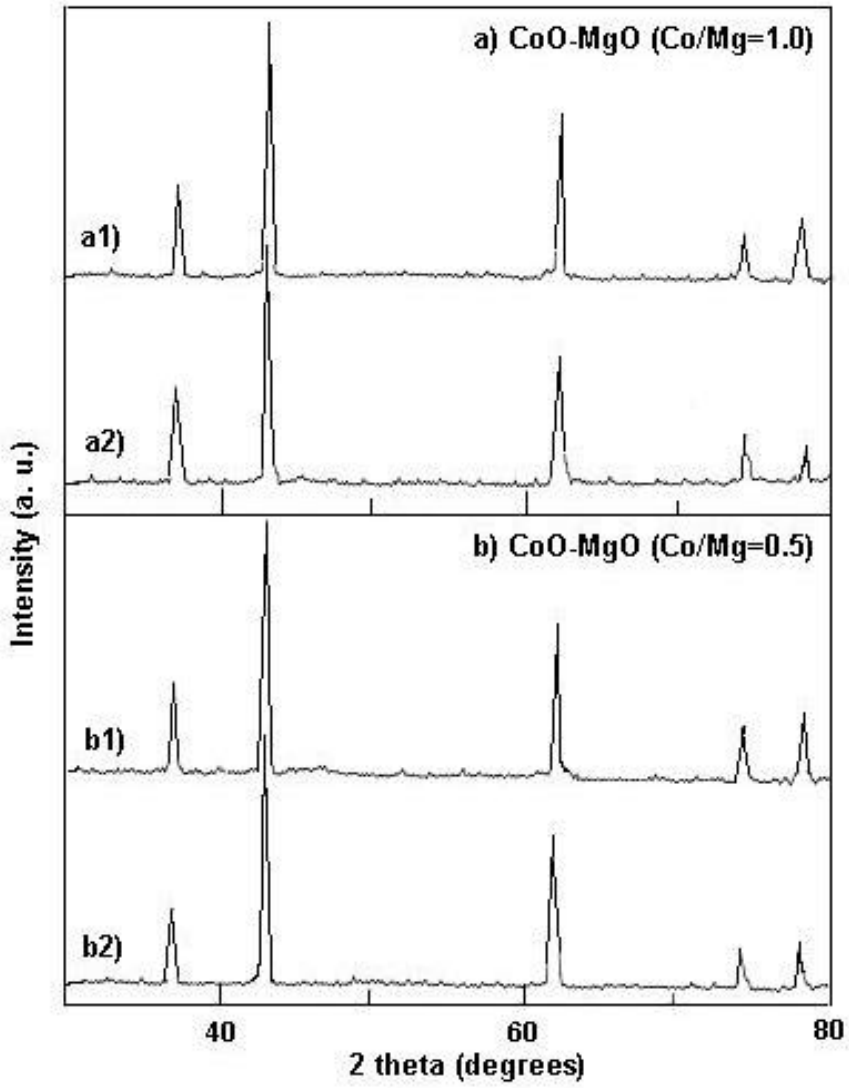


**Figure 4.5.1.** The X-ray diffraction spectra of different CoO-MgO catalysts with Co/Mg ratio 1.0 (a) calcined at 1200°C (a1) and at 900°C (a2) and Co/Mg ratio 0.5 (b) calcined at 1400°C (b1) and at 900°C (b2)

### *4.5.3.2. Methane combustion*

Results showing the influence of Co/Mg and calcination temperature of the catalyst on its surface area and methane combustion activity (in terms of the temperature required for half the combustion at different space velocities) are presented in Table-4.5.1. Effect of space velocity on the methane conversion in the methane combustion over the CoO-MgO catalysts calcined at different temperatures is shown in Figs. 4.5.4 and 4.5.5. The temperature dependence of the rate of methane

combustion at 50% methane conversion over the CoO-MgO catalysts is shown in Fig. 4.5.6. The data showing the influence of Co/Mg ratio and calcination temperature on the activation energy and frequency factor for the combustion are given in Table 4.5.2. The activation energy was obtained from the temperature dependence of the methane combustion rate at the half reaction (50% conversion) according to the Arrhenius type equation.

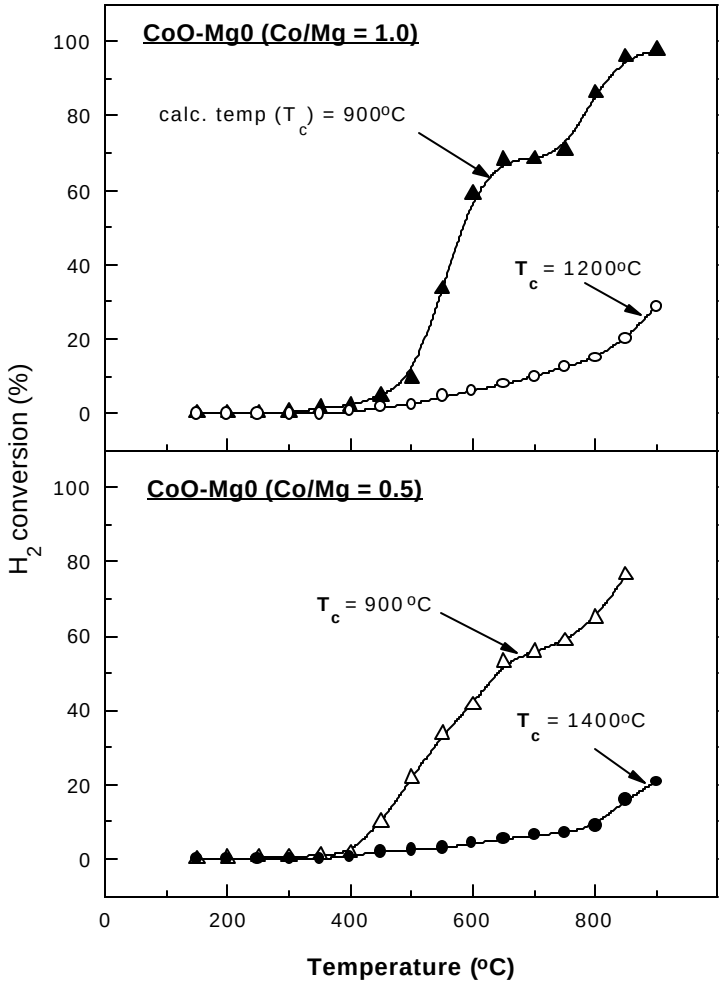


**Figure 4.5.2.** Effect of calcination temperature on the reduction of CoO for the catalyst

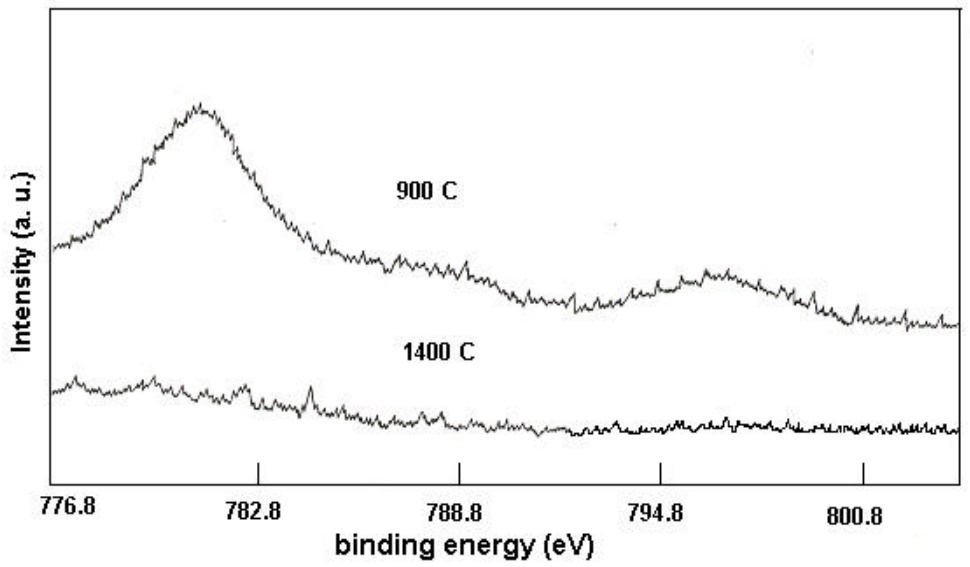


**Figure 4.5.3.** The X-ray photoelectron spectra of Co ($2p_{3/2}$) electron of CoO-MgO catalyst (Co/Mg = 1.0) calcined at 1400°C and 900°C

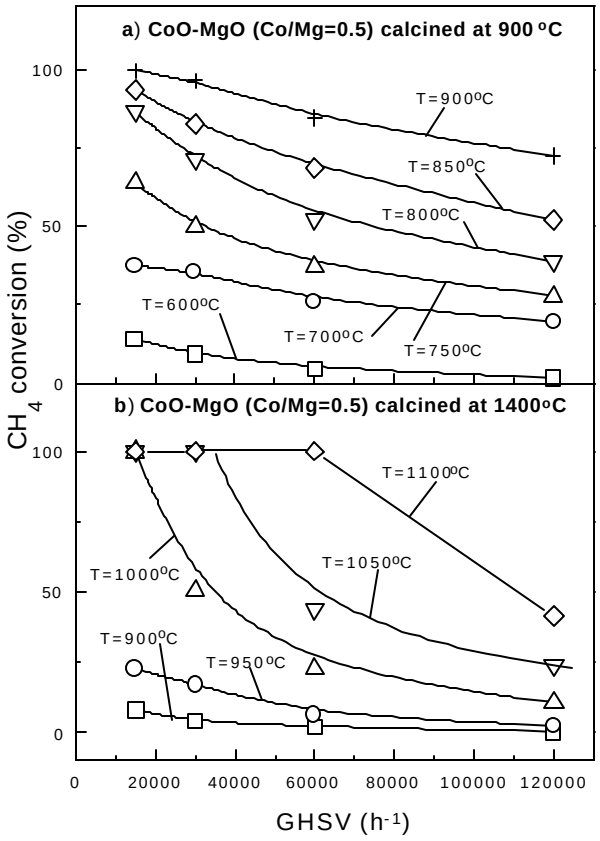


**Figure 4.5.4.** Influence of gas hourly space velocity on the conversion of methane in the methane combustion at different temperatures over CoO-MgO catalyst with Co/Mg ratio of 0.5

**Table 4.5.1.** Temperature required for half the methane combustion reaction over the CoO-MgO catalysts

| Co/Mg ratio in the catalysts | Calcination temperature ($^oC$) | Surface area ($m^2.g^{-1}$) | Temperature ($^oC$) for half reaction | | | |
|---|---|---|---|---|---|---|
| | | | GHSV ($h^{-1}$) x $10^{-3}$ | | | |
| | | | 15 | 30 | 60 | 120 |
| 0.5 | 900 | 4.8 | 723 | 748 | 792 | 840 |
| 1.0 | 900 | 1.4 | 660 | 724 | 766 | 784 |
| 1.0 | 1200 | 0.1 | 883 | 937 | 972 | 1021 |
| 0.5 | 1400 | 0.2 | 972 | 1003 | 1050 | - |

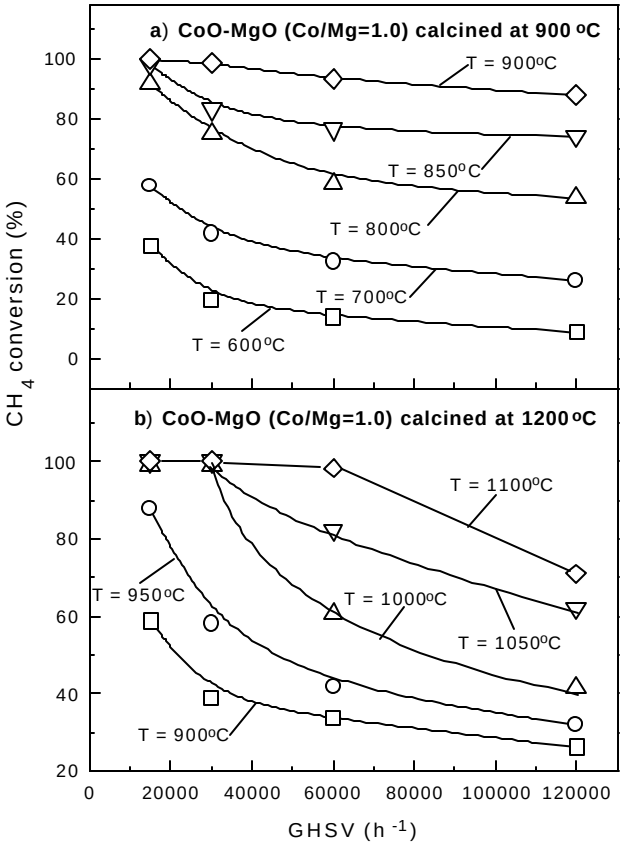


**Figure 4.5.5.** Influence of gas hourly space velocity (GHSV) on the conversion of methane in the methane combustion at different temperature over CoO-MgO catalyst with Co/Mg ratio of 1.0

From these results, following important observations can be made:

When the Co/Mg ratio of the catalyst is increased, its surface area is decreased but its combustion activity is increased appreciably and also the activation energy is decreased significantly. The increase in the catalyst calcination temperature from 900°C to 1200°C or 1400°C, has resulted in a large decrease in the surface area and a large increase in the activation energy. However, the catalyst calcined at a very high temperature shows high methane combustion activity (Figs. 4.5.4b and 4.5.5b)

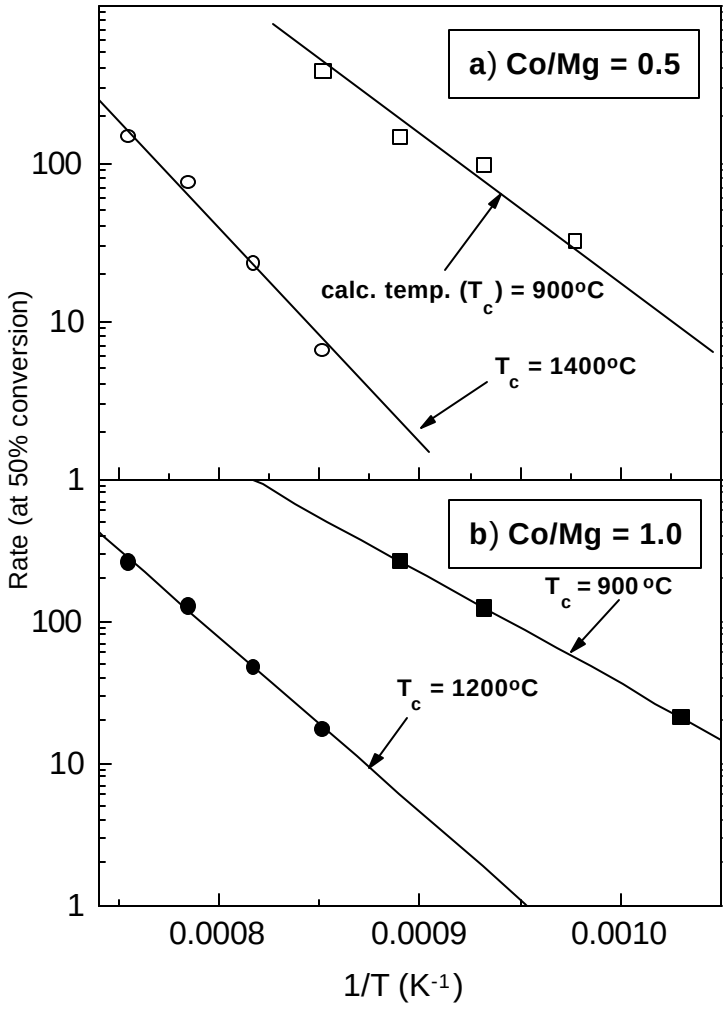


**Figure 4.5.6.** Temperature dependence of the methane combustion rate (at 50% conversion) over the CoO-MgO catalyst

**Table 4.5.2.** Activation energy and frequency factor (A) for the combustion of methane over the CoO-MgO catalysts

| Co/Mg ratio in the catalyst | Calcination temperature ($^oC$) | Activation energy ($kcal.mol^{-1}$) | A x $10^{-10}$ ($mole.h^{-1}$) |
|---|---|---|---|
| 0.5 | 900 | 37.7 | 0.34 |
| 1.0 | 900 | 36.2 | 0.26 |
| 1.0 | 1200 | 56.6 | 52.5 |
| 0.5 | 1400 | 65.8 | 1072 |

In the pulse reaction of pure methane over the catalyst (Fig. 4.5.7), the conversion is decreased with increasing the pulse number. At the 9$^{th}$ pulse, the conversion is reduced to a very low value (0.6%). However, the initial high conversion (≈ 29%) is regained after reoxidation of the catalyst by air. This clearly shows the involvement of lattice oxygen with redox mechanism in the methane combustion over the catalyst.

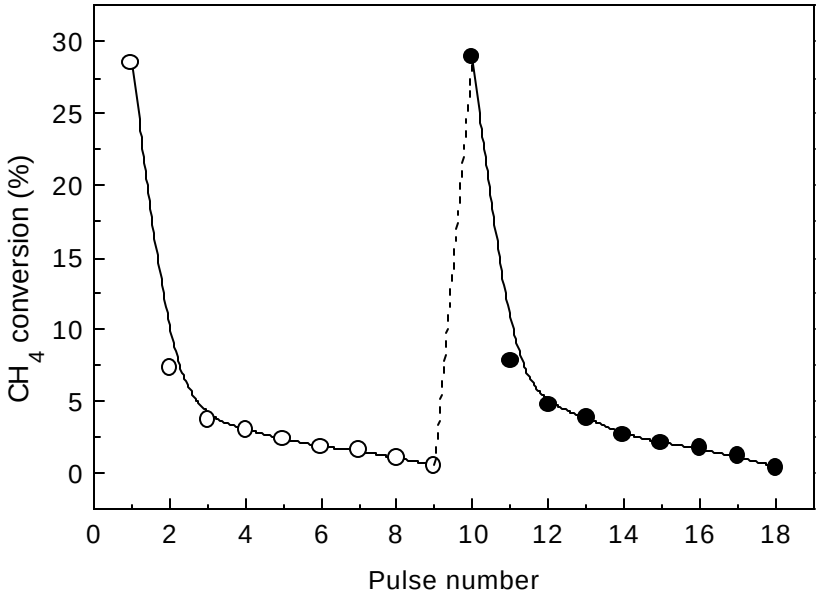


**Figure 4.5.7.** Pulse reaction of pure methane (at 800oC) over fresh and reoxidized CoO-MgO (Co/Mg = 1.0) catalyst (calcined at 900$^o$C) [○ - fresh catalyst and - after reoxidation of the catalyst at 800$^o$C in a flow of air for 1h followed by treating it under He flow for 0.5h]

It may be noted that, in spite of its very low surface area, the catalyst calcined at the high temperatures shows high methane combustion activity, making this catalyst useful for the high temperature combustion of methane (at a very low concentration) from the hot furnace effluent gases. This catalyst may also be used for the combustion of methane at ≤1500°C for reducing the formation of $NO_x$ in the gas power plants and gas-fired furnaces. It would be interesting to study further a supported CoO-MgO solid solution, using a support, which does not undergo solid-solid reaction with CoO and/or MgO at high temperatures, for the combustion of methane.

### 4.5.4. Conclusions

From this investigation, following important conclusions have been drawn:

1. CoO-MgO forms a complete solid solution at high temperatures (≥900°C) and it is a promising catalyst for the high temperature (≥900°C) combustion of dilute methane.
2. The methane combustion over the catalyst involves its lattice oxygen with a redox mechanism.
3. The activation energy of the methane combustion is increased with increasing the calcination temperature and/or decreasing the Co/Mg ratio of the catalyst.

### 4.5.5. References


1. E.M., Johansson, D. Papadias, P.O. Thevenin, A.G., Ersson, R. Gabrielsson, P.G. Menon, P.H. Bjornbom, S.G. Jaras, A Specialist Periodic Report - Catalysis, vol. 14, page 183-235, The Royal Society of Chemistry, Cambridge, UK, 1999.
2. V. R. Choudhary, S. Banerjee and R. E. Babcock, 6th International Petroleum Environmental Conference, Nov. 16-19, 1999, Houston, TX
3. J. J. Spivey, Ind. Eng. Chem. Res., 26 (1987) 2165.
4. J. J. Spivey and J.B. Butt, Catal. Today, 11 (1992) 465.
5. V. R. Choudhary, B. S. Uphade, S. G. Pataskar, and A. Keshavaraja, Angew. Chem. Int. Ed. Engl., 35 (1996) 2393.
6. V. R. Choudhary, B. S. Uphade, S. G. Pataskar, and G. A. Thite, Chem. Commun., (1996) 1021-2.
7. V. R. Choudhary, B. S. Uphade and S. G. Pataskar, Fuel, 78 (1999) 919.
8. J. G. Highfield, A. Bossi, F. S. Stone, Stud. Surf. Sci. Catal., 16 (1983) 181.
9. V. R. Choudhary, V. H. Rane, J. Catal., 135 (1992) 310.

## PUBLICATIONS AND PATENTS BASED ON THE WORK REPORTED IN THE THESIS

### A Papers Published/Communicated

1. *Activation by hydrothermal treatment of low surface area $ABO_3$ type perovskite oxide catalysts*
   V. R. Choudhary, **S. Banerjee** and B. S. Uphade
   Appl. Catal. A: Gen. **197** (2000) L183-L186.

2. *Complete combustion of methane over transition metal oxide(s) containing acidic $ZrO_2$ catalysts*
   **S. Banerjee**, T. V. Choudhary and V. R. Choudhary
   Recent Trends in Catalysis, Edited by. V. Murugesan, B. Arabindoo and M. Palanichamy, pp. 481, Narosa Publishing House, New Delhi, 1999.

3. *A method for increasing the surface area of perovskite-type oxide*
   **S. Banerjee** and V. R. Choudhary
   Proc. Ind. Ac. Sci.-Chem. Sci. **112** (2000) 535-542.

4. *Continuous production of $H_2$ at low temperature from methane decomposition over Ni-containing catalyst followed by gasification by steam of the carbon on the catalyst in two parallel reactors operated in cyclic manner*
   V. R. Choudhary, **S. Banerjee** and A. M. Rajput, J. Catal 198 (2001) 136.

5. *Control of methane emissions from oil/gas-fired furnaces by high temperature combustion of methane over thermally stable CoO-MgO catalyst,*
   Vasant R. Choudhary, Ajit S. Mamman, Suryakant G. Pataskar and **Subhabrata Banerjee**
   Preprint - Fuel Chem. Div., Am. Chem. Soc. 42 (2001) 83.

6. *Aromatization of dilute ethylene over Ga-modified ZSM-5 type zeolite catalysts*
   V. R. Choudhary, P. Devadas, **S. Banerjee** and A. K. Kinage
   Microporous and Mesoporous Materials, (2001) (in press).

7. *Aromatization of propene and n-butene over H-galloaluminosilicate (ZSM-5 type) Zeolite*
   V. R. Choudhary, P. Devadas and **S. Banerjee**
   (revised manuscript communicated to Applied Catalysis A: General).

8. *Product distribution in the aromatization of dilute ethene over H-GaAlMFI zeolite: Effect of space velocity*
   V. R. Choudhary, **S. Banerjee** and P. Devadas
   (communicated to Microporous Mesoporous Materials).

9. *Influence of temperature on the product selectivity and distribution of aromatics and $C_8$ aromatic isomers in the conversion of dilute ethene over H-galloaluminosilicate (ZSM-5 type) zeolite*
   V. R. Choudhary, S. Banerjee and P. Devadas
   (revised manuscript communicated to Journal of Catalysis)

10. *High temperature combustion of methane over thermally stable CoO-MgO catalyst for controlling methane emissions from oil/gas-fired furnaces*
    V. R. Choudhary, **S. Banerjee,** A. S. Mamman and S. G. Pataskar

"Environmental Challenges and Greenhouse Gas Control for Fossil Fuel Utilization in the 21st Century" (M. M. Maroto-Valer, C. Song and Soong, Eds.), Kluwer Academic/Plenum Publishers, New York (2001).

11. *Pulse reaction of methane in the presence or absence of $O_2$ over Pd (or PdO)/$Al_2O_3$ oxidized (or reduced) to different extents*
V. R. Choudhary and **S. Banerjee,** (communicated to Journal of Catalysis).

12. *Low temperature complete combustion of dilute propane over Mn-doped $ZrO_2$ (cubic) catalyst*
V. R. Choudhary, **S. Banerjee** and S. G. Pataskar (communicated to Applied Catalysis B: Environmental).

13. *Complete combustion of dilute propane over transition metal-doped $ZrO_2$ catalyst*
V. R. Choudhary, **S. Banerjee** and S. G. Pataskar (communicated to Applied Catalysis A: General).

14. *Catalysts for Catalytic Combustion* (A Review)
T. V. Choudhary, **S. Banerjee** and V. R. Choudhary (communicated to Applied Catalysis A:General).

15. *Hydrogen from step-wise steam reforming of methane over Ni/$ZrO_2$: Factors affecting catalytic methane decomposition and gasification by steam of carbon formed on the catalysts*
V. R. Choudhary, **S. Banerjee** and A. M. Rajput (communicated to Journal of Catalysis)

## B. Papers Presented in International Symposiums

1. *Low Temperature (1300° – 1500°C) Combustion of Methane/Natural Gas for Reducing NOx Formation,* Vasant R. Choudhary, **Subhabrata Banerjee** and R. E. Babcock, presented at Sixth Annual International Petroleum Environmental Conference, Nov. 16-19, 1999, Houston, Texas.

2. *Low temperature catalytic oxidative destruction of volatile organic compounds* ***(VOCs),*** Vasant R. Choudhary, **Subhabrata Banerjee** and R. E. Babcock, presented at Sixth Annual International Petroleum Environmental Conference, Nov. 16-19, 1999, Houston, Texas.

3. *Complete combustion of toluene from waste gases over Co-, Fe-, Cr- and Ni-doped $ZrO_2$ catalysts,* **S. Banerjee**, S. G. Pataskar and V. R. Choudhary (to be presented at 2nd Indo-Pacific Catalysis Symposium to be held at National Chemical Laboratory, Pune, India from 24th-26th January, 2000)

4. *CO-free hydrogen from low temperature methane decomposition followed by carbon gasification with steam over Ni/$ZrO_2$ catalyst in two parallel reactors*, A. M. Rajput, **S. Banerjee** and V. R. Choudhary (to be presented at 2nd Indo-Pacific Catalysis Symposium to be held at National Chemical Laboratory, Pune, India from 24th-26th January, 2000)

5. *Control of methane emissions from oil/gas-fired furnaces by high temperature combustion of methane over thermally stable CoO-MgO catalyst,* Vasant R. Choudhary, Ajit S. Mamman, Suryakant G. Pataskar and **Subhabrata Banerjee** (presented in 221st ACS National Meeting, held at San Diego, 1-4th April, 2000.

## C. Papers Presented in National Symposium

1. *Complete Combustion of Methane over Transition Metal Oxide(s) Containing Acidic $ZrO_2$ Catalysts*, **Subhabrata Banerjee**, Tushar V. Choudhary and Vasant R. Choudhary (Paper presented in 14th National Symposium on Catalysis (CATSYMP-98) at Anna University, Chennai, 16-18th Dec.,1998.

2. *Complete Combustion of Methane at Low Concentrations using Nickel and Cobalt containing Catalysts*, A. G. Gaikwad, **S. Banerjee**, S. G. Pataskar and V. R. Choudhary (Poster presented in NCL Golden Jubilee Symposium on Catalysis, 1999)

3. *Aromatization of n-Heptane over H-GaMFI, Ga/H-ZSM-5 and H-GaAlMFI Zeolites*, **S. Banerjee**, S. A. R. Mulla and V. R. Choudhary (Poster presented in NCL Golden Jubilee Symposium on Catalysis, 1999)

4. *A Method for Increasing the Surface Area of Perovskite-type Oxide*, **S. Banerjee** and V. R. Choudhary, presented in Catworkshop 2000, IICT, Hyderabad, 7-8th January, 2000.

## D. US Patents Granted/Filed

Process for the activation of perovskite-type oxide
Vasant. R. Choudhary and **Subhabrata Banerjee**
**US 6,197,719** (6th March, 2001).

*Low Temperature production of hydrogen from methane or methane-rich hydrocarbons and steam using a group VIII metal oxide(s) containing solid catalyst in two parallel reactors*
Vasant R. Choudhary, Amarjeet M. Rajput and Subhabrata Banerjee,
(Filed both Indian and US patent application) (2000).